

Identification of proteins controlling AQP2 translocation by large-scale siRNA screening of the mouse kinome

DISSERTATION

zur Erlangung des akademischen Grades des
Doktors der Naturwissenschaften
(Dr. rer. nat.)

eingereicht im Fachbereich Biologie, Chemie, Pharmazie
der Freien Universität Berlin

vorgelegt von

Dörte Faust

aus Lauchhammer

Berlin 2014

Diese Arbeit wurde von August 2009 bis März 2014 am Max-Delbrück-Centrum für Molekulare Medizin (MDC) in Berlin unter der Leitung von Priv.-Doz. Dr. Enno Klußmann angefertigt.

Dissertation eingereicht am: 27.03.2014

1. Gutachter: PD Dr. Enno Klußmann
2. Gutachter: Prof. Dr. Christian Freund

Disputation am: 17.07.2014

SELBSTÄNDIGKEITSERKLÄRUNG

Hiermit erkläre ich, dass ich die vorliegende Arbeit selbständig und nur unter Verwendung der angegebenen Literatur und Hilfsmittel angefertigt habe. Des Weiteren versichere ich, dass die vorliegende Arbeit nie Gegenstand eines früheren Promotionsverfahrens war. Die dem Verfahren zugrunde liegende Promotionsordnung ist mir bekannt.

Dörte Faust
Berlin, März 2014

TABLE OF CONTENTS

TABLE OF CONTENTS	5
ABBREVIATIONS	7
LIST OF FIGURES	9
LIST OF TABLES	10
1 INTRODUCTION	11
1.1 The nephron.....	11
1.2 Vasopressin-mediated antidiuresis.....	12
1.3 The water channel aquaporin-2.....	13
1.3.1 Exocytosis-like AQP2 trafficking.....	16
1.3.2 Endocytosis of AQP2 bearing vesicles.....	18
1.3.3 Regulators of AQP2 trafficking	19
1.3.3.1 Bradykinin.....	19
1.3.3.2 Calcium	19
1.3.3.3 Dopamine	20
1.3.3.4 Nitric oxide.....	21
1.3.3.5 Prostaglandin E ₂	21
1.3.3.6 Purines	22
1.3.4 Proteins controlling AQP2	22
1.3.5 AQP2 pathology.....	25
1.3.5.1 Diabetes insipidus.....	25
1.3.5.2 Extracellular fluid volume expansion	26
1.4 Aim of the thesis	27
2 MATERIALS AND METHODS	28
2.1 Materials	28
2.1.1 Equipment and software	28
2.1.2 Antibodies.....	29
2.1.3 Mouse siGENOME siRNA library-SMART pool	29
2.1.3.1 Plate layout.....	29
2.1.4 Oligonucleotides	30
2.1.4.1 DNA oligonucleotides.....	30
2.1.4.2 siRNAs	31
2.1.5 Chemicals and buffers	31
2.1.6 Eukaryotic cells.....	32
2.2 Methods	33
2.2.1 Isolation and purification of DNA	33
2.2.1.1 Isolation of genomic DNA from cell lines	33
2.2.1.2 Purification of DNA fragments from agarose gels.....	33
2.2.2 Analysis and modification of DNA	33
2.2.2.1 Polymerase chain reaction.....	33
2.2.2.2 Agarose gel electrophoresis for separation of DNA fragments	34
2.2.2.3 DNA sequencing.....	34
2.2.3 Biochemical methods.....	35
2.2.3.1 Cell lysis	35
2.2.3.2 Bradford assay	35
2.2.3.3 Western Blotting	35
2.2.4 Mammalian cell culture	36

2.2.4.1 Culturing of rat primary inner medullary collecting duct (IMCD) cells	36
2.2.4.2 Culturing of mammalian cells	36
2.2.4.3 Cell counting	36
2.2.4.4 Freezing and thawing of mammalian cell lines	36
2.2.4.5 Reverse siRNA transfection of MCD4 cells	37
2.2.4.6 Determination of cell viability via alamarBlue®	37
2.2.5 Immunofluorescence microscopy	38
2.2.5.1 Immunofluorescent detection of proteins	38
2.2.5.2 Microscope settings	39
2.2.5.2.1 Arrayscan VTI HCS Reader	39
2.2.5.2.2 LSM 780	39
2.2.6 CellProfiler	39
2.2.7 Statistics	43
3 RESULTS	44
3.1 MCD4 cells are appropriate for the analysis of the AQP2 redistribution	44
3.2 Experimental design	46
3.3 Mouse Protein Kinases siRNA sublibrary	47
3.4 Reverse siRNA transfection of MCD4 cells	47
3.5 Automated immunofluorescence microscopy	50
3.6 Image analysis using CellProfiler	53
3.7 Data analysis using KNIME	56
3.7.1 Transfection efficiency	56
3.7.2 siRNA affects cell viability	58
3.7.3 Multilayer perceptron	59
3.7.4 Z-score based analysis	62
3.7.5 Hits	63
3.8 Hit validation	67
4 DISCUSSION	74
4.1 Strengths and limitations of siRNA screenings	74
4.2 Specificity of siRNAs of the Mouse Protein Kinases sublibrary	76
4.3 Characterisation of MCD4 cells	77
4.4 Transfection efficiency	79
4.5 High content image analysis	79
4.6 Profiling the translocation of AQP2 using MLP machine learning	81
4.7 Z-score-based analysis of AQP2 redistribution	82
4.8 Hit validation	83
4.8.1 CDK18	85
4.8.2 PKIA	86
4.8.3 Proteins involved in AQP2 control	87
5 PERSPECTIVE	88
6 SUMMARY	90
7 ZUSAMMENFASSUNG	91
8 BIBLIOGRAPHY	92
9 PUBLICATIONS	106
10 SUPPLEMENTARY DATA	107
10.1 Supplementary figures	107
10.2 Supplementary tables	117

ABBREVIATIONS

Amino acids are abbreviated in one-letter-code.

aa	amino acid
AC	adenylate cyclase
<i>A. dest.</i>	aqua destillata
ADH	antidiuretic hormone
AKAP	A-kinase anchoring protein
AMP	adenosine-5'-monophosphate
AngII	angiotensin II
ATP	adenosine-5'-triphosphate
AQP	aquaporin
<i>AQP2</i>	aquaporin-2, human gene
AQP2	aquaporin-2, protein
AVP	arginine-vasopressin
BSA	bovine serum albumin
bp	base pair(s)
CD	collecting duct
CDI	central diabetes insipidus
CaM	calmodulin
cAMP	cyclic adenosine-3',5'-monophosphate
cDNA	complementary deoxyribonucleic acid
<i>Cdk18</i>	cyclin-dependent kinase 18, mouse gene
CDK18	cyclin-dependent kinase 18, protein
cGMP	cyclic guanosine-3',5'-monophosphate
CHF	congestive heart failure
CSNK	casein kinase
DAPI	4', 6'-diamidine-2-phenylindole
DCT	distal convoluted tubule
DI	diabetes insipidus
DMEM	Dulbecco's modified eagle medium
DMSO	dimethyl sulphoxide
DNA	deoxyribonucleic acid
dNTP	deoxyribonucleotide triphosphate
DTT	dithiothreitol
EDTA	ethylenediaminetetraacetic acid
<i>EGTA</i>	<i>ethylene glycol tetraacetic acid</i>
ENaC	epithelial sodium channel
Epac	exchange protein activated by cAMP
ER	endoplasmatic reticulum
ERK	extracellular signal-related kinase
EtOH	ethanol
FCS	fetal calve serum
FMP	Leibniz-Institut für Molekulare Pharmakologie
FSK	forskolin
forw	forward (primer)
<i>Gapdh</i>	glyceraldehyde-3-phosphate dehydrogenase, mouse gene
GAPDH	glyceraldehyde-3-phosphate dehydrogenase, mouse protein
GEF	guanine nucleotide exchange factor
GFP	green fluorescent protein
G protein	GTP-binding protein
GPCR	G protein-coupled receptor
GSK3B	glycogen synthase kinase 3 beta
GTP	guanosine-5'-triphosphate
H27	rabbit-derived anti-AQP2 antibody
H27-Cy3	rabbit-derived anti-AQP2 antibody plus Cy3-conjugated secondary antibody
HRP	horseradish peroxidase
IC	intercalated cell(s)

IgG	immunoglobulin G
IMCD	inner medullary collecting duct
JNK	c-Jun N-terminal kinase
l	litre
KNIME	Konstanz Information Miner
LSM	laser scanning microscope
mA	milliampere
MAL	lymphocyte-associated protein
MAPK	mitogen-activated protein kinase
MCD4	mouse collecting duct
MDC	Max Delbrück Center for Molecular Medicine
min	minute(s)
MLCK	myosin light chain kinase
MLP	multilayer perceptron
MVB	multi vesicular bodies
NDI	nephrogenic diabetes insipidus
NO	nitric oxide
NT#2	non-targeting siRNA
PAGE	polyacrylamide gel electrophoresis
PBS	phosphate buffered saline
PCR	polymerase chain reaction
PFA	paraformaldehyde
PGE ₂	prostaglandin E ₂
PI3K	phosphoinositide-3-kinase
PKA	protein kinase A
PKB	protein kinase B
PKC	protein kinase C
PKG	protein kinase G
<i>Pkia</i>	protein kinase a inhibitor alpha, mouse gene
PKIA	protein kinase a inhibitor alpha, protein
PLC	phospholipase C
PMSF	phenylmethylsulphonyl fluoride
PP1	protein phosphatase 1
PP2A	protein phosphatase 2A
pS256	AQP2, phosphorylated at serine 256
pS261	AQP2, phosphorylated at serine 261
pS264	AQP2, phosphorylated at serine 264
pS269	AQP2, phosphorylated at serine 269
PVDF	polyvinylidene fluoride
rev	reverse (primer)
RhoA	Ras homolog family member A
RNA	ribonucleic acid
RNAi	RNA interference
rpm	revolutions per minute
SDS	sodium dodecylsulfate
SEM	standard error of mean
shRNA	short hairpin RNA
SIADH	syndrome of inappropriate antidiuretic hormone secretion
siRNA	short interfering RNA
SLB	standard lysis buffer
SNARE	soluble N-ethylmaleimide-sensitive-factor-attachment receptor
TAE	Tris/acetate/EDTA buffer
TBS	Tris buffered saline
TBS-T	TBS with Tween 20
TOX	toxic siRNA
Tris	Tris(hydroxymethyl)-aminomethane
ut	unstimulated
UTR	untranslated region
V	Volt
V2R	vasopressin receptor type 2

LIST OF FIGURES

Fig. 1. The nephron.....	11
Fig. 2. AQP2 structure.....	14
Fig. 3. AQP2 redistribution in renal principal cells.....	16
Fig. 4. Assay plate layout.....	30
Fig. 5. Images field per well.....	39
Fig. 6. Summary of CellProfiler pipeline.....	42
Fig. 7. AQP2 protein expression in mammalian kidney cells.....	44
Fig. 8. The microscopic detection of the AQP2 translocation in MCD4 and primary IMCD cells.....	45
Fig. 9. The expression of human AQP2 but not V2R in MCD4 cells.....	46
Fig. 10. The experimental design.....	46
Fig. 11. Seeding of 400 cells per well of a microtiter plate results in optimal density for microscopic analysis.....	47
Fig. 12. Effect of Lipofectamine® 2000 transfection reagent on MCD4 cells.....	48
Fig. 13. Viability of MCD4 cells upon TOX-transfection.....	49
Fig. 14. siRNA transfection reduces target gene expression.....	49
Fig. 15. Fluorescent staining of nuclei, AQP2 and F-actin of MCD4 cells.....	50
Fig. 16. Immunofluorescent staining of AQP2 in MCD4 cells using H27 and different secondary antibodies.....	51
Fig. 17. Intensity of AQP2 signals within defined plasma membrane regions.....	53
Fig. 18. CellProfiler pipeline modules in detail.....	54
Fig. 19. Summary of CellProfiler pipeline modules.....	55
Fig. 20. Excluded images.....	56
Fig. 21. MCD4 cells were efficiently transfected with siRNAs of the Mouse Protein Kinases sublibrary.....	57
Fig. 22. Differently sized expansions of nucleus outlines.....	59
Fig. 23. The distribution of AQP2 speckles per cell.....	60
Fig. 24. Cellular phenotypes were classified using a multilayer perceptron (MLP).....	61
Fig. 25. Hit maps of four different microtiter plates.....	64
Fig. 26. AQP2 translocation is impaired upon silencing of hits.....	65
Fig. 27. Efficiency of CDK18 and PKIA down regulation.....	67
Fig. 28. The detection of PKIA by Western Blotting.....	68
Fig. 29. FSK-induced AQP2 translocation in MCD4 cells is impaired after transfection with <i>Pkia</i> and <i>Cdk18</i> pooled but not single siRNAs.....	69
Fig. 30. The down regulation of AQP2 was accompanied by reduced <i>Cdk18</i> and <i>Pkia</i> gene expression.....	70
Fig. 31. The down regulation of PKIA did not affect AQP2 protein abundance.....	71
Fig. 32. CDK18 down regulation affects AQP2 protein abundance and its phosphorylation at S261.....	73
Fig. 33. Diverse phenotypes of MCD4 cells.....	78
Fig. 34. Differently sized perinuclear regions.....	80
Fig. S 1. Mouse and rat V2R share 98 % amino acid sequence identity.....	107
Fig. S 2. Protocol for automated siRNA transfer using TECAN Freedom EVO.....	108
Fig. S 3. Protocol for automated transfer of Lipofectamine® 2000 using TECAN Freedom EVO.....	109
Fig. S 4. High quality imaging of MCD4 cells in microtiter plates.....	110
Fig. S 5. Mouse-derived α -rabbit Cy3-conjugated secondary antibody showed weak background staining on MCD4 cells.....	110
Fig. S 6. Down regulation of indicated genes impaired the AQP2 translocation to the plasma membrane in MCD4 cells.....	111
Fig. S 7. Down regulation of proteins or protein subunits that are involved in AQP2 control did not impair the AQP2 translocation to the plasma membrane.....	112
Fig. S 8. The predicted phosphorylation sites of mouse CDK18.....	115
Fig. S 9. Human and mouse CDK18 share 91 % amino acid identity.....	116

LIST OF TABLES

Tab. 1. Mammalian aquaporins.	15
Tab. 2. Proteins controlling the AQP2 expression and/or localisation.	23
Tab. 3. Equipment and disposal.	28
Tab. 4. Software.	28
Tab. 5. Antibodies used for Western Blotting and immunofluorescence microscopy.	29
Tab. 6. Sublibraries of the Mouse siGENOME siRNA Library.	29
Tab. 7. DNA oligonucleotides used for PCR or sequencing.	30
Tab. 8. siRNAs for control and validation experiments.	31
Tab. 9. Buffers and solutions.	31
Tab. 10. Chemicals and fluorescent dyes.	32
Tab. 11. Eukaryotic cell lines and primary cells.	32
Tab. 12. Composition of PCR reaction.	34
Tab. 13. PCR protocol.	34
Tab. 14. MCD4 cell viability is decreased upon the down regulation of the listed genes.	58
Tab. 15. Optimal parameters for AQP2 speckles identification.	60
Tab. 16. Results of MLP classification.	62
Tab. 17. Z' factors.	63
Tab. 18. Hit list.	64
Tab. 19. Interaction partners of human CDK18.	86
Tab. S 1. MCD4 cell viability upon the down regulation of listed genes.	117
Tab. S 2. Different mRNA regions are targeted by pooled and single siRNAs.	131
Tab. S 3. Settings of prime program <i>PRIME_200</i> of BioTek ELx405 Select CW Microtiter plate Washer.	131
Tab. S 4. Settings of aspiration program <i>GREINER 10</i> of BioTek ELx405 Select CW Microtiter plate Washer.	131
Tab. S 5. Settings of washing program <i>GREINER</i> of BioTek ELx405 Select CW Microtiter plate Washer.	132
Tab. S 6. MCD4 cell viability upon the siRNA-mediated down regulation of proteins that are involved in the AQP2 control.	132
Tab. S 7. siRNA molecules that are not complementary to target mRNA.	133
Tab. S 8. Sequences of siRNAs directed against 13 hits.	135

1 INTRODUCTION

The kidney regulates various vital processes. It participates in the regulation of blood pH and blood pressure by controlling acid-base balance and salt- and water homeostasis. It filters the blood, thereby reabsorbing solutes and excreting toxic substances into the urine. The functional unit of the kidney is the nephron.

1.1 The nephron

The kidney contains approximately one million nephrons. They filter the entire blood several times a day, leading to the production of 180 l pre-urine, which is mainly composed of water. Of this, less than 1 % is excreted as final urine. Upon initial filtration of the blood through the glomerulus into the surrounding Bowman's capsule, the resulting filtrate passes a tubular system, starting with the proximal tubule and the descending limb of Henle (Fig. 1). In these segments 90 % of the total water retention occurs¹, which is mediated by the water channel aquaporin-1 (AQP1). In contrast, the ascending limb of Henle and the distal convoluted tubule (DCT) are water impermeable. Here, sodium and chloride are reabsorbed to maintain the osmotic gradient, being the driving force for water. Water permeability of the last part of

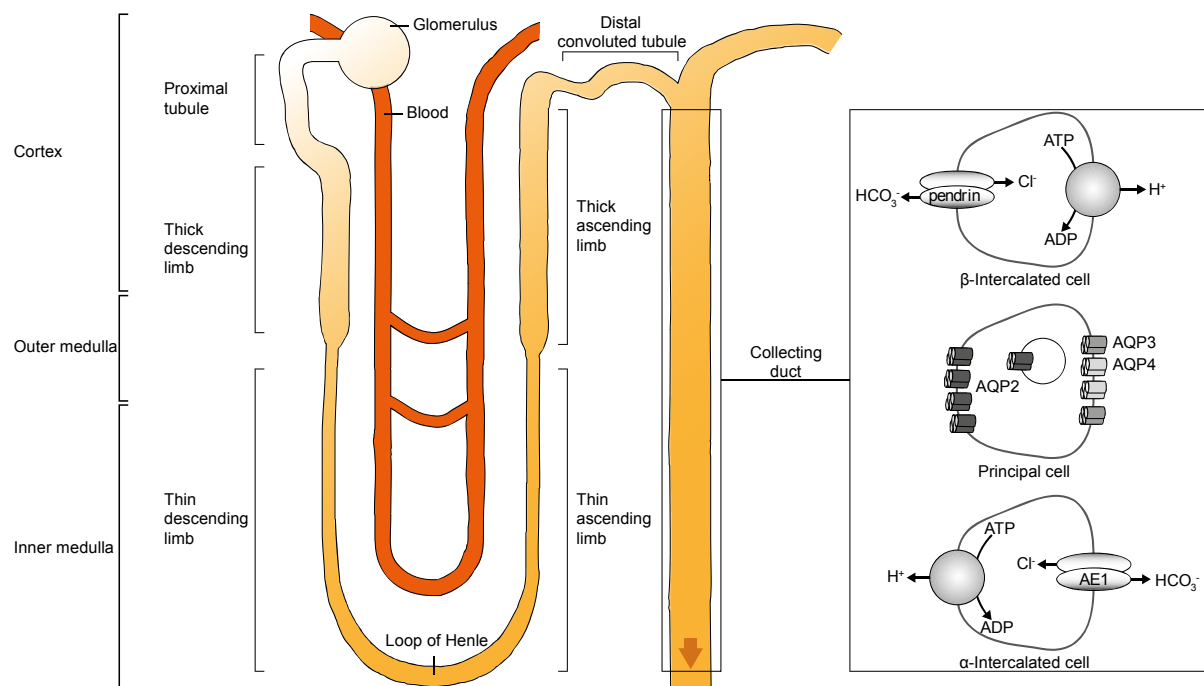


Fig. 1. The nephron. Blood is filtered in the glomerulus and the remaining filtrate is concentrated along the tubular system to generate final urine. In the cortical collecting duct epithelium β -intercalated cells (IC) secrete bicarbonate into the urine *via* pendrin-mediated chloride exchange. ATP-dependently protons are pumped into the interstitium, thereby lowering its pH. *Vice versa*, inner medullary α -IC acidify the urine and lead to increased interstitial pH by the secretion of bicarbonate along the anion exchanger 1 (AE1). In renal principal cells the water channels aquaporin-2, -3 and -4 (AQP2, AQP3, AQP4) are expressed, enabling these cells to reabsorb water. (Adapted from King *et al.*²).

the nephron, the collecting duct (CD), is controlled hormonally and accounts for the remaining 10 % of total water retention, which is 10-20 litres a day³. Here, the final urine is generated before it is collected in the bladder.

The CD epithelium comprises two cell types (Fig. 1), intercalated cells (IC) and principal cells. The former are further classified into cortical β -IC and medullary α -IC. By secreting or retaining protons and bicarbonate, respectively, ICs adjust the acid-base-homeostasis. In principal cells, the water channels aquaporin-2, -3 and 4 (AQP2, AQP3 and AQP4) are expressed, facilitating the reabsorption of water from the primary urine.

The major regulation of sodium and water reabsorption occurs through the renin-angiotensin-aldosterone-system (RAAS). RAAS increases blood pressure by inducing vasoconstriction and renal sodium and water retention⁴. If arterial blood pressure decreases or distal sodium concentration drops, renin is synthesised in the juxtaglomerular apparatus, a specialised region of DCT, located in close proximity to the afferent arteriole. Renin converts angiotensinogen into angiotensin I, which subsequently is cleaved to the biologically active angiotensin II (AngII) by angiotensin converting enzyme (ACE). AngII stimulates aldosterone secretion from the adrenal gland⁵. Both, AngII and aldosterone stimulate the activity of the epithelial sodium channel (ENaC) located in the CD, which in turn leads to increased water reabsorption^{6,7}. Maximal urinary concentration is achieved by synergistic action of AngII, aldosterone and arginine-vasopressin⁸ (AVP; antidiuretic hormone, ADH).

1.2 Vasopressin-mediated antidiuresis

The nona-peptide AVP is produced in the hypothalamus and reaches the pituitary glands *via* axonal transport. From there it is secreted into the blood. This is initiated if endothelial baroreceptors sense a decrease in blood plasma volume (hypovolemia) or hypothalamic osmoreceptors detect increased blood electrolyte concentration (hypernatremia)⁹.

AVP signals *via* two G protein-coupled receptors (GPCR), the vasopressin receptor type 1 (V1R) and 2 (V2R), the former comprises two subclasses V1AR and V1BR (V3R). Both subtypes of V1R are mainly located in the brain, liver and peripheral vasculature. However, Nonoguchi and co-workers described V1AR expression also in intercalated cells of the collecting duct^{10,11}. In contrast, V2R is expressed in the ear¹² and is highly abundant in kidney CD and thick ascending limb¹³. All vasopressin receptors consist of seven membrane-spanning domains, an extracellular N- and an intracellular C-terminus. Coupled to the stimulatory G protein $G\alpha_s$, their stimulation leads to the activation of adenylate cyclase (AC) and an increase in the cytosolic concentration of the second messenger cyclic adenosine-3',5'-monophosphate (cAMP)¹⁴.

AVP controls several cellular processes. It promotes NaCl reabsorption by activating Na⁺-K⁺-Cl⁻-cotransporter (NKCC) in the thick ascending limb of Henle¹⁵. Thereby, renal sodium excretion is decreased and the medullary osmotic gradient increased¹⁶. Retained K⁺-ions are secreted *via* the simultaneously activated renal outer medullary potassium channel (ROMK). In addition, AVP facilitates medullary urea and Na⁺-reabsorption by increasing the cell surface expression of urea transporter 1 (UT1)¹⁷ and ENaC¹⁵. AVP enhances AQP2 total protein abundance^{18,19} by stimulating its transcription²⁰ and translation²¹ and preventing its degradation^{22,23}. Upon AVP stimulation, AQP2 inserts into the apical plasma membrane^{18,24} facing the urinary volume, thus facilitating water reabsorption. Further, AVP elevates the intracellular Ca²⁺ concentration²⁵, which was suggested to be involved in water retention (1.3.3.2). Overall, AVP exerts an antidiuretic effect by simultaneously increasing the osmotic gradient and enhancing the plasma membrane water permeability. Beside its role in maintaining water homeostasis, AVP was supposed to exert an anti apoptotic effect, to promote Wnt signalling and to influence several mitogen-activated protein (MAP) kinases^{23,26}.

1.3 The water channel aquaporin-2

Water channels were discovered by Peter Agre²⁷, who was honoured with the Nobel Prize in 2003. They are integral membrane proteins and facilitate the transport of water. All aquaporins assemble to homotetramers with each monomer providing an independent water pore, which is formed by two membrane-embedded NPA-motifs (asparagine-proline-alanine)²⁸. Of 13 known mammalian aquaporins (0-12, Tab. 1), nine are expressed in the kidney, namely AQP1-8 and 11 (Tab. 1). They are arranged in three groups²⁹: class I comprises the water selective classical aquaporins (AQP0, 1, 2, 4, 5, 6 and 8); class II aquaglycero-proteins are permeable for water and small neutral solutes like urea and glycerol (AQP3, 7, 9 and 10)³⁰; AQP11 and AQP12 belong to class III and are so called supraaquaporins, which have a deviated NPA-motif in common. The alanine in their first NPA motif is replaced by cysteine (C) and threonine (W), resulting in NPC and NPW, respectively³¹. With the exception of AQP8, class I, class II and class III aquaporins are encoded by four, six or three exons (Tab. 1).

AQP1 is highly abundant in the proximal tubule and the descending limb of Henle^{32,33}, whereas AQP2, 3 and 4 are expressed in CD principal cells³⁴⁻³⁹ (Fig. 1, Tab. 1). AQP5 and AQP6 were detected in β- and α-IC, respectively^{40,41} and AQP7, 8 and 11 are expressed in the proximal tubule⁴²⁻⁴⁵. AQP2 was discovered in 1993⁴⁶ and is the most intensively studied water channel today. Its relevance becomes apparent when considering that mice globally lacking AQP2, fail to thrive and die shortly after birth⁴⁷. The protein sequence is highly conserved among species (Fig. 2) and includes residues for post-translational

phosphorylation (serines 256, 261, 264 269)⁴⁸ and ubiquitination (lysine 270)²², determining AQP2s localisation and stability, as well as for glycosylation (asparagine 123)^{49,50}, whose role is poorly understood⁵¹. Upon folding and homotetramerisation in the endoplasmatic reticulum (ER), high mannose glycans are attached and AQP2 is forwarded to the GOLGI⁵⁰, where the sugars of one or two molecules of the AQP2 homotetramer are further processed to form complex N-glycosylation⁵². Since glycosylation is species-specific⁵³, results obtained in different cell lines and animal models are hardly comparable. However, the water conductivity of AQP2 seems not to be affected by glycosylation⁵⁴.

The membrane abundance of AQP2 is determined by the equilibrium of its exocytosis-like insertion into the plasma membrane and its endocytic retrieval. AQP2 underlies constitutive recycling, depending on the crosstalk of AQP2 phosphorylation and ubiquitination. Enhanced cell surface expression results from increased trafficking or decreased internalisation^{55,56}.

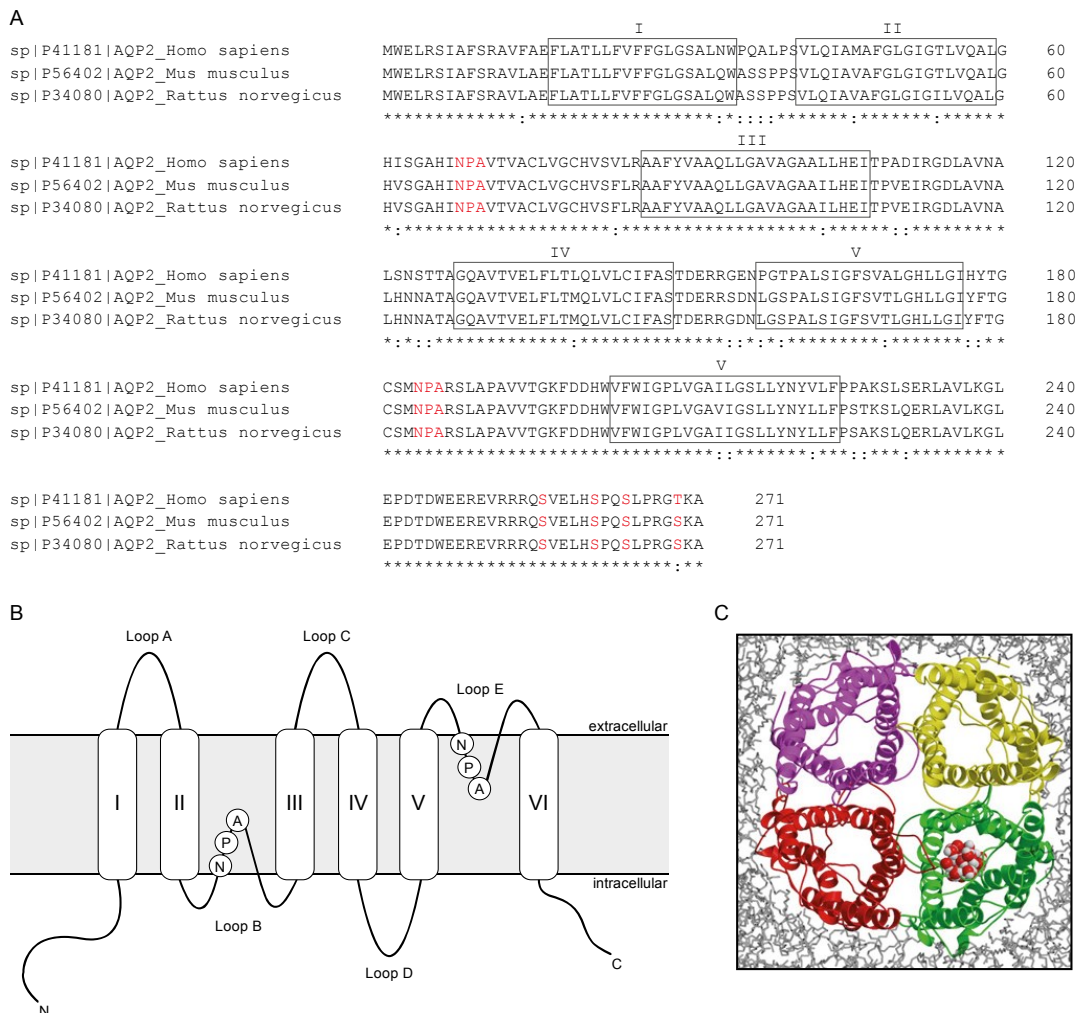


Fig. 2. AQP2 structure. **A.** The AQP2 amino acid sequence is highly conserved among species. Six membrane domains (I-VI), conserved NPA-motif and serines 256, 261, 264 and 269 are highlighted. Within the 271 amino acids, matches and mismatches between the three sequences are marked with a star and colon below, respectively. **B.** The transmembrane domains of AQP2 (I-VI) form three extracellular (A, C and E) and two cytosolic loops (B and D). The conserved NPA motif, which forms the water pore, is embedded in the membrane (adapted from Kruse *et al.* 2006⁵⁷). **C.** Crystal structure of the AQP2 homotetramer according to Ikeguchi 2009⁵⁸. A water molecule passes the green monomer.

Tab. 1. Mammalian aquaporins.

Name	Class	Exons	Synonyms	Kidney segment	Extrarenal localisation	Subcellular distribution	Function	KO mice show	Reference
AQP0	I	4	Lens fibre major intrinsic protein, MIP26	-	Eye	Apical and basolateral PM	Regulation of lens osmolality, cell adhesion	Cataracts	59-65
AQP1	I	4	AQP-CHIP, CHIP28	PT, DL	Brain, erythrocytes, eye, heart, lung, pancreas, skeletal muscle, vagina	Apical and basolateral PM	Constitutive water reabsorption from pre-urine, tubular cell migration, angiogenesis	Impaired pain sensation, polyuria	66-75
AQP2	I	4	AQP-CD, WCH-CD	CD-PC	Ear, epididymis, vagina	Intracellular vesicles, apical and basolateral PM	AVP-stimulated water reabsorption from urine	Fail to thrive, polyuria	46,47,74-78
AQP3	II	6	GLIP	CD-PC	Erythrocytes, eye, colon, conjunctiva, lung, skin, vagina	Basolateral PM	Water exit of kidney CD-PC, regulation of epidermal glycerol content	Impaired wound healing, reduced skin hydration, urinary concentration defects	35,74,79-85
AQP4	I	4	MIWC, WCH4	CD-PC	Brain, eye, lung, muscle, retinal glia, skin, stomach	Basolateral PM	Water exit of kidney CD-PC, regulation of water flow in central nervous system	Impaired vision, hearing, olfaction; urinary concentration defects	34,86-93
AQP5	I	4	-	CNT, CD-βIC	Ear, eye, lung, salivary glands, placenta, pancreas, vagina	Apical PM	Generation of saliva, tears and pulmonary secretion, unknown renal function	Impaired salivary and sweat secretion, decreased osmotic water permeability across alveolar epithelium	41,74,81,94-103
AQP6	I	4	AQP2L, HKID, KID	CNT, CD-αIC	Brain, vagina	Intracellular vesicles	Urinary acid secretion, nitrate and chloride transport	-	40,74,104-109
AQP7	II	6	AQPap	PT	Adipose tissue, brain, heart, intestine, skeletal muscle, testis	Apical PM	Glycerol metabolism, arsenite uptake	Glyceroluria, obesity, smaller islet cells	42,43,110-117
AQP8	I	6	-	PT	Brain, pancreas, placenta, salivary glands, sperm, testis	Intracellular vesicles, PM	Urea, ammonia and ROS transport	Mild hypertriglyceridemia	44,118-123
AQP9	II	6	SSC1	-	Brain, epididymis, leukocytes, liver, skeletal muscle, spleen, testis	Apical PM	Arsenite uptake, glycerol transport, cell motility	-	75,112,122,124-130
AQP10	II	6	Small intestine aquaporin	-	Adipose tissue, intestine	Apical PM	Glycerol transport	-	117,131-135
AQP11	III	3	AQPX1	PT	Brain, intestine, liver, testis, thymus	ER	ER homeostasis, spermiogenesis, salivary gland development	Polycystic kidney disease	31,45,136-141
AQP12	III	3	AQPX2	-	Pancreas	ER	Suggested to be involved in digestion	Mild impairment of pancreatic secretion	31,136,142,143

AQPap, AQP adipose; AQP2L, AQP2 like; CD-αIC, collecting duct α-intercalated cells; CD-βIC, collecting duct β-intercalated cells; CD-PC, collecting duct principal cells; Class I, classical aquaporins; Class II, aquaglyceroporins; Class III, superaquaporins, unorthodox AQPs, subcellular AQPs; CNT, connecting tubule; DL, descending limb of Henle; ER, endoplasmic reticulum; GLIP, glucagon-like insulinotropic peptide; HKID, original name of the clone¹⁰⁴; KO, knock out; MIP, major intrinsic protein; MIWC, mercurial-insensitive water channel; PM, plasma membrane; PT, proximal tubule; SSC1, small solute channel 1; WCH4, water channel 4.

1.3.1 Exocytosis-like AQP2 trafficking

The CD epithelium becomes water permeable upon the insertion of AQP2 into the apical plasma membrane^{144,145}. AVP binds to the V2R located in the basolateral plasma membrane of renal principal cells (Fig. 3). Thereupon, the stimulatory G protein $G\alpha_s$ activates adenylyl cyclase (AC), probably AC3^{146,147} and AC6¹⁴⁷⁻¹⁴⁹, converting ATP into the second messenger cAMP. Cyclic AMP binds to the regulatory subunits of protein kinase A (PKA), leading to a release of its two catalytically active subunits. A subpool of PKA is tethered to perinuclear

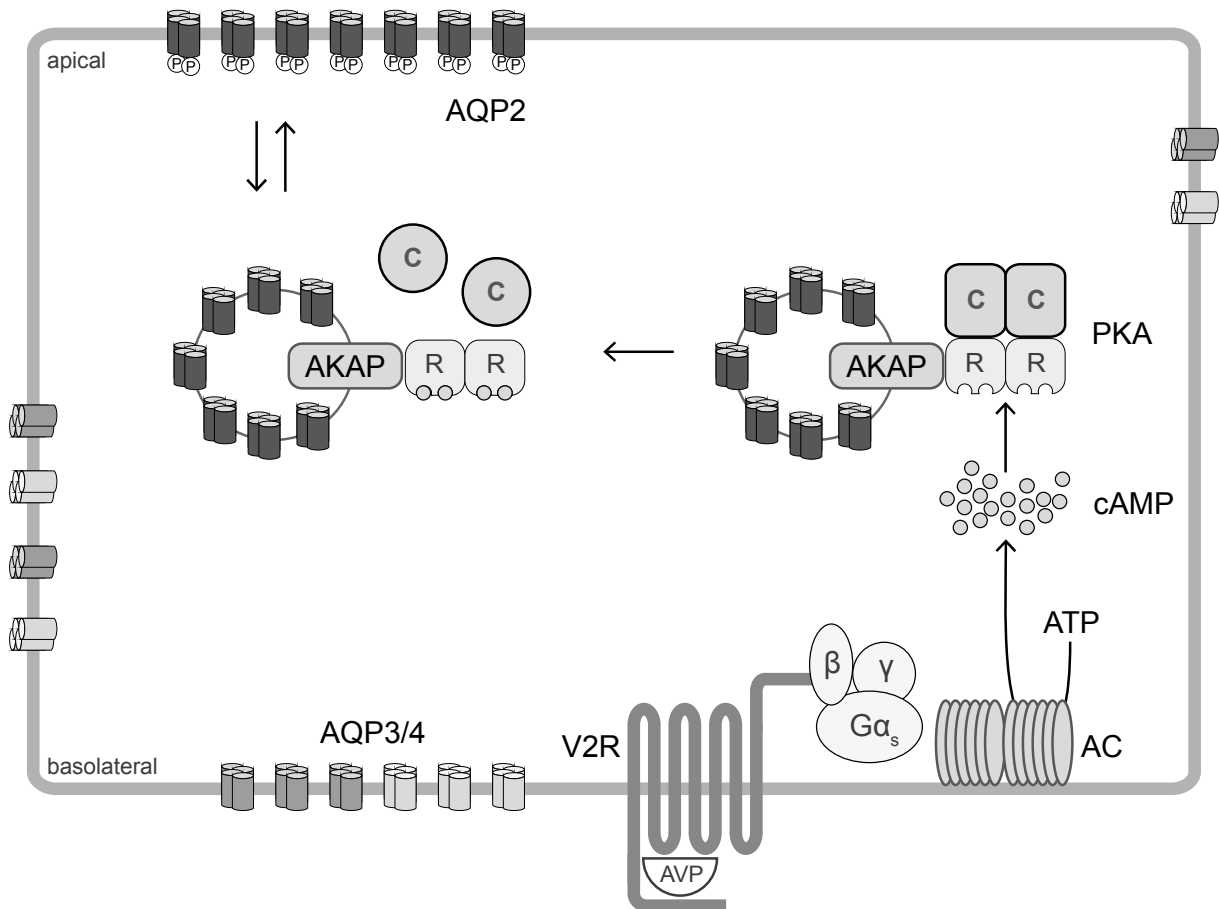


Fig. 3. AQP2 redistribution in renal principal cells. AQP2 translocates to the apical plasma membrane upon increase of intracellular cAMP levels. After binding of AVP to the V2R, the stimulatory G protein $G\alpha_s$ activates the AC, leading to an increase in cytosolic cAMP. cAMP binds to the regulatory subunit of PKA, which is tethered to AQP2-bearing vesicles by an AKAP. Subsequently the catalytic subunits of PKA are released, which phosphorylate AQP2 at serine 256 and thereby trigger its insertion predominantly into the apical plasma membrane. Following an osmotic gradient water enters the cell and exits *via* AQP3 and AQP4. AC, adenylyl cyclase; AKAP, A-kinase-anchoring-protein; AQP2/3/4, aquaporin-2/3/4; AVP, arginine-vasopressin; C, catalytic subunit of PKA, PKA, protein kinase A, R, regulatory subunit of PKA, V2R, vasopressin receptor type 2; P, Pi.

AQP2-bearing vesicles by A-kinase anchoring proteins (AKAPs)¹⁵⁰⁻¹⁵², which compartmentalise the players of PKA-signalling cascades to subcellular sites^{153,154}. Facilitated by their close proximity to each other, PKA phosphorylates serine 256 (S256) in the intracellular C-terminus of AQP2^{155,156}. If at least three of four AQP2 monomers per homotetramer are phosphorylated, it redistributes to the apical plasma membrane¹⁵⁷. In addition to S256, the phosphorylation of serines 264 and 269 (S264 and S269) by yet

unknown kinases increases in response to AVP¹⁵⁸⁻¹⁶⁰. Whereas AQP2 phosphorylated at S264 (pS264) is localised in the plasma membrane and endocytotic retrieval compartments¹⁵⁸, AQP2 phosphorylated at S269 (pS269) was detected only in the apical plasma membrane¹⁶⁰, probably preventing AQP2 internalisation^{159,160}. pS264 and pS269 do not affect AQP2 activity, as mutations, mimicking constant de-phosphorylation by serine-to-alanine exchange at 264 and 269 (S264A, S269A) showed the same conductivity¹⁶¹. The phosphorylation of both S264 and S269 was suggested to require prior phosphorylation of S256^{159,161}. However, we recently detected pS269 independently of pS256¹⁶². Upon the direct stimulation of AC by forskolin (FSK) and simultaneous treatment with selective blocker of vacuolar H⁺-ATPase 4AD (4-acteyldiphyllin), the phosphorylation of S256 but not of S269 was reduced. In contrast to the phosphorylation of S256, S264 and S269, the phosphorylation of serine 261 (S261) is diminished upon AVP challenge^{23,163,164}.

After PKA phosphorylation, AQP2 dissociates from G-actin and assembles with tropomyosin 5b (TM5b), which induces a destabilisation of the F-actin network¹⁶⁵. In parallel PKA phosphorylates and thus inhibits the Ras homolog family member A (RhoA)¹⁶⁶, leading to reduced binding of RhoA to RhoA kinase¹⁶⁷. Consequently, the F-actin cytoskeleton depolymerises promoting AQP2s translocation to the plasma membrane^{168,169}.

The membrane insertion of AQP2 is achieved by the interaction of vesicular N-ethylmaleimide-sensitive fusion factor¹⁷⁰ and its soluble N-ethylmaleimide attachment protein target receptors (SNARE). Vesicle-associated membrane protein 2 and/or 3 (VAMP2, VAMP3) interact/s specifically with apical syntaxins (Stx) and synaptosome associated proteins (SNAPs) to form the SNARE complex that mediates the fusion of vesicle and plasma membrane¹⁷¹. This formation is inhibited by Munc18b¹⁷², which is a functional partner of syntaxin 3 (Stx3)¹⁷³.

The cell surface location of AQP2 is maintained by its interaction with myelin- and lymphocyte-associated protein (MAL), which is abundantly expressed in the apical plasma membrane of epithelial CD cells¹⁷⁴. As reported by Kamsteeg *et al.*, MAL interacts with AQP2-S256D and increases its cell surface expression probably by preventing its dephosphorylation and subsequent internalisation¹⁷⁵.

The insertion of AQP2 into the apical plasma membrane facilitates water entry into the cell. Water exits the cells through AQP3 and AQP4, both located in the basolateral plasma membrane. Trafficking of AQP2 to the basolateral plasma membrane was also observed^{24,39,176} and might be involved in cell migration and tubulogenesis¹⁷⁷.

1.3.2 Endocytosis of AQP2 bearing vesicles

The internalisation of AQP2 occurs in a clathrin-mediated way¹⁷⁸; *via* direct interaction of AQP2 with the endocytotic machinery^{179,180}, clathrin-coated vesicles are formed¹⁷⁸ and AQP2 is internalised into early endosomes, which bud into multi vesicular bodies (MVB). MVB contain several luminal vesicles mediating lysosomal degradation^{181,182}. The formation of luminal vesicles is assisted by lysyl-interacting protein 5 (LIP5)¹⁸³⁻¹⁸⁵, which directly binds AQP2 and facilitates its degradation¹⁸⁶. Alternatively, the MVB outer membrane fuses with the apical plasma membrane and releases AQP2 exosomes into the lumen to be excreted with the urine^{187,188}.

Kamsteeg *et al.* reported that AQP2 endocytosis is increased upon short-chain ubiquitination at K270²². Three enzymes are necessary to covalently attach ubiquitin (Ub) to a target protein and elicit its subsequent degradation^{189,190}. After the activation and conjugation of Ub by enzymes E1 and E2, respectively, E3 ligase transfers Ub to the specific target protein. The E3 ligase involved in AQP2 endocytosis is presently not known. By mapping E3 genes expressed in the CD, Lee *et al.*¹⁹¹ suggested a possible involvement of three proteins in AQP2 ubiquitin ligation: RING-finger protein 40 (BRE1B), cullin-5 (CUL5, alternative name VACM1, vasopressin-activated calcium mobilizing)¹⁹² and neural precursor cell expressed, developmentally down regulated gene 4-like (NEDD4), whose nuclear expression increases upon AVP challenge, as recently reported by Schenk *et al.*¹⁹³. Besides, AQP2 can enter the Ras-related protein Rab11 (Rab11)-dependent recycling pathway upon deubiquitination¹⁹⁴⁻¹⁹⁶ or be targeted for proteasomal degradation upon polyubiquitination²³.

The internalisation of AQP2 is enhanced by the activation of protein kinase C (PKC)^{197,198}, which induces AQP2 short-chain ubiquitination and subsequent degradation²². Although several putative PKC phosphorylation sites were identified in AQP2, PKC probably does not phosphorylate it directly^{48,199}. The phosphorylation of S261, possibly by p38-mitogen-activated protein kinase (p38-MAPK)²³, follows AQP2 ubiquitination and endocytosis¹⁶⁴. pS256 and pS269 reduce internalisation^{159,160,200} by trapping AQP2 in “endocytosis-resistant” domains of the membrane during AVP stimulation²⁰¹. In line, phosphomimetic S256D and S269D have a significantly increased half-life, probably due to decreased internalisation and degradation²⁰². The interaction of endocytosis-mediators like dynamin and clathrin heavy chain²⁰² or the clathrin-decoating ATPase hsc70¹⁸⁰ with AQP2-pS256 or -pS269 was decreased compared to wildtype AQP2. As reported by several groups though, pS256 alone is not sufficient to tether AQP2 in the plasma membrane²⁰³ and AQP2 internalisation occurred independently of its prior dephosphorylation^{198,204}.

1.3.3 Regulators of AQP2 trafficking

Apart from AVP, other regulators control the AQP2 localisation.

1.3.3.1 Bradykinin

The peptide hormone bradykinin activates two $G_{\alpha_{q/11}}$ -coupled bradykinin receptors B1R and B2R²⁰⁵. While B1R is involved in tissue injury and inflammatory responses, B2R induces vasodilation leading to natriuresis and decreased blood pressure²⁰⁶. Upon B2R activation phospholipase C (PLC) is stimulated, which converts phosphatidylinositol 4,5-bisphosphate (PIP₂) into inositol 1,4,5-triphosphate (IP₃) and diacylglycerol²⁰⁷. IP₃ leads to the elevation of cytosolic Ca²⁺ concentration, which together with DAG activates PKC²⁰⁸. As described earlier (1.3.2), PKC is associated with increased AQP2 ubiquitination, known to precede internalisation^{22,198,209}. Additionally, bradykinin stimulates the production of prostaglandin E₂ (PGE₂) and nitric oxide (NO)^{210,211} and activates RhoA²¹². RhoA activates Rho kinases, which facilitate the peripheral polymerisation of actin fibres, hence blocking AQP2 membrane trafficking by a physical barrier^{168,169,213}. Accordingly, bradykinin counteracts AVP signalling by multiple actions.

1.3.3.2 Calcium

Cytosolic Ca²⁺-concentration rises upon extracellular entry or release from intracellular stores. In the apical plasma membrane of inner medullary collecting duct cells (IMCD), the Calcium-sensing receptor (CaR) responds to luminal Ca²⁺ and transduces signals *via* G_{α_q} , G_{α_i} or $G_{\alpha_{12/13}}$ ²⁰⁵. Downstream of G_{α_q} receptors, transient receptor potential (TRP) cation channels are activated through which Ca²⁺ enters²¹⁴. Besides, Ca²⁺ is transported along voltage-gated ion channels²⁰⁵ or is released from intracellular stores by ryanodine receptors (RyR), probably RyR-1 in IMCD²¹⁵.

The activation of the luminal CaR by extracellular Ca²⁺ reduces the expression and membrane targeting of AQP2²¹⁶⁻²¹⁸. Procino *et al.* observed that CaR-signalling decreases the FSK-stimulated rise in cAMP, activates PKC and down-regulates RhoA, explaining the inhibitory effect of Ca²⁺ on the AVP-induced redistribution of AQP2^{219,220}. According to Bustamante *et al.* AVP- but not FSK-triggered AQP2 transcription was reduced upon Ca²⁺ challenge, indicating an uncoupling of V2R and AC, which leads to decreased PKA activity²¹⁸. As water reabsorption increases the luminal Ca²⁺ concentration, the diuretic effect elicited by extracellular Ca²⁺ is protecting against urinary calcium oversaturation, which might result in intratubular precipitation and stone formation^{221,222}.

Cytosolic Ca²⁺ is bound by the calcium-modulated protein Calmodulin (CaM)¹⁴, which in turn triggers three downstream signalling cascades that are relevant for AQP2. First, CaM

activates the myosin light chain kinase (MLCK), which phosphorylates the myosin regulatory light chain (MLC) and thereby facilitates AVP-triggered routing of AQP2-bearing vesicles to the plasma membrane by regulating the actin filament organisation^{223,224}. Second, CaM activates the serine-threonine phosphatase calcineurin, which enhances AQP2 transcription²²⁵. In addition, calcineurin dephosphorylates AQP2 during GOLGI and/or vesicular routing, allowing normal intracellular trafficking²²⁶. Third, the AC-catalysed generation of cAMP underlies Ca²⁺/CaM control²²⁷. Whereas it is widely accepted that cytosolic Ca²⁺ inhibits AC6^{228,229}, there is contradicting data regarding AC3 regulation. Storm and co-workers suggested that CaM activates the Calmodulin-dependent protein kinase II (CaMKII), which in turn blocks AC3 by phosphorylation²³⁰⁻²³². In contrast, other groups observed Ca²⁺/CaM-dependent stimulation of AC3^{233,234}, suggesting a synergistic control of AC3 and AC6 by alternating activation¹⁴⁶.

Apparently, also AVP-V2R signalling elevates the intracellular Ca²⁺ concentration^{25,235-239}. Apart from PKA, the exchange protein activated by cAMP (EPAC) is stimulated upon G α_s -signalling²⁴⁰. This triggers intracellular Ca²⁺-mobilisation²⁴¹, down regulates Rho GTPase activation²⁴² and thus enhances AQP2 trafficking²⁴¹. However, AQP2 trafficking in the absence of Ca²⁺ occurs just as efficiently, at least in rat primary inner medullary collecting duct (IMCD) cells²⁴³.

1.3.3.3 Dopamine

Dopamine is a neurotransmitter in the central nervous system, which is implicated in reward, motivation, motor control, learning and cognition. Outside the nervous system dopamine is synthesised in the proximal tubule, *inter alia*, where it acts in a paracrine manner²⁴⁴. Dopamine receptors are divided into D₁-like (D₁ and D₅, also called D_{1A} and D_{1B}) and D₂-like (D₂, D₃ and D₄) families, which are coupled to G α_s and G α_i , respectively, and all are expressed in the kidney²⁴⁵. The presence of opposing receptors however, raises the question which effect dominates and leads to contrary discussions regarding the underlying molecular mechanism. Li *et al.* observed a decrease of cytosolic cAMP in principal cells upon dopamine challenge, leading to reduced AQP2 transcription and membrane targeting^{246,247}. In line, Nejsum *et al.* reported increased endocytosis of AQP2 after dopamine treatment, independent of S256 phosphorylation²⁰³. As demonstrated by Peter Deen and co-workers, the dopamine-induced internalisation of AQP2 depends on its ubiquitination at K270, which precedes the phosphorylation of S261 and is associated with its lysosomal degradation²⁴⁷. They propose a bimodal action of dopamine. Next to the G α_i -mediated decrease in cytosolic cAMP, an activation of PKC could also increase AQP2 endocytosis. Presumably, dopamine antagonises the AVP effect but the precise mechanism remains to be established.

1.3.3.4 Nitric oxide

The gaseous signalling molecule nitric oxide (NO) diffuses through the cytoplasm and the plasma membrane. NO triggers an increase in cytosolic cyclic guanosine monophosphate (cGMP), which activates cGMP-dependent protein kinase G (PKG). According to Bouley *et al.*, this results in the increased plasma membrane localisation of AQP2, possibly due to phosphorylation of S256 by PKG²⁴⁸. In contrast, other groups observed reduced AVP-mediated water permeability in the collecting duct upon NO treatment, which they suggest to be the result of a PKG-mediated decrease in cytosolic cAMP and thus reduced PKA activity²⁴⁹⁻²⁵². In line, Kortenoeven *et al.* observed that NO lowers AQP2 protein abundance, apparently without affecting its gene transcription²⁵³. However, Borghese and co-workers proposed enhanced AQP2 promoter activity upon NO challenge²⁵⁴. Thus, regarding AQP2 control the role of NO and NO-donors like L-arginine is not entirely understood yet.

1.3.3.5 Prostaglandin E₂

Prostaglandin E₂ (PGE₂) can bind to four different G protein-coupled E-prostanoid receptors EP₁-EP₄²⁵⁵. PGE₂-EP₁-signalling elicits a diuretic effect *via* the G α_q -mediated activation of PKC, triggering AQP2 internalisation²⁵⁶. However, until today an EP₁-mediated decrease in AQP2-induced water permeability was only shown in frog urinary bladder, but not in CD cells²⁵⁶. EP₃ is coupled to G α_i and reduces cAMP synthesis upon activation²⁵⁷, thus decreasing AQP2 expression and membrane localisation²⁰⁴. EP₃-signalling also stimulates RhoA²⁵⁸, probably mediated by the G $\alpha_{12/13}$ -dependent activation of Rho guanine nucleotide exchange factors (GEFs)^{259,260}, which directly activate RhoA and thus attenuate AQP2 membrane trafficking^{168,169}. These alternative functional effects are due to different EP₃ splice variants, which signal *via* different G proteins^{261,262}. As recently reviewed by Olesen and Fenton, the observation of various cellular responses might also be the result of the differential expression of PGE₂-receptors in model systems derived from different renal sections of diverse species²⁶³.

Like the V2R, EP₂ and EP₄ couple to G α_s ²⁰⁵. Olesen *et al.* reported that the stimulation of both receptors results in the increased phosphorylation of AQP2-S264, whose effect is presently unknown²⁶⁴. However, only EP₂-signalling increases the cytosolic cAMP concentration AVP-independently²⁶⁵ and stimulates the phosphorylation of AQP2-S256 and -S269²⁶⁴. Presumably, EP₂ and EP₄ might act *via* different signalling pathways²⁶⁴. Apart from that, there are contradictory data on whether EP₂ is expressed in the CD at all^{255,266-270}. EP₄ is widely spread in the CD²⁷¹ and its activation enhances AQP2 membrane trafficking, although cytosolic cAMP concentration remains unaffected²⁶⁴. This might result from promiscuous G protein coupling²⁷² as speculated to occur upon the PKA phosphorylation of EP₄²⁶³. In line,

EP₄ activation was shown to stimulate phosphatidylinositol 3-kinase (PI3K)²⁷³, which is, beside being involved in cancer and inflammation, suggested to regulate AQP2 expression and endosomal retrieval^{274,275}. Altogether, the molecular details of PGE₂-signalling remain to be completely understood.

1.3.3.6 Purines

Purine signalling occurs *via* three classes of purinergic receptors, P1 adenosine GPCRs, P2X ligand-gated ion channels and P2Y GPCRs. In the CD P2Y receptors are predominantly expressed and activated by extracellular adenosine- or uridine- di- and triphosphates (ADP, ATP, UDP, UTP)²⁷⁶. They are divided into six G α_q -coupled (P2Y₁, P2Y₂, P2Y₄, P2Y₆, P2Y₁₁, P2Y₁₄) and two G α_i -coupled subtypes (P2Y₁₂, P2Y₁₃)²⁰⁵. Until today most studies focussed on P2Y₂, whose activation by ATP or UTP induces two cascades, which are relevant for AQP2 regulation. First, G $\alpha_{q/11}$ -mediated signalling of basolateral P2Y₂ or apical P2Y₄ receptors elicits the PLC-PKC-signalling-cascade²⁷⁷, which alleviates AQP2 membrane localisation as described earlier. In addition, the ubiquitination of AQP2 is increased upon ATP challenge²⁴⁷, which is a prerequisite for its internalisation²². At the same time, ATP-P2Y₂-signalling attenuates the AVP-triggered increase in cytosolic cAMP^{247,278}. In line, Boone *et al.* observed reduced AQP2 mRNA levels upon ATP treatment, likely to be a consequence of reduced cAMP levels²⁴⁷. However, these effects might also be a consequence of G α_i -coupled receptors P2Y₁₂ or P2Y₁₃ but not P2Y₂^{277,279}. Second, upon P2Y₂ activation the release of arachidonic acid is triggered, which is converted to PGE₂²⁸⁰ by cyclooxygenase (COX). P2Y₂ antagonism reduces EP₃ levels, which in turn leads to decreased AQP2 expression and activity (1.3.3.5)²⁸¹. Besides, Sauzeau *et al.* reported that P2Y₁-, P2Y₂-, P2Y₄- and P2Y₆-stimulation activates RhoA in aortic myocytes²⁸². Since RhoA alleviates AQP2 plasma membrane trafficking in renal principal cells^{168,169}, this mechanism might also account for the AVP-opposing effect of purine signalling.

1.3.4 Proteins controlling AQP2

The expression and localisation of AQP2 are controlled by numerous proteins of several pathways. However, in many cases their significance remains unclear, as a proof for their direct involvement is missing.

Tab. 2. Proteins controlling the AQP2 expression and/or localisation.

Protein	Suggested functional implication	Reference
Actin	Actin-depolymerisation promotes AQP2 trafficking to the plasma membrane	165,168,169,213,283-285
AKAP18 δ	AKAP18 δ tethers PKA to AQP2-bearing vesicles, most likely facilitating its PKA phosphorylation	151
AKAP220	AKAP220 tethers PKA to AQP2-bearing vesicles, most likely facilitating its PKA phosphorylation	152
Annexin	Annexin II is required for AQP2 trafficking to and/or fusion with the plasma membrane; annexins II and VI belong to a motor complex binding to AQP2; annexins I, II, IV, and V are located on AQP2-bearing vesicles	285-288
AP1/2	AP1/2 mediates clathrin-mediated endocytosis of AQP2	180,201,286
AP-1	AP-1 increases AQP2 transcription	289,290
BIP	BiP selectively binds to phosphorylated AQP2; its functional implication regarding AQP2 is currently unknown	288,291
Calcineurin	Calcineurin enhances AQP2 transcription and dephosphorylates AQP2 during GOLGI/vesicle routing, allowing normal trafficking	225,226,292-294
Calcitonin	Calcitonin induces cAMP-dependent AQP2 trafficking to the plasma membrane	295
Caveolin	Caveolin-1 was suggested to mediate AQP2 internalisation	296
CDK	CDK1 and CDK5 were shown to phosphorylate AQP2 at S261	297
Clathrin	Clathrin forms coated pits for AQP2 endocytosis	178,298-300
COXII	COXII is involved in renal prostanoid synthesis and its inhibition leads to enhanced AQP2 protein abundance	301-307
CREB	CREB and CREB-like transcription factors increase AQP2 transcription	20,289,308-310
CSNK	CSNK phosphorylates S256 during GOLGI transition of AQP2	311,312
Dynactin	Dynactin is located on AQP2-bearing vesicles and probably links them to the dynein complex	179
Dynamin	Dynamin binds to AQP2 and is involved in the scission of clathrin-coated AQP2-bearing vesicles during endocytosis	178,180,202,286,313
Dynein	Dynein mediates the microtubule-associated transport of endocytotic AQP2-bearing vesicles	179,194
EPAC	Epac triggers AQP2 translocation to the plasma membrane Ca ²⁺ -dependently	241,309,314
ERK	ERK1/2 increases AQP2 transcription <i>via</i> the cAMP/Epac/ERK/CREB pathway; ERK1/2 may mediate S256 phosphorylation under hypertonic conditions; ERK1/2 phosphorylates S261 <i>in vitro</i>	48,275,297,309,315,316
GSK3B	GSK3B enhances PGE2 production by stimulation of COXII, which causes endocytic retrieval of AQP2; GSK3 β inhibition was suggested to reduce AVP-induced AC activity	199,317-319
HSC70, HSP70	Hsc70 and Hsp70 are involved in clathrin-mediated endocytosis of AQP2, were shown to bind AQP2 and suggested to affect AQP2 trafficking to the plasma membrane	180,202,288,320,321
Integrin	Integrins α 1, α 2, α 5 and β 1 are located on AQP2-bearing vesicles; Integrins α 5 and β 1 bind to AQP2; Interaction of AQP2 with Integrin β 1 promotes renal epithelial cell migration and might regulate AQP2 trafficking <i>via</i> cAMP and Ca ²⁺	286,322-324
JNK	JNK1/2 may mediate phosphorylation of S261 and S256	297,315,316
LIP5	LIP5 interacts with AQP2 and facilitates its lysosomal degradation	186,325
MAL	MAL attenuates AQP2 internalisation	175,326
MLCK	MLCK phosphorylates myosin regulatory light chain (MLC) and facilitates apical sorting of AQP2 by regulating actin filament organisation	223
Moesin	Moesin was suggested to support the transport of AQP2 to the plasma membrane by modulating actin depolymerisation	327
MUNC18b	Munc18b inhibits fusion of AQP2-bearing vesicle to the plasma membrane by counteracting SNARE complex formation	172
Myosin	Myosins and associate proteins were localised on AQP2-bearing vesicles and/or bind to AQP2, Myosin regulatory light chain might facilitate apical sorting of AQP2 by actin reorganisation	195,223,285,286
NF κ B	NF κ B reduces AQP2 gene transcription	328-330
p38-MAPK	p38-MAPK phosphorylates AQP2-S261 that is associated with ubiquitination and proteasomal degradation of AQP2	23,48,199,297,316
PI3K	PI3K potentiates AVP-mediated increase of AQP2 expression; PI3K mediates endosomal retrieval of AQP2-bearing vesicles	274,275,331
PKA	PKA phosphorylates AQP2-S256 and induces its trafficking to the apical plasma membrane	155-157,332-334

Protein	Suggested functional implication	Reference
PKB	PKB- inhibits GSK3 β , which increases the COX-mediated PGE2-production, resulting in reduced AQP2 membrane abundance; PKB inhibits Akt substrate of 160 kDa (AS160), which was suggested to increase plasma membrane abundance of AQP2	275,315,331,335,336
PKC	PKC induces short-chain ubiquitination of AQP2, leading to its endocytosis and degradation; PKC activation leads to depolymerisation of α -tubulin and intracellular localisation of AQP2; PKC was suggested to maintain AQP2 transcription by phosphorylation of CREB, PKC is suggested to phosphorylate S256 and S264	22,48,198,199,209,337-340
PKG	PKG was suggested to phosphorylate AQP2-S256, thus increasing its plasma membrane abundance; PKG was suggested to inhibit AVP-dependent AQP2 trafficking by atrial natriuretic peptide (ANP)	199,248,251
PP1/PP2A	PP1 and PP2A inhibition induces AQP2 redistribution to the apical plasma membrane; PP1 binds to AQP2	288,293
RAB	RAB GTPases are located on AQP2-bearing vesicles and regulate its endosomal trafficking	194,195,286,341-343
RAN	RAN binds to AQP2 but its significance regarding AQP2 control is not known	288
RHOA	RHOA stimulates actin-polymerisation, which inhibits AQP2 trafficking to the plasma membrane	168,169,344
SNAP	SNAP23 and SNAP25 are located on AQP2-bearing vesicles and participate in SNARE complex formation during vesicle and plasma membrane fusion	345,346
SPA-1	SPA-1 binds to AQP2 and stimulates AQP2 trafficking to the apical plasma membrane	347
Synaptotagmin	Synaptotagmin-13 is located on AQP2-bearing vesicles and might be involved in SNARE complex formation during vesicle and plasma membrane formation	286,348
Syntaxin	Syntaxins are involved in SNARE complex formation during fusion of AQP2 vesicle and plasma membrane; syntaxins 1A, 2, 3 and 4 are located in the plasma membrane of kidney epithelial cells, syntaxins 5A, 7, 12, 13 and 16 are located on AQP2-bearing vesicles	172,286,349-353
TM5b	α -TM5b binds to AQP2, which results in F-actin destabilisation and facilitates apical sorting of AQP2	165,285,286,321,354
TONEBP	ToneBP increases AQP2 transcription during hypertonic stress response	225,330,355-358
TRPC3	TRPC3 interacts and translocates with AQP2 upon AVP stimulation, its functional implication is presently unknown	359,360
TRPV4	TRPV4 interacts with AQP2, the functional implication is presently unknown	361
Tubulin	α - and β -tubulin are located on AQP2-bearing vesicles; tubulin forms microtubules, which participate in AVP-elicited apical sorting of AQP2-bearing vesicles and perinuclear positioning of AQP2 after endocytosis	177,179,194,286,326,339,342,362-364
Ubiquitin	Ubiquitination at AQP2-K270 mediates AQP2 endocytosis and regulates its proteasomal degradation	22,191,247,286,365
VACM-1	VACM-1 targets E3 ligase formation and decreases AQP2 protein abundance	191,192
VAMP	VAMP2 and 3 are located both on AQP2-bearing vesicles and in the plasma membrane and are involved in SNARE complex formation during vesicle and plasma membrane fusion; VAMP8 was suggested to be located on AQP2-bearing vesicles and to be implicated in SNARE complex formation	172,286,341,345,351,366-370

Several proteins were shown to regulate AQP2 expression, abundance, subcellular localisation and degradation. Listed proteins act downstream of receptor activation. For most of them a direct evidence as well as *in vitro* data supporting their role in AQP2-mediated water reabsorption, is missing. AKAP, A-kinase anchor protein, AKAP18 δ /AKAP7, AKAP220/AKAP11; AP1/2, adaptor protein; AP-1, activator protein; BIP/GRP78/HSP50-5/HSPA5/HSP70-5, Heat shock 70 kDa protein 5/Immunoglobulin heavy chain-binding protein/78 kDa glucose-regulated protein precursor; Calcineurin, Protein phosphatase 2B, PP2B; CSNK, Golgi casein kinase, casein kinase; CDK, Cyclin-dependent kinase; COX, Cyclooxygenase-2; CREB, Cyclic AMP responsive element binding protein; EPAC, Exchange protein activated by cAMP; ERK, Extracellular signal-regulated kinase, ERK1/MAPK3, ERK2/MAPK1; GSK3B, Glycogen synthase kinase 3 β ; HSC, Heat shock cognate; HSP, Heat shock protein; JNK, c-Jun NH2-terminal kinase; LIP5, Lysosomal trafficking regulator interacting protein-5; MAL, Myelin and lymphocyte associated protein, JNK1/MAPK8, JNK2/MAPK9; MAPK, mitogen activated protein kinase; MLCK, Myosin light chain kinase; Moesin, part of ERM (ezrin/radixin/moesin) protein complex; Munc18b, Unc18-2, Syntaxin-binding protein 2; NF κ B, Nuclear factor "kappa-light-chain-enhancer" of activated B-cells; P38-MAPK, p38 mitogen activated protein kinase, MAPK14; PI3K, Phosphoinositide-3-kinase, MAPK14; PKA/B/C/G, Protein kinase A/B/C/G; PP1, Serine/threonine-protein phosphatase 1; PKB/AKT; RAB, Ras-related protein; RAN, Ras-related nuclear protein; RHOA, Ras homolog family member A; SNAP, Synaptosomal-associated protein 25; SPA-1, Signal-induced proliferation-associated protein 1; TM5b, α -Tropomyosin 5b; TONEBP, tonicity-responsive enhancer binding protein/NFAT5, Nuclear factor of activated T-cells 5/OREBP, Osmotic response element binding protein; TRPC3, Transient receptor potential cation channel subfamily C member 3; TRPV4, Transient receptor potential cation channel subfamily V member 4; VACM, Vasopressin-activated calcium mobilizing, Cullin 5; VAMP2, Vesicle associated membrane protein/Synaptobrevin; VAMP3, Vesicle associated membrane protein/Cellubrevin.

1.3.5 AQP2 pathology

The dysregulation of AQP2 is associated with impaired urinary concentration or enhanced water retention, leading to pathophysiologic conditions.

1.3.5.1 Diabetes insipidus

Aberrations in AVP-mediated water reabsorption cause diabetes insipidus (DI), which is divided in central (also termed neurohypophyseal) and nephrogenic DI (CDI and NDI). Whereas CDI is characterised by impaired AVP production or release³⁷¹, in NDI the kidney is resistant to AVP and thus fails to concentrate urine. One distinguishes between acquired and less common inherited (congenital) NDI.

Beside urinary tract obstruction and electrolyte disturbances, acquired NDI is most commonly caused by lithium³⁷², which is used to treat bipolar disorders³⁷³, the most serious and prevalent mental illness in the world³⁷⁴. Lithium enters principal cells *via* apically expressed ENaC³⁷⁵ and impairs AQP2-mediated water reabsorption by multiple pathways³¹⁵. It reduces AVP-stimulated cAMP production in rats and isolated rabbit cortical collecting tubules^{376,377}, but not in mouse cortical collecting duct mpkCCD cells³⁷⁸. According to Nielsen *et al.*, lithium affects the expression of 74 proteins, mostly involved in apoptosis, cell morphology and proliferation³¹⁵. Chronic lithium intake reduces AQP2 transcription^{307,378}, as well as the apical trafficking and excretion of AQP2^{379,380} whereas AQP2 protein stability remains unaffected³⁷⁸. However, Kortenoeven *et al.* suggested an implication of lithium in AQP2s lysosomal degradation³⁰⁷.

Congenital NDI was already reported in 1892³⁸¹ and comprises X-linked NDI (XNDI), which occurs in 90 % of the patients³⁸² and is due to a loss-of-function mutation in the *AVPR2* gene³⁸³, located on the X-chromosome and encoding for V2R^{384,385}, or the rare autosomal NDI, due to a mutated *AQP2* gene^{386,387}. Until today, more than 200 *AVPR2*- and 50 *AQP2*-mutations are described to cause NDI³⁸⁸.

All forms of DI can lead to polyuria, followed by dehydration and electrolyte imbalance. The symptoms include persistent need for drinking, frequent voiding, constipation, dryness of skin, recessed eyeballs, intermittent high fever, seizures and developmental retardation^{382,389}. Apart from AVP deficiency, which can be compensated by treatment with the AVP analogue desmopressin (dDAVP)³⁹⁰, DI can rarely be corrected^{388,389}. Current medication aims to reduce the symptoms but mostly does not eliminate fully. Thus patients have to adapt to low sodium diet and to ensure sufficient water intake.

1.3.5.2 Extracellular fluid volume expansion

Next to polyuric states, AQP2 dysregulation can cause excessive water retention, which contributes to the development of hyponatremia. In the syndrome of inappropriate antidiuretic hormone secretion (SIADH, Schwartz-Bartter-syndrome)³⁹¹, an exaggerated production and release of AVP, which is often accompanied by malignancies³⁹², results in persistent AQP2-mediated water reabsorption^{393,394} and thus inappropriately concentrated urine. Besides, gain-of-function mutations in the *AVPR2* gene cause the constitutive activation of V2R, resulting in increased water retention even under hypovasopressinergic conditions, which is termed nephrogenic syndrome of inappropriate antidiuresis (NSIAD)^{395,396}. Both, SIADH and NSIAD, are characterised by euvolemic hyponatremia^{396,397}.

In addition, an expansion of extracellular fluid volume due to elevated water retention is associated with congestive heart failure (CHF), hepatic cirrhosis and nephrotic syndrome³⁹². According to Xu *et al.*, patients suffering from CHF display elevated plasma AVP level and thus increased AQP2 expression and membrane abundance³⁹⁸. Severe CHF is associated with hypervolemic hyponatremia³⁹⁹. In contrast, excessive water retention during nephrotic syndrome is accompanied by increased sodium reabsorption. Although circulating AVP-levels are elevated, AQP2 is down regulated, probably attributable to an escape reaction, in which water reabsorption is decreased AVP-independently leading to enhanced diuresis^{394,400-403}. The expression level of AQP2 in different cirrhosis animal models considerably varies, suggesting that AQP2 is not the main determinant³⁹².

Consequences of extracellular fluid volume expansion and hyponatremia can include shortness of breath, leg swelling, headache, vomiting and can even lead to convulsion, neurological impairment or coma. The treatment includes the administration of saline, fluid restriction and diuretics.

1.4 Aim of the thesis

Arginine-vasopressin (AVP) controls water reabsorption in renal collecting duct principal cells and thereby fine-tunes body water homeostasis. By binding to the basolateral vasopressin receptor type 2 (V2R), AVP stimulates an increase in cytosolic cAMP, which activates protein kinase A (PKA). PKA phosphorylates the water channel aquaporin-2 (AQP2) and triggers its translocation from perinuclear vesicles into the plasma membrane, where it facilitates water reabsorption from the primary urine. However, details of the molecular mechanisms underlying AQP2 redistribution are largely unknown. Aberrations in AVP-mediated signalling are associated with severe water balance disorders like nephrogenic diabetes insipidus (NDI), the syndrome of inappropriate antidiuretic hormone secretion (SIADH) or congestive heart failure (CHF).

The aim of this thesis was to identify proteins, which control the location of AQP2 and thus to contribute to understanding the molecular details of its translocation. Therefore, a large-scale siRNA screen had to be established. The major objectives were the identification of a cell line suitable for high-throughput analysis of AQP2 redistribution in a 384 well format, the upscaling of siRNA transfection, the establishment of automated immunofluorescence microscopy, the development of an image analysis pipeline using CellProfiler software and the hit identification utilizing KNIME software.

2 MATERIALS AND METHODS

2.1 Materials

2.1.1 Equipment and software

Tab. 3. Equipment and disposal.

Equipment	Description	Vendor
ArrayScan V ^{II} HCS Reader	Automated microscope	Thermo Fisher Scientific/Cellomics (Bonn, DE)
Cryo-container 5100-0001	Freezing container	Thermo Fisher Scientific /NALGENE (Bonn, DE)
EL406 TM	Microplate washer dispenser	BioTek (Bad Freidrichshall, DE)
ELx405 TM Selet CW	Microplate washer	BioTek (Bad Freidrichshall, DE)
Enspire® 2300	Microplate reader	PerkinElmer (Rodgau, DE)
Eppendorf Research pro	Multichannel pipette	Eppendorf AG(Wesseling-Berzdorf, DE)
FreedomEVO	Liquid handling robotic system	Tecan Deutschland GmbH (Crailsheim, DE)
GelDoc 2000	Gel documentation system	Bio-Rad Laboratories GmbH (München, DE)
LSM780	Confocal microscope	Carl Zeiss MicroImaging GmbH (Jena, DE)
MiniProtean®	Polyacrylamide gel electrophoresis	Bio-Rad Laboratories GmbH (München, DE)
Odyssey Imager	Western Blot detection system	LI-COR Biosciences (Bad-Homburg, DE)
PerfectBlue mini L	Agarose gel electrophoresis chamber	PeqLab Biotechnologie GmbH (Erlangen, DE)
Potter	Cell homogeniser	Braun Biotech Int. GmbH (Melsungen, DE)
Scepter TM 2.0	Cell counting	Merck Millipore (Schwalbach, DE)
Sonopuls HD 2070	Ultrasound homogeniser	Bandelin electronic GmbH & Co.KG (Berlin, DE)
TProfessional TRIO	Thermocycler	Biometra (Göttingen, DE)
TransBlot	Semi-Dry Western Blot module	Bio-Rad Laboratories GmbH (München, DE)
Disposal		
6 well plate 92006	6 well cell culture plate	TPP (Trasadingen, CH)
96 Well Microplate 655101	96 well microplate	Greiner bio-one (Solingen, DE)
384 Well Microplate 3985	384 well cell culture microplate	Corning (Amsterdam, NL)
384 Well Microplate 781091	384 well cell culture microplate	Greiner bio-one (Solingen, DE)
Cryo-vials E309.1	Cryoconservation of cells	Carl Roth GmbH & Co KG (Karlsruhe, DE)
Filtertop 99505	Filtertop 500 ml	TPP (Trasadingen, CH)
PVDF membranes T830.1	Western Blotting membranes	Carl Roth GmbH & Co KG (Karlsruhe, DE)
Scepter TM Sensors 60 µM PHCC60050	Cell counting	Merck Millipore (Schwalbach, DE)
T75 cell culture flask	Cell culture flask	TPP (Trasadingen, CH)

Tab. 4. Software.

Software	Purpose	Vendor/URL
CellProfiler 2.0	Image analysis	www.cellprofiler.org
ClustalW	Sequence alignment	www.ebi.ac.uk/Tools/msa/clustalw2/
DAVID	Functional annotations and gene conversion	david.abcc.ncifcrf.gov/
EndNote X6	Reference manager	endnote.dom
Excel 2011	Spreadsheet	Microsoft (Redmond, US)
GraphPad Prism 5	Statistical analysis	GraphPad Software, Inc. (La Jolla, US)
Illustrator	Graphics, drawing	Adobe Systems, Inc. (San Jose, US)
Image J	Image processing	rsb.info.nih.gov/ij/
Image Studio Ver 2.0	Western Blot analysis	LI-COR Biosciences (Bad-Homburg, DE)
KNIME	Data mining	knime.org
Photoshop	Image processing	Adobe Systems, Inc. (San Jose, US)
Power Point	Presentations	Microsoft (Redmond, US)
SerialCloner	Sequence analysis	serialbasics.free.fr/Serial_Cloner.html
Word 2011	Word processing	Microsoft (Redmond, US)
ZEN 2011	Confocal microscopy, image acquisition and analysis	Carl Zeiss MicroImaging GmbH (Jena, DE)

2.1.2 Antibodies

Tab. 5. Antibodies used for Western Blotting and immunofluorescence microscopy.

Primary antibody	Origin	Vendor, article number (#)
α -Tubulin (DM1a)	Mouse	Calbiochem; #CP06
AQP2 (C17)	Goat	Santa Cruz; #9882
AQP2 H27	Rabbit	Custom-made ⁴⁰⁴
AQP2-pS256	Rabbit	Custom-made (Eurogentec ZDE12147_0798)
AQP2-pS261	Rabbit	Abcam; #ab72383
CDK18	Rabbit	Santa Cruz, #176
GAPDH (14C10)	Rabbit	Cell Signaling; #2118S
PKIA	Goat	Santa Cruz; #1943
Pan-cadherin	Rabbit	SIGMA; #C3678
V2R (K3)	Rabbit	Custom-made in Bachmann group, Charité Berlin
Secondary antibody		
Alexa647-anti Rabbit IgG	Donkey	Jackson ImmunoResearch Laboratories; #711-605-152
Alexa647-F(ab') ₂ -anti Rabbit IgG	Donkey	Jackson ImmunoResearch Laboratories; #711-606-152
Cy2-anti-Rabbit-IgG	Goat	Jackson ImmunoResearch Laboratories; #111-225-144
Cy3-anti-Rabbit IgG	Mouse	Jackson ImmunoResearch Laboratories; #211-165-109
Cy3-F(ab') ₂ -anti-Rabbit IgG	Donkey	Jackson ImmunoResearch Laboratories; #711-166-152
Cy5-anti-Rabbit IgG	Donkey	Jackson ImmunoResearch Laboratories; #711-175-152
Cy5-F(ab') ₂ -anti-Rabbit IgG	Donkey	Jackson ImmunoResearch Laboratories; #711-176-152
FITC-anti-Rabbit IgG	Goat	Jackson ImmunoResearch Laboratories; #111-095-003
Peroxidase (POD)-anti-goat IgG	Donkey	Jackson ImmunoResearch Laboratories; #705-035-147
POD-anti-mouse IgG	Donkey	Jackson ImmunoResearch Laboratories; #715-035-151
POD-F(ab') ₂ -anti-rabbit IgG	Donkey	Jackson ImmunoResearch Laboratories; #711-036-152

2.1.3 Mouse siGENOME siRNA library-SMART pool

The Mouse siGENOME siRNA Library-SMARTpool (Thermo Fisher Scientific; #G-015005-E2-025, 0.25 nmol) comprises 55x 384 well microplates (Thermo Fisher Scientific; #AB-0781) and is divided into four sublibraries (Tab. 6).

Tab. 6. Sublibraries of the Mouse siGENOME siRNA Library.

Sublibrary	384 well microplates	Targeted genes
Mouse GPCR	2	474
Mouse Protein Kinases	3	719
Mouse Druggable	17	5169
Mouse Genome	33	10510

In total, 16,872 genes are targeted by 67,488 different siRNAs, all of which are 19 nucleotides in length without chemical modification. Four siRNAs directed against the same target mRNA are pooled per well.

2.1.3.1 Plate layout

Upon resuspension of desalted lyophilised siRNAs of the library with siRNA buffer (Thermo Fisher Scientific; #B-002000-UB-100) in storage plates (Thermo Fisher Scientific; #AB-0781), assay plates (GREINER bio-one; #781091) were prepared with 0.5 μ M siRNA in 4 μ l RNase-free water per well, resulting in 50 nm siRNA (2 pmol) in 40 μ l final transfection volume including Lipofectamine®2000 and MCD4 cells. Both, storage and assay plates were stored

at -20°C . Maximal 320 of 384 wells per microplate are occupied, leaving the outer two rows of each 384 well microplate for controls (Fig. 4). Equivalent to the concentration of library siRNAs, 4 μl of 0.5 μM control Aqp2 siRNA, toxic (TOX) siRNA and scrambled non-targeting (NT#2) siRNA (Tab. 8) were added manually to each assay plate on the day of transfection. Including siRNA-free mock transfection, in which only Lipofectamine® 2000 and cells were present, four controls were placed in central and outer parts of both sides of the microplate (Fig. 4).

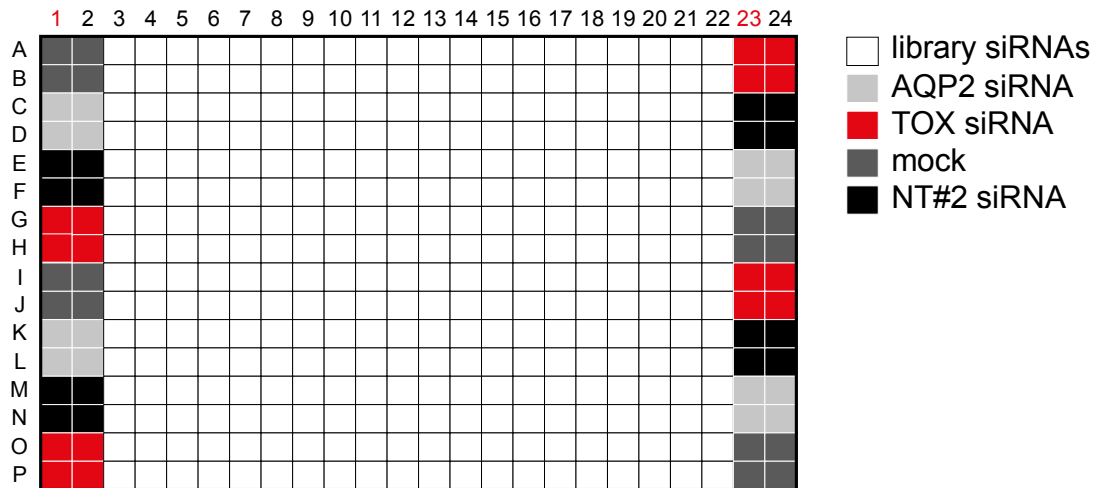


Fig. 4. Assay plate layout. Surrounding library siRNAs, the controls mock, Aqp2, TOX, and NT#2 siRNAs were arranged in the indicated parts of the microplate. Except for rows 1 and 23, FSK was added to all wells.

2.1.4 Oligonucleotides

2.1.4.1 DNA oligonucleotides

Tab. 7. DNA oligonucleotides used for PCR or sequencing.

Name	Use	DNA Sequence 5'-3'
hAQP2-forw-1	PCR	GAATTCATGTGGGAGCTCCGC
hAQP2-rev-816	PCR	GCGGCCGCTCAGGCCTTGGTACC
hAQP2-forw-442	Sequencing	TCCACCGATGAGCGCCGCGGA
hAQP2-rev-474	Sequencing	CCCCGCGGATGTCTGCTGGCG
mGAPDH for	PCR	AGGTTGTCTCCTGCGACTTCA
mGAPDH rev	PCR	CCAGGAAATGAGCTTGACAAAGTT

Oligonucleotides were purchased from BioTeZ Berlin Buch GmbH (Berlin, DE). They were synthesised in 10 nmol scale, dissolved in *A. dest.* and stored as 100 mM stock and 10 μM solutions at -20°C .

2.1.4.2 siRNAs

Tab. 8. siRNAs for control and validation experiments.

Name	Target/sequence (5'-3')	Source, article number (#)
Aqp2 (Aqp2 Stealth siRNA)	Human AQP2/ GAGCTCCGCTCCATAGCCTTCTCCA	Life Technologies GmbH (Darmstadt, DE); #1299001/AQP2HSS179907
Gapdh (Silencer® GAPDH siRNA)	Human, mouse, rat GAPDH/ Proprietary	Life Technologies GmbH (Darmstadt, DE); #AM4624
TOX (TOX Transfection Control)	Proprietary	Thermo Fisher Scientific (Bonn, DE), #D-001500-01-20
NT#2 (siGENOME Non-targeting siRNA Pool #2)	Firefly luciferase/ UAAGGCUAUGAAGAGAUAC, AUGUAUJGGCCUGUAUUAG, AUGAACGUGAAUUGCUCAA, UGGUUUACAUGUCGACUAA	Thermo Fisher Scientific (Bonn, DE), #D-001206-14-20
Cdk18 (siGENOME SMART pool)	Mouse Cdk18/CCAAAUCAGUGCCUACAAA, ACAGUGACCUGAAACAGUA, GGAAACAUAUGUGAAACUG, GAAACACGCCAAUUAUUGUG	Thermo Fisher Scientific (Bonn, DE), #M-040145-01-0005/18557
Cdk18 single (Silencer Predesigned)	Mouse Cdk18/ CCAACUCCACACUCAGACG	Life Technologies GmbH (Darmstadt, DE); #AM16708A; ID, 155801
Pkia pool (siGENOME SMART pool)	Mouse Pkia/AAACUAGCAGGCCUUGAUA, CAGCAAUGAAUUAGCCUUA, GAGAAGCUCCACCGAACAA, GAAGAAAUGCAAUCAUGA	Thermo Fisher Scientific (Bonn, DE), #M-058432-01-0005/18767
Pkia single (Silencer Predesigned)	Mouse Pkia/ CCAAAUGUACCAUUCAGUU	Life Technologies GmbH (Darmstadt, DE); #AM16708A; ID, 150159

siRNAs were ordered in 20 nmol scale, resuspended in RNase-free water and stored as 100 μ M stock solutions at -20°C.

2.1.5 Chemicals and buffers

All chemicals used for preparing buffers and solutions (Tab. 9) were obtained from Sigma-Aldrich (Taufkirchen, DE) or Carl Roth GmbH & Co. KG (Karlsruhe, DE), unless indicated otherwise. All buffers were prepared with *A. dest.*

Tab. 9. Buffers and solutions.

Buffer/solution	Composition
Blocking buffer (IF)	1x PBS; 0.27 % fish skin gelatine
Blocking buffer (Western Blot)	1x TBS-T; 1 % bovine serum albumine (BSA)
Lysis buffer	SLB; PhosSTOP EASY (Tab. 10), Complete mini EDTA-free (Tab. 10)
Opti-MEM®	Life Technologies GmbH (Darmstadt, DE); #11058-021
Phosphate-buffered saline (PBS)	137 mM NaCl; 2.7 mM KCl; 1.5 mM KH ₂ PO ₄ ; 8.1 mM Na ₂ HPO ₄ ; pH 7.4
Sample buffer 3x	30 % glycerine; 3 % SDS; 200 mM Tris-HCl; 30 mM DTT; pH 6.8
SDS-polyacrylamide gel electrophoresis (PAGE) running buffer	25 mM Tris; 192 mM glycine; 0.1 % SDS
Semi-dry transfer buffer (Western Blot)	48 mM Tris; 39 mM glycine; 1.3 mM SDS; 20 % (v/v) methanol
Separating gel buffer (SDS-PAGE)	0.625 M Tris-HCl; pH 6.8
Standard lysis buffer (SLB)	10 mM K ₂ HPO ₄ ; 150 mM NaCl; 5 mM EDTA; 5 mM EGTA; 0.5 % Triton X-100; pH 7.4
Stacking gel buffer (SDS-PAGE)	0.75 M Tris-HCl; pH 8.8

Buffer/solution	Composition
TBS + Tween (TBS-T)	1x TBS; 0.05 % Tween-20
Tris-acetate-EDTA (TAE) buffer	40 mM Tris; 1 mM EDTA; 1.14 % (v/v) glacial acetic acid
Tris-buffered saline (TBS)	10 mM Tris-HCl; 150 mM NaCl; pH 7.4
Trypsin-EDTA	Biochrom AG (Berlin, DE); #L2153

Tab. 10. Chemicals and fluorescent dyes.

Substance	Vendor; article number (#)
4', 6-Diamidine-2'-phenylindole dihydrochloride (DAPI)	Roche Diagnostics GmbH (Mannheim, DE); #10236276001
alamarBlue®	Life Technologies GmbH (Darmstadt, DE); #DAL1025
Arginine-vasopressin (AVP)	M. Beyermann, Leibniz-Institut für Molekulare Pharmacologie (FMP; Berlin, DE)
Complete mini EDTA-free	Roche Diagnostics (Mannheim, DE); #REF0693159001
Coomassie Plus™ Protein Assay Reagent	Thermo Fisher Scientific (Bonn, DE); #1856210
Forskolin (FSK)	Biaffin GmbH & Co KG Life Sciences Institute (Kassel, DE); #PKE-FORS-050
HyperLadder II (HyperLadder™ 50bp)	BioLine GmbH (Luckenwalde, DE); #BIO33054
Immobilon™ Western Chemiluminescent HRP substrate	Merck Millipore (Schwalbach, DE); #WBKLS0500
Immu-Mount™	Thermo Fisher Scientific (Bonn, DE); #99-904-12
PhosSTOP EASY pack	Roche Diagnostics (Mannheim, DE); #REF04906837001
Precision Plus Protein Standard Dual Color	Bio-Rad Laboratories GmbH (München, DE)
Redsafe	Intron Biotechnology (Seongnam, KR); #21141
TRITC-Phalloidin	Sigma-Aldrich (Taufkirchen, DE); #P1951

2.1.6 Eukaryotic cells

Tab. 11. Eukaryotic cell lines and primary cells.

Cell lines	Description	Culture medium	Vendor; article number (#)
HEK293	Human embryonic kidney cell line ⁴⁰⁵	DMEM- GlutaMAX™(Life Technologies GmbH (Darmstadt, DE; #21885108); 10 % fetal calf serum (FCS); 1 % penicillin/streptomycin (100 U/ml)	Deutsche Sammlung von Mikroorganismen und Zellkulturen GmbH (DSMZ; Braunschweig, DE); #ACC305
HK2	Human kidney cell line, proximal tubule	K-SFM (Life Technologies GmbH (Darmstadt, G; #17005-042); 2 % FCS; 1 % penicillin/streptomycin (100 U/ml)	LGC Standards GmbH (Wesel, DE); #CRL-2190
HKC8	Human kidney cell line, proximal tubule	DMEM/F-12-GlutaMAX™(Life Technologies GmbH (Darmstadt, DE; #31331028); 2.5 % FCS; 1 % penicillin/streptomycin (100 U/ml); 1 % insulin/transferrin/selenium (ITS)	M. Goppelt-Strübe, Universitätsklinikum Erlangen (Erlangen, DE)
M1	Mouse cortical collecting duct cell line ⁴⁰⁶	DMEM/F-12-GlutaMAX™(Life Technologies GmbH (Darmstadt, DE; #31331028); 5 % FCS, 5 µM dexamethasone	LGC Standards GmbH (Wesel, DE); #CRL-2038
MCD4	Mouse collecting duct cell line, stably expressing human AQP2 ⁴⁰⁷	DMEM/F-12-GlutaMAX™(Life Technologies GmbH (Darmstadt, DE; #31331028); 5 % FCS, 5 µM dexamethasone	G. Valenti, Dipartimento di Fisiologia Generale ed Ambientale, (Bari, I)

Cell lines	Description	Culture medium	Vendor; article number (#)
mTERT	Mouse collecting duct cells ⁴⁰⁸	DMEM/F-12 – GlutaMAX™ (Life Technologies GmbH (Darmstadt, DE; #31331028); 5 % FCS; 1 % penicillin/streptomycin (100 U/ml); 5 µM dexamethasone; 1 % ITS; 10 nm 3, 3', 5-Triido-L-thyronine sodium salt (T3)	Stacy L. Steele, Medical University of South Carolina (South Carolina, US)
Primary cells			
IMCD	Inner medullary collecting duct cells from rats	DMEM- GlutaMAX™ (Life Technologies GmbH (Darmstadt, DE; #21885108); 1 % non-essential amino acids (Biochrom AG; Berlin, DE; #C2-22; 1 % ultrosor G (Cytogen GmbH, Sinn, DE; #15950-017); 500 µM DBcAMP, 20 U/ml nystatin (Sigma Aldrich; #N4014); 0.25 µg/ml gentamicin (Life Technologies GmbH (Darmstadt, DE; #15710); 4.5 g/l glucose; 100 mM NaCl; 100 mM urea	Made inhouse; ^{404,409}

2.2 Methods

2.2.1 Isolation and purification of DNA

2.2.1.1 Isolation of genomic DNA from cell lines

For the isolation of genomic DNA from cell lines, cells were grown to confluency in T75 cell culture flasks, trypsinised and resuspended in 5 ml medium. Cells were counted using the Scepter™ pipette (see Cell counting) and up to 10⁷ cells were transferred to a 2 ml reaction tube for centrifugation (2 min, 1500x g, room temperature). DNA was purified using the GeneMATRIX Tissue DNA Purification kit (Roboklon GmbH, Berlin, DE; #E3550).

2.2.1.2 Purification of DNA fragments from agarose gels

DNA was purified from agarose gels using the NucleoSpin® Extract II kit (Macherey-Nagel, Düren, DE; #740609.250) according to manufacturer's instructions.

2.2.2 Analysis and modification of DNA

2.2.2.1 Polymerase chain reaction

The polymerase chain reaction (PCR) was used to amplify specific DNA regions from *AQP2* for subsequent sequencing. Specific forward (hAQP2-for-1) and reverse (hAQP2-rev-816) primers and thermostable OptiQa DNA polymerase were used. PCR reactions were performed in 35 cycles in the TProfessional TRIO thermocycler (Biometra, Göttingen, DE) using the protocol outlined in Tab. 13.

Tab. 12. Composition of PCR reaction.

Component	Volume [μ l]	Final concentration
Template DNA	1	50-200 ng
hAQP2-forw-1 (10 μ M)	0,4	0,2 μ M
hAQP2-rev-816 (10 μ M)	0,4	0,2 μ M
dNTP mix (5 mM)	0,8	0,2 mM
OptiTaq polymerase (5 U/ μ l)	0,1	0,025 U
10x Buffer C (15 mM MgCl ₂ <i>inter alia</i>)	2	1x (1,5 mM Mg Cl ₂)
<i>Aqua dest.</i>	<i>ad 20 μl</i>	

OptiTaq thermostable DNA polymerase (#E2600-02), reaction buffer (#011211) and dNTPs (#E2800-04) were purchased from Roboklon GmbH (Berlin, DE).

Tab. 13. PCR protocol.

Step		Temperature	Time	
1	Preheating	80°C	2 min	
2	Initial denaturation	95°C	3 min	
3	Denaturation	95°C	1 min	} 35x
	Annealing	61°C	1 min	
	Elongation	72°C	1 min	
4	Final elongation	72°C	7 min	
5	Precooling	25°C	5 min	
6	Cooling	4°C	∞	

2.2.2.2 Agarose gel electrophoresis for separation of DNA fragments

DNA fragments were analysed by agarose gel electrophoresis. TAE buffer containing 1.5 % (w/v) agarose was boiled in a microwave until the solution became clear. After the solution cooled to approximately 60°C the DNA stain Redsafe was added and the gels were mounted. 10 μ l of the PCR reaction (Tab. 12), containing Buffer C, were loaded per well. To determine the size of DNA fragments, HyperLadder II was run as the molecular weight standard. The gels were run at 100 V for 50-60 min in 1x TAE buffer, DNA was visualised with GelDoc 2000 using a 520 nm filter.

2.2.2.3 DNA sequencing

For DNA sequencing, the Value Read Tube Service by Eurofins MWG Operon (Ebersberg, DE) was used and custom-made primers hAQP2-for-442 and hAQP2-rev-474 (Tab. 7) were applied.

2.2.3 Biochemical methods

2.2.3.1 Cell lysis

Eukaryotic cells were lysed by ultrasound. Confluent cells were washed with ice-cold PBS and scraped into lysis buffer. In a 1,5 ml reaction tube cells were disrupted by six ultrasonic impulses (65 % amplitude) at 4°C, using Sonoplus HD 2070. Cell debris was removed by centrifugation (30 min, 15,000x g, 4°C). The supernatant was used for Bradford assays and Western Blot analyses.

2.2.3.2 Bradford assay

Protein concentration of cell lysates was determined using the colorimetric Bradford assay⁴¹⁰. Per well of a 96 well microplate, 5 µl of sample lysate or standard samples (defined concentration of 0.125-2 mg/ml) and 250 µl Coomassie PlusTM Protein Assay Reagent were mixed and incubated for 10 min at room temperature, protected from light. Using the Enspire®2300 microplate reader, absorbance at 595 nm was measured. According to the extinction of standards, protein concentration of samples was determined.

2.2.3.3 Western Blotting

Protein samples were denatured in 1x sample buffer for 10 min at 95°C, separated by SDS-PAGE and transferred from the polyacrylamide gel to polyvinylidene fluoride (PVDF) membranes using the TransBlot Semi-dry Western Blot module (20 V for 90 min). Membranes were blocked for 60 min at room temperature (blocking buffer) and agitated with primary antibody, diluted in blocking buffer, at 4°C over night. Membranes were washed 3x 10 min in TBS-T and incubated with POD-labelled secondary antibodies, diluted in blocking buffer, for one hour at room temperature. Finally, membranes were washed 3x 10 min in TBS-T and proteins were detected by Immobilon® Western Chemiluminescent HRP substrate. Signals were visualised using Odyssey Imager. Precision Plus Protein Standard Dual Color was applied to determine protein sizes. Image Studio Ver. 2.0 and Image J were used for image processing and densitometric analysis, respectively.

To confirm specific antibody binding to antigen the antibody was pre-absorbed with the peptide, representing the respective epitope. The dilution at which the antibody consistently gives positive results was determined. The antibody was pre-incubated with a 1000 fold molecular excess of peptide in 500 µl PBS for 2 hours at room temperature. Antibody/peptide mixture was diluted in blocking buffer and the PVDF membrane was incubated with the mixture at 4°C over night.

2.2.4 Mammalian cell culture

2.2.4.1 Culturing of rat primary inner medullary collecting duct (IMCD) cells

IMCD cells were prepared according to Faust *et al.* 2013⁴⁰⁹. In brief, 10 to 12 weeks old rats (Wistar Han, Charles River Laboratories International, Inc., Sulzfeld, DE) were anaesthetised and decapitated. Inner medullae were dissected and digested enzymatically by hyaluronidase and collagenase. IMCD cells were resuspended in fully supplemented medium (Tab. 11) and seeded in collagen type IV (BD Biosciences, Heidelberg, DE; #356233)-coated dishes. Six to eight days after seeding, cells were used for experiments. 24 hours before starting the experiment, cells were incubated in medium without DBcAMP and nystatin in order to increase the perinuclear location of AQP2.

2.2.4.2 Culturing of mammalian cells

HEK293, HK1, HKC8, M1, MCD4 and mTERT cells were grown in appropriate medium (Tab. 11) and subcultured twice a week. Confluent cells were washed with ice-cold PBS and incubated with 1x Trypsin-EDTA for 2-10 min at 37°C. After detachment of the cells, trypsinisation was stopped by serum containing medium. A defined volume of cell suspension was transferred into a new cell culture flask with freshly added medium. After cell transfer, the cell passage (P) increased by a factor of one.

2.2.4.3 Cell counting

Cells were detached from plastic surfaces of culture dishes by trypsinisation. The cell suspension was diluted 1:10 in a 1.5 ml reaction tube using PBS. Using the Scepter™ 2.0 pipette with 60 µM tips, cells of 9-21 µM size were counted.

2.2.4.4 Freezing and thawing of mammalian cell lines

When confluency was reached cells were trypsinised and centrifuged (2 min, 300x g, room temperature). The pellet was resuspended in 3 ml medium without antibiotics per T75 cell culture flask. The equal volume of FCS containing 20 % dimethyl sulfoxide (DMSO) was added. The cell suspension was aliquoted in 3x 2 ml vials, which were stored at -80°C in a Cryo-container to achieve a cooling rate of 1°C/min. After a minimum of 3 hours, the cell-containing vials were transferred to liquid nitrogen.

To re-culture cells, frozen vials were quickly thawed by slight agitation in a water bath at 37°C. With a sterile Pasteur pipette, cells of one vial were slowly transferred in a T75 cell culture flask, containing 15 ml medium. After 2-4 days cells were grown confluent.

2.2.4.5 Reverse siRNA transfection of MCD4 cells

Transfection of double stranded short interfering RNAs (ds siRNAs) is widely used to specifically inhibit the expression of a target gene and to study its biological function. siRNA is a key component of RNA interference (RNAi⁴¹¹) and mediates posttranscriptional gene silencing (PTGS). With approximately 20 nucleotides in length, siRNA duplexes escape dsRNA-induced mammalian defence mechanisms⁴¹² but assemble with the RNA-induced silencing complex (RISC⁴¹³). The siRNA duplex is dissociated into its single strands, of which the guide strand is incorporated into RISC (called activated RISC) and the passenger strand is degraded⁴¹⁴. Activated RISC is directed to the homologous mRNA target and catalyses its cleavage^{415,416}. The expression of a single gene is then inhibited sequence-specifically.

siRNA was resuspended in RNase-free water and incubated with Lipofectamine® 2000 for 15 min at room temperature. MCD4 cells were reversely transfected by seeding cells onto the siRNA-liposome complex and incubation for 72 hours at 37°C. Transfections were conducted manually in 6 well plates or 384 well microplates or robot-assisted in 384 well microplates. In 6-well format, 200 µl of 500 nm siRNA were mixed with 200 µl Opti-MEM®, containing 6 µl Lipofectamine® 2000. After 15 min incubation at room temperature, 45,000 MCD4 cells (P42) in 1600 µl medium were added, resulting in 50 nm final siRNA concentration in 2000 µl transfection volume per well. In 384 well microplates, 5 µl of 500 nm siRNA were mixed with 5 µl Opti-MEM®, containing 0.15 µl Lipofectamine® 2000, and incubated for 10-15 min at room temperature. 500 MCD4 cells (P42) in 40 µl medium were added, resulting in 50 nm final siRNA concentration in 50 µl per well.

For automated reverse siRNA transfection in 384 well microplates, Tecan Freedom EVO liquid handling robot was used. Transfection volume was reduced to 40 µl in order to safe siRNA. 4 µl of 500 nm siRNA and 6 µl OptiMEM® including 0.15 µl Lipofectamine® 2000 were transferred to assay plates (GREINER 781091) by following the protocol instructions *Transfer_siRNAs* and *Transfer_Lipofectamine2000*, respectively (Fig. S 2, Fig. S 3). The siRNA-liposome-complex was incubated for 15 min at room temperature and finally 500 MCD4 cells in 30 µl medium were added, using the EL406™ dispenser module.

2.2.4.6 Determination of cell viability *via* alamarBlue®

In 384 well format, MCD4 cell viability was determined using alamarBlue® cell health indicator. According to the protocol, 5 µl alamarBlue® cell viability reagent were added to 50 µl cell suspension. After incubation for four hours at 37°C, the absorbance of alamarBlue® was measured at 570 nm, using 600 nm as a reference wavelength, utilizing the Enspire®2300. The alamarBlue® absorbance at 570 nm is proportional to the amount of living cells.

2.2.5 Immunofluorescence microscopy

2.2.5.1 Immunofluorescent detection of proteins

Cells were grown to confluency on cover slides with 12 mm diameter. Medium was aspirated and the cells were fixed with 2.5 % PFA for 15 min at room temperature. Cells were washed three times with 1x PBS and permeabilised with 0.1 % Triton X-100 for 5 min at room temperature. Unspecific binding was inhibited by blocking with 0.27 % fish skin gelatine for 60 min at 37°C. Cells were incubated with anti-AQP2 antibody H27 (1:500 dilution of H27, stored with glycerol 1:1; resulting in final 1:1000 dilution) for 60 min at 37°C and washed afterwards three times with 1x PBS. Cells were incubated with secondary anti-rabbit antibody (1:500) and 1x DAPI for 60 min at 37°C and finally were washed with 1x PBS. Using Imm-mount™, cover slides were fixed on microscope slides and stored at 4°C overnight.

Using 384 well GREINER microplates 781091, the BioTEK microplate washer was used for aspiration and washing steps. Detailed settings are appended (Tab. S 1, Tab. S 2, Tab. S 3, Tab. S 4) and protocol names are indicated in italics. Initially, the washer was primed with 1x PBS, starting *PRIME_200*. Medium was aspirated by running *GREINER 10*, leaving 10 µl residual volume per well. Using either the BioTEK Elx406 dispenser module or an Eppendorf Research Pro multichannel pipette, 40 µl of 3.125 %PFA were added per well, resulting in 2.5 % PFA in 50 µl. After 15 min incubation at room temperature, cells were washed three times with 1x PBS by running *GREINER*. The remaining volume was reduced to 10 µl per well by activating *GREINER 10*. 40 µl of 0.125 % Triton X-100 were added to each well. Cells were incubated for 5 min at room temperature and washed afterwards (*GREINER*). Again, the remaining volume was reduced to 10 µl (*GREINER 10*). 40 µl blocking buffer per well were added and microplates were incubated for 60 min at 37°C. Upon aspiration (*GREINER 10*), 20 µl of H27 (1:333 of H27, diluted 1:1 in glycerol, results in final 1:1000 H27 in 30 µl) were dispensed and microplates were incubated for 60 min at 37°C. Cells were washed (*GREINER*), PBS was aspirated (*GREINER 10*) and 20 µl 1.5x DAPI plus 1:400 fluorescently labelled anti-rabbit secondary antibody, diluted 1:1 in glycerol, were dispensed. Finally, cells were washed three times with 1x PBS (*GREINER*) and stored at 4°C before microscopic analysis.

2.2.5.2 Microscope settings

2.2.5.2.1 Arrayscan VTI HCS Reader

384 well microplates were analysed by automated microscopy, using the ArrayScan V^{TI} HCS Reader (Thermo Fisher Scientific/Cellomics, Bonn, DE). Two channels were recorded, applying the filters BGRFR_386_23 and BGRFR_549_15 to detect DAPI and Cy3 signals, respectively. With 20x magnification, 81 image fields (Fig. 5) per well and channel were acquired, resulting in 62,208 images per microplate (384 x 81 x 2). Images were acquired in high resolution camera mode (1024 x 1024). Exposure was set manually. Auto focus on DAPI signal in channel 1 was applied in each image field.

80	79	78	77	76	75	74	73	72
49	48	47	46	45	44	43	42	71
50	25	24	23	22	21	20	41	70
51	26	9	8	7	6	19	40	69
52	27	10	1	0	5	18	39	68
53	28	11	2	3	4	17	38	67
54	29	12	13	14	15	16	37	66
55	30	31	32	33	34	35	36	65
56	57	58	59	60	61	62	63	64

Fig. 5. Images field per well. ArrayScan VTI HCS Reader acquires 81 image fields per well of a 384 well microplate when set to 20x magnification. Pictures are recorded in spiral order starting with image field 0 from the centre of the well.

2.2.5.2.2 LSM 780

Object slides were analysed with LSM780 confocal laser scanning microscope, applying 40x magnification. Two channels were acquired: (i) DAPI, using a 405 nm laser and filter for 415-502 nm, and (ii) Cy3, using a 561 nm laser and filter for 563-699 nm. Pinholes were set to 100-130 μ M, digital gain remained 1.00 and master gain was adjusted to approximately 550 for both channels.

2.2.6 CellProfiler

The software CellProfiler was used for detailed image analysis. AQP2 speckles and nuclei were identified as objects and specific image and object features were extracted. The settings of these measurements are defined in so-called modules. All modules together form a pipeline, which was applied on 8 bit TIFF images.

A-MeasureImageIntensity:

Image to measure:OrigBlue,[OrigRed]

ExportToSpreadsheet:

Intensity_MinIntensity_OrigBlue,[Intensity_MinIntensity_OrigRed]
 Intensity_StdIntensity_OrigBlue,[Intensity_StdIntensity_OrigRed]
 Intensity_TotalIntensity_OrigBlue,[Intensity_TotalIntensity_OrigRed]
 Intensity_PercentMaximal_OrigBlue,[Intensity_PercentMaximal_OrigRed]
 Intensity_TotalArea_OrigBlue,[Intensity_TotalArea_OrigRed]
 Intensity_MADIntensity_OrigBlue,[Intensity_MADIntensity_OrigRed]
 Intensity_MeanIntensity_OrigBlue,[Intensity_MeanIntensity_OrigRed]
 Intensity_MaxIntensity_OrigBlue,[Intensity_MaxIntensity_OrigRed]
 Intensity_MedianIntensity_OrigBlue,[Intensity_MedianIntensity_OrigRed]

B-IdentifyPrimaryObjects:

Input image:OrigBlue

Primary objects to be identified:Nuclei

Typical diameter of objects, in pixel units (Min,Max):25,100

Discard objects outside the diameter range?:Yes

Try to merge too small objects with nearby larger objects?:Yes

Discard objects touching the border of the image?:No

Select the thresholding method:Otsu Global

Threshold correction factor:1

Lower and upper bounds on threshold:0.0125,1.0

Approximate fraction of image covered by objects?:0.01

Method to distinguish clumped objects:Shape

Method to draw dividing lines between clumped objects:Shape

Size of smoothing filter:10

Suppress local maxima that are closer than this minimum allowed distance:7

Speed up by using lower-resolution image to find local maxima?:No

Name the outline image:NucleiOutlines

Fill holes in identified objects?:Yes

Automatically calculate size of smoothing filter?:Yes

Automatically calculate minimum allowed distance between local maxima?:Yes

Manual threshold:0.0

Select binary image:None

Retain outlines of the identified objects?:Yes

Automatically calculate the threshold using the Otsu method?:Yes

Enter Laplacian of Gaussian threshold:0.5

Two-class or three-class thresholding?:Three classes

Minimise the weighted variance or the entropy?:Weighted variance

Assign pixels in the middle intensity class to the foreground or the background?:Background

Automatically calculate the size of objects for the Laplacian of Gaussian filter?:Yes

Enter LoG filter diameter:5

Handling of objects if excessive number of objects identified:Continue

Maximum number of objects:500

C-ExpandOrShrinkObjects:

Input objects:Nuclei

Output objects: ExpandedNuclei4,[5,6,7,8,9]

Select the operation:Expand objects by a specified number of pixels

Number of pixels by which to expand or shrink:4,[5,6,7,8,9]

Fill holes in objects so that all objects shrink to a single point?:No

Retain the outlines of the identified objects for use later in the pipeline:Yes

Name the outline image:ExpandedNucleiOutlines4,[5,6,7,8,9]

D-MeasureObjectIntensity:

Image to measure:OrigBlue, [OrigRed]

Objects to measure:Nuclei, [ExpandedNuclei4,5,6,7,8,9]

ExportToSpreadsheet:

Intensity_StdIntensityEdge_OrigBlue,[Intensity_StdIntensityEdge_OrigRed]

Intensity_MinIntensity_OrigBlue,[Intensity_MinIntensity_OrigRed]
 Intensity_IntegratedIntensityEdge_OrigBlue,[Intensity_IntegratedIntensityEdge_OrigRed]
 Intensity_StdIntensity_OrigBlue,[Intensity_StdIntensity_OrigRed]
 Intensity_MassDisplacement_OrigBlue,[Intensity_MassDisplacement_OrigRed]
 Intensity_UpperQuartileIntensity_OrigBlue,[Intensity_UpperQuartileIntensity_OrigRed]
 Intensity_LowerQuartileIntensity_OrigBlue,[Intensity_LowerQuartileIntensity_OrigRed]
 Intensity_MinIntensityEdge_OrigBlue,[Intensity_MinIntensityEdge_OrigRed]
 Intensity_MeanIntensity_OrigBlue,[Intensity_MeanIntensity_OrigRed]
 Intensity_MeanIntensityEdge_OrigBlue,[Intensity_MeanIntensityEdge_OrigRed]
 Intensity_MaxIntensity_OrigBlue,[Intensity_MaxIntensity_OrigRed]
 Intensity_MedianIntensity_OrigBlue,[Intensity_MedianIntensity_OrigRed]
 Intensity_IntegratedIntensity_OrigBlue,[Intensity_IntegratedIntensity_OrigRed]
 Intensity_MaxIntensityEdge_OrigBlue,[Intensity_MaxIntensityEdge_OrigRed]

E-MeasureTexture:

Image to measure:OrigRed
 Objects to measure:Nuclei, [ExpandedNuclei4,5,6,7,8,9]
 Texture scale to measure:3
 Texture scale to measure:4
 Measure Gabor features?:No
 Number of angles to compute for Gabor:4
 ExportToSpreadsheet: [of ExpandedNuclei4,5,6,7,8,9]
 Texture_DifferenceEntropy_OrigRed_3,[4]
 Texture_InfoMeas1_OrigRed_3,[4]
 Texture_DifferenceVariance_OrigRed_3,[4]
 Texture_SumVariance_OrigRed_3,[4]
 Texture_AngularSecondMoment_OrigRed_3,[4]
 Texture_Entropy_OrigRed_3,[4]
 Texture_Correlation_OrigRed_3,[4]
 Texture_SumAverage_OrigRed_3,[4]
 Texture_Variance_OrigRed_3,[4]
 Texture_InverseDifferenceMoment_OrigRed_3,[4]
 Texture_SumEntropy_OrigRed_3,[4]
 Texture_Contrast_OrigRed_3,[4]
 Texture_InfoMeas2_OrigRed_3,[4]

F-MeasureObjectSizeShape:

Objects to measure:Nuclei, [ExpandedNuclei4,5,6,7,8,9]
 ExportToSpreadsheet: [ExpandedNuclei4,5,6,7,8,9]
 AreaShape_Perimeter,
 AreaShape_FormFactor,
 AreaShape_Orientation,
 AreaShape_Area,
 AreaShape_Solidity,
 AreaShape_EulerNumber,
 AreaShape_Compactness,
 AreaShape_Extent,
 AreaShape_Eccentricity,
 AreaShape_MinorAxisLength,
 AreaShape_MajorAxisLength,
 AreaShape_Center_Y,
 AreaShape_Center_X,

G-EnhanceOrSuppressFeatures:

Input image:OrigRed
 Output image:EnhancedRed3,[EnhancedRed4]
 Select the operation:Enhance
 Feature size:3,[4]
 Feature type:Speckles
 Range of hole sizes:1,10

H-IdentifyPrimaryObjects:

Input image:EnhancedRed3,[EnhancedRed4]
 Primary objects to be identified:Speckles3-1,[3-2,3-3,3-4,3-5,3-6,4-1,4-2,4-3,4-4,4-5,4-6]
 Typical diameter of objects, in pixel units (Min,Max):3,5
 Discard objects outside the diameter range?:Yes
 Try to merge too small objects with nearby larger objects?:No
 Discard objects touching the border of the image?:Yes
 Select the thresholding method:RobustBackground PerObject
 Threshold correction factor:0.55,[0,60;0,65;0,70;0,75;0,80]
 Lower and upper bounds on threshold:0.01,0.7
 Approximate fraction of image covered by objects?:0.01
 Method to distinguish clumped objects:Intensity
 Method to draw dividing lines between clumped objects:Intensity
 Size of smoothing filter:1
 Suppress local maxima that are closer than this minimum allowed distance:2
 Speed up by using lower-resolution image to find local maxima?:No
 Name the outline image:SpecklesOutlines3-1, [3-2,3-3,3-4,3-5,3-6,4-1,4-2,4-3,4-4,4-5,4-6]
 Fill holes in identified objects?:Yes
 Automatically calculate size of smoothing filter?:No
 Automatically calculate minimum allowed distance between local maxima?:No
 Manual threshold:0.0
 Select binary image:None
 Retain outlines of the identified objects?:Yes
 Automatically calculate the threshold using the Otsu method?:Yes
 Enter Laplacian of Gaussian threshold:0.5
 Two-class or three-class thresholding?:Two classes
 Minimise the weighted variance or the entropy?:Weighted variance
 Assign pixels in the middle intensity class to the foreground or the background?:Foreground
 Automatically calculate the size of objects for the Laplacian of Gaussian filter?:Yes
 Enter LoG filter diameter:5
 Handling of objects if excessive number of objects identified:Continue
 Maximum number of objects:500
 Select the measurement to threshold with:None

I-RelateObjects:

Input child objects:Speckles3-1 [3-2,3-3,3-4,3-5,3-6,4-1,4-2,4-3,4-4,4-5,4-6]
 Input parent objects:ExpandedNuclei4[5,6,7,8,9]
 Calculate distances?:None
 Calculate per-parent means for all child measurements?:No
 Calculate distances to other parents?:No
 Parent name:None

J-ExportToSpreadsheet:

Count_Nuclei,
 Count_Speckles3-1[3-2,3-3,3-4,3-5,3-6,4-1,4-2,4-3,4-4,4-5,4-6]

Fig. 6. Summary of CellProfiler pipeline. Settings of major 10 of in total 194 modules are described (A-J). Square brackets indicate other objects or images on which the same module with identical parameters was applied. A Intensity parameters of images OrigBlue (DAPI channel) and OrigRed (H27-Cy3 channel) were measured and exported. B Nuclei were identified as primary objects and (C) expanded by 4, 5, 6, 7, 8 or 9 pixels. D Intensity of OrigBlue image within nuclei objects and intensity of OrigRed image within nuclei and expanded nuclei objects were measured and exported. E Texture parameters of OrigRed image within nuclei and expanded nuclei were measured and exported. F Area shape characteristics of nuclei and expanded nuclei were measured and exported. G OrigRed image was enhanced by a factor of 3 or 4. H Based on OrigRed enhancements by 3 or 4 AQP2 speckles were identified applying threshold corrections factors 0.55, 0.60, 0.65, 0.70, 0.75 or 0.80. I Speckles were related to expanded nuclei. J Number of nuclei and speckles was measured and exported.

2.2.7 Statistics

Statistical analysis was performed using GraphPad Prism5. Unpaired t-test or one-way ANOVA with posthoc Bonferonni were applied. Significant differences are indicated as $p \leq 0.05 = *$, $p \leq 0.01 = **$, $p \leq 0.001 = ***$. Mean plus standard error of mean (SEM) are plotted.

The quality of an assay can be evaluated by the Z'-factor (Z'^{417}). It is calculated from means (μ) and standard deviations (σ) of positive (p) and negative (n) controls: μ_p , μ_n , σ_p , σ_n :

$$Z' = 1 - 3(\sigma_p + \sigma_n) / |\mu_p - \mu_n|$$

Z' can never exceed 1.0. Z' between 0.5 – 1.0 describes an excellent, between 0.0 – 0.5 a marginal readout. Z' below 0.0 marks poor quality assay setups.

3 RESULTS

In order to investigate the AQP2 redistribution, a kidney cell line was needed in which AQP2 is expressed and inserted into the plasma membrane upon the elevation of cAMP. With regard to screening procedures strongly adherent cells are sought as detaching during automated washing procedure is minimised.

3.1 MCD4 cells are appropriate for the analysis of the AQP2 redistribution

AQP2 protein expression in five mammalian kidney cell lines was analysed by Western Blotting. In mouse collecting duct (MCD4) cells high AQP2 protein abundance was detected but neither in mouse-derived cortical collecting duct (mTERT-CCD) nor in the human kidney cell lines HEK293, HK2 and HKC8 (Fig. 7).

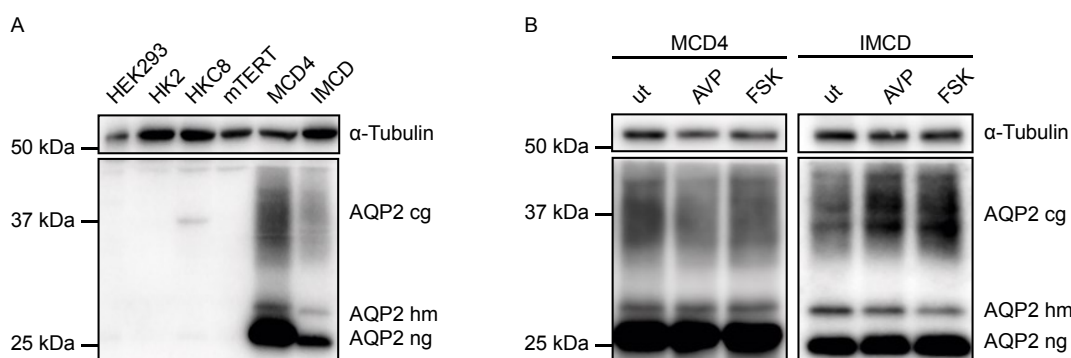


Fig. 7. AQP2 protein expression in mammalian kidney cells. A) AQP2 was expressed in MCD4 and rat primary IMCD cells. Glycosylation forms are indicated. **B)** Protein abundance of AQP2 cg increased upon stimulation with AVP or FSK in IMCD but not MCD4 cells. Cells were stimulated with 100 nM AVP or 30 μ M FSK for 30 min and lysed (2.2.3.1). Western Blotting was carried out with AQP2 (C17) and α -Tubulin (DM1a) antibodies. HEK293, human embryonic kidney cell line⁴⁰⁵; HK2, human kidney cell line; HKC8, human kidney cell line; mTERT, mouse collecting duct cells⁴⁰⁸; MCD4, mouse collecting duct cells⁴⁰⁷; IMCD, inner medullary collecting duct⁴⁰⁹; cg, complex glycosylated; hm, high mannose; ng, non-glycosylated; ut, unstimulated AVP, arginine-vasopressin, FSK, forskolin.

As expected, AQP2 is expressed in rat primary inner medullary collecting duct (IMCD) cells that were used as a positive control. Bands representing non glycosylated (ng), high mannose glycosylated (hm) and complex glycosylated (cg) AQP2 were observed. In rat primary IMCD cells, AQP2 protein abundance increased, if the cAMP level was elevated upon the V2R activation by AVP or the direct stimulation of AC by FSK^{404,409} (Fig. 7B). In MCD4 cells no cAMP-dependent increase of AQP2 protein level was detected upon FSK- or AVP-stimulation (Fig. 7B). The most likely explanation for this observation might be that the transcription of AQP2 in MCD4 cells is controlled by human cytomegalovirus immediate early promoter (CMV), driving constitutively high expression^{407,418}.

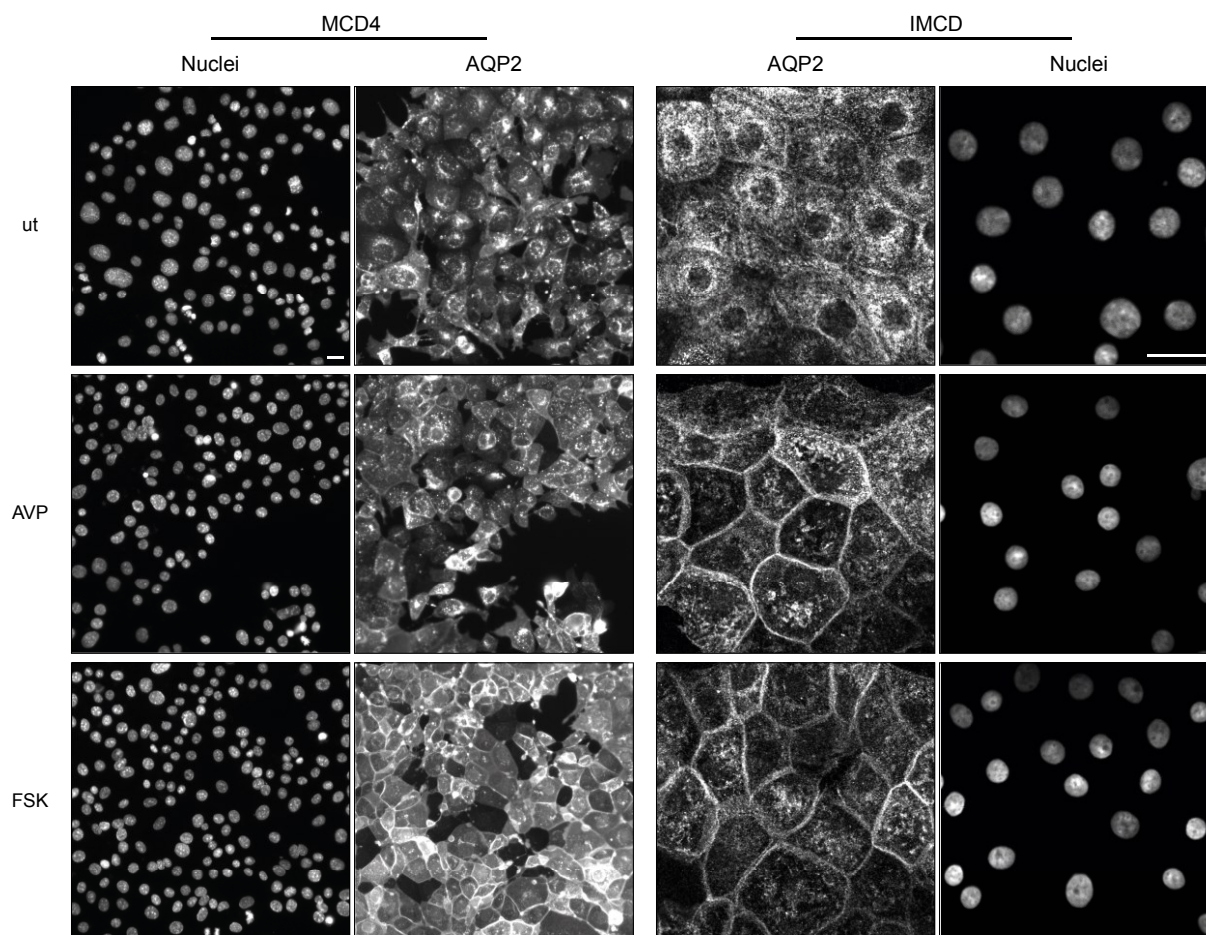


Fig. 8. The microscopic detection of the AQP2 translocation in MCD4 and primary IMCD cells. In IMCD cells, AQP2 inserted into the plasma membrane upon cAMP elevation in response to AVP and FSK. After stimulation with FSK but not AVP, the AQP2 redistribution was detected in MCD4 cells. Cells were treated with 100 nM AVP or 30 μ M FSK for 30 min. Nuclei and AQP2 were visualised with DAPI and H27 plus Cy5-labelled secondary antibody (Jackson ImmunoResearch, Newmarket, UK; #711-176-152), respectively. Images were acquired with confocal laser scanning microscope LSM780 using 40x magnification (IMCD) and ArrayScan V^{TI} HCS Reader using 20x magnification (MCD4). The scale bars indicate 20 μ m. ut, unstimulated; AVP, arginine-vasopressin; FSK, forskolin. Representative images are shown.

Rat primary IMCD cells show AQP2 plasma membrane localisation after stimulation with both FSK or AVP (Fig. 8). In contrast, AQP2 redistribution in MCD4 cells was observed upon FSK but not AVP treatment. The resistance of MCD4 cells towards AVP is explained by the lack of V2R expression (Fig. 9B). The cell line was generated by stably transfecting mouse cortical M1 cells⁴⁰⁶ with human *AQP2* cDNA⁴⁰⁷ (Fig. 9A). To confirm the *AQP2* sequence, genomic DNA was isolated from M1 and MCD4 cells. The *AQP2* cDNA was amplified *via* PCR using specific primers hAQP2-forw-1 and hAQP2-rev-816 (Tab. 7). The amplicon was subjected to agarose gel electrophoresis, excised from the gel, purified and validated by sequence analysis. Thus, MCD4 cells are appropriate for the analysis of the AQP2 redistribution. With a mean diameter of 20 to 40 μ m MCD4 cells are of similar size as rat primary IMCD cells. They are attached tightly to the cell culture dish, which facilitates automated washing procedures during large-scale experiments.

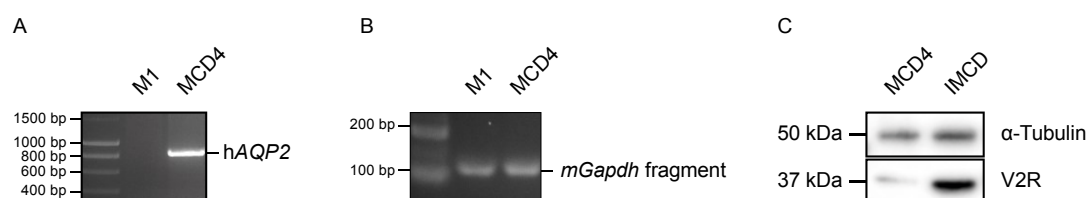


Fig. 9. The expression of human AQP2 but not V2R in MCD4 cells. MCD4 cells were generated by stably transfecting M1 cells with human (h) AQP2 cDNA⁴⁰⁷. Genomic DNA of M1 and MCD4 cells was isolated and (A) hAQP2 and (B) a fragment of mouse (m) *Gapdh* were amplified via PCR using specific primers (Tab. 7). DNA was subjected to agarose gel electrophoresis. hAQP2 cDNA comprises 816 base pairs (bp), *mGapdh* fragment comprises 101 bp. (C) Cells were lysed and proteins were detected by Western Blotting with V2R (K3) and α -Tubulin (DM1a) antibodies. The antibody K3 (provided by Prof. Dr. Bachman, Charité, Berlin) targets the second intracellular loop of the V2R, whose amino acids are identical in murine and rat receptors (Fig. S 1).

3.2 Experimental design

RNA interference (RNAi) is used to inhibit the expression of specific genes and to analyse its biological function. Gene expression is silenced post-transcriptionally by short interfering ribonucleic acids (siRNA), which block the translation of specific mRNA transcripts (2.2.4.5). This mechanism was utilised to investigate the AQP2 redistribution in MCD4 cells and to identify involved proteins. Gene products, whose knockdown prevents the insertion of AQP2 into the plasma membrane were to be identified. In 384 well microtiter plates MCD4 cells were transfected with a Mouse Protein Kinase sublibrary (Fig. 10A, 3.4, 2.2.4.5) that is part of a genome-wide siRNA library (2.1.3, 3.3). Three days after transfection cells were stimulated with FSK to elevate cAMP and thereby, to trigger the AQP2 translocation (Fig. 10B). Cells were fixed and labelled fluorescently.

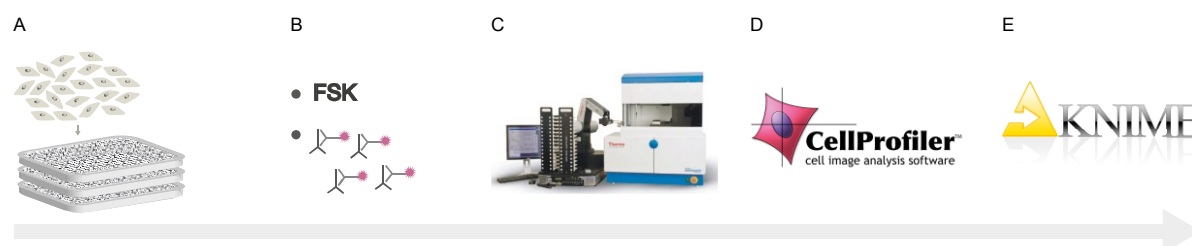


Fig. 10. The experimental design. A) MCD4 cells were transfected with a Mouse Protein Kinases siRNA library in 384 well plates. B) Three days after transfection, cells were stimulated with 30 μ M FSK for 60 min. Cells were fixed and labelled fluorescently. C) Images were acquired via automated immunofluorescence microscopy, using an ArrayScan V^{TI} HCS Reader. D) Applying CellProfiler software, images were analysed in detail and image features were extracted. E) Based on metadata generated by the CellProfiler, cells were classified and hits were visualised using KNIME software. All steps were performed in cooperation with Sabrina Kleissle, Dr. Katina Lazarow, Dr. Martin Neuenschwander and Marc Wippich from the FMP Screening Unit, headed by Dr. Jens Peter von Kries. The CellProfiler-based image analysis was run on a computer cluster that was provided by Dr. Jean-Fred Fontaine and Dr. Miguel Andrade.

Images were obtained by automated immunofluorescence microscopy using an ArrayScan V^{TI} HCS Reader (Fig. 10C, 3.5) and analysed with the software CellProfiler⁴¹⁹ (Fig. 10D, 3.6). Extracted image features were forwarded to KNIME (Konstanz Information Miner, www.knime.org) to classify cellular phenotypes and thereby, to identify hits (Fig. 10E, 3.7). The experimental steps are explained in detail in the following section.

3.3 Mouse Protein Kinases siRNA sublibrary

The Mouse Protein Kinases siRNA sublibrary is part of the Mouse siGENOME siRNA library-SMART pool (2.1.3). Within the genome-wide siRNA library 16,872 genes are targeted. Four different siRNAs directed against various positions of one mRNA transcript are pooled per well (Tab. S 2). siRNA molecules were generated in 2008, based on annotations of Reference Sequence Database release 32 (RefSeq, <ftp://ftp.ncbi.nlm.nih.gov/refseq/release/release-catalog/archive/>) published by the National Center for Biotechnology Information (NCBI, www.ncbi.nlm.nih.gov). The genome-wide library comprises three additional sublibraries: Mouse GPCR, Mouse Druggable and Mouse Genome (2.1.3). As MCD4 cells do not express V2R (Fig. 9B) and downstream AC was to be stimulated in order to raise the cytosolic cAMP level, the Mouse GPCR sublibrary was not considered relevant for this experiment. For the present work, the Mouse Protein Kinases sublibrary was screened, comprising three 384 well microtiter plates and targeting a total of 719 genes (Tab. S 1).

3.4 Reverse siRNA transfection of MCD4 cells

MCD4 cells were transfected reversely, i.e. seeded onto the siRNA-liposome complexes. For maximal transfection efficiency optimum cell number, siRNA concentration and amount of transfection reagent were determined. Seeding of 1000 MCD4 cells per well resulted in a 100 % confluent layer after 72 hours (Fig. 11). Single cells could not be identified, as cells grew in multilayers and cell borders were not detectable. The mean cell area was smaller compared to cells in less confluent cell layers. 400 MCD4 cells per well grew to 80-90 % confluency within three days, representing the optimum density for microscopic analysis.

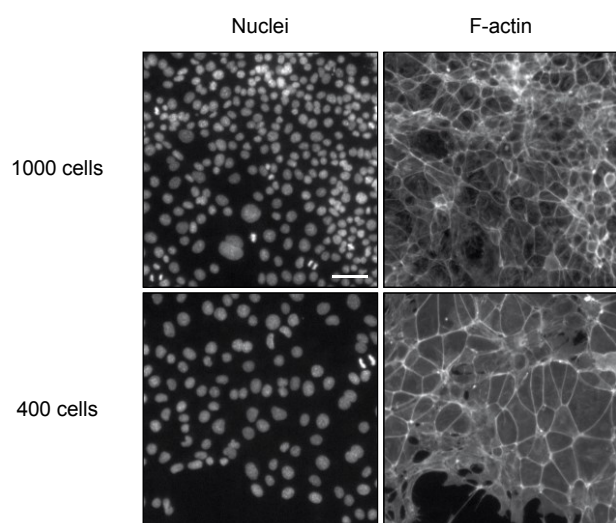


Fig. 11. Seeding of 400 cells per well of a microtiter plate results in optimal density for microscopic analysis. Nuclei and F-actin were visualised with DAPI and TRITC-Phalloidin, respectively. Images were acquired using an LSM780 confocal microscope (20x magnification). The scale bar indicates 50 μ m. Representative images are shown.

Thus, transfections were conducted with 400 cells per well. All experiments were performed exclusively with cell passage 42. To determine an ideal amount of transfection reagent cells were incubated with different amounts of Lipofectamine® 2000 in the absence of siRNA (mock transfection). After three days, cell viability was monitored using alamarBlue® cell health indicator and additionally by counting of nuclei (Fig. 12). The addition of 0.20 µl Lipofectamine® 2000 to a total transfection volume of 50 µl significantly reduced MCD4 cell viability (Fig. 12A) and number (Fig. 12B) compared to cells that were left untreated.

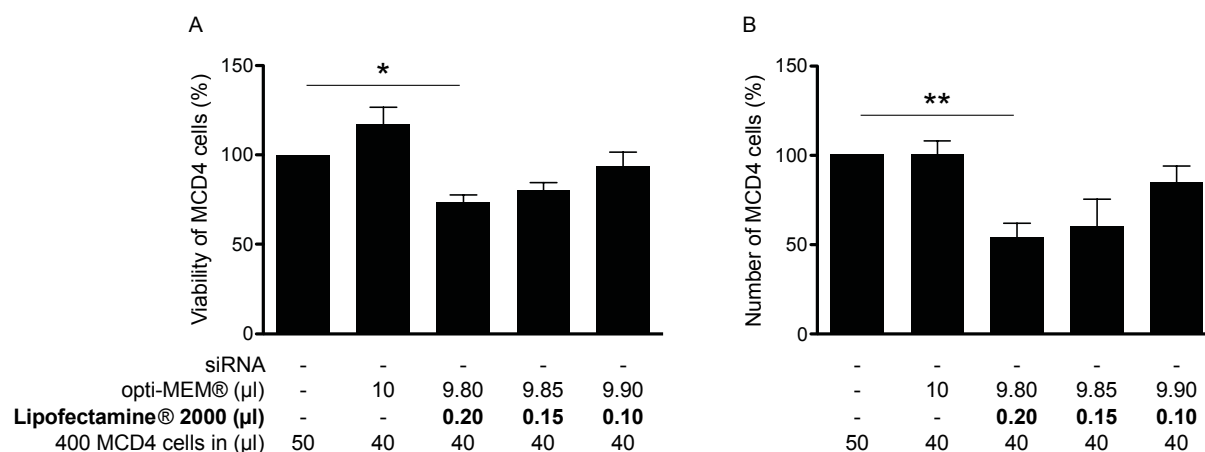


Fig. 12. Effect of Lipofectamine® 2000 transfection reagent on MCD4 cells. In each of the 384 wells of the microtiter plates 400 MCD4 cells were mock-transfected (without siRNA) using Lipofectamine® 2000. After 72 hours, viability of MCD4 cells was determined using alamarBlue® cell health indicator (A) and number of cells was monitored by nuclei counting (B). The addition of 0.2 µl transfection reagent per well significantly reduced cell viability and cell number. Lipofectamine® 2000 was diluted in opti-MEM® serum free medium, cells grew in the absence of antibiotics. Statistically significant differences were determined applying one-way ANOVA with posthoc Bonferroni. *, $p \leq 0.05$, **, $p \leq 0.01$. Mean \pm SEM are plotted.

The following experiments were conducted with 0.15 µl Lipofectamine® 2000 per well and were evaluated using the alamarBlue® assay. In order to define the most effective siRNA concentration, MCD4 cells were transfected with 20-70 nM toxic siRNA (TOX, Fig. 13). Compared to cells transfected with scrambled non-targeting siRNA (NT#2) in an equal concentration, TOX transfection resulted in the significant reduction of cell viability. Transfection with NT#2 led to a reduction in cell viability by approximately 10 % compared to mock transfection, indicating general off-target effects of siRNA. Up to 70 % transfection efficiency was reached using 50 nM siRNA, 0.15 µl Lipofectamine® 2000 and 400 MCD4 cells. Additionally, transfection efficiency was verified using 50 nM siRNA directed against hAQP2 mRNA or the expression of the housekeeping gene *Gapdh*. As confirmed by Western Blotting, abundance of specific target proteins was strongly reduced (Fig. 14). Complex glycosylated and high mannose AQP2 protein was efficiently knocked down, whereas α -Tubulin and GAPDH remained unaffected upon Aqp2 siRNA transfection. Transfection with 50 nM *Gapdh* siRNA led to the down regulation of GAPDH but neither of α -Tubulin nor of AQP2 protein.

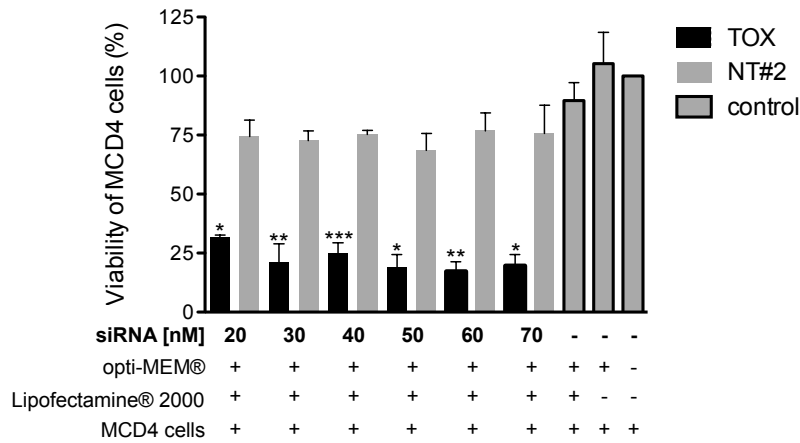


Fig. 13. Viability of MCD4 cells upon TOX-transfection. The transfection of 20-70 nM toxic siRNA (TOX) significantly reduced cell viability compared to transfection with scrambled non targeting siRNA (NT#2). In 50 μ l total volume, 400 MCD4 cells were transfected using 0.15 μ l Lipofectamine® 2000. After three days, cell viability was monitored using alamarBlue® cell health indicator. Cells were left untreated or as controls supplemented with opti-MEM® serum free medium only or mock-transfected. Statistically significant differences were determined applying one-way ANOVA with posthoc Bonferroni. *, $p \leq 0.05$, **, $p \leq 0.01$, *** $p \leq 0.001$. Mean \pm SEM are plotted.

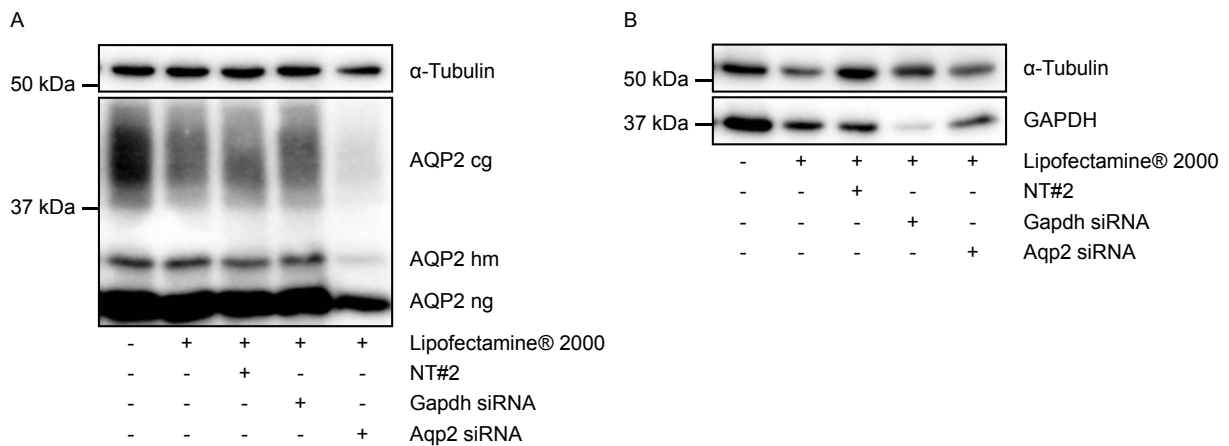


Fig. 14. siRNA transfection reduces target gene expression. **A)** AQP2 protein abundance was reduced upon transfection with Aqp2 siRNA but was not affected by transfection with Gapdh siRNA. **B)** After transfection with Gapdh but not Aqp2 siRNA the GAPDH protein level was decreased. The loading control α -Tubulin was not affected by Gapdh or Aqp2 siRNA transfection. MCD4 cells were transfected with 50 nM siRNA. Three days after transfection, cells were lysed and proteins were detected by Western Blotting with AQP2 (C17), GAPDH (14C10) and α -Tubulin (DM1a) antibodies.

3.5 Automated immunofluorescence microscopy

One strategy to investigate the redistribution of AQP2 is to analyse the co-localisation of AQP2 and the plasma membrane *via* automated immunofluorescence microscopy. Therefore, in 384 well microtiter plates the near plasma membrane region of MCD4 cells was detected by F-actin staining using TRITC-labelled Phalloidin. AQP2 was visualised with primary antibody H27⁴⁰⁴ in combination with Cy5-conjugated F(ab')₂ fragment donkey anti-rabbit secondary antibody (Fig. 15; Jackson ImmunoResearch Laboratories, #711-176-152). Early findings suggested that GFP-tagged AQP2 is useful to study AQP2 trafficking⁴²⁰. This could not be reproduced by other studies and until today image-based investigations of AQP2 localisation depend on immunofluorescent staining using specific antibodies.

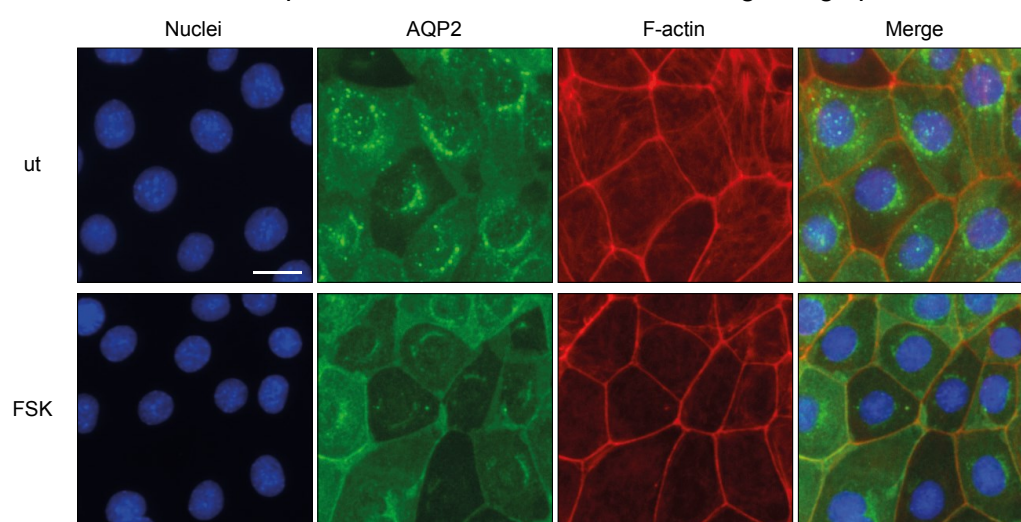


Fig. 15. Fluorescent staining of nuclei, AQP2 and F-actin of MCD4 cells. In 384 well plates nuclei, AQP2 and F-actin were visualised with DAPI, anti AQP2 antibody H27 plus Cy5-labelled secondary antibody (Jackson ImmunoResearch Laboratories; #711-176-152) and TRITC-Phalloidin, respectively. Images were acquired using an ArrayScan V^{TI} HCS Reader (20x magnification). The scale bar indicates 20 μ m. ut, unstimulated; FSK, forskolin. Representative images are shown.

During the optimisation of experimental conditions Jackson ImmunoResearch stopped producing the antibody #711-176-152. The fluorophore Cy5 was replaced by Alexa Fluor 647, having similar excitation and emission spectra (Fig. 16A-D). Alexa Fluor 647-conjugated antibodies did, however, reveal extracellular aggregates and high background staining (Fig. 16B,C). Unexpectedly, neither the Cy5-labelled IgG antibody (Fig. 16D) nor the Cy3-conjugated F(ab')₂ fragment (Fig. 16E) did result in high quality staining that is indispensable for image analysis. By testing secondary antibodies that were not raised in donkey (Fig. 16F-H), the combination of the anti AQP2 antibody H27 and Cy3-conjugated mouse anti-rabbit IgG (H27-Cy3, #211-165-109; Fig. 16H) resulted in specific AQP2 staining. Unlike initial conditions (Fig. 16A, Fig. S 5) background staining was observed. However, in contrast to other secondary antibodies (Fig. 16B-G) extracellular aggregates were not visible (Fig. 16H). Thus, the following experiments were performed with the secondary antibody #211-165-109.

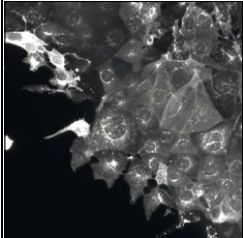
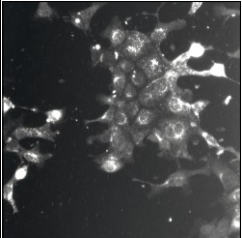
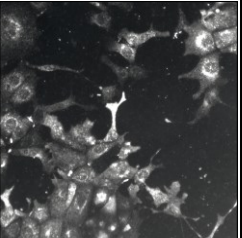
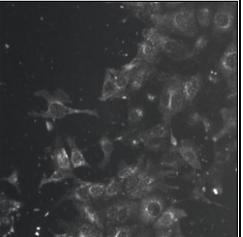
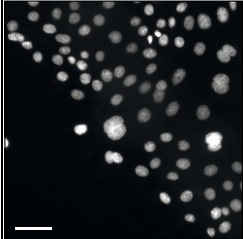
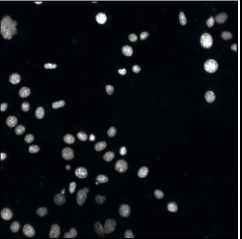
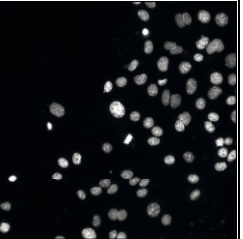
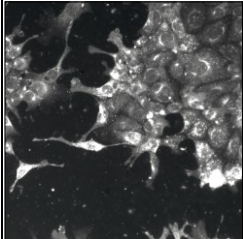
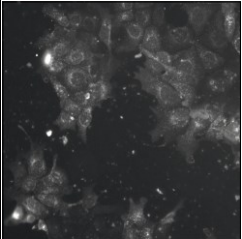
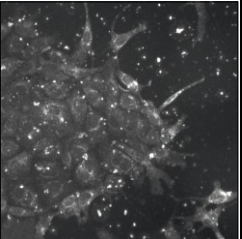
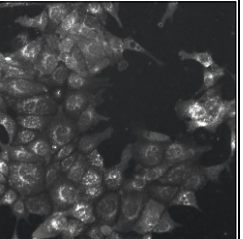
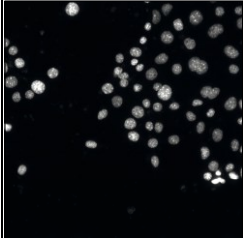
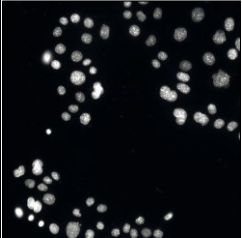
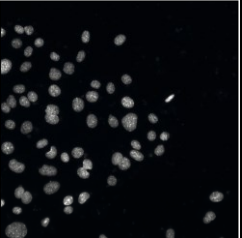
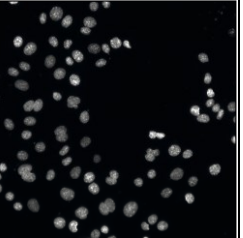
	A	B	C	D
Article number #	711-176-152	711-606-152	711-605-152	711-175-152
Raised in	donkey	donkey	donkey	donkey
Against	rabbit	rabbit	rabbit	rabbit
IgG-form	F(ab') ₂	F(ab') ₂	whole IgG	whole IgG
Conjugated dye	Cy5	Alexa Fluor 647	Alexa Fluor 647	Cy5
Excitation peak (nm)	650	651	651	650
Emission peak (nm)	670	667	667	670
H27 +				
DAPI				
	E	F	G	H
Article number #	711-166-152	111-095-003	111-225-144	211-165-109
Raised in	donkey	goat	goat	mouse
Against	rabbit	rabbit	rabbit	rabbit
IgG-form	F(ab') ₂	whole IgG	whole IgG	whole IgG
Conjugated dye	Cy3	FITC	Cy2	Cy3
Excitation peak (nm)	550	492	492	550
Emission peak (nm)	570	520	510	570
H27 +				
DAPI				

Fig. 16. Immunofluorescent staining of AQP2 in MCD4 cells using H27 and different secondary antibodies. AQP2 was visualised using rabbit-derived H27 primary antibody in combination with one of eight secondary anti-rabbit antibodies. Secondary antibodies were purchased from Jackson ImmunoResearch Laboratories, article numbers are indicated. **A)** The production of #711-176-152 was stopped. **B-G)** H27 plus secondary antibodies revealed unspecific extracellular signals. **H)** #211-165-109 specifically recognised AQP2-H27. Nuclei were stained with DAPI. Images were acquired using an ArrayScan V^{II} HCS Reader (20x magnification). The scale bar indicates 50 µm. Representative images are shown.

Microscopic analysis was conducted within seven days after fluorescent staining to avoid time-dependent signal decrease⁴²¹. Images were acquired using an ArrayScan V^{TI} HCS Reader automated microscope. Using the high resolution camera mode 1024 x 1024 pixel sized images were generated. Best imaging results were obtained by using ultrathin optical bottom (190 μ m) 384 well microtiter plates (GREINER, μ clear, Fig. S 4). Applying 20 fold magnification one well splits into 81 image fields, requiring 81 focussing events (Fig. 5). The acquisition of three channels (nuclei, AQP2, plasma membrane) per image field resulted in 243 images per well and required approximately 24 hours per microtiter plate. Files generated by the ArrayScan V^{TI} HCS Reader were saved in a proprietary file format (12 bit Cellomics C01), which cannot be processed by common image analysis programs and thus, were exported to 8 bit TIFF files. In doing so, the number of grey values was reduced to $2^8 = 256$. Alternatively, 16 bit TIFF files could have been created providing $2^{16} = 65,536$ possible grey values per pixel. However, in order to avoid the distortion of the original data by generating additional grey values that were not recorded, images would have to be rescaled to equivalent ranges in downstream applications. Overall, this would double storage space from approximately 60 GB to 120 GB per microtiter plate considering raw images only and was therefore not performed in this work. Depending on cell density and the duration of focussing, image acquisition and subsequent file conversion required up to 30 hours per microtiter plate.

3.6 Image analysis using CellProfiler

Images, generated by automated immunofluorescence microscopy were analysed automatically to quantitatively evaluate cellular phenotypes in an unbiased approach. Specific image features were extracted using CellProfiler advanced image analysis software. Within several so-called modules thresholds, smoothing filters and segmentation methods were defined to identify nuclei, plasma membrane and AQP2. In order to distinguish phenotypes of unstimulated and FSK-stimulated cells, AQP2 plasma membrane signals, predicted to increase upon AQP2 redistribution, were quantified. However, this strategy failed for two reasons. First, F-actin-labelling was variable as it depends on the cytosolic cAMP level¹⁶⁸. Although the F-actin signal was consistently most intense at the plasma membrane, overall intensity decreased upon FSK stimulation (Fig. 15) as previously observed in IMCD and CD8 cells^{168,169}. The precise and transferable identification of the plasma membrane could not be achieved (Fig. 17A). Second, the difference of AQP2 mean signal ratios in

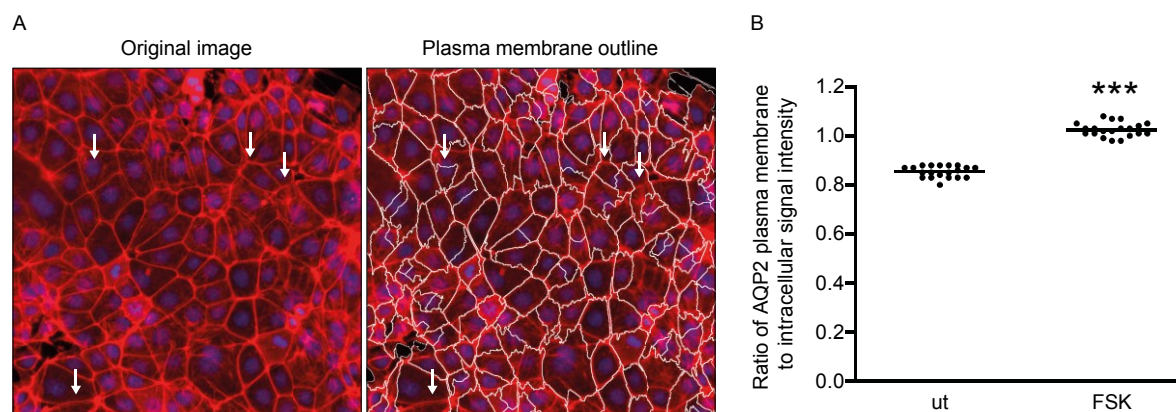


Fig. 17. Intensity of AQP2 signals within defined plasma membrane regions. **A)** Plasma membrane identification using CellProfiler image analysis software did not result in precisely defined regions. Based on F-actin staining, plasma membrane was defined using the Watershed-Gradient method, three classes Otsu per object thresholding applying threshold correction factor 0.4 within 0.0001-0.095 lower and upper limits of threshold. Nuclei are shown in blue, F-actin is depicted in red. White arrows highlight examples for identification errors. **B)** Ratios of AQP2 plasma membrane to intracellular signal intensity increased upon FSK treatment. The signal window between control and stimulated condition was too small to assign unknown phenotypes. Statistically significant differences were determined applying the unpaired t-test. *** $p \leq 0.001$. ut, unstimulated; FSK, forskolin.

plasma membrane regions under control and FSK-stimulated conditions, which is defined as separation band, was not big enough, albeit significant (Fig. 17B). The separation band forms a “signal window”, in which hits can be identified. It is evaluated by the Z' -factor (Z'), a statistical parameter to judge an assays quality. Z' integrates means and standard deviations of positive and negative controls and needs to exceed 0.5 to guarantee an excellent readout (2.2.7). The signal window emerging from analysis of AQP2 plasma membrane to intracellular signal intensities under unstimulated and stimulated conditions resulted in $Z' = -0.047$ and thus, was not suitable for the detection of an AQP2 redistribution. An alternative strategy to quantify the AQP2 redistribution is to monitor perinuclear AQP2 speckles that decrease upon FSK stimulation (Fig. 15). A CellProfiler pipeline comprising 194

modules was generated (Fig. 6) to first identify nuclei and expand nucleus outlines by 4, 5, 6, 7, 8 or 9 pixels in order to include differently sized perinuclear regions; second, to define AQP2 speckles applying 6 different thresholds (0.55, 0.60, 0.65, 0.70, 0.75 or 0.80) based on prior signal expansion by a factor of 3 or 4; and third, to relate all AQP2 speckles to each of the six nucleus outlines (Fig. 18). In total, AQP2 speckles per nucleus were determined by 72 alternative settings (Fig. 19), which allows applying the pipeline on different microtiter plates without prior adjustment. If performed on a standard desktop computer, image analysis by the CellProfiler pipeline requires 385 hours to process 62,208 images derived from one 384 well microtiter plate. The time was reduced to 5 hours per microtiter plate by running the pipeline on a computer cluster, which uses 500 processors simultaneously.

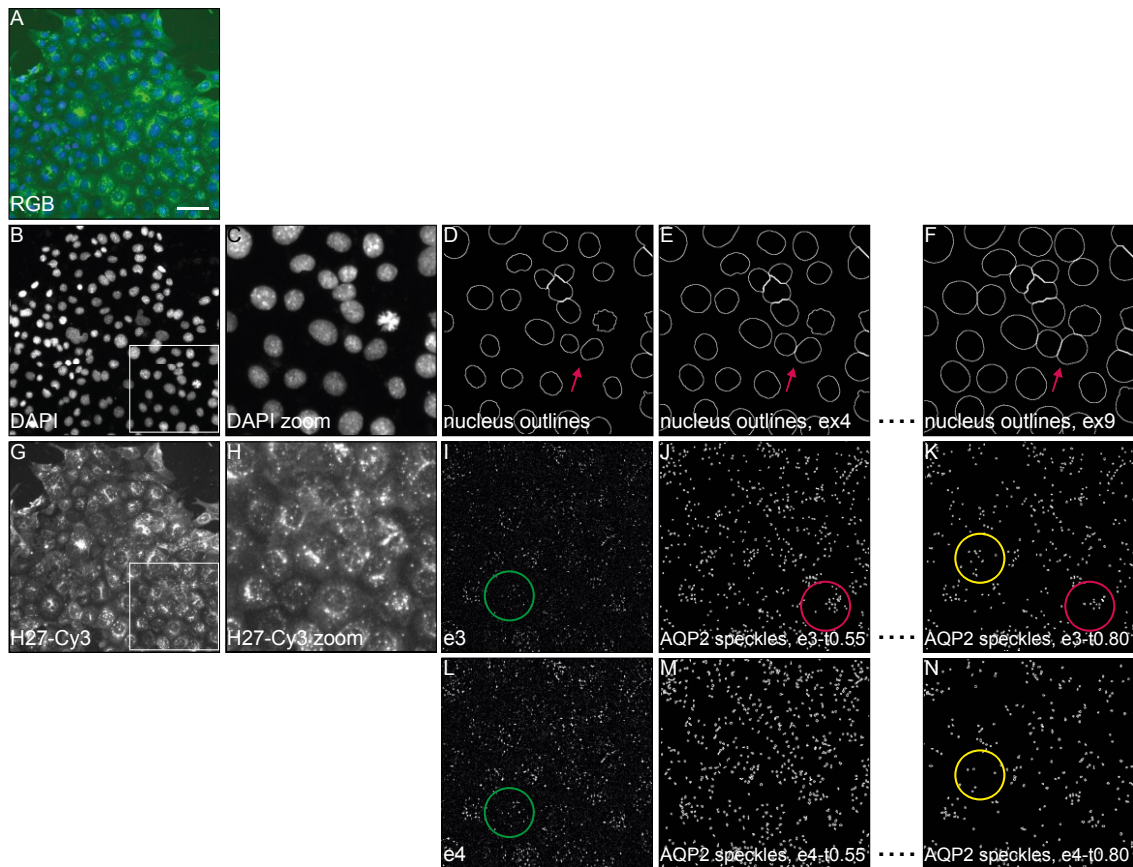


Fig. 18. CellProfiler pipeline modules in detail. **A)** The RGB immunofluorescent image depicts an overlay of both channels: **B)** DAPI, showing nuclei and **G)** H27-Cy3 (rabbit-derived anti-AQP2 antibody plus Cy3-conjugated secondary antibody), staining AQP2. **D)** Nucleus outlines were identified based on DAPI staining (**C)** and expanded by 4 (**E**), 5, 6, 7, 8 or 9 (**F**) pixels. Outlines did not overlap (red arrow) to avoid double measurement of the same region. Pixels were exclusively assigned to one nucleus. H27-Cy3-signal (**H**) was enhanced by a factor of 3 (**I**) or 4 (**L**). Based on each enhancement AQP2 speckles were identified using a threshold of 0.55 (**J**, **M**), 0.60, 0.65, 0.70, 0.75 or 0.80 (**K**, **N**). The number of identified speckles depends on both thresholds (red circles) and enhancements (green and yellow circles). e, enhanced; ex, expansion; t, threshold correction factor. The scale bar indicates 50 μm .

3.7 Data analysis using KNIME

Handling of huge data amounts is facilitated by KNIME software, whose use in combination with CellProfiler is well established⁴²². The program was used to summarise the data of identified nuclei and AQP2 speckles per image field and to relate all 6,156 files of 81 image fields to the corresponding well. First, pictures distorting the analysis were excluded (Fig. 20).

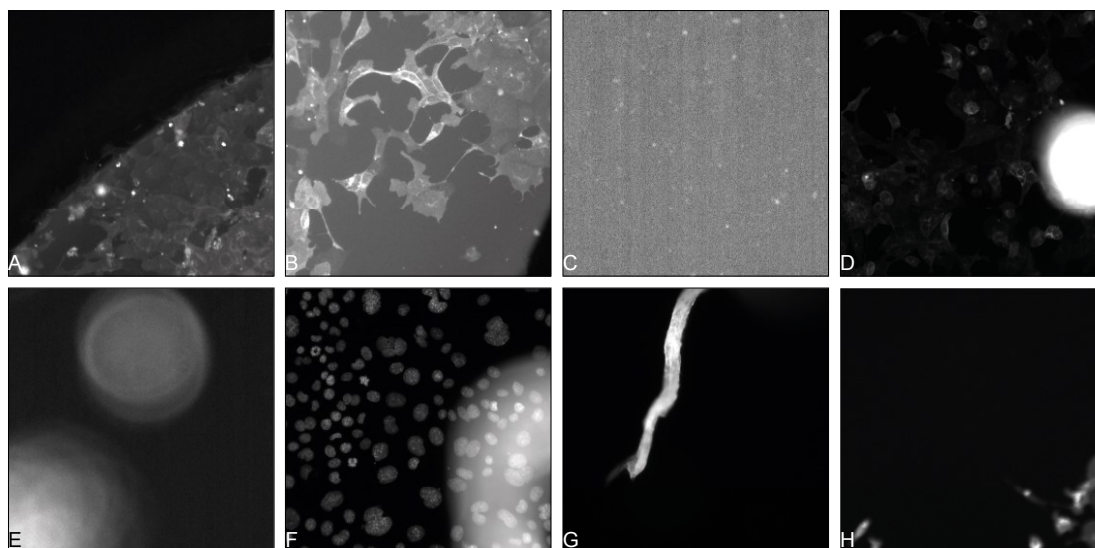


Fig. 20. Excluded images. Images were excluded from the data analysis when the edge of a well is depicted (**A**), mean (**B**) or median (**C**) signal intensity exceeded 0.25, percent maximum signal intensity was above 0.2 (**D**), the standard deviation of signal intensity exceeded 0.15 (**E**), focus score was not in the range of 0.11-0.24 (**F**) or power logarithmic slope in channel 1 (nuclei; **G**) or channel 2 (AQP2; **H**) was below -2.0. Images were acquired using an ArrayScan V^{TI} HCS Reader (20x magnification). The scale bar indicates 50 μm .

Image fields 49, 56, 64, 71, 72, 73, 79 and 80 (Fig. 20A, Fig. 5) were not considered as they are depicting the edge of the well. Besides, if the signal exceeded mean (Fig. 20B), median (Fig. 20C) or maximum intensity (Fig. 20D) or if the standard deviation of its intensity was above 0.15 (Fig. 20E) in either channel, images were excluded. Also out of focus recordings (Fig. 20F) and imaging artefacts (Fig. 20G,H) were not taken into consideration. Metadata of filtered images were used to evaluate cellular phenotypes.

3.7.1 Transfection efficiency

To control transfection efficiency NT#2 and TOX siRNA were placed manually in the middle and outer regions on both sides of each microtiter plate, accounting for 16 wells per condition (Fig. 21A). Nuclei number of NT#2- and TOX-transfected cells was related to each other. The transfection of MCD4 cells with TOX siRNA led to a 64-72 % reduction of cell number compared to NT#2-transfected cells (Fig. 21B,C,E). Compared to mock-transfected cells, scrambled NT#2 siRNA did not affect MCD4 cell number, indicating that it did not have off-target effects. Additionally, AQP2 siRNA was placed manually on each microtiter plate (Fig. 21A). As expected, the down regulation of AQP2 led to reduced immunofluorescent

signals elicited by rabbit-derived anti-AQP2 antibody H27 plus Cy3-conjugated secondary antibody (H27-Cy3; Fig. 21D,F).

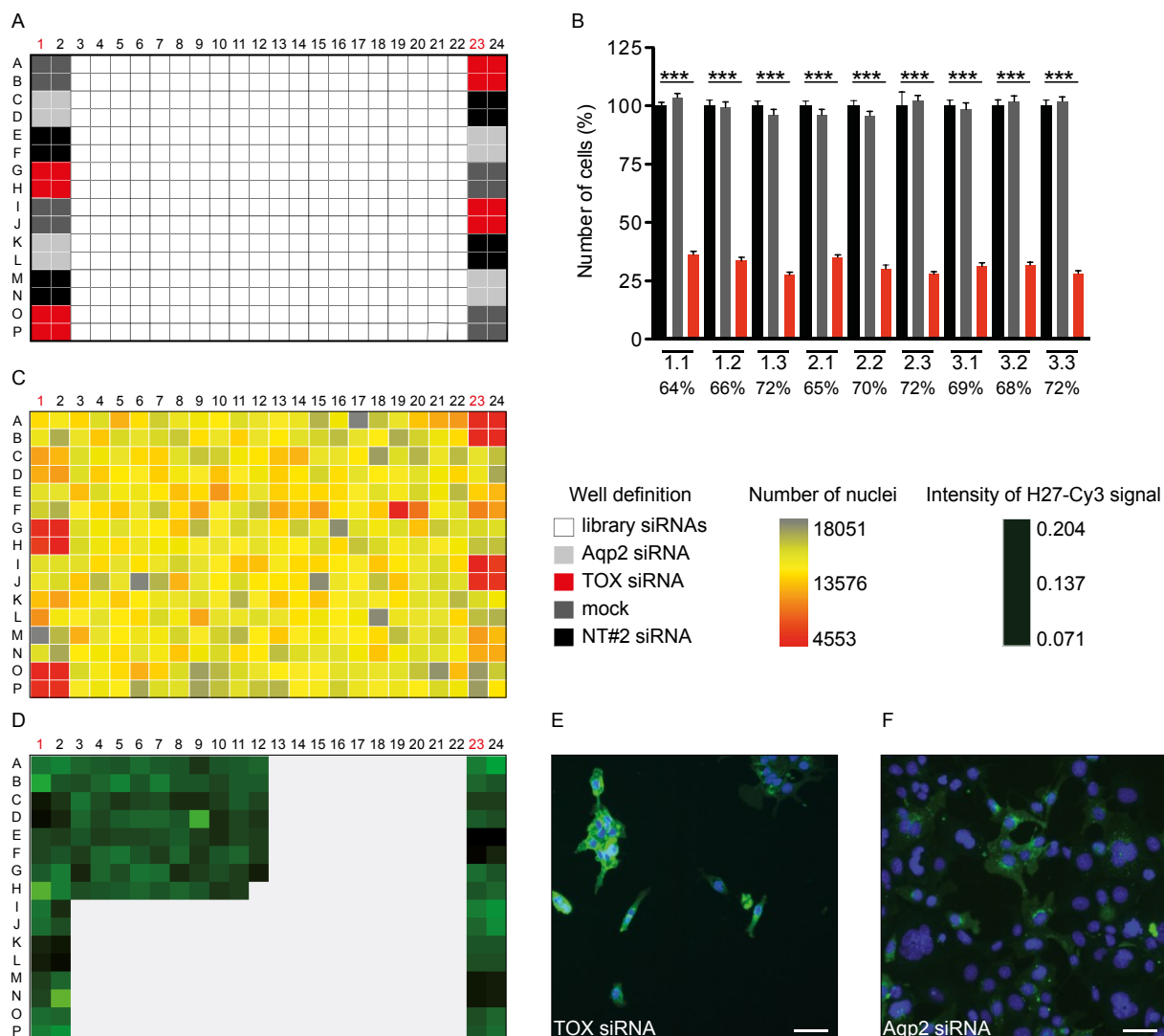


Fig. 21. MCD4 cells were efficiently transfected with siRNAs of the Mouse Protein Kinases sublibrary. **A)** Library siRNAs were located in the central 320 wells of columns 3-22 of 384 well plates. Controls were arranged on either side and included cells transfected with AQP2 siRNA, TOX siRNA, NT#2 siRNA and mock-transfected cells. Except for rows 1 and 23 20 μ l of 90 μ M FSK were added to all wells resulting in final concentrations of 30 μ M FSK. **B)** The experiment was performed three times independently, i.e. microtiter plates 1-3 were analysed in triplicate (1.1, 1.2, 1.3, 2.1, 2.2, 2.3, 3.1, 3.2, 3.3). The transfection of TOX siRNA reduced the cell number to 64-72% compared to NT#2 transfected cells. Colour code relates to well definition. **C)** A graphical overview of nuclei counts of microtiter plate 2.1. The lowest cell number was detected in TOX-transfected cells. Also, in well F19 a decreased cell number was detected, implying that transfection with siRNA in that well elicits a toxic effect on MCD4 cells. **D)** Heatmap of recorded H27-Cy3 intensities on microtiter plate 2.3, on which 79 of central 320 wells were occupied with library siRNAs. The lowest AQP2 intensity was detected upon AQP2 siRNA transfection. Representative images of cells transfected with TOX and AQP2 siRNA are shown in **(E)** and **(F)**. Images were acquired using an ArrayScan V^{TI} HCS Reader (20x magnification). The scale bars indicate 50 μ m. AQP2 is depicted in green, nuclei are shown in blue. H27-Cy3, rabbit-derived anti-AQP2 antibody H27 plus Cy3-conjugated secondary antibody. Statistically significant differences were determined applying one-way ANOVA with posthoc Bonferroni. ***, $p \leq 0.001$. Mean \pm SEM are plotted.

3.7.2 siRNA affects cell viability

Beside TOX siRNA, the transfection of several siRNAs included in the Mouse Protein Kinases sublibrary led to strongly reduced cell number. Out of 719 tested genes, the knockdown of 24 kinases decreased cell viability to less than 60 % compared to NT#2-transfected cells (Tab. 14). To identify targeted genes, siRNA sequences were re-annotated with RefSeq version 58 (www.ncbi.nlm.nih.gov/refseq/announcements/), released in 2013.

Tab. 14. MCD4 cell viability is decreased upon the down regulation of the listed genes.

Position	Viability (%)	Protein symbol	Gene name	Accession
1	3/H07	WEE1	<i>WEE1 homolog 1</i>	NM_009516
2	1/D20	COPB2	<i>Coatomer protein complex subunit beta 2 (beta prime)</i>	NM_015827
3	2/F19	PLK1	<i>Polo-like kinase 1</i>	NM_011121
4	1/I04	AURKB	<i>Aurora kinase B</i>	NM_011496
5	1/A11	STK36	<i>Serine/threonine kinase 36</i>	NM_175031
6	1/J06	EVI5L	<i>Ecotropic viral integration site 5 like</i>	NM_153536
7	2/F20	PLK2	<i>Polo-like kinase 2</i>	NM_152804
8	3/C10	AURKA	<i>Aurora kinase A</i>	NM_011497
9	3/F10	TRPM6	<i>Transient receptor potential cation channel subfamily M member 6</i>	NM_153417
10	2/F09	MAP3K2	<i>Mitogen-activated protein kinase kinase kinase 2</i>	NM_011946
11	1/A22	CDKL3	<i>Cyclin-dependent kinase-like 3</i>	NM_153785
12	1/K06	PDIK1L	<i>PDLIM1 interacting kinase 1 like</i>	NM_146156
13	1/I12	THNSL1	<i>Threonine synthase-like 1</i>	NM_0010012
14	1/F10	XYLB	<i>Xylulokinase homolog</i>	NM_0010332
15	3/D03	TEC	<i>Tec protein tyrosine kinase</i>	NM_013689
16	1/C05	MAGI3	<i>Membrane associated guanylate kinase WW and PDZ domain containing 3</i>	NM_133853
17	2/E10	MAP2K4	<i>Mitogen-activated protein kinase kinase 4</i>	NM_009157
18	1/O04	CARD14	<i>Caspase recruitment domain family member 14</i>	NM_130886
19	1/G10	AKAP13	<i>A kinase (PRKA) anchor protein 13</i>	NM_029332
20	3/C07	STK38L	<i>Serine/threonine kinase 38 like</i>	NM_172734
21	2/I12	MARK3	<i>MAP/microtubule affinity-regulating kinase 3</i>	NM_021516
22	3/D05	TESK1	<i>Testis specific protein kinase 1</i>	NM_011571
23	1/H11	ARAF	<i>V-raf murine sarcoma 3611 viral oncogene homolog</i>	NM_009703
24	1/M10	C230081A13RIK	<i>RIKEN cDNA C230081A13 gene</i>	NM_172924

Cells were transfected with siRNA targeting mRNA transcripts of the indicated genes. Three days after transfection, cells were analysed *via* automated immunofluorescence microscopy. During image analysis number of nuclei were determined within the CellProfiler pipeline. 'Position' indicates on which microtiter plate and in which well respective siRNAs were located. Mean viability of three independent experiments is shown (repetitions 1.1-1.3 are averaged to 1, 2.1-2.3 to 2, 3.1-3.3 to 3). NT#2-transfected cells were considered as 100 % viable. Position indicates the microtiter plate and well of detected candidates. Accession numbers refer to National Center for Biotechnology Information (NCBI, www.ncbi.nlm.nih.gov/) entries.

Many of these proteins are involved in cell cycle regulation (EVI5L⁴²³, PLK2⁴²⁴, AURKA⁴²⁵, STK38L⁴²⁶, MARK3⁴²⁷) and mitosis (PLK1⁴²⁸, WEE1, AURKB⁴²⁹, ARAF⁴³⁰, CDKL3⁴³¹). TEC plays a role in inflammation and bone destruction⁴³². TESK1 and C230081A13RIK that is also known as atypical kinase SGK269 participate in diverse signalling processes and are involved in cytoskeletal organisation^{433,434}. STK36 participates in cilogenesis⁴³⁵; MAP3K2 acts as transcriptional regulator⁴³⁶. MAGI3 participates in extracellular signal-related kinase (ERK) signalling⁴³⁷ and MAP2K4 is involved in stress-activated c-Jun N-terminal kinases (JNK) and p38 MAPK signalling pathways⁴³⁸. AKAP13 is also called AKAP-Lbc and functions as PKA-targeting protein and as GEF that activates RhoA⁴³⁹. COPB2 is a coat protein that regulates vesicle transport from ER to GOLGI⁴⁴⁰ and TRPM6 acts as cation channel mediating Ca²⁺ and Mg²⁺ transport⁴⁴¹. XYLB is suggested to participate in the carbohydrate metabolism⁴⁴². The function of CARD14⁴⁴³, PDIK1L⁴⁴⁴ and THNSL1 is currently not known.

The expression of these genes is indispensable for MCD4 cell survival. On the other hand, the down regulation of 22 other kinases led to slightly increased cell number (Tab. S 1). However, viability increased maximal by 15 %.

3.7.3 Multilayer perceptron

In order to automatically analyse the AQP2 localisation, cellular phenotypes were classified using a multilayer perceptron (MLP), which is integrated into KNIME. MLP is a powerful machine learning model that is able to autonomously identify complex data patterns and to map them to defined groups. It belongs to the class of artificial neural networks that are widely used for gene identification approaches⁴⁴⁵. Machine learning algorithms can be successfully trained even for phenotypes that cannot be distinguished by humans⁴⁴⁶. MLP was trained with CellProfiler-derived metadata of unstimulated and FSK-stimulated mock-transfected cells, showing many and few perinuclear AQP2 speckles, respectively. Data of each microtiter plate were classified separately. Out of 72 sets of AQP2 speckle identifications one was used for MLP classification. First, input information was restricted to metadata from 9-pixel-expanded nucleus outlines. Compared to expansions by 4-8 pixels, more perinuclear AQP2 speckles were included within this region (Fig. 22). Second, considering feature enhancements and threshold correction factors of each of the remaining 12 sets of AQP2 speckle identifications (Fig. 19) the number of AQP2 speckles in 9-pixels-

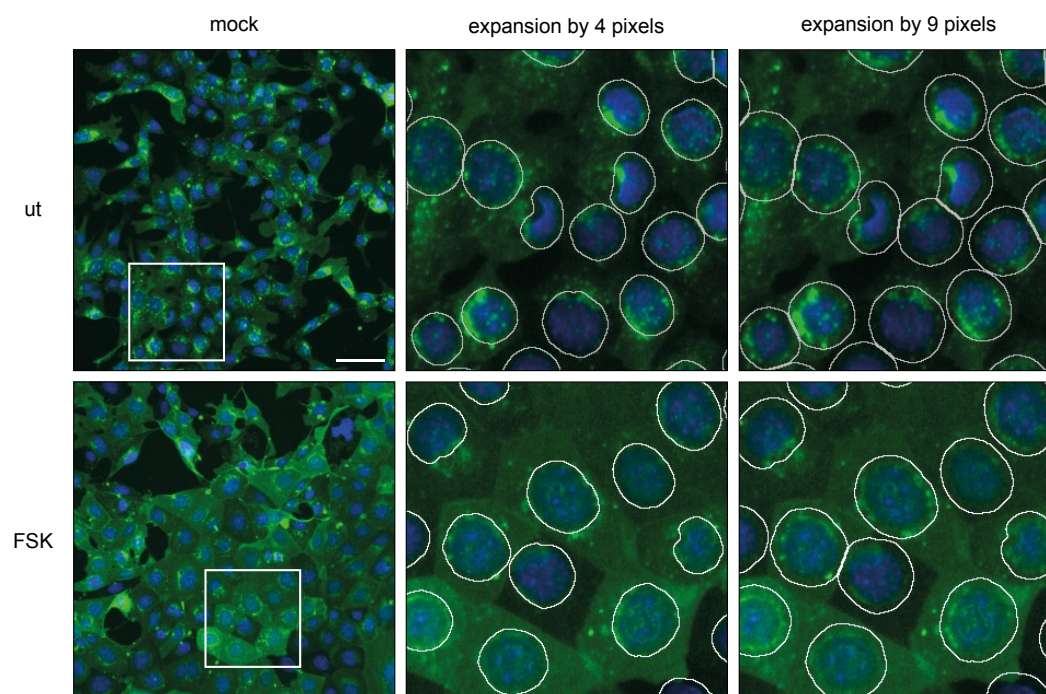


Fig. 22. Differently sized expansions of nucleus outlines. Perinuclear AQP2 speckles were included entirely in nucleus outlines that are expanded by 9 pixels but not in smaller 4 pixel-expansions. Mock-transfected cells were left unstimulated (ut) or stimulated with 30 μM FSK for 60 minutes (FSK). Cells were analysed *via* automated immunofluorescence microscopy. Using CellProfiler image analysis nuclei (blue) were identified. Nucleus outlines were increased by 4-9 pixels in order to surround perinuclear AQP2 signals (green). Expansions of nucleus outlines by 4 and 9 pixels of identical nuclei are indicated by white lines. Images were acquired using an ArrayScan V^{TI} HCS Reader (20x magnification). The scale bar indicates 50 μm . ut, unstimulated; FSK, forskolin.

-expanded nuclei of unstimulated and FSK-stimulated mock-transfected cells was compared (Fig. 23). The dataset displaying the maximal difference in the distribution of AQP2 speckles in the presence and absence of FSK (Fig. 23A) was used for microtiter plate-specific MLP training (Tab. 15).

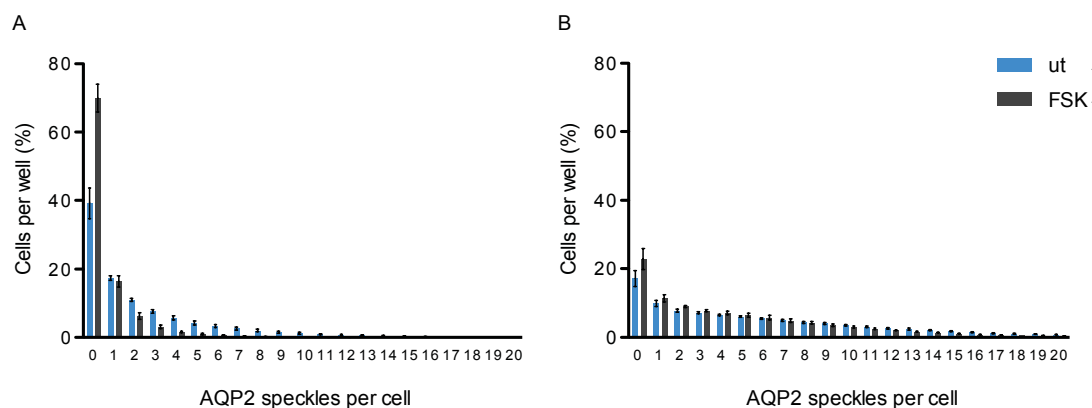


Fig. 23. The distribution of AQP2 speckles per cell. Number of unstimulated and FSK-stimulated mock-transfected cells displaying 0-20 AQP2 speckles within 9-pixels-expanded nucleus outlines, were compared with regard to the corresponding speckle identification parameters. **A)** AQP2 speckles were defined after signal enhancement by a factor of 4 and the application of the threshold correction factor 0.80. Upon stimulation with FSK more cells showed 0 AQP2 speckles (70 %) compared to unstimulated cells (40 %). The majority of unstimulated cells showed AQP2 speckles. **B)** Signal enhancement factor 3 and threshold correction factor 0.55 were applied for AQP2 speckle identification. The difference between unstimulated and FSK-stimulated cells displaying 0 AQP2 speckles was lower compared to A. In most of the cells 1-20 AQP2 speckles were detected in the presence or absence of FSK. Cells were stimulated with 30 μ M FSK for 60 minutes. ut, unstimulated; FSK, forskolin.

Tab. 15. Optimal parameters for AQP2 speckles identification.

Microtiter plate	Feature enhancement	Threshold correction factor
1.1	4	0.75
1.2	3	0.65
1.3	4	0.75
2.1	4	0.80
2.2	3	0.80
2.3	3	0.70
3.1	4	0.60
3.2	3	0.65
3.3	4	0.80

Parameters of AQP2 speckle identification, which led to a maximally different distribution of AQP2 speckles in unstimulated and FSK-stimulated MCD4 cells. Parameters are indicated for each microtiter plate screened and relate to 9-pixels-expanded nucleus outlines.

The dataset was imported as MLP input information and was processed by perceptrons that are arranged in so-called layers (Fig. 24). A perceptron is comparable to a biological neuron, as it fires if input values are above a certain threshold⁴⁴⁷. MLP learns to exert the desired classification by defining the expected output of control input data in a process referred to as training⁴⁴⁵. In other words, the weight of single perceptrons is adjusted to a predefined output and a rule is generated to recognise specific phenotypes. The hidden layer contained 10 perceptrons, in which multiple unknown algorithms were applied to filter and prioritise relevant input information in order to achieve the predefined binary output, being hit YES if many or hit NO if few APQ2 speckles are present (Fig. 24A).

After MLP training with metadata of mock-transfected cells, images of unstimulated and FSK-stimulated NT#2-transfected MCD4 cells were classified applying the previously trained hidden algorithms. If the classification of these controls resulted in the expected output, i.e. hit YES for unstimulated and hit NO for FSK-stimulated NT#2-transfected cells, successful MLP training was confirmed (Fig. 24B). In this case, the trained MLP was used to classify CellProfiler-derived metadata of siRNA transfected cells with unknown phenotype that were derived from the same microtiter plate. If the MLP classification of NT#2-transfected cells failed (Fig. 24C), MLP training was repeated using metadata from the remaining 11 sets of speckle identifications. However, none of these additional trainings proved to be correct, i.e. led to the expected classification of NT#2-transfected cells.

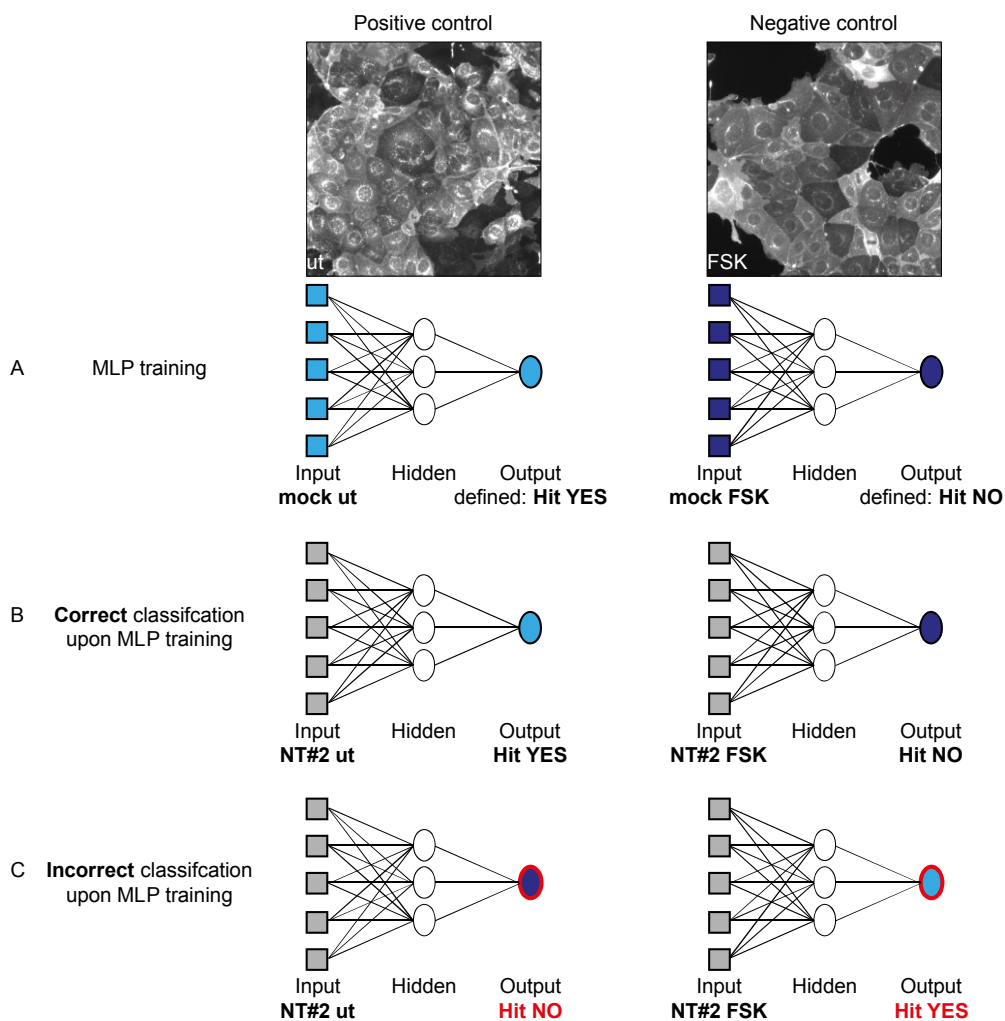


Fig. 24. Cellular phenotypes were classified using a multilayer perceptron (MLP). The MLP consists of two layers, hidden and output layer. The hidden layer contains 10 perceptrons (only three are depicted), the output layer is made of one perceptron. CellProfiler-derived metadata were used as input information. Input information and perceptrons of the hidden layer were not connected within each other but were linked to all perceptrons of the following layer, which represents a characteristic feature of feedforward artificial neural networks. **A)** Given the metadata of images of unstimulated and FSK-stimulated mock-transfected cells, the MLP was trained to result in defined output information hit YES and NO, respectively. **B)** Upon training, MLP classification was tested on images derived from NT#2-transfected cells. If unstimulated cells were classified to be a hit and FSK-stimulated cells not to be, MLP classification was used for the analysis of the whole microtiter plate. **C)** If NT#2-transfected controls were classified incorrectly, microtiter plates were excluded from the analysis. ut, unstimulated; FSK, forskolin.

In total, five of nine microtiter plates were excluded from further analysis: 1.1, 1.2, 2.2, 3.1 and 3.2 (Tab. 16). MLP classification proved to be correct on four microtiter plates 1.3, 2.1, 2.3 and 3.3. Each plate of the Mouse Protein Kinase sublibrary was represented at least once. The AQP2 redistribution upon the siRNA-mediated knockdown of all 719 kinases could be analysed using machine learning.

Tab. 16. Results of MLP classification.

Well	Stimulation	Output of MLP classifier								
		1.1	1.2	1.3	2.1	2.2	2.3	3.1	3.2	3.3
C23	ut	YES	YES	YES	YES	YES	YES	YES	YES	YES
C24	+FSK	NO	NO	NO	NO	NO	NO	NO	NO	NO
D23	ut	YES	YES	YES	YES	YES	YES	YES	YES	YES
D24	+FSK	NO	NO	NO	NO	NO	NO	NO	NO	NO
E01	ut	YES	YES	YES	YES	YES	YES	YES	YES	YES
E02	+FSK	NO	NO	NO	NO	NO	NO	NO	NO	NO
F01	ut	YES	YES	YES	YES	YES	YES	YES	YES	YES
F02	+FSK	NO	NO	NO	NO	NO	NO	NO	NO	NO
K23	ut	YES	NO	YES	YES	NO	YES	NO	NO	YES
K24	+FSK	NO	NO	NO	NO	NO	NO	NO	NO	NO
L23	ut	YES	YES	YES	YES	NO	YES	YES	YES	YES
L24	+FSK	NO	NO	NO	NO	NO	NO	NO	NO	NO
M01	ut	YES	NO	YES	YES	NO	YES	NO	NO	YES
M02	+FSK	NO	NO	NO	NO	NO	NO	NO	NO	NO
N01	ut	YES	NO	YES	YES	NO	YES	NO	NO	YES
N02	+FSK	YES	NO							

Microtiter plates were excluded from the analysis if the MLP classification of metadata from NT#2 transfected cells did not result in the predicted categories. On microtiter plates 1.1, 1.2, 2.2, 3.1 and 3.2 several controls were not classified correctly (red), whereas MLP classification proved to be correct on microtiter plates 1.3, 2.1, 2.3 and 3.3. ut, unstimulated; FSK, forskolin.

Additionally, the screening was evaluated based on standard statistical methods using Z-score-based analysis. Whereas MLP classification is based on plate-specific controls, the Z-score describes the performance of a single sample related to the mean of all samples per microtiter plate.

3.7.4 Z-score based analysis

Z-score-based analysis of large data sets is meaningful if the signal window between positive and negative controls is big enough and variability of control values is low. Statistically, this can be expressed by the Z'-factor, a dimensionless parameter describing the capability of hit identification for a given assay at defined screening conditions⁴¹⁷. Based on means and standard deviations, the Z'-factor describes the dynamic range of positive and negative controls. Although marginal readout is possible if Z' is between 0.0 - 0.5, excellent analysis is only guaranteed if Z' exceeds 0.5⁴¹⁷ (2.2.7). A negative Z'-factor indicates that hits cannot be separated from background noise. In contrast to the Z'-factor, the Z-score integrates samples values only and represents the deviation of a phenotype from the mean of a screen.

The Z'-factor was determined for each microtiter plate with regard to 12 different settings of AQP2 speckle identifications related to 9-pixels enhanced nucleus outlines (Tab. 17). Mock- and NT#2-transfected cells were considered separately. A positive Z'-factor of 0.5 was

detected once in 108 measurements (Tab. 17, microtiter plate 2.1, feature enhancement 3, threshold correction factor 0.70). Thus, in addition to MLP classification the metadata of one microtiter plate were analysed by Z-score. This conventional analysis was not possible on the remaining eight microtiter plates. A siRNA pool was regarded positive if it scored >2 standard deviations above the mean, i.e. if the Z-score was larger than 2.

Tab. 17. Z' factors.

Microtiter plate	siRNA	Feature enhancement: 3						Feature enhancement: 4					
		Threshold correction factor:						Threshold correction factor:					
		0.55	0.60	0.65	0.70	0.75	0.80	0.55	0.60	0.65	0.70	0.75	0.80
1.1	mock	0.0	0.1	-0.1	-0.4	-0.4	-0.4	-0.3	-0.4	-0.4	-0.4	-0.4	-0.5
1.1	NT#2	-0.7	0.1	-0.4	-0.8	-1.2	-1.4	-0.3	-0.9	-1.3	-1.5	-1.7	-1.8
1.2	mock	-2.8	-1.7	-1.8	-1.6	-1.9	-1.7	-1.5	-1.6	-1.6	-1.8	-2.1	-2.4
1.2	NT#2	-10.8	-9.7	-6.3	-4.8	-4.1	-3.9	-5.1	-3.9	-3.6	-3.9	-4.1	-4.6
1.3	mock	-1.0	0.0	0.0	-0.2	-0.3	-0.3	-0.3	-0.1	-0.1	-0.1	-0.2	-0.3
1.3	NT#2	-0.1	-0.4	-0.8	-1.3	-1.5	-1.6	-1.1	-1.4	-1.5	-1.7	-1.8	-2.0
2.1	mock	-2.1	-0.1	0.0	0.4	0.3	0.2	0.0	0.1	-0.1	-0.1	-0.1	0.0
2.1	NT#2	-2.0	-0.5	0.2	0.5	0.4	0.2	0.1	0.3	0.3	0.2	0.2	0.2
2.2	mock	-5.3	-2.1	-2.5	-1.7	-1.6	-1.8	-1.4	-1.3	-2.0	-2.4	-2.9	-3.3
2.2	NT#2	-8.3	-5.8	-4.3	-4.4	-5.0	-5.1	-3.7	-4.4	-4.7	-5.0	-5.2	-5.3
2.3	mock	-2.7	-0.6	0.2	0.4	0.3	0.3	0.4	0.3	0.2	0.1	0.0	-0.1
2.3	NT#2	-0.6	0.2	0.1	0.1	-0.1	-0.3	0.2	-0.1	-0.3	-0.4	-0.4	-0.5
3.1	mock	-2.8	-2.4	-4.1	-6.5	-7.4	-13.8	-5.8	-7.1	-17.0	-31.5	-73.4	-649.0
3.1	NT#2	-2.0	-2.1	-3.4	-7.4	-9.3	-9.9	-6.3	-9.0	-10.5	-14.7	-19.1	-25.3
3.2	mock	-4.0	-3.6	-2.3	-1.7	-2.1	-2.1	-2.0	-1.9	-1.9	-1.9	-1.6	-1.6
3.2	NT#2	-2.6	-3.7	-3.0	-3.5	-3.8	-5.4	-3.3	-4.3	-5.7	-6.7	-7.4	-7.8
3.3	mock	-0.4	0.0	0.2	0.3	-0.3	-0.7	0.1	-0.5	-0.4	-0.4	-0.5	-0.5
3.3	NT#2	-2.0	-0.3	0.0	-0.2	-0.3	-0.4	0.0	-0.2	-0.4	-0.6	-0.6	-0.6

Based on indicated speckle identification parameters (feature enhancement and threshold correction factor) metadata of filtered images were normalised per well and Z' factors were determined. Positive values are highlighted in grey, bold numbers mark settings that allow high quality analysis.

3.7.5 Hits

On four microtiter plates that were included in the analysis of the AQP2 redistribution, 137 hits were identified (Fig. 25A). On microtiter plates 1.3, 2.1 and 3.3 six to eight candidates were detected by MLP machine learning. On microtiter plate 2.3 108 candidates were localised (Fig. 25A). This represents 34 % of all 320 siRNA pools per plate and is far above a reasonable number of hits^{448,449}, indicating plate-specific misclassification. To avoid false positives these candidates were not considered but it was focussed on MLP classification and Z-score based analysis of microtiter plate 2.1, harbouring identical siRNAs as microtiter plate 2.3. Considering only candidates that were identified by both methods on microtiter plate 2.1, the overall number of hits was reduced to 19, three of which were detected twice (Fig. 25). No microtiter plate- or well-specific effects were observed and thus systemic errors could be excluded. Of the 19 hits the down regulation of 6 candidates decreased cell viability to less than 60 % compared to NT#2-transfected cells (Tab. 14, Tab. 18). The expression of genes 14-19 listed in Tab. 18 is necessary for MCD4 cell survival and respective candidates were excluded from downstream analysis. The remaining 13 candidates reduced MCD4 cell viability to 64-97 % (1-13 in Tab. 18). The decreased expression of each of these 13 genes

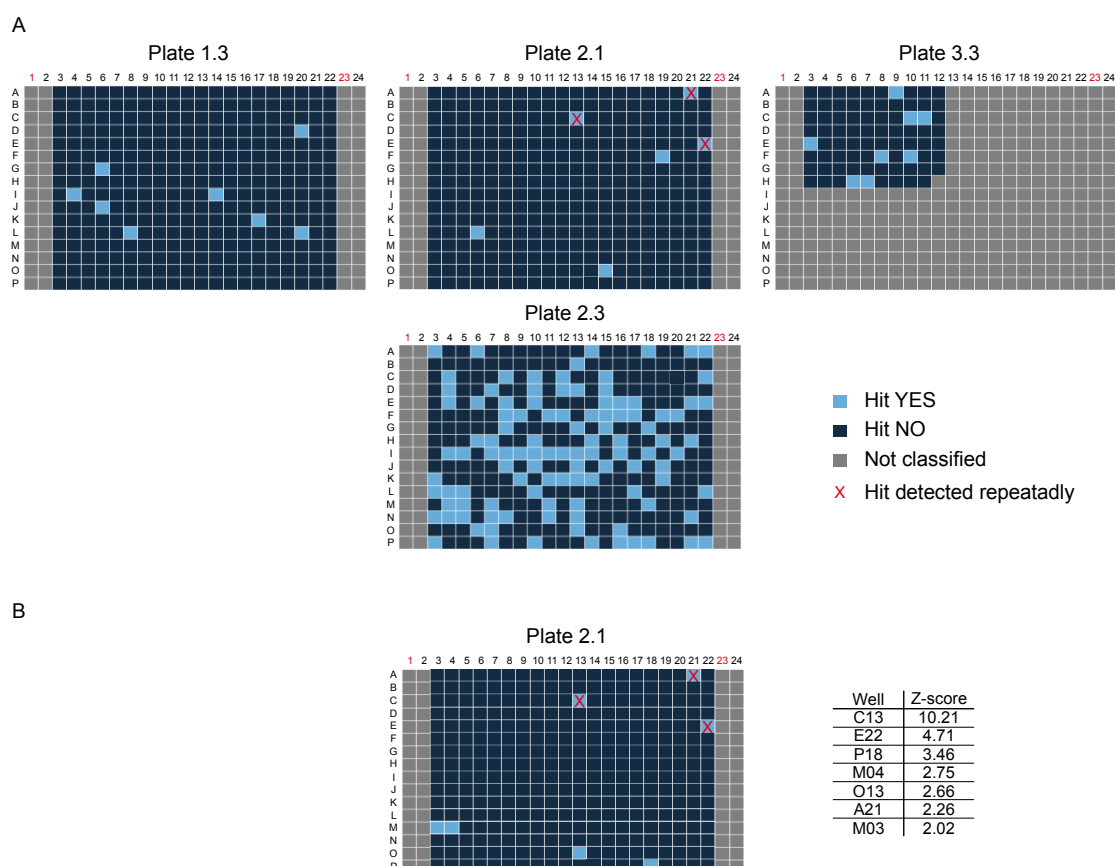


Fig. 25. Hit maps of four different microtiter plates. A) On microtiter plates 1.3, 2.1, 2.3 and 3.3 8, 6, 108 and 8 hits, respectively, were identified by MLP machine learning. **B)** Z-score-based analysis of microtiter plate 2.1 revealed 7 hits, three of which were also detected by MLP (red cross). Hit ranking according to Z-scores is depicted. For targeted genes, refer to Tab. 18 and Tab. S 1.

Tab. 18. Hit list.

	Microtiter plate/well	Viability (%)	Protein symbol	Gene name	Accession
1	2.1/E22	97	PKIA	<i>cAMP-dependent protein kinase inhibitor</i>	NM_008862.3
2	3.3/A09	87	STK11	<i>Serine/threonine kinase 11</i>	NM_011492.3
3	1.3/L20	79	FGFR1	<i>Fibroblast growth factor receptor 1</i>	NM_010206.2
4	1.3/K17	78	EPHB3	<i>Eph receptor B3</i>	NM_010143.1
5	1.3/L08	75	BMPR1B	<i>Bone morphogenetic protein receptor type 1B</i>	NM_007560.3
6	3.3/H06	70	VRK3	<i>Vaccinia related kinase 3</i>	NM_133945.1
7	3.3/F08	70	TRIM27	<i>Tripartite motif-containing 27</i>	NM_009054.3
8	2.1/A21	70	CDK18	<i>Cyclin-dependent kinase 18</i>	NM_008795.2
9	1.3/G06	69	AK3	<i>Adenylate kinase 3</i>	NM_021299.1
10	3.3/C11	69	SYK	<i>Spleen tyrosine kinase</i>	NM_011518.2
11	3.3/E03	66	TK2	<i>Thymidine kinase 2, mitochondrial</i>	NM_021028.3
12	1.3/I14	65	DUSP2	<i>Dual specificity phosphatase 2</i>	NM_010090.2
13	2.1/C13	64	PFKP	<i>Phosphofructokinase 1</i>	NM_019703
14	3.3/F10	52	TRPM6	<i>Transient receptor potential cation channel subfamily M member 6</i>	NM_153417.1
15	3.3/C10	52	AURKA	<i>Aurora kinase A</i>	NM_011497.3
16	1.3/J06	50	EVI5I	<i>Ecotropic viral integration site 5 like</i>	NM_001039578.3
17	1.3/I04	33	AURKB	<i>Aurora kinase B</i>	NM_011496.1
18	1.3/D20	25	COPB2	<i>Coatamer protein complex subunit beta 2 (beta prime)</i>	NM_015827.2
19	3.3/H07	18	WEE1	<i>WEE 1 homolog 1</i>	NM_009516.3

Upon the down regulation of the expression of the indicated genes the AQP2 redistribution in MCD4 cells was inhibited. Hits are listed according to MCD4 cell viability caused by siRNA-mediated silencing of gene expression. Viability of NT#2-transfected cells was considered 100 %. Three genes that were detected twice are highlighted. The down regulation of candidates 1-6 decreased MCD4 cell viability to less than 60 %. Accession numbers refer to National Center for Biotechnology Information (NCBI, www.ncbi.nlm.nih.gov/) entries.

inhibited the AQP2 redistribution upon FSK- stimulation in MCD4 cells (Fig. 26, Fig. S 6). None of them was previously related to AQP2 control (Tab. 2).

PKIA blocks PKA activity by binding to its catalytic subunits upon their cAMP-dependent dissociation from its regulatory subunits⁴⁵⁰. It regulates the nuclear export of the free catalytical PKA subunits⁴⁵¹. STK11 controls the activity of AMP-activated protein kinases (AMPK) and thus, is involved in various processes such as cell growth, energy metabolism and cell polarity⁴⁵². FGFR1 acts as receptor for fibroblast growth factors and is involved in embryonic development, cell proliferation, differentiation and migration⁴⁵³. The tyrosine-protein kinase mediates the activation of RAS/MEK/MAPK signalling pathways⁴⁵⁴. The receptor tyrosine kinase EPHB3 binds transmembrane ephrin-B ligands and leads to contact-dependent signalling into neighbouring cells⁴⁵⁵. It controls cell migration and adhesion and is involved in axon guidance⁴⁵⁶, angiogenesis⁴⁵⁷ and intestinal epithelium differentiation⁴⁵⁸. BMPR1B forms a receptor complex, which activates SMAD transcription factors in response to particular cytokines, the transformation growth factor (TGF β) and bone morphogenic protein (BMP) families²⁰⁵. The kinase is important in skeletal and bone development⁴⁵⁹. VRK3 activates the phosphatase activity of DUSP3 (dual specificity phosphatase 3), leading to ERK dephosphorylation and hence, inactivation⁴⁶⁰. It plays a role during embryonic development

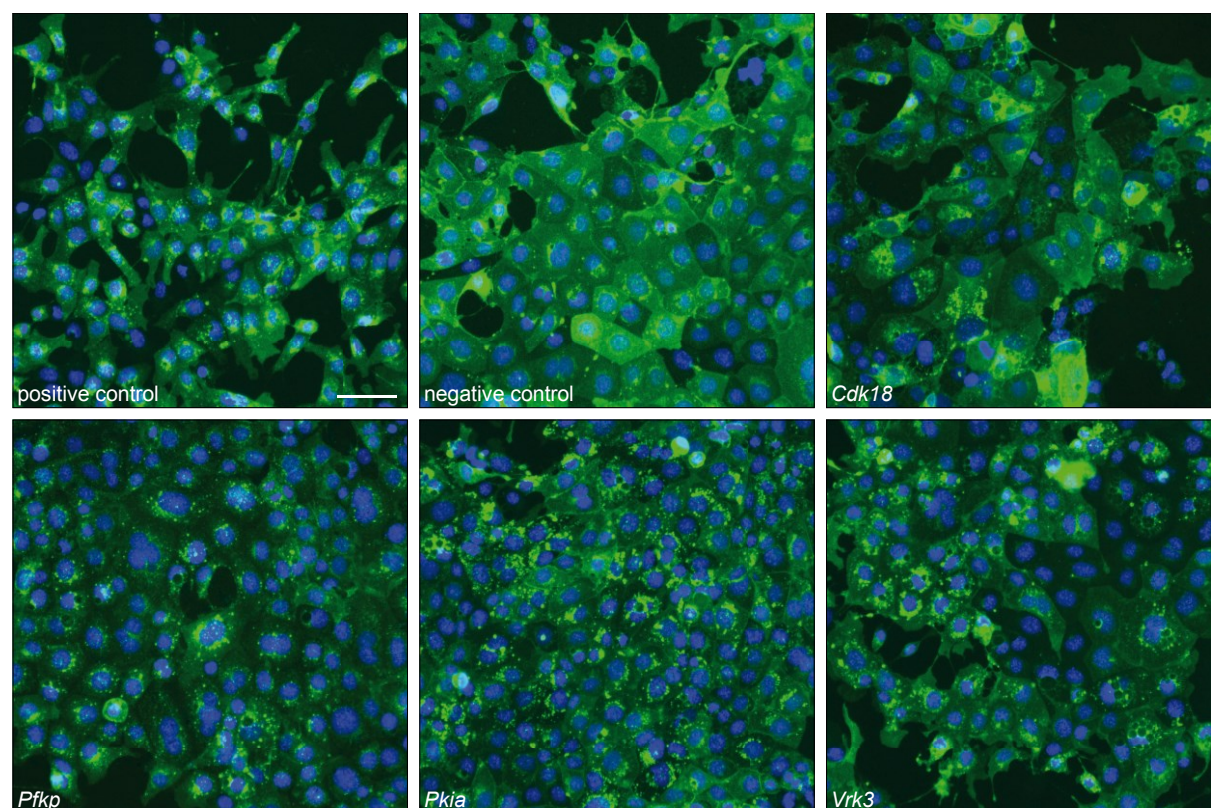


Fig. 26. AQP2 translocation is impaired upon silencing of hits. The knockdown of *Cdk18*-, *Pfkp*-, *Pkia*- or *Vrk3*- gene expression inhibits the AQP2 insertion into the plasma membrane. Except for the positive control, in which cells were left unstimulated all wells were treated with 30 μ M FSK for 60 min. Control images show NT#2-transfected cells. Images were acquired using an ArrayScan V^{TI} HCS Reader (20x magnification). The scale bar indicates 50 μ m. AQP2 is depicted in green, nuclei are shown in blue. Representative images are shown.

of hematopoiesis⁴⁶¹. TRIM27 is associated with tumorigenesis⁴⁶². It mediates epigenetic gene silencing and was suggested to function as E3 ubiquitin ligase⁴⁶³.

CDK18 belongs to the family of cyclin-dependent kinases; its function is unclear⁴⁶⁴. AK3 maintains homeostasis of cellular guanine and adenine nucleotides by catalysing the conversion between nucleosides and phosphates⁴⁶⁵. SYK mediates signal transduction downstream of various plasma membrane receptors and is involved in the regulation of innate and adaptive immunity⁴⁶⁶ and vascular development⁴⁶⁷. It regulates CFTR (cystic fibrosis transmembrane conductance regulator) trafficking and activation⁴⁶⁸. Amongst others, it activates the PKC signalling pathway⁴⁶⁹. TK2 has a key function in the synthesis of mitochondrial DNA⁴⁷⁰. It catalyses the phosphorylation of pyrimidine deoxyribonucleosides to deoxyribonucleoside 5'-monophosphates⁴⁷¹. DUSP2 is a crucial player in the regulation of immune responses. It controls mitogenic signal transduction by dephosphorylating ERK1/2 and p38 MAPK leading to their inactivation⁴⁷². PFKF is a key enzyme of the glycolysis. It catalyses the phosphorylation of fructose-6-phosphate to fructose-1,6-bisphosphate⁴⁷³.

Regarding proteins shown to play a role in the control of AQP2 (Tab. 2), 26 proteins or protein subunits were targeted within the Mouse Protein Kinase sublibrary. None of them was identified as hit (Fig. S 7); i.e. the decreased expression of each of these genes did not impair the AQP2 redistribution in MCD4 cells. With the exception of PI3K2C, whose down regulation decreased cell viability to less than 60 %, silencing of these genes did not affect MCD4 cell viability (Tab. S 6).

3.8 Hit validation

Screening of the Mouse Protein Kinases sublibrary revealed 13 genes, whose expression is relevant for the AQP2 redistribution (Tab. 18). To confirm the results of the automated image and data analysis and thus, to judge the assays quality, experiments were repeated on a small scale. As for the screening, MCD4 cells of passage 42 were transfected with the siRNA pools that are included in the library and three days after transfection the AQP2 localisation was monitored by laser scanning microscopy. The efficiency of protein knockdown was monitored by Western Blotting. Exemplarily, siRNA pools targeting *Pkia* and *Cdk18* transcripts, were chosen (Tab. 18, Fig. 26) as both of them were detected by MLP machine learning and Z-score-based analysis (Fig. 25) and their down regulation did not reduce MCD4 cell viability as strongly as the silencing of other hits did (Tab. 18).

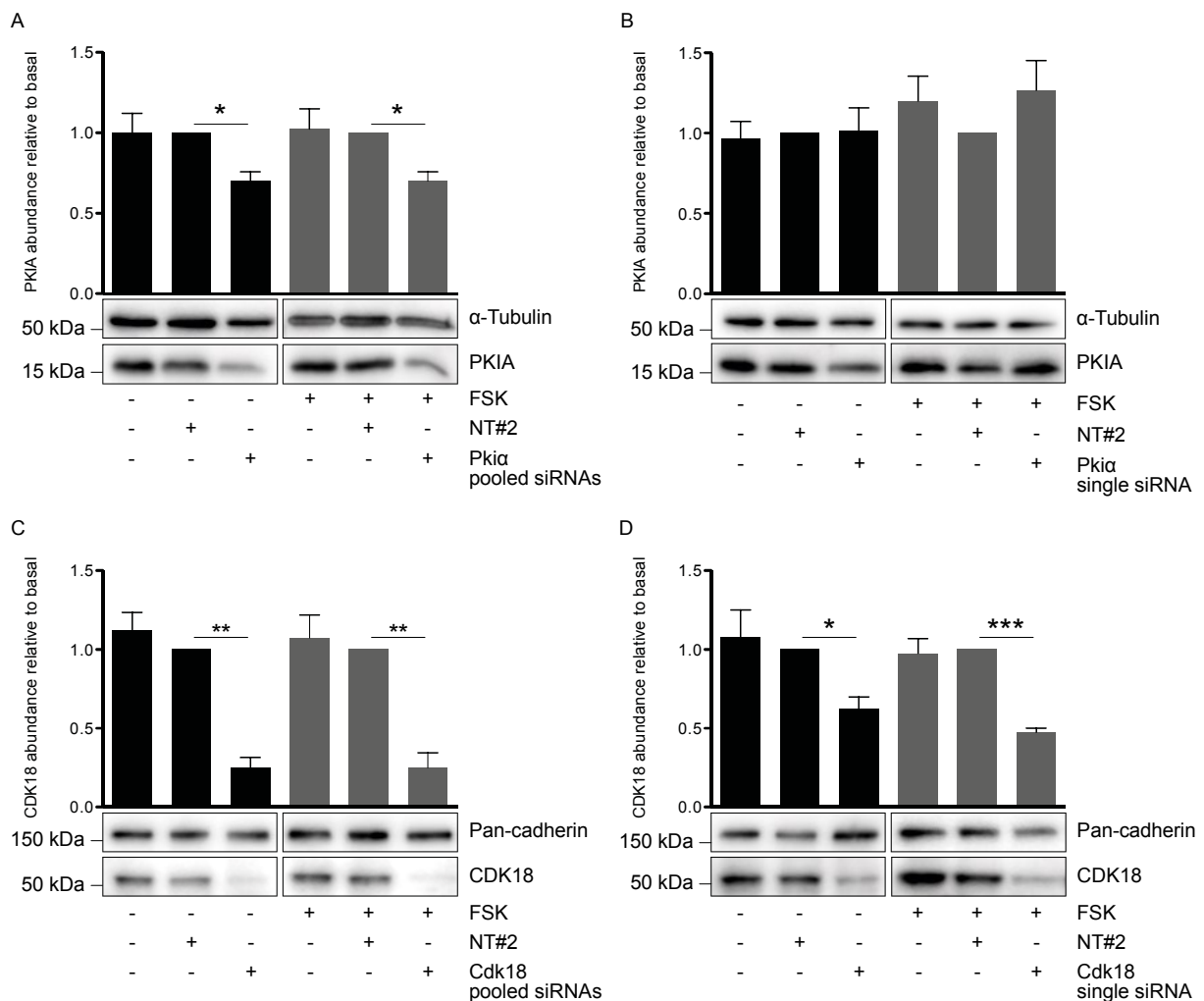


Fig. 27. Efficiency of CDK18 and PKIA down regulation. **A)** After the transfection of MCD4 cells with pooled *Pkia* siRNAs, PKIA abundance was significantly reduced compared to NT#2-transfected cells. **B)** *Pkia* single siRNA did not reduce target protein abundance. The down regulation of CDK18 is more effective upon transfection with pooled *Cdk18* siRNAs (**C**) than after *Cdk18* single siRNA transfection (**D**). MCD4 cells were transfected with 50 nM siRNAs as indicated or left untreated. After three days, cells were stimulated with 30 μ M FSK for 60 min, lysed and proteins were detected by Western Blotting with *Cdk18* (C17), *Pkia* (N20), Pan-cadherin (C3678) and α -Tubulin (CM1a) antibodies. Signals were quantified by densitometric analysis. Statistical analysis was performed using the unpaired t-test. Statistical significant differences are indicated. *, $p \leq 0.05$; **, $p \leq 0.01$; ***, $p \leq 0.001$. Mean \pm SEM are plotted, $n = 3-6$ independent experiments. FSK, forskolin.

The transfection of MCD4 cells with pooled Pk α siRNAs led to 30 % reduction of PKIA protein abundance compared to NT#2-transfected cells (Fig. 27A). Comprising 76 amino acids, PKIA has a mass of approximately 8 kDa. However, a distinct signal at 16 kDa was detected by Western Blotting (Fig. 27A). Since the signal disappeared upon blocking of the antibody with the peptide representing its epitope (Fig. 28), the band was considered as specifically representing PKIA.

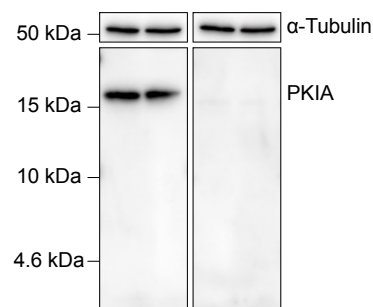


Fig. 28. The detection of PKIA by Western Blotting. PKIA was detected using the antibody sc-1943 (Tab. 5) alone (left) or upon blocking with 1000x molecular excess of peptide sc-1943P representing its epitope (2.2.3.3). As loading control α -Tubulin was detected using antibody DM1a (Calbiochem, CP06).

Immunofluorescence microscopy revealed that AQP2 resides intracellularly upon PKIA down regulation by pooled Pk α siRNAs (Fig. 29). With and without FSK stimulation distinct AQP2 speckles were detected perinuclearly. Compared to unstimulated NT#2-transfected cells, AQP2 was less spread throughout the cytoplasm but was exclusively located close to the nucleus. Transfection with pooled Cdk18 siRNAs led to a 75 % reduction of target protein abundance compared to NT#2-transfected cells (Fig. 27C). The down regulation of CDK18 by pooled Cdk18 siRNAs abolished the AQP2 transport to the plasma membrane (Fig. 29). Thus, screening results obtained by automated image and data analysis were confirmed.

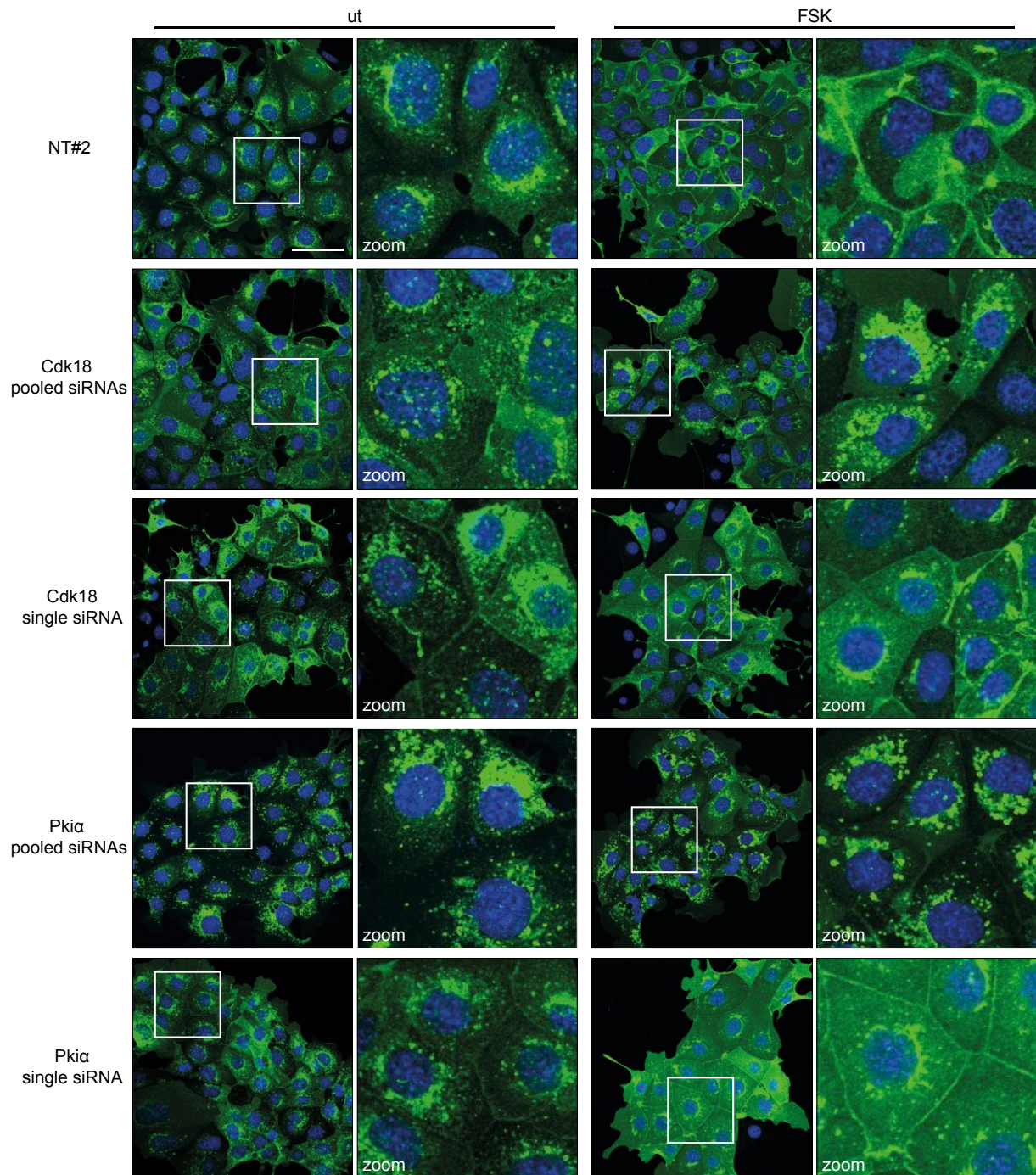


Fig. 29. FSK-induced AQP2 translocation in MCD4 cells is impaired after transfection with Pki α and Cdk18 pooled but not single siRNAs. MCD4 cells were transfected with 50 nM siRNA as indicated. After three days, cells were left untreated or stimulated with 30 μ M FSK for 60 min, fixed and analysed *via* immunofluorescence microscopy. Images were acquired with confocal laser scanning microscope LSM780 (40x magnification). The scale bar indicates 50 μ m. AQP2 is depicted in green, nuclei are shown in blue. ut, unstimulated; FSK, forskolin. Representative images are shown.

To validate the potential role of PKIA and CDK18 in the AQP2 redistribution, their involvement was to be shown by alternative methods. One possibility is to block target proteins by specific inhibitors and thereupon, monitor the AQP2 localisation. However, according to OpenPHACTS, a database that provides pharmacological and physiochemical information no substances or compounds selectively inhibiting any of the identified hits are known (Open Pharmacological Space, www.openphacts.org/explorer). Thus, gene expression was down regulated by RNAi as established before. MCD4 cells were transfected with single siRNAs targeting *Pkia* and *Cdk18* mRNA, respectively. Single siRNAs were directed against mRNA regions that were not targeted by any of the four pooled siRNAs applied before (Tab. 8, Tab. S 2). Three days after transfection, the efficiency of protein knockdown was detected by Western Blotting and AQP2 location was analysed by

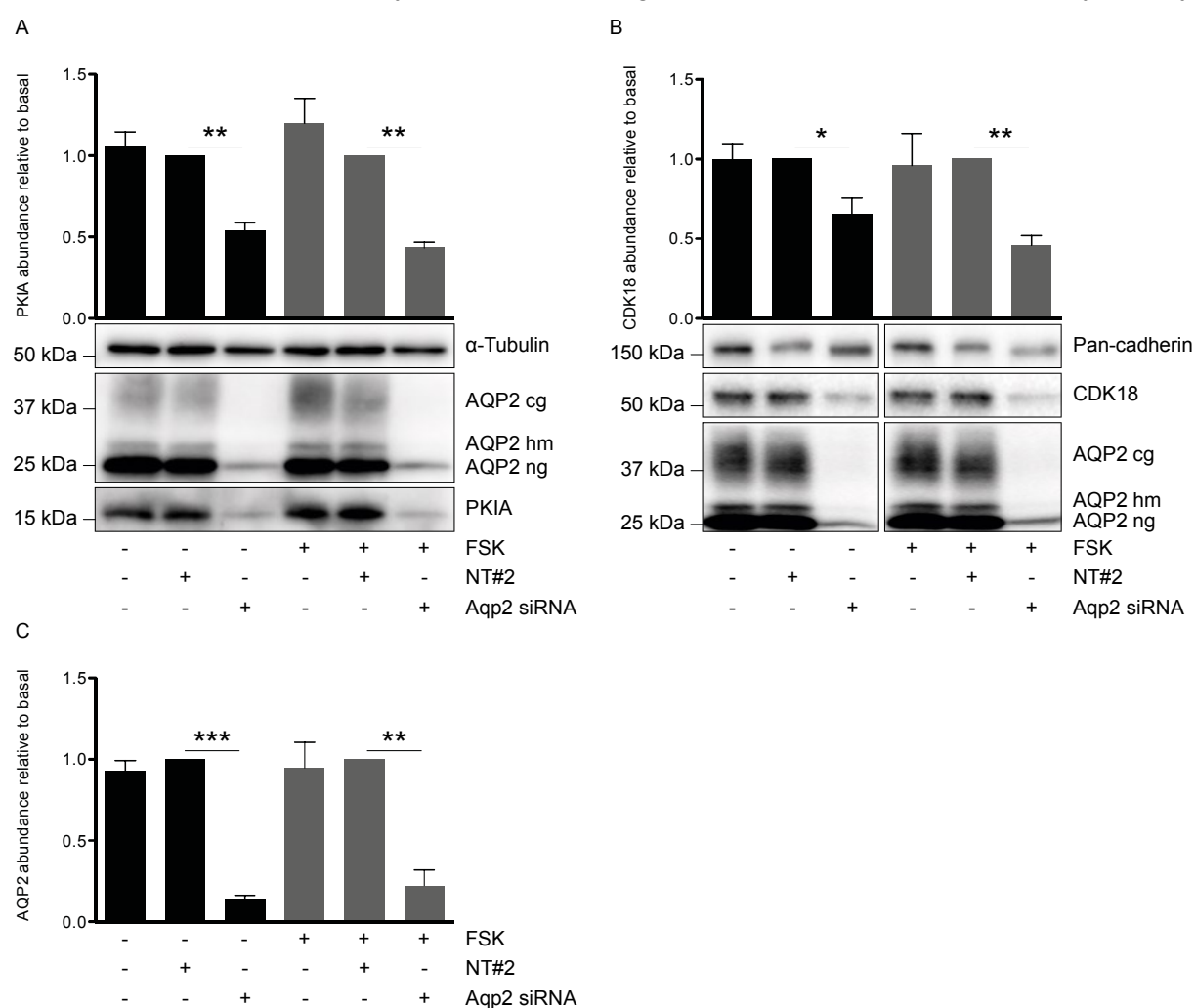


Fig. 30. The down regulation of AQP2 was accompanied by reduced *Cdk18* and *Pkia* gene expression. MCD4 cells were transfected with 50 nM Aqp2 or NT#2 siRNA or left untreated. The knockdown of AQP2 led to a approximately 50 % reduction of PKIA (A) and CDK18 (B) abundance compared to NT#2-transfected cells. C) AQP2 protein abundance was significantly reduced up to 85 % upon transfection with Aqp2 siRNA compared to NT#2-transfected cells. Cells were stimulated with 30 μ M FSK for 60 min, lysed afterwards and proteins were detected by Western Blotting with AQP2 (C17), Cdk18 (C17), Pkia (N20), Pan-cadherin (C3678) and α -Tubulin (CM1a) antibodies. Signals were quantified by densitometric analysis. Statistical analysis was performed using the unpaired t-test. Statistical significant differences are indicated. *, $p \leq 0.05$; **, $p \leq 0.01$; *** $p \leq 0.001$. Mean \pm SEM are plotted, $n = 3-7$ independent experiments. FSK, forskolin.

immunofluorescence microscopy. Pk α single siRNA did not inhibit target mRNA translation as PKIA protein abundance was not reduced compared to NT#2-transfected cells (Fig. 27B). Since a down regulation of PKIA using pooled siRNAs was observed after three days (Fig. 27A), it can be excluded that PKIA protein half life exceeds the assay's duration. In line, AQP2 redistribution did not change upon transfection with Pk α single siRNA compared to NT#2-transfected controls (Fig. 29).

Transfection with Cdk18 single siRNA led to a 37-50 % reduction of CDK18 protein abundance (Fig. 27D) and thus, was less effective than knockdown with pooled siRNAs (Fig. 27C). A 50 % decrease of CDK18 expression did not prevent the AQP2 redistribution completely (Fig. 29).

To gain further insight into the regulation of AQP2 by PKIA and CDK18, it was investigated whether a decrease in their gene expression affects AQP2 protein abundance and *vice versa*. MCD4 cells were transfected with pooled Cdk18 or Pk α siRNAs or single Aqp2 siRNA, and were analysed by Western Blotting. The down regulation of AQP2 of up to 85 % (Fig. 30C) significantly reduced the expression of both CDK18 and PKIA (Fig. 30A,B) by approximately 50 %.

Vice versa, a reduction of PKIA protein level did not alter AQP2 expression (Fig. 31). The knockdown of CDK18 was accompanied by a twofold increase of AQP2 protein abundance, in the absence or presence of FSK (Fig. 32A). Since AQP2 protein stability and intracellular

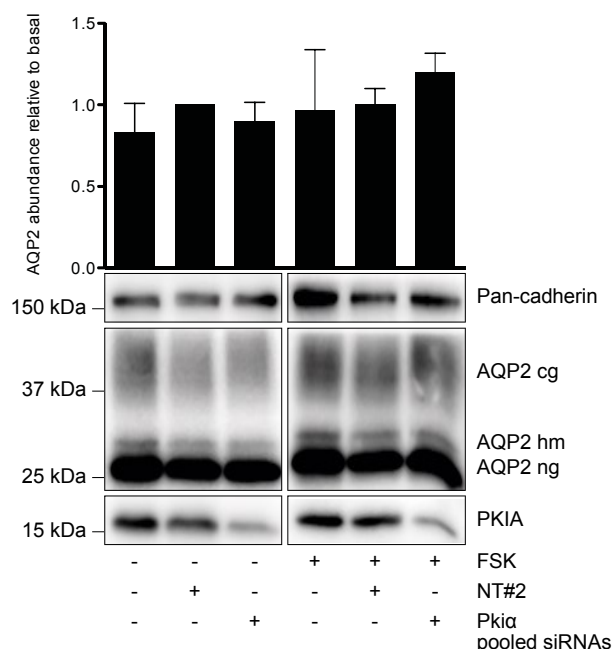


Fig. 31. The down regulation of PKIA did not affect AQP2 protein abundance. Cells were transfected with 50 nM pooled siRNAs where indicated. After three days cells were stimulated with 30 μ M FSK for 60 min, lysed and proteins were detected by Western Blotting with AQP2 (C17), Pk α (N20), Pan-cadherin (C3678) and α -Tubulin (CM1a) antibodies. Signals were quantified by densitometric analysis. Statistical analysis was performed using the unpaired t-test. Mean \pm SEM are plotted, n = 3 independent experiments. FSK, forskolin.

localisation are tightly regulated by its phosphorylation (1.3.1) it was investigated, whether AQP2 phosphorylation is influenced by CDK18 knockdown. Out of four relevant residues in the C-terminus of human AQP2 (1.3.1) the phosphorylation of two serines was analysed by Western Blotting: pS256 and pS261. The Phosphorylation of S264 and T269 could not be detected as no phospho-specific antibodies are available. Phosphorylation at S256 is triggering the AQP2 translocation to the plasma membrane. Surprisingly, a significantly increased pS256 abundance was observed in cells lacking CDK18 (Fig. 32B). The ratio of pS256/total AQP2 remained unchanged after the down regulation of CDK18 (Fig. 32D). pS261 levels correlate with AQP2 degradation²³. Since CDK18 knockdown leads to the elevation of total AQP2 levels, a reduction of pS261 was expected. Indeed, less pS261 was observed in cells lacking CDK18 compared to NT#2-transfected cells (Fig. 32C). As anticipated, stimulation with FSK led to the reduction of pS261 in untreated, mock-transfected and Cdk18-transfected cells. The ratio of pS261 to total AQP2 was decreased in cells lacking CDK18 compared to NT#2-transfected cells (Fig. 32E).

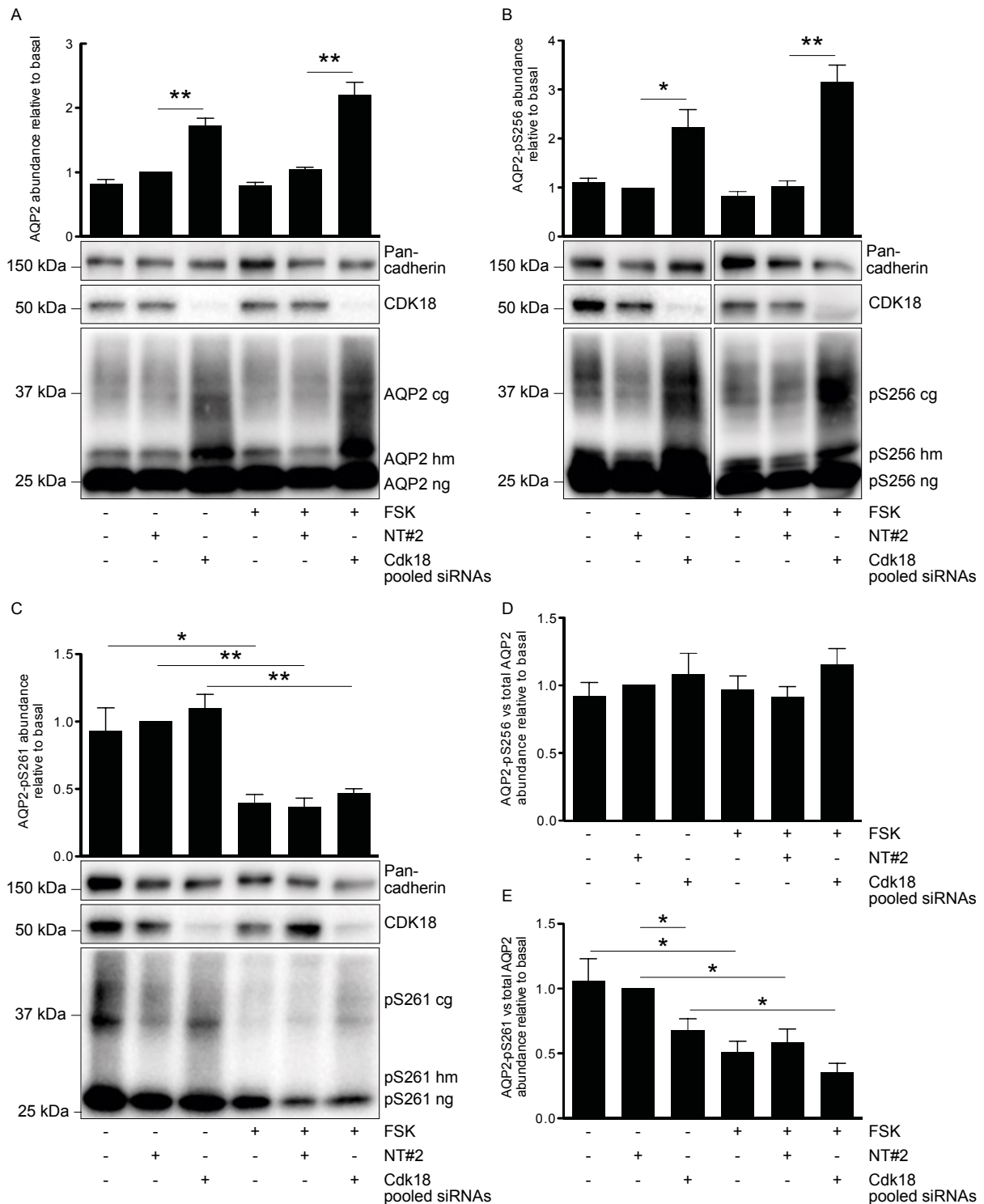


Fig. 32. CDK18 down regulation affects AQP2 protein abundance and its phosphorylation at S261. **A)** The knockdown of CDK18 was accompanied by significantly elevated AQP2 expression. **B)** Abundance of pS256 significantly increased after CDK18 silencing compared to NT#2-transfected cells. **C)** The level of pS261 significantly decreased upon FSK stimulation in untransfected, NT#2-transfected and Cdk18-transfected cells. **D)** Compared to total AQP2 expression the level of pS256 did not change upon CDK18 down regulation or FSK stimulation. **E)** Related to total AQP2 expression the level of pS261 was significantly reduced in cells lacking CDK18 and upon FSK stimulation. Cells were transfected with 50 nM pooled siRNAs as indicated or were left untreated. After three days cells were stimulated with 30 μ M FSK for 60 min, lysed and proteins were detected by Western Blotting with AQP2 (C17), pS256 (custommade), pS261 (ab72383), Cdk18 (C17), Pan-cadherin (C3678) and α -Tubulin (CM1a) antibodies. Signals were quantified by densitometric analysis. Statistical analysis was performed using the unpaired t-test. Statistical significant differences are indicated. *, $p \leq 0.05$; **, $p \leq 0.01$. Mean \pm SEM are plotted, $n = 3-4$ independent experiments. pS256, AQP2-pS256; pS261, AQP2-pS261; Cg, complexly glycosylated; hm, high mannose; ng, non glycosylated. FSK, forskolin.

4 DISCUSSION

Within the last decade comprehensive large scale studies revealed the proteome⁴⁷⁴, phosphoproteome⁴⁸, membrane proteome⁴⁷⁵ and transcriptome⁴⁷⁶ of kidney collecting duct cells, trying to unmask the complex AVP signalling network and to understand the molecular details of renal water reabsorption. However, none of them directly addressed the translocation of AQP2, the key player of collecting duct water transport.

In the present thesis the first loss of function study investigating the regulation of AQP2 trafficking was established. By sophisticated image and data analysis the difficult scorable phenotypes of MCD4 cells were automatically classified. Silencing of the mouse kinome revealed 13 genes, whose expression is necessary for the AQP2 transport to the plasma membrane and additional 24 genes, whose expression is indispensable for MCD4 viability. So far, none of these candidates was related to AQP2 or MCD4 survival.

The herein established method provides a powerful technique to investigate the AQP2 translocation in an unbiased genome-wide manner and thereby to provide fascinating new insight into the regulation of AQP2 as well as exciting therapeutic strategies.

4.1 Strengths and limitations of siRNA screenings

With large-scale RNAi screenings a powerful technology for high throughput analysis of gene function emerged. Genes involved in biological processes of interest can be identified in an unbiased genome wide approach.

Mammalian RNAi screens largely focussed on cancer biology aiming to identify genes that relate to drug resistance or are involved in cell cycle arrest, proliferation, DNA damage repair and cell migration^{448,477}. The assay readout is usually based on colorimetric, fluorescence or luminescence detection⁴⁷⁷. The minority of large-scale siRNA screens was conducted in mouse cell lines and even less focussed on image-based analysis of subcellular protein localisation⁴⁷⁷.

As in the present work, RNAi screenings are usually performed in duplicates or triplicates to minimise the false-positive and false-negative rates⁴⁴⁸. Transient transfection of siRNA leads to the short-term down regulation of gene expression and requires readouts within 48-96 hours⁴⁷⁸. This time might not be sufficient for the depletion of proteins with extended half lifes or the detection of long term effects as epigenetic changes. The down regulation of gene expression over a longer period (not to a larger extend) can be achieved by using short hairpin RNAs (shRNAs)⁴⁷⁹. Comprising approximately 65 nucleotides shRNAs are encoded

in adeno- or lentiviral vectors that stably incorporate into the genome of target cells⁴⁸⁰. A disadvantage in using shRNA is that the handling of infectious amphotropic viruses requires extra safety precautions as experiments are carried out under biosafety level 2⁴⁸¹ and thus, in the present thesis effects of siRNA-mediated gene silencing were investigated. Large-scale experiments often yield false positive and false negative results⁴⁸². In RNAi experiments these can result from off-target effects that are independent of the siRNA delivery method but are mediated by the oligonucleotides⁴⁸³. Unintended targets can be down regulated for three reasons. First, if the 3' UTR (untranslated region) of the transcript shows perfect complementarity to the siRNA hexa- or heptameric seed region, i.e. to bases 2-7/8 in its 5' end⁴⁸² that mediate specific target recognition. Second, if the siRNA oligonucleotide contains microRNA (miRNA) seed regions, defined as six to eight nucleotides at the 5' end of miRNAs that are essential for specific mRNA binding⁴⁸⁴ and therefore, acts like a miRNA. A third possibility is that the cellular RNAi machinery is saturated with exogenous siRNA, preventing endogenous miRNA function^{485,486}. Genes, whose expression is controlled by miRNA might be upregulated and therefore, might alter the cellular phenotype.

Potential off-target effects of the siRNAs used in this work were minimised by the development of predictive algorithms and enhanced siRNA design by the manufacturer Dharmacon⁴⁸². Additionally, effective screening design reduced the detection of off-targets as on every microtiter plate not only mock but also scrambled NT#2-transfected cells were included under both stimulated and unstimulated conditions (Fig. 21A). Thus, multiple treatments were considered for the phenotypic characterisation of controls and non-specific effects due to delivery or RNAi itself were taken into account.

In general, the RNAi-mediated knockdown of target proteins is not complete and a residual protein activity might remain⁴⁸¹. Also, silencing of redundant genes may not result in a detectable phenotype.

Results of RNAi screens are acutely sensitive to cell system, assay design, readout and statistical analysis. For example, in 2008 three groups independently conducted genome-wide siRNA screenings in either HeLa or HEK293 cells, aiming to identify genes that are critical for HIV replication⁴⁸⁷⁻⁴⁸⁹. All of them transfected pooled siRNAs and monitored reporter gene expression for assay readout. Surprisingly, there was only an overlap of hits of 7 %^{481,490}. Therefore, much effort is being made to create guidelines providing minimum information about RNAi experiments (MIARE⁴⁹¹) to enable the unambiguous interpretation and reproduction of the results⁴⁴⁹.

4.2 Specificity of siRNAs of the Mouse Protein Kinases sublibrary

The Mouse siGENOME siRNA library targets 16,872 genes (Tab. 1, Tab. 6). Out of 23,139 genes within the mouse genome (useast.ensembl.org/Mus_musculus/Info/Annotation), current siRNA libraries address approximately 19,000. Within the library four synthetic siRNA oligonucleotides directed against the same transcript are pooled (Tab. S 2). In comparison to transfection with single oligonucleotides of equal concentration, usage of pooled siRNAs increases knockdown efficiency and reduces off-target effects⁴⁸².

In the Mouse Protein Kinases sublibrary 719 genes are targeted by 2876 unique siRNA duplexes (Tab. S 1) that were assembled in 2008 based on NCBI RefSeq version 32 (3.3). Since genome annotations are continuously evolving the siRNA sequences were compared to NCBI RefSeq version 58 released in 2013. This revealed that 65 of 2876 duplexes do not bind to currently annotated transcripts (Tab. S 7). Even single base pair mismatches can dramatically alter siRNA functionality and lead to off-target effects⁴⁹². Whether the 65 duplexes bind to any other than originally targeted transcripts cannot be defined. Using the genome-wide basic local alignment search tool (BLAST⁴⁹³) no unique targets of 19 bp oligonucleotides were identified, as multiple genes scored equally. In 44 cases, one of four siRNAs did not match with indicated transcripts (Tab. S 7), i.e. only three duplexes were complementary to target mRNA: amongst them two gene products might be involved in the AQP2 redistribution, *Tk2* and *Trim27* (Tab. 18, Fig. S 6); three gene products were shown to be essential for MCD4 cell viability as their down regulation reduced MCD4 cell number to less than 60 % compared to NT#2-transfected cells, *Akap13*, *Evi5l* and *Mark3* (Tab. 14); and four genes encoding proteins that are known to regulate AQP2 (Tab. 2), *Pkba*, *Myo3a*, *Pp2cb* and *Pkcd* (Tab. S 7). Seven genes were targeted by two and additional two genes by either only one or none out of four siRNA oligonucleotides (Tab. S 7). Neither cellular viability (Tab. 14, Tab. S 1) nor AQP2 translocation (Tab. 18) was affected upon transfection with any of these siRNA pools. In total, 53 of 719 targets were not addressed by four siRNAs, which might have lowered efficiency of gene silencing.

siRNAs of the Dharmacon library are arranged in central 320 wells of a 384 well plate, leaving two rows on both sides for controls (Fig. 4). According to Zhang *et al.* an alternative is to place controls all over the plate but not only in outer regions⁴⁹⁴. Thereby, the normalisation of plate position-related effects i.e. well-, column- or row-specific effects would be more precise. Due to automated handling procedures systematic errors can occur, leading to misinterpretation of results⁴⁹⁵. Besides, wells at the edges are more exposed to

variations in temperature, humidity and oxygen than central wells⁴⁹⁶. However, no systematic errors were detected in this experiment as no gradient of cell number or fluorescent signal was identified (Fig. 21C,D) and gene products affecting both cellular viability (Tab. 14, Tab. S 1) and AQP2 redistribution (Tab. 18, Fig. 29) were identified in different regions of the microtiter plates. This proves robust assay setup and exact robotic liquid handling.

4.3 Characterisation of MCD4 cells

MCD4 cells express human AQP2 (Fig. 9) that inserts into the plasma membrane upon FSK stimulation (Fig. 8). Consequently, the molecular machinery relevant for the translocation of AQP2 is functional and MCD4 cells are appropriate for the analysis of proteins involved in the exocytosis-like AQP2 redistribution.

However, MCD4 cells do not express the V2R (Fig. 9C), which activates many pathways that might affect AQP2 trafficking²⁶. Regulators of AQP2 trafficking (1.3.3) upstream of AC cannot be detected in MCD4 cells. Accordingly, effects of bradykinin, dopamine and purine as well as the influence of Ca^{2+} , PGE_2 or NO on AQP2 translocation were not considered in the assay performed in this work. As MCD4 cells are not polarised it was not differentiated between AQP2 transport to apical or basolateral plasma membranes.

In rat primary IMCD cells, AQP2 protein abundance increases in response to AVP or FSK stimulation (Fig. 7B). Increased cytosolic cAMP leads to the stimulation of AQP2 transcription²⁸⁹ and in parallel to the inhibition of proteasomal AQP2 degradation²³. The underlying mechanism involves blocking of p38 MAPK and thus, reduction of the destabilizing phosphorylation of AQP2 at S261²³. As observed in rat primary IMCD cells¹⁶², the level of pS261 in MCD4 cells is decreased in response to FSK (Fig. 32C), indicating that AQP2 is not destabilised upon the elevation of the cAMP level. Thus, MCD4 cells are suitable for the analysis of phosphorylation-dependent changes in AQP2 stability and localisation. However, in MCD4 cells AQP2 expression remained unchanged after FSK treatment (Fig. 7B). The most likely explanation for this observation is that the transcription of hAQP2 is not controlled by its endogenous promoter. The cDNA was cloned into the *EcoRI-NotI* sites of the mammalian expression vector pcDNA3⁴¹⁸ (Invitrogen). The transcription of hAQP2 is controlled by the human cytomegalovirus (CMV) immediate early promoter, driving constitutively high expression. Most likely maximal expression level is reached already under unstimulated conditions.

Analysis of MCD4 cells by immunofluorescence microscopy revealed diverse cellular phenotypes. Stimulation with FSK resulted either in the detection of strong AQP2 plasma membrane (Fig. 33C) or homogenous AQP2 signals (Fig. 33D), which might represent an intermediate state between exclusive perinuclear and exclusive plasma membrane localisation. However, both phenotypes clearly differ from cells under resting conditions, in which AQP2 is localised perinuclearly (Fig. 33B). The presence and absence of perinuclear AQP2 speckles appears to be most suitable for quantitatively scoring these phenotypes. A fraction of the cells showed large intracellular compartments (Fig. 33A), whose number increased with increased passage number. Such structures suggest that cells undergo autophagy⁴⁹⁷. To minimise experimental variations, all experiments were conducted with the lowest possible cellular passage (42) using always the same lot of serum in the growth medium. Similar to rat primary IMCD cells⁴⁰⁹, 10-20 % of MCD4 cells completely lack AQP2 (Fig. 33B). Cells that did not express AQP2 (Fig. 33B) and cells showing large intracellular compartments (Fig. 33A) were not excluded during image analysis. Thus, hit identification by either method is based on the assumption that a relative constant number of cells shows these phenotypes (Fig. 33A, B).

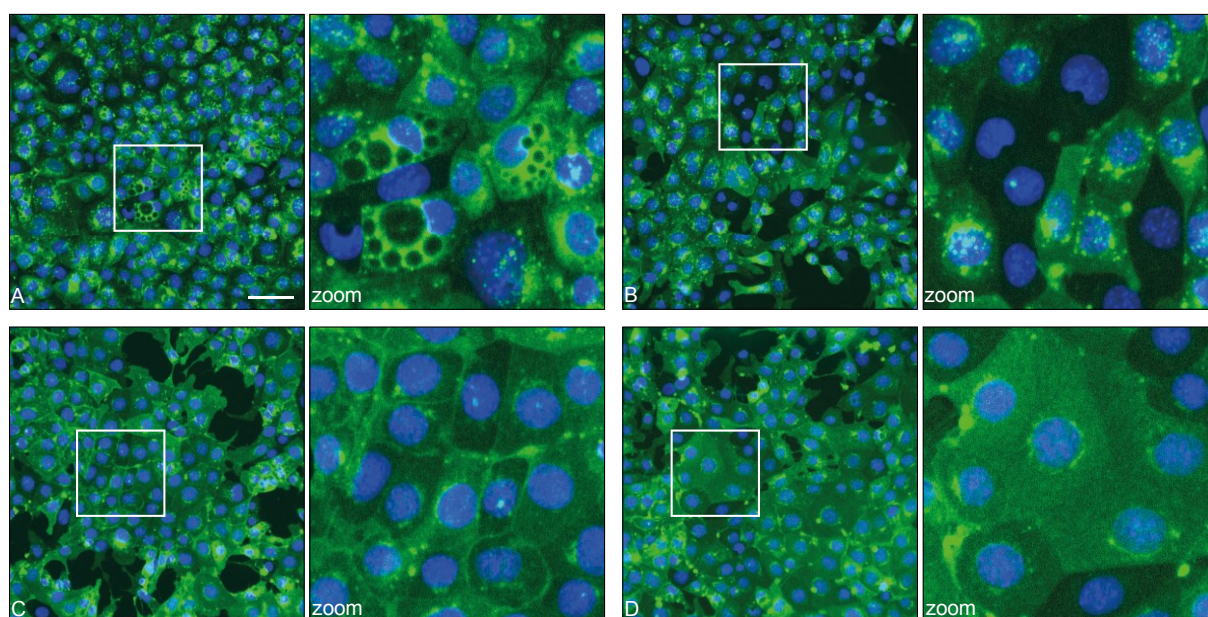


Fig. 33. Diverse phenotypes of MCD4 cells. **A)** Single MCD4 cells show large intracellular compartments, independently of prior treatment. Depicted cells were left untransfected and unstimulated. **B)** About 10-20 % of MCD4 cells show little or no AQP2 expression. Stimulation with 30 μ M FSK for 60 min decreased the number of perinuclear AQP2 speckles and led to increased AQP2 plasma membrane (**C**) as well as homogenous AQP2 signals (**D**). Images were acquired using an ArrayScan V^{TI} HCS Reader (20x magnification). The scale bar indicates 50 μ m. AQP2 is depicted in green, nuclei are shown in blue.

4.4 Transfection efficiency

A prerequisite for siRNA screenings is the sufficient delivery of siRNAs into the cells. The applied concentration of 50 nM is in the range of commonly used 25-100 nM final siRNA concentration in high throughput screenings⁴⁹⁸⁻⁵⁰⁰. Upscaling of the procedure to automated handling conditions did not impair the transfection efficiency as equivalent to manually conducted experiments a down regulation of up to 72 % was achieved (Fig. 21B). Gene silencing was constant within triplicates proving a robust assay that produces reliable results under normal experimental variation (Fig. 21B).

Commonly, transfection efficiency is not monitored in an arrayed format but shown exemplarily by the detection of fluorescent siRNAs or quantitative analysis of mRNA or protein levels of selected hits. Using Hepa-1 mouse epithelial hepatoma cells⁴⁹⁸ and CGR8 mouse embryonic stem cells⁵⁰¹, siRNA-mediated reduction in target transcripts of 54-79 % and 34-86 % was reported, respectively. In the present work, a target protein reduction of up to 85 % was achieved (Fig. 30C). Gene silencing was monitored on protein rather than mRNA level since a reduction in target transcripts does not necessarily imply a down regulation of respective proteins⁵⁰². In summary, the level of gene silencing is in range with comparable siRNA screenings and the down regulation is sufficient for loss of function studies.

4.5 High content image analysis

Automated image analysis enables the extraction of multiple cellular information, including intensity, localisation, shape and textures of defined subcellular compartments, whereas human observers typically score only one or a few obvious features⁴¹⁹. In this work, images were analysed using CellProfiler, an open source software for cell image analysis capable of extracting high information content. Created by the Broad Institute of MIT (Massachusetts Institute of Technology) and Harvard University, CellProfiler was the first of constantly emerging open-source software packages to profile microscopic images like GCellIQ⁵⁰³, CellCognition⁵⁰⁴, micropilot⁵⁰⁵, Icy⁵⁰⁶, Fiji⁵⁰⁷ or PhenoRipper⁵⁰⁸ (reviewed in Li *et al.* 2013⁵⁰⁹). Five of them were published in Nature within the last 3 years, highlighting the growing relevance of bioinformatic image analyses.

CellProfiler generates consistent, quantitative measures for every image and creates specific phenotypic fingerprints for each cell. In a so-called pipeline single modules are aligned, in which images are sequentially processed in a manually defined manner⁵¹⁰. Every image travels along the pipeline and is analysed by all modules⁴¹⁹. Visual information is reduced to a single numerical output⁵¹¹. The specific pipeline can be saved and rerun by other users.

In this work, a sophisticated image analysis was established; not only the absence or presence of fluorescence signals per well but also its subcellular localisation was measured (Fig. 18). Based on nuclei staining, differently sized perinuclear regions were defined, in which AQP2 speckles were detected. Based on various parameters AQP2 speckles were identified (Fig. 18), resulting in 72 different ways for analysing AQP2 speckles per nucleus (Fig. 19). This complex analysis allowed the evaluation of images derived from different microtiter plates on different days with the same pipeline without prior adjustment of the settings. The software generated 2,363,904 files per microtiter plate, amounting to a total of approximately 200 GB of data per plate.

In a first step, nucleus outlines were defined and expanded by 4-9 pixels (Fig. 18D-F). As in 4-8 pixel expansions only a fraction of perinuclear AQP2 speckles was included (Fig. 22), they were not considered in the downstream analysis. Nuclei expansions are not relative to overall cell size but fixed pixel definitions, indicating that in large cells a relatively smaller area is considered perinuclear than in small cells and hence, less AQP2 speckles are considered (Fig. 34).

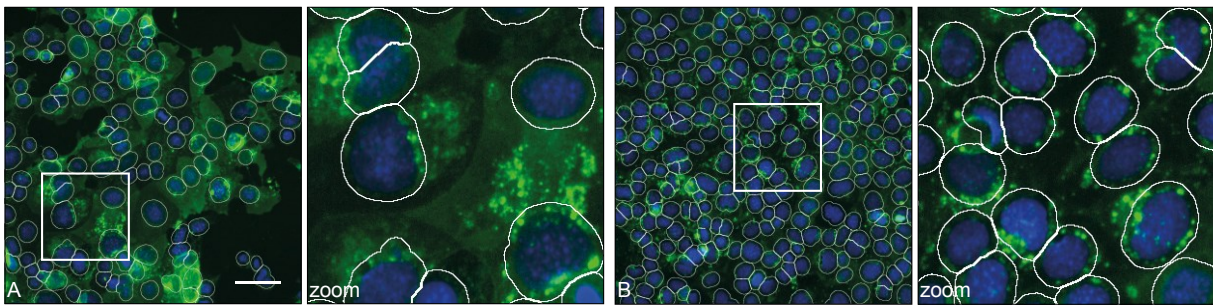


Fig. 34. Differently sized perinuclear regions. **A)** Nucleus outlines include the minority of AQP2 speckles. After transfection with Cdk18 siRNA MCD4 cell viability was reduced to 70 % compared to NT#2-transfected cells. **B)** Nucleus outlines include the majority of AQP2 speckles. Upon transfection with Pkia siRNA MCD4 cell viability remained unchanged in comparison to NT#2-transfected cells. Images were acquired using an ArrayScan VTI HCS Reader (20x magnification). The scale bar indicates 50 μ m. AQP2 is depicted in green, nuclei are shown in blue.

Gene silencing usually affects cellular viability. Although the down regulation of only 24 of in total 719 tested genes decreased MCD4 cell viability to less than 60 % (Tab. 14), in 83 % of all transfections MCD4 viability was lower than 90 % and in approximately 50 % of all transfections lower than 80 % compared to NT#2-transfected cells (Tab. S 1). Thus, siRNA-transfected cells have more space to spread than mock-transfected cells. Therefore, in future experiments it might be feasible to expand nuclei by more than 9 pixels. Alternatively, nuclei could be enlarged relative to corresponding cell size. In order to do so, plasma membranes would have to be defined and the ratio of nucleus to total cell area to be determined. However, this would markedly increase image acquisition and processing time.

AQP2 speckles were defined after fluorescent signals were computationally enhanced by a factor of 3 or 4 and one of six different threshold correction factors was applied (Fig. 19). Of in total 12 different settings of AQP2 speckle identification per nucleus outline expansion

the one detecting the biggest difference between both control conditions (Fig. 23) or resulting in highest Z'-factor (Tab. 17) was used for MLP classification (4.6) and Z-score-based analysis (4.7), respectively. Since the method used to analyse high throughput screenings has a tremendous impact on the hit identification⁵¹², both strategies were applied to reliably identify hits.

4.6 Profiling the translocation of AQP2 using MLP machine learning

In the present work the AQP2 localisation was analysed by the automated classification of cellular phenotypes using MLP machine learning. In contrast to other tools like the Advanced or Enhanced Cell Classifier (ACC⁵¹³; ECC⁵¹⁴) single cells did not have to be scored manually and thus, unbiased data evaluation was guaranteed.

MLP was trained with CellProfiler-derived metadata of mock-transfected cells that were left unstimulated or stimulated with FSK, representing positive and negative controls, respectively (Fig. 24A). Experimental variation was taken into account by creating training sets for every microtiter plate, which is a more robust approach than applying the same rule on all replicates⁵¹⁰. To verify the trained algorithms, metadata of NT#2-transfected cells were classified without predefining the output. MLP classification proved correct if all wells with unstimulated or FSK-stimulated NT#2-transfected cells were classified to be hits or no hits, respectively (Fig. 24B). Four of nine microtiter plates were classifiable, amongst them each plate of the Mouse Protein Kinase sublibrary was represented at least once (Tab. 16). In the remaining five plates, the MLP classification algorithms were not sufficient to group controls correctly, indicating that phenotypes of mock- and NT#2-transfected cells were too divergent or too similar to each other. Classification errors occurred on either side but only in rows K, L, M and N in the lower half of the microtiter plate (Tab. 16). In the majority of misclassifications unstimulated cells were grouped to be hits, suggesting that too few speckles were recognised. The reason for this is not known. Cells are seeded and stimulated using an automated dispenser module operating from the left to the right side of the microtiter plate, i.e. from column 1 to 24. Incorrect dispensation would result in a column- but not row-specific gradient. In addition, MLP was trained with metadata of mock-transfected cells, including wells located in the lower part of the microtiter plate. Consequently, effects of potential handling errors were considered in training algorithms.

Alternatively, metadata of NT#2-transfected cells could have been used for MLP training in addition to metadata of mock-transfected cells and thereby broaden the range of control specific parameters or could have been used for MLP backpropagation. Backpropagation

describes the correction of classification errors by readjusting the perceptrons weights⁴⁴⁵. However, in this case MLP classification could not have been verified plate-specifically.

Upon down regulation of 6 of 19 identified hits MCD4 cell viability was reduced to less than 60 % compared to NT#2-transfected cells (Tab. 18). These candidates were referred to as false positive and hence, excluded from the validation process. Wells showing reduced cell number were not already excluded during upstream image analysis as the absolute count varies microtiter plate-specifically and thus, no fix minimum could be set.

A common criticism of artificial neural networks such as MLP is that they operate as a black box and how or why an output is achieved remains elusive⁴⁴⁵. Algorithms of perceptrons in the hidden layer are not known. However, by restricting the input information MLP users can preselect relevant data. Here, classification was based on the relative distribution of perinuclear AQP2 speckles in unstimulated and FSK-stimulated mock-transfected cells (Fig. 23).

A drawback of machine learning is that novel phenotypes are not identified but grouped into predefined classes. As in the present work the morphology of single MCD4 cells was investigated in detail by sophisticated image analysis more insight into cellular phenotypes apart from AQP2 localisation can be gained. For example, the entire CellProfiler-derived metadata could be plotted and outliers could be visualised. Thereby, effects of gene silencing on for instance nuclei size and shape would be detectable and could hint to a gene's role in MCD4 cells.

4.7 Z-score-based analysis of AQP2 redistribution

Z-score-based analysis is reasonable if the Z'-factor exceeds 0.5⁴¹⁷, a criterion that is widely used to assess cell-based high throughput experiments⁵¹⁵. With regard to six different threshold correction factors each related to one of two different feature enhancements, metadata from mock- and NT#2-transfected cells were used for Z' calculation (Tab. 17). Positive Z'-factors were detected on four of nine microtiter plates (1.1, 1.3; 2.1 and 2.3), three of which were classifiable by MLP machine learning (1.3, 2.1 and 2.3; Tab. 16). Of in total 108 pairs of controls 15 resulted in positive Z'-factors in either mock-or NT#2-transfected cells and additional eight measurements showed positive Z'-factors for both control conditions. Multiple image analysis settings scored similar on the same microtiter plate. These findings highlight that the analysability largely depends on microtiter plate- and cell-specific parameters. Despite cellular variability sophisticated image analysis allowed the evaluation of diverse MCD4 phenotypes and reliable hit identification.

The majority of the settings did not allow standard Z-score-based analysis since discrepancies between control phenotypes were too large and the signal window between mean positive and mean negative controls was too small as expressed by negative Z'-factors. Microtiter plate 2.1 was suitable to undergo Z-score-based evaluation, with regard to the identification of AQP2 speckles upon feature enhancement by a factor 3 and application of a threshold correction factor of 0.70 that revealed a Z'-factor of 0.5 (Tab. 17). Any other of the remaining 11 settings of AQP2 speckle identification parameters led to dramatically decreased Z'-factors on microtiter plate 2.1. Thus, based on the same cellular phenotype Z'-factor variability depends on prior image analysis. The application of feature enhancement 3 and threshold correction factor 0.70 did not score highest on other plates. Therefore, the prioritisation of a single method to identify AQP2 speckles is not possible.

On microtiter plate 2.1, Z-score-based analysis was conducted, i.e. the number of standard deviations a sample is different from the mean was determined based on the ratio of AQP2 speckles per nucleus. A siRNA pool was considered as hit if it scored >2 standard deviations above the mean of all values (Fig. 25B). In contrast to MLP classification Z-score-based analysis did not result in a binary output but in a hit list with associated Z-scores allowing a ranking of the identified candidates. Theoretically, the microtiter plate-wise Z-score-based analysis might produce misleading results if a cluster of "active siRNA pools" is located on the same plate⁵¹⁶. However, of in total seven hits that were determined by using the Z-score tool, three candidates were also revealed by MLP machine learning that did not consider other sample but control values only (Fig. 25). This confirms the reliable detection of hits. None of them showed viability of less than 60 % compared to NT#2-transfected cells (Tab. 14). In contrast, the MLP classification of metadata derived from the same microtiter plate revealed one gene, whose down regulation led to 25 % remaining viability (well F19, pooled siRNAs targeting *Plk1* mRNA, Tab. 14, Fig. 25A). This indicates that Z-score-based analysis reduces the identification of false positives. However, as only one of nine microtiter plates was analysable by this statistical tool, MLP machine learning is the method of choice to automatically evaluate the phenotype of MCD4 cells.

4.8 Hit validation

The collecting duct kinome comprises 154 kinases out of 518 that exist in the whole genome⁵¹⁷. 60 of these 154 kinases likely participate in AVP signalling⁵¹⁷ as they were up or down regulated in response to AVP⁵¹⁷; 15 were described to be involved in the control of AQP2 expression and/or localisation (Tab. 2). In the work presented here, 13 hits were identified to be relevant for the AQP2 redistribution, amongst them 10 genes encoding kinases or subunits of kinases (Tab. 18).

Validation experiments were conducted to verify the performance of automated image and data analysis and to gain insight into the functional implication of selected hits with regard to the AQP2 control. MCD4 cells were transfected with siRNAs targeting *Cdk18* and *Pkia*, both of which were detected by MLP machine learning as well as Z-score-based analysis (Fig. 25). The down regulation of both, *Cdk18* or *Pkia* expression, impaired the translocation of AQP2 to the plasma membrane upon FSK stimulation and led to the perinuclear accumulation of AQP2. Thus, the here established workflow composed of a combination of sophisticated image analysis with microtiter plate-specific data evaluation using MLP machine learning and common statistical tools did result in reliable and robust hit identification.

Although hit identification was confirmed, it cannot be ruled out that observed effects were elicited by siRNA-mediated off-target effects, i.e. by the down regulation of unintended targets due to afore mentioned reasons (4.1). However, according to the microRNA database miRBase⁵¹⁸ siRNAs directed against the identified hits (Tab. S 8) are not complementary to any mouse miRNA, providing strong evidence that the siRNAs target the specific mRNAs.

To detect off-target effects, most commonly smart pools are deconvoluted into their constituent siRNAs and rescreened using the same assay⁴⁴⁸. The effect is confirmed if transfection with at least two of four different siRNAs duplexes results in the same phenotype. However, this strategy focuses on an identical readout as the primary screen, i.e. this approach may rely on the detection of secondary effects but does not directly prove specific gene silencing. In the work presented here, specificity of siRNA pools was investigated by monitoring target protein abundance three days after transfection. Western Blotting revealed the significant down regulation of CDK18 and PKIA upon transfection with the respective siRNA pools (Fig. 27A,B). Additionally, MCD4 cells were transfected with single *Cdk18* and *Pkia* siRNAs that are directed against yet untargeted regions of the mRNAs (Tab. 8, Tab. S 2). PKIA abundance was not reduced (Fig. 27B), indicating that single *Pkia* siRNA was ineffective. In line, the AQP2 redistribution was not impaired (Fig. 29). The use of single *Pkia* siRNA was not sufficient to down regulate PKIA and did not affect AQP2 localisation. Although this does not validate this target it shows the specificity of the approach. The CDK18 protein level was significantly decreased after transfection with *Cdk18* single siRNA (Fig. 27D), albeit not as drastic as upon transfection with pooled *Cdk18* siRNAs (Fig. 27C). CDK18 reduction by approximately 40 % did not completely inhibit the AQP2 redistribution (Fig. 29). However, although AQP2 was detected in the plasma membrane, perinuclear AQP2 abundance was increased upon transfection with *Cdk18* single siRNA. The positive correlation between protein knockdown and phenotype penetrance underlines that CDK18 is involved in the control of AQP2.

4.8.1 CDK18

The down regulation of CDK18 reduced the viability of MCD4 cells by 30 % (Tab. 14), impaired the AQP2 translocation (Fig. 26, Fig. 29) and led to significantly increased AQP2 abundance independently of FSK stimulation (Fig. 32A). Surprisingly, CDK18 down regulation did not lower AQP2 phosphorylation at S256 (Fig. 32B), which is the key trigger for the AQP2 redistribution¹⁵⁷. Since this phosphorylation is catalysed by PKA¹⁵⁵ or PKG²⁴⁸ one possible explanation might be that the down regulation of CDK18 reduces PKA and/or PKG activity.

Upon CDK18 silencing, AQP2 phosphorylation at S261 was decreased by 32 % (Fig. 32E). Since the phosphorylation at S261 is associated with the proteasomal degradation of AQP2^{23,164}, the down regulation of CDK18 and the associated decrease of S261 phosphorylation is likely to account for the increase in AQP2 protein abundance. As a putative kinase phosphorylating AQP2 at S261 is p38-MAPK²³, a possible explanation would be that active CDK18 lowers p38-MAPK activity.

Vice versa, it was investigated whether the knockdown of AQP2 affects CDK18 abundance. The down regulation of AQP2 of up to 85 % (Fig. 30C) led to significantly decreased CDK18 abundance (Fig. 30B), which emphasises a mutual regulation of both proteins.

CDK18 belongs to the CDK family of serine/threonine protein kinases that are involved in various processes such as proliferation, transcription, mRNA processing, translation or the control of differentiation and function of neurons⁵¹⁹. Whereas the majority of CDKs is well characterised, the function of CDK18 is poorly understood. CDK18 shows highest expression in brain, kidney and intestine⁵²⁰. Increased CDK18 expression was reported in Alzheimer's disease⁴⁶⁴; large-scale RNAi studies revealed an involvement of CDK18 in mitosis⁵²¹. Whether CDK18 exhibits kinase activity is unknown⁴⁶⁴. Mouse CDK18 contains multiple phosphorylation sites, including consensus sequences for PKA and PKC (Fig. S 8). Although the CDK18 sequence strongly varies amongst species⁵¹⁹, mouse and human CDK18 share 91 % amino acid identity (Fig. S 9). Human CDK18 is associated with the plasma membrane⁵¹⁹ and was shown to interact with 22 proteins (Tab. 19). Amongst them, two proteins are known to participate in the control of AQP2, CDK5 and PP2A (PPP2CB; Tab. 2). CDK5 phosphorylates AQP2 at S261²⁹⁷. Since CDK18 knockdown was associated with decreased phosphorylation of AQP2 at S261 (Fig. 32E), the CDK5-mediated phosphorylation of AQP2 might depend on CDK18. The inhibition of PP2A by okadaic acid induces the AQP2 redistribution without affecting its phosphorylation at S256²⁹³, indicating that the phosphatase counteracts the AQP2 transport PKG and/or PKA-independently. Although CDK18 and PP2A exert opposing effects on AQP2 trafficking, they both regulate AQP2 localisation independently of the phosphorylation at S256. One possible explanation would be that CDK18 negatively regulates PP2A.

Tab. 19. Interaction partners of human CDK18.

	Protein symbol	Protein name	Reference
1	BAG6	Large proline-rich protein BAG6	522
2	CCDC85B	Coiled-coil domain-containing protein 85B	523
3	CCNK	Cyclin-K	523
4	CDK5	Cyclin-dependent kinase 5	522
5	EEF2	Elongation factor 2	522
6	EIF3I	Eukaryotic translation initiation factor 3 subunit I	522
7	GNB4	Guanine nucleotide-binding protein subunit beta-4	522
8	HSP90AB1	Heat shock protein HSP 90 beta	524
9	LARP4B	La-related protein 4B	522
10	MAGED2	Melanoma-associated antigen D2	522
11	MTR	Methionine synthase	522
12	NSRP1	Nuclear speckle splicing regulatory protein 1	522
13	NTPCR	Cancer-related nucleoside-triphosphatase	522
14	PPP2CB	Serine/threonine-protein phosphatase 2A catalytic subunit beta isoform	522
15	PPP5C	Serine/threonine-protein phosphatase 5	522
16	SEC23A	Protein transport protein Sec23A	525
17	SEC24D	Protein transport protein Sec24D	525
18	STUB1	E3 ubiquitin-protein ligase CHIP	522
19	UBL4A	Ubiquitin-like protein 4A	522
20	YWHAB	14-3-3 protein beta/alpha	526
21	YWHAH	14-3-3 protein eta	526
22	YWHAZ	14-3-3 protein zeta/delta	526

Interaction partners of human CDK18 were listed according to the NextProt database (www.nextprot.org).

4.8.2 PKIA

A reduction of PKIA protein by just 30 % (Fig. 27A) completely blocked the AQP2 transport to the plasma membrane and led to the exclusive perinuclear localisation of AQP2 (Fig. 26, Fig. 29). Whereas PKIA down regulation did not affect AQP2 protein abundance (Fig. 31), the knockdown of AQP2 significantly reduced the PKIA level by 50 % (Fig. 30A). The down regulation of PKIA did not affect MCD4 viability (Tab. 18).

PKIA is a potent inhibitor of PKA⁵²⁷. Following the cAMP-mediated dissociation of the PKA holoenzyme into its regulatory and catalytic subunits, PKIA functions as a pseudo-substrate and selectively binds and thereby inhibits the catalytic subunits⁴⁵⁰. Thus, the phosphorylation of PKA substrates is prevented. In addition, PKIA controls the intracellular distribution of active PKA by regulating the nuclear export of free catalytic subunits into the cytoplasm⁴⁵¹. Upon down regulation of PKIA and stimulation with FSK the catalytic subunits of PKA might be trapped within the nucleus and therefore, cannot phosphorylate AQP2.

According to the STRING database that describes functional protein association networks⁵²⁸ PKIA is predicted to bind to Profilin 2 (PFN2), as both proteins show similar patterns of mRNA expression. PFN2 is required for actin polymerisation in the synapse⁵²⁹. Since actin depolymerisation promotes AQP2 transport to the plasma membrane^{168,169}, Pfn could possibly be involved in the control of AQP2 redistribution. However, if and how PKIA interacts with PFN2 *in vivo* and whether this is controlled by PKA remains to be established.

4.8.3 Proteins involved in AQP2 control

Proteins indicated in Tab. 2 are known to participate in the control of AQP2. Of these, 26 proteins or protein subunits are targeted by siRNA pools of the Mouse Protein Kinase sublibrary. In the present thesis, none of them was identified to be essential for the FSK-stimulated AQP2 translocation in MCD4 cells (Tab. 18, Fig. S 7):

AKAP220 is thought to facilitate AQP2 phosphorylation by targeting PKA to AQP2-bearing vesicles¹⁵². Apparently, its expression is not crucial for the AQP2 translocation in MCD4 cells as a down regulation of AKAP220 did not impair the FSK-induced AQP2 redistribution (Fig. S 7). CSNK phosphorylates AQP2 at S256 during its GOLGI transition^{311,312}. As cells were stimulated with FSK, PKA was highly likely to be fully activated, which might have overwhelmed potential effects of CSNK knockdown. Possibly, a perinuclear pool of PKA outside the GOLGI is activated¹⁵³ and thus, AQP2 is phosphorylated at S256. MLCK was suggested to facilitate the translocation of AQP2 by regulating the interaction of myosin and actin²²³ that is predominantly responsible for AQP2 transport to the plasma membrane¹⁹⁴. However, AQP2 localisation is mediated only in part through activation of MLCK²²³ and thus, possible effects of MLCK down regulation might have been overwhelmed by constantly activated PKA. The knockdown of PKG did not block the AQP2 redistribution in response to FSK (Fig. S 7). Possibly, the down regulation of the PKG-mediated phosphorylation of AQP2 at S256²⁴⁸ triggering the AQP2 redistribution was compensated by constantly activated PKA activity. Down regulation of five PKA subunits (Fig. S 7; PKACA, PKACB, PKAR1A, PKAR2A, PKAR2B) did not inhibit AQP2 translocation, indicating that they are functionally redundant.

As expected, silencing of CDK1, CDK5, ERK1/2, GSK3B, JNK1/2, p38-MAPK, PI3K, PKC, PP1/2A did not affect the FSK-stimulated translocation of AQP2; most of them do not participate in AQP2 exocytosis-like transport (Tab. 2). ERK1/2 and JNK1/2 may mediate the phosphorylation of AQP2 at S256 under hypotonic conditions, which were not tested in this experiment (Tab. 2, 4.3) and inhibition of the phosphatases PP1/2A induces AQP2 transport to the apical plasma membrane²⁹³.

Of note, none of these effects was validated, yet. Bearing in mind that on the one hand the degree of siRNA-mediated protein reduction might not be sufficient to elicit a detectable effect and on the other hand that decreased gene expression might be compensated by redundant proteins, these findings need to be verified in additional experiments.

The redistribution of AQP2 was measured by analysing perinuclear AQP2 speckles. Thus, it cannot be distinguished between the sub-plasma membrane and plasma membrane localisation of AQP2. Accordingly, in this assay it cannot be detected whether gene products are necessary for vesicle to plasma membrane fusion.

5 PERSPECTIVE

In the present thesis a powerful technique to automatically analyse the AQP2 trafficking in an unbiased large-scale manner was established. After siRNA-mediated silencing of the murine kinome, the localisation of AQP2 was investigated on a single-cell level and the expression of 13 genes was shown to be essential for its exocytosis-like transport to the plasma membrane. To our knowledge, this is the first high throughput analysis of gene function regarding the control of AQP2.

The here presented method is a suitable tool to screen the complete Mouse siGENOME siRNA library and thereby extend the analysis to a genome-scale range. Thus, global networks controlling cAMP-induced AQP2 redistribution could be identified. Using bioinformatics resources like DAVID, FuncAssociate or MAPPFinder (Huang *et al.*⁵³⁰) the biological significance of the identified genes could be analysed systematically and thereby reveal exciting insight into the AQP2 control. Novel drug targets could be identified for the treatment of diseases associated with high level of AVP, such as CHF.

In addition, the screening could be conducted without prior FSK stimulation of the cells and thereby, genes whose down regulation triggers AQP2 translocation could be identified.

In future experiments the involvement of the 13 identified gene products in the control of the AQP2 redistribution should be validated, first, by investigating specific target protein reduction *via* Western Blotting and second, by using another non image-based readout. Exemplarily, cell surface proteins (including AQP2) could be biotinylated and precipitated using streptavidin. By Western Blotting AQP2 abundance in response to FSK and after the specific down regulation of gene expression could be analysed. Another approach to validate candidates is to rescue the phenotype by expressing a RNAi resistant version of the target in the presence of siRNA⁴⁸¹. For this, siRNAs targeting the 3' UTR of targets and cDNA encoding the respective gene product without its 3' UTR should be utilised. The validation should be extended to cells that express the V2R such as rat primary IMCD cells.

In this work, it was observed that knockdown of PKIA and CDK18 inhibited the AQP2 translocation in response to FSK (Fig. 26, Fig. 29). Knockdown of PKIA did not alter AQP2 protein abundance (Fig. 31). In future experiments, the phosphorylation status of AQP2 as well as total PKA activity upon the knockdown of PKIA should be analysed. Further, the localisation of the catalytic subunit of PKA could be investigated by immunofluorescence microscopy.

Knockdown of CDK18 led to significantly increased AQP2 protein abundance (Fig. 32A). Whereas the phosphorylation of AQP2 at S256 was not altered (Fig. 32D), phosphorylation at S261 was impaired upon down regulation of CDK18 (Fig. 32E). In future experiments activities of PKA phosphorylating S256 and p38-MAPK phosphorylating S261 should be investigated. In contrast to human CDK18, the interaction proteins of mouse CDK18 are not known. Thus, interaction partners of CDK18 in MCD4 cells could be identified by mass spectrometry upon CDK18 precipitation. Of note, human CDK18 interacts with the E3 ubiquitin-protein ligase CHIP (carboxyl terminus of Hsp70-interacting protein; STUB1). As the E3 ligase mediating AQP2 degradation is presently unknown (1.3.2) and since CDK18 regulates AQP2 stability through controlling S261 phosphorylation (Fig. 32A), a possible involvement of STUB1 in AQP2 ubiquitination could be investigated in future experiments.

6 SUMMARY

Water reabsorption in the renal collecting duct is controlled by arginine-vasopressin (AVP). By binding to vasopressin-type-2 receptors (V2R) on the basolateral surface of renal principal cells, AVP elicits an increase in cAMP and thus, the activation of protein kinase A (PKA). PKA phosphorylates the water channel aquaporin-2 (AQP2), which induces its translocation from perinuclear vesicles to the plasma membrane. This causes a 10-100 fold increase in water reuptake from the primary urine. The molecular details of AQP2 transport are largely unknown. Aberrations in AVP-mediated water reabsorption are associated with nephrogenic diabetes insipidus (NDI), the syndrome of inappropriate antidiuretic hormone secretion (SIADH) and congestive heart failure (CHF).

Here, an image-based siRNA screening was established to identify genes whose expression is essential for the AQP2 redistribution. In mouse collecting duct (MCD4) cells, stably expressing human AQP2, the 719 genes comprising kinome was silenced and the subcellular AQP2 localisation was analysed by automated immunofluorescence microscopy. Sophisticated image analysis using CellProfiler software and the combination of phenotypic classification applying artificial neural networks and the evaluation by standard statistical metrics revealed 13 so far unknown gene products that are essential for the AQP2 translocation. One candidate is cyclin-dependent kinase 18 (CDK18), whose down regulation impaired AQP2 plasma membrane targeting and in parallel led to significantly increased AQP2 protein abundance.

By integrating biological and computational approaches, the herein established method represents a powerful technique to elucidate molecular mechanisms underlying the AQP2 redistribution in an unbiased genome-wide manner. This contributes to the identification of potential therapeutic targets for the treatment of diseases associated with aberrant AVP-mediated water reabsorption.

7 ZUSAMMENFASSUNG

Die Wasserrückresorption im renalen Sammelrohr wird durch Arginin-Vasopressin (AVP; Antidiuretisches Hormon, ADH) reguliert. Durch Bindung an den Vasopressin-Typ-2 Rezeptor auf der basolateralen Oberfläche renaler Hauptzellen bewirkt AVP einen Anstieg von intrazellulärem cAMP und folglich die Aktivierung der Proteinkinase A (PKA). PKA phosphoryliert den Wasserkanal Aquaporin-2 (AQP2), wodurch dessen Translokation von peri-nukleären Vesikeln zur Plasmamembran induziert wird. Dies bewirkt einen bis zu 100-fachen Anstieg der Rückresorption von Wasser aus dem Primärharn. Die molekularen Mechanismen des AQP2 Transportes sind größtenteils unbekannt. Störungen AVP-vermittelter Wasserrückresorption sind mit nephrogenem Diabetes insipidus (NDI), dem Syndrom der inadäquaten ADH-Sekretion (SIADH) und Herzinsuffizienz assoziiert.

In der vorliegenden Arbeit wurde ein siRNA screening etabliert um Gene zu identifizieren, dessen Expression für die AQP2 Translokation essenziell ist. In murinen Sammelrohrzellen, welche stabil humanes AQP2 exprimieren (MCD4-Zellen), wurde die Expression des 719 Gene umfassenden Kinoms inhibiert und die subzelluläre Lokalisierung von AQP2 durch automatische Immunfluoreszenzmikroskopie analysiert. Hochkomplexe Bildanalyse und die Kombination von Zellklassifizierung mit Hilfe eines artifiziellen neuronalen Netzes sowie die Analyse anhand statistischer Standardmethoden ergaben 13 bisher unbekannte Gene, dessen Expression für die AQP2 Umverteilung unerlässlich ist. Ein Kandidat ist *Cyclin-dependent kinase 18* (CDK18), dessen Herunterregulierung die AQP2 Translokation inhibierte und gleichzeitig zu einem signifikanten Anstieg der AQP2 Abundanz führte.

Durch das Integrieren molekularbiologischer und bioinformatischer Methoden bildet die in dieser Arbeit etablierte Analyse eine leistungsstarke Technik, um die molekularen Mechanismen der AQP2 Umverteilung genomweit zu erforschen. Dies trägt zur Identifizierung potenzieller therapeutischer Angriffspunkte zur Behandlung von Erkrankungen bei, welche mit gestörter AVP-vermittelter Wasserrückresorption assoziiert sind.

8 BIBLIOGRAPHY

- 1 Boone, M. *et al.* Physiology and pathophysiology of the vasopressin-regulated renal water reabsorption. *Pflugers Arch* 456, 1005-1024 (2008).
- 2 King, L. S. *et al.* From structure to disease: the evolving tale of aquaporin biology. *Nat. Rev. Mol. Cell Biol.* 5, 687-698 (2004).
- 3 Kamsteeg, E.-J. *et al.* Repulsion between Lys258 and upstream arginines explains the missorting of the AQP2 mutant p.Glu258Lys in nephrogenic diabetes insipidus. *Hum. Mut.* 30, 1387-1396 (2009).
- 4 Skeggs, L. T. *et al.* The biochemistry of the renin-angiotensin system and its role in hypertension. *Am. J. Med.* 60, 737-748 (1976).
- 5 Quinn, S. J. *et al.* Regulation of aldosterone secretion. *Annu. Rev. Physiol.* 50, 409-426 (1988).
- 6 Pacha, J. *et al.* Regulation of Na channels of the rat cortical collecting tubule by aldosterone. *J. Gen. Physiol.* 102, 25-42 (1993).
- 7 Peti-Peterdi, J. *et al.* Angiotensin II directly stimulates ENaC activity in the cortical collecting duct via AT(1) receptors. *J. Am. Soc. Nephrol.* 13, 1131-1135 (2002).
- 8 Klingler, C. *et al.* Angiotensin II potentiates vasopressin-dependent cAMP accumulation in CHO transfected cells. Mechanisms of cross-talk between AT1A and V2 receptors. *Cell. Signal.* 10, 65-74 (1998).
- 9 Bourque, C. W. *et al.* Osmoreceptors, osmoreception, and osmoregulation. *Front. Neuroendocrinol.* 15, 231-274 (1994).
- 10 Tashima, Y. *et al.* Intranephron localization and regulation of the V1a vasopressin receptor during chronic metabolic acidosis and dehydration in rats. *Pflugers Arch* 442, 652-661 (2001).
- 11 Izumi, Y. *et al.* Aldosterone requires vasopressin V1a receptors on intercalated cells to mediate acid-base homeostasis. *J. Am. Soc. Nephrol.* 22, 673-680 (2011).
- 12 Kitano, H. *et al.* Vasopressin and oxytocin receptor mRNAs are expressed in the rat inner ear. *Neuroreport* 8, 2289-2292 (1997).
- 13 Morel, F. *et al.* Receptors to vasopressin and other hormones in the mammalian kidney. *Kidney Int.* 31, 512-520 (1987).
- 14 Bolignano, D. *et al.* Aquaretic inhibits renal cancer proliferation: Role of vasopressin receptor-2 (V2-R)☆. *Urol. Ocol.-Semin. Ori.* 28, 642-647 (2010).
- 15 Bugaj, V. *et al.* Activation of the epithelial Na⁺ channel in the collecting duct by vasopressin contributes to water reabsorption. *Am. J. Physiol. Renal Physiol.* 297, F1411-1418 (2009).
- 16 Bankir, L. Antidiuretic action of vasopressin: quantitative aspects and interaction between V1a and V2 receptor-mediated effects. *Cardiovasc. Res.* 51, 372-390 (2001).
- 17 Sands, J. M. Molecular mechanisms of urea transport. *J. Membr. Biol.* 191, 149-163 (2003).
- 18 Hayashi, M. *et al.* Expression and distribution of aquaporin of collecting duct are regulated by vasopressin V2 receptor in rat kidney. *J. Clin. Invest.* 94, 1778-1783 (1994).
- 19 DiGiovanni, S. R. *et al.* Regulation of collecting duct water channel expression by vasopressin in Brattleboro rat. *Proc. Natl. Acad. Sci. U. S. A.* 91, 8984-8988 (1994).
- 20 Hozawa, S. *et al.* cAMP motifs regulating transcription in the aquaporin 2 gene. *Am. J. Physiol. Renal Physiol.* 270, C1695-1702 (1996).
- 21 Sandoval, P. C. *et al.* Proteome-Wide Measurement of Protein Half-Lives and Translation Rates in Vasopressin-Sensitive Collecting Duct Cells. *J. Am. Soc. Nephrol.* (2013).
- 22 Kamsteeg, E. J. *et al.* Short-chain ubiquitination mediates the regulated endocytosis of the aquaporin-2 water channel. *Proc. Natl. Acad. Sci. U. S. A.* 103, 18344-18349 (2006).
- 23 Nedvetsky, P. I. *et al.* Reciprocal Regulation of Aquaporin-2 Abundance and Degradation by Protein Kinase A and p38-MAP Kinase. *J. Am. Soc. Nephrol.* 21, 1645-1656 (2010).
- 24 Nielsen, S. *et al.* Cellular and subcellular immunolocalization of vasopressin-regulated water channel in rat kidney. *Proc. Natl. Acad. Sci. U. S. A.* 90, 11663-11667 (1993).
- 25 Star, R. A. *et al.* Calcium and cyclic adenosine monophosphate as second messengers for vasopressin in the rat inner medullary collecting duct. *J. Clin. Invest.* 81, 1879-1888 (1988).
- 26 Hoffert, J. D. *et al.* Dynamics of the G protein-coupled vasopressin V2 receptor signaling network revealed by quantitative phosphoproteomics. *Mol. Cell. Proteomics* 11, M111 014613 (2012).
- 27 Preston, G. M. *et al.* Appearance of water channels in *Xenopus* oocytes expressing red cell CHIP28 protein. *Science* 256, 385-387 (1992).
- 28 Reizer, J. *et al.* The MIP family of integral membrane channel proteins: sequence comparisons, evolutionary relationships, reconstructed pathway of evolution, and proposed functional differentiation of the two repeated halves of the proteins. *Crit. Rev. Biochem. Mol. Biol.* 28, 235-257 (1993).
- 29 Ishibashi, K. *et al.* Aquaporin water channels in mammals. *Clin. Exp. Nephrol.* 13, 107-117 (2009).
- 30 Rojek, A. *et al.* A current view of the mammalian aquaglyceroporins. *Annu. Rev. Physiol.* 70, 301-327 (2008).
- 31 Ishibashi, K. Aquaporin superfamily with unusual npa boxes: S-aquaporins (superfamily, sip-like and subcellular-aquaporins). *Biochim. Biophys. Acta* 52, 20-27 (2006).
- 32 Nielsen, S. *et al.* CHIP28 water channels are localized in constitutively water-permeable segments of the nephron. *J. Cell Biol.* 120, 371-383 (1993).
- 33 Sabolic, I. *et al.* Localization of the CHIP28 water channel in rat kidney. *Am. J. Physiol. Cell Physiol.* 263, C1225-1233 (1992).
- 34 Hasegawa, H. *et al.* Molecular cloning of a mercurial-insensitive water channel expressed in selected water-transporting tissues. *J. Biol. Chem.* 269, 5497-5500 (1994).
- 35 Ecelbarger, C. A. *et al.* Aquaporin-3 water channel localization and regulation in rat kidney. *Am. J. Physiol. Renal Physiol.* 269, F663-672 (1995).
- 36 Frigeri, A. *et al.* Immunolocalization of the mercurial-insensitive water channel and glycerol intrinsic protein in epithelial cell plasma membranes. *Proc. Natl. Acad. Sci. U. S. A.* 92, 4328-4331 (1995).

- 37 Terris, J. *et al.* Distribution of aquaporin-4 water channel expression within rat kidney. *Am. J. Physiol. Renal Physiol.* 269, F775-785 (1995).
- 38 Ishibashi, K. *et al.* Immunolocalization and effect of dehydration on AQP3, a basolateral water channel of kidney collecting ducts. *Am. J. Physiol. Renal Physiol.* 272, F235-241 (1997).
- 39 Coleman, R. A. *et al.* Expression of aquaporins in the renal connecting tubule. *Am. J. Physiol. Renal Physiol.* 279, F874-883 (2000).
- 40 Yasui, M. *et al.* Aquaporin-6: An intracellular vesicle water channel protein in renal epithelia. *Proc. Natl. Acad. Sci. U. S. A.* 96, 5808-5813 (1999).
- 41 Procino, G. *et al.* AQP5 is expressed in type-B intercalated cells in the collecting duct system of the rat, mouse and human kidney. *Cell. Physiol. Biochem.* 28, 683-692 (2011).
- 42 Ishibashi, K. *et al.* Cellular localization of aquaporin 7 in the rat kidney. *Exp. Nephrol.* 8, 252-257 (2000).
- 43 Nejsum, L. N. *et al.* Localization of aquaporin-7 in rat and mouse kidney using RT-PCR, immunoblotting, and immunocytochemistry. *Biochem. Biophys. Res. Commun.* 277, 164-170 (2000).
- 44 Elkjaer, M. L. *et al.* Immunolocalization of aquaporin-8 in rat kidney, gastrointestinal tract, testis, and airways. *Am. J. Physiol. Renal Physiol.* 281, F1047-1057 (2001).
- 45 Morishita, Y. *et al.* Disruption of aquaporin-11 produces polycystic kidneys following vacuolization of the proximal tubule. *Mol. Cell. Biol.* 25, 7770-7779 (2005).
- 46 Fushimi, K. *et al.* Cloning and expression of apical membrane water channel of rat kidney collecting tubule. *Nature* 361, 549-552 (1993).
- 47 Rojek, A. *et al.* Severe urinary concentrating defect in renal collecting duct-selective AQP2 conditional-knockout mice. *Proc. Natl. Acad. Sci. U. S. A.* 103, 6037-6042 (2006).
- 48 Hoffert, J. D. Quantitative phosphoproteomics of vasopressin-sensitive renal cells: Regulation of aquaporin-2 phosphorylation at two sites. *Proc. Natl. Acad. Sci. U. S. A.* 103, 7159-7164 (2006).
- 49 Ma, T. *et al.* Cloning of a novel rat kidney cDNA homologous to CHIP28 and WCH-CD water channels. *Biochem. Biophys. Res. Commun.* 197, 654-659 (1993).
- 50 Hendriks, G. *et al.* Glycosylation is important for cell surface expression of the water channel aquaporin-2 but is not essential for tetramerization in the endoplasmic reticulum. *J. Biol. Chem.* 279, 2975-2983 (2004).
- 51 Moeller, H. B. *et al.* Invited Review- Regulation of the water channel Aquaporin-2 by post-translational modifications. *Am. J. Physiol. Renal Physiol.* (2011).
- 52 Baumgarten, R. *et al.* Glycosylation is not essential for vasopressin-dependent routing of aquaporin-2 in transfected Madin-Darby canine kidney cells. *J. Am. Soc. Nephrol.* 9, 1553-1559 (1998).
- 53 Bizal, G. L. *et al.* Glycosylation of the Na⁺/H⁺ exchanger isoform NHE-3 is species specific. *J. Lab. Clin. Med.* 128, 304-312 (1996).
- 54 Bai, L. *et al.* Structure of aquaporin-2 vasopressin water channel. *J. Biol. Chem.* 271, 5171-5176 (1996).
- 55 Knepper, M. A. *et al.* Kinetic model of water and urea permeability regulation by vasopressin in collecting duct. *Am. J. Physiol. Renal Physiol.* 265, F214-224 (1993).
- 56 Brown, D. The ins and outs of aquaporin-2 trafficking. *Am. J. Physiol. Renal Physiol.* 284, F893-901 (2003).
- 57 Kruse, E. *et al.* The aquaporins. *Genome Biol.* 7, 206 (2006).
- 58 Ikeguchi, M. Water transport in aquaporins: molecular dynamics simulations. *Front. Biosci.* 14, 1283-1291 (2009).
- 59 Alcalá, J. *et al.* Protein composition of bovine lens cortical fiber cell membranes. *Exp. Eye Res.* 21, 581-595 (1975).
- 60 Fitzgerald, P. G. *et al.* Immunocytochemical localization of the main intrinsic polypeptide (MIP) in ultrathin frozen sections of rat lens. *J. Cell Biol.* 97, 1491-1499 (1983).
- 61 Mulders, S. M. *et al.* Water channel properties of major intrinsic protein of lens. *J. Biol. Chem.* 270, 9010-9016 (1995).
- 62 Shiels, A. *et al.* Mutations in the founder of the MIP gene family underlie cataract development in the mouse. *Nat. Genet.* 12, 212-215 (1996).
- 63 Shiels, A. *et al.* Optical dysfunction of the crystalline lens in aquaporin-0-deficient mice. *Physiol. Genomics* 7, 179-186 (2001).
- 64 Golestaneh, N. *et al.* PKC putative phosphorylation site Ser235 is required for MIP/AQP0 translocation to the plasma membrane. *Mol. Vis.* 14, 1006-1014 (2008).
- 65 Varadaraj, K. *et al.* Functional characterization of a human aquaporin 0 mutation that leads to a congenital dominant lens cataract. *Exp. Eye Res.* 87, 9-21 (2008).
- 66 Preston, G. M. *et al.* Isolation of the cDNA for erythrocyte integral membrane protein of 28 kilodaltons: member of an ancient channel family. *Proc. Natl. Acad. Sci. U. S. A.* 88, 11110-11114 (1991).
- 67 Ma, T. *et al.* Severely impaired urinary concentrating ability in transgenic mice lacking aquaporin-1 water channels. *J. Biol. Chem.* 273, 4296-4299 (1998).
- 68 Bai, C. *et al.* Lung fluid transport in aquaporin-1 and aquaporin-4 knockout mice. *J. Clin. Invest.* 103, 555-561 (1999).
- 69 Pallone, T. L. *et al.* Requirement of aquaporin-1 for NaCl-driven water transport across descending vasa recta. *J. Clin. Invest.* 105, 215-222 (2000).
- 70 Vacca, A. *et al.* Microvessel overexpression of aquaporin 1 parallels bone marrow angiogenesis in patients with active multiple myeloma. *Br. J. Haematol.* 113, 415-421 (2001).
- 71 Saadoun, S. *et al.* Impairment of angiogenesis and cell migration by targeted aquaporin-1 gene disruption. *Nature* 434, 786-792 (2005).
- 72 Hara-Chikuma, M. *et al.* Aquaporin-1 facilitates epithelial cell migration in kidney proximal tubule. *J. Am. Soc. Nephrol.* 17, 39-45 (2006).
- 73 Wang, W. *et al.* Role of AQP1 in endotoxemia-induced acute kidney injury. *Am. J. Physiol. Renal Physiol.* 294, F1473-1480 (2008).
- 74 Kim, S. O. *et al.* Expression of aquaporin water channels in the vagina in premenopausal women. *J. Sex. Med.* 8, 1925-1930 (2011).
- 75 Arrighi, S. *et al.* Immunolocalization of Aquaporin Water Channels in the Domestic Cat Male Genital Tract. *Reproduction in domestic animals = Zuchthygiene* (2013).
- 76 Nielsen, S. *et al.* The aquaporin family of water channels in kidney. *Kidney Int.* 48, 1057-1068 (1995).
- 77 Nelson, R. D. *et al.* Expression of an AQP2 Cre recombinase transgene in kidney and male reproductive system of transgenic mice. *Am. J. Physiol. Renal Physiol.* 275, C216-226 (1998).
- 78 Merves, M. *et al.* Developmental expression of aquaporin 2 in the mouse inner ear. *Laryngoscope* 110, 1925-1930 (2000).

- 79 Ishibashi, K. *et al.* Molecular cloning and expression of a member of the aquaporin family with permeability to glycerol and urea in addition to water expressed at the basolateral membrane of kidney collecting duct cells. *Proc. Natl. Acad. Sci. U. S. A.* 91, 6269-6273 (1994).
- 80 Echevarria, M. *et al.* Cloning and expression of AQP3, a water channel from the medullary collecting duct of rat kidney. *Proc. Natl. Acad. Sci. U. S. A.* 91, 10997-11001 (1994).
- 81 Ma, T. *et al.* Lung fluid transport in aquaporin-5 knockout mice. *J. Clin. Invest.* 105, 93-100 (2000).
- 82 Ma, T. *et al.* Impaired stratum corneum hydration in mice lacking epidermal water channel aquaporin-3. *J. Biol. Chem.* 277, 17147-17153 (2002).
- 83 Hara, M. *et al.* Selectively reduced glycerol in skin of aquaporin-3-deficient mice may account for impaired skin hydration, elasticity, and barrier recovery. *J. Biol. Chem.* 277, 46616-46621 (2002).
- 84 Kwon, T. H. *et al.* Regulation of collecting duct AQP3 expression: response to mineralocorticoid. *Am. J. Physiol. Renal Physiol.* 283, F1403-1421 (2002).
- 85 Roudier, N. *et al.* AQP3 deficiency in humans and the molecular basis of a novel blood group system, GIL. *J. Biol. Chem.* 277, 45854-45859 (2002).
- 86 Ma, T. *et al.* Cloning of a water channel homolog expressed in brain meningeal cells and kidney collecting duct that functions as a stilbene-sensitive glycerol transporter. *J. Biol. Chem.* 269, 21845-21849 (1994).
- 87 Ma, T. *et al.* Generation and phenotype of a transgenic knockout mouse lacking the mercurial-insensitive water channel aquaporin-4. *J. Clin. Invest.* 100, 957-962 (1997).
- 88 Yang, B. *et al.* Very high single channel water permeability of aquaporin-4 in baculovirus-infected insect cells and liposomes reconstituted with purified aquaporin-4. *Biochemistry* 36, 7625-7632 (1997).
- 89 Manley, G. T. *et al.* Aquaporin-4 deletion in mice reduces brain edema after acute water intoxication and ischemic stroke. *Nat. Med.* 6, 159-163 (2000).
- 90 Li, J. *et al.* Impaired hearing in mice lacking aquaporin-4 water channels. *J. Biol. Chem.* 276, 31233-31237 (2001).
- 91 Zelenina, M. *et al.* Water permeability of aquaporin-4 is decreased by protein kinase C and dopamine. *Am. J. Physiol. Renal Physiol.* 283, F309-318 (2002).
- 92 Hiroaki, Y. *et al.* Implications of the aquaporin-4 structure on array formation and cell adhesion. *J. Mol. Biol.* 355, 628-639 (2006).
- 93 Ho, J. D. *et al.* Crystal structure of human aquaporin 4 at 1.8 Å and its mechanism of conductance. *Proc. Natl. Acad. Sci. U. S. A.* 106, 7437-7442 (2009).
- 94 Raina, S. *et al.* Molecular cloning and characterization of an aquaporin cDNA from salivary, lacrimal, and respiratory tissues. *J. Biol. Chem.* 270, 1908-1912 (1995).
- 95 He, X. *et al.* Polarized distribution of key membrane transport proteins in the rat submandibular gland. *Pflugers Arch* 433, 260-268 (1997).
- 96 Ishida, N. *et al.* Immunolocalization of aquaporin homologs in mouse lacrimal glands. *Biochem. Biophys. Res. Commun.* 238, 891-895 (1997).
- 97 Ma, T. *et al.* Defective secretion of saliva in transgenic mice lacking aquaporin-5 water channels. *J. Biol. Chem.* 274, 20071-20074 (1999).
- 98 Mhatre, A. N. *et al.* Identification of aquaporin 5 (AQP5) within the cochlea: cDNA cloning and in situ localization. *Biochem. Biophys. Res. Commun.* 264, 157-162 (1999).
- 99 Song, Y. *et al.* Aquaporin-5 dependent fluid secretion in airway submucosal glands. *J. Biol. Chem.* 276, 41288-41292 (2001).
- 100 Krane, C. M. *et al.* Salivary acinar cells from aquaporin 5-deficient mice have decreased membrane water permeability and altered cell volume regulation. *J. Biol. Chem.* 276, 23413-23420 (2001).
- 101 Krane, C. M. *et al.* Aquaporin 5-deficient mouse lungs are hyperresponsive to cholinergic stimulation. *Proc. Natl. Acad. Sci. U. S. A.* 98, 14114-14119 (2001).
- 102 Nejsum, L. N. *et al.* Functional requirement of aquaporin-5 in plasma membranes of sweat glands. *Proc. Natl. Acad. Sci. U. S. A.* 99, 511-516 (2002).
- 103 Wu, H. *et al.* Aqp5 is a new transcriptional target of Dot1a and a regulator of Aqp2. *PLoS One* 8, e53342 (2013).
- 104 Ma, T. *et al.* cDNA cloning and gene structure of a novel water channel expressed exclusively in human kidney: evidence for a gene cluster of aquaporins at chromosome locus 12q13. *Genomics* 35, 543-550 (1996).
- 105 Yasui, M. *et al.* Rapid gating and anion permeability of an intracellular aquaporin. *Nature* 402, 184-187 (1999).
- 106 Ohshiro, K. *et al.* Expression and immunolocalization of AQP6 in intercalated cells of the rat kidney collecting duct. *Arch. Histol. Cytol.* 64, 329-338 (2001).
- 107 Ikeda, M. *et al.* Characterization of aquaporin-6 as a nitrate channel in mammalian cells. Requirement of pore-lining residue threonine 63. *J. Biol. Chem.* 277, 39873-39879 (2002).
- 108 Liu, K. *et al.* Conversion of aquaporin 6 from an anion channel to a water-selective channel by a single amino acid substitution. *Proc. Natl. Acad. Sci. U. S. A.* 102, 2192-2197 (2005).
- 109 Yasui, M. pH regulated anion permeability of aquaporin-6. *Handb. Exp. Pharmacol.*, 299-308 (2009).
- 110 Ishibashi, K. *et al.* Cloning and functional expression of a new water channel abundantly expressed in the testis permeable to water, glycerol, and urea. *J. Biol. Chem.* 272, 20782-20786 (1997).
- 111 Kishida, K. *et al.* Aquaporin adipose, a putative glycerol channel in adipocytes. *J. Biol. Chem.* 275, 20896-20902 (2000).
- 112 Liu, Z. *et al.* Arsenite transport by mammalian aquaglyceroporins AQP7 and AQP9. *Proc. Natl. Acad. Sci. U. S. A.* 99, 6053-6058 (2002).
- 113 Sohara, E. *et al.* Defective water and glycerol transport in the proximal tubules of AQP7 knockout mice. *Am. J. Physiol. Renal Physiol.* 289, F1195-1200 (2005).
- 114 Hara-Chikuma, M. *et al.* Progressive adipocyte hypertrophy in aquaporin-7-deficient mice: adipocyte glycerol permeability as a novel regulator of fat accumulation. *J. Biol. Chem.* 280, 15493-15496 (2005).
- 115 Hibuse, T. *et al.* Aquaporin 7 deficiency is associated with development of obesity through activation of adipose glycerol kinase. *Proc. Natl. Acad. Sci. U. S. A.* 102, 10993-10998 (2005).
- 116 Sohara, E. *et al.* Physiological roles of AQP7 in the kidney: Lessons from AQP7 knockout mice. *Biochim. Biophys. Acta* 1758, 1106-1110 (2006).
- 117 Laforenza, U. *et al.* Aquaporin-10 represents an alternative pathway for glycerol efflux from human adipocytes. *PLoS One* 8, e54474 (2013).
- 118 Ishibashi, K. *et al.* Cloning and functional expression of a second new aquaporin abundantly expressed in testis. *Biochem. Biophys. Res. Commun.* 237, 714-718 (1997).
- 119 Yang, B. *et al.* Phenotype analysis of aquaporin-8 null mice. *Am. J. Physiol. Cell Physiol.* 288, C1161-1170 (2005).

- 120 Saporov, S. M. *et al.* Fast and selective ammonia transport by aquaporin-8. *J. Biol. Chem.* 282, 5296-5301 (2007).
- 121 Bienert, G. P. *et al.* Specific aquaporins facilitate the diffusion of hydrogen peroxide across membranes. *J. Biol. Chem.* 282, 1183-1192 (2007).
- 122 Kobayashi, K. *et al.* Cellular and subcellular localization of aquaporins 1, 3, 8, and 9 in amniotic membranes during pregnancy in mice. *Cell Tissue Res.* 342, 307-316 (2010).
- 123 Tamma, G. *et al.* Cell culture models and animal models for studying the patho-physiological role of renal aquaporins. *Cell. Mol. Life Sci.* (2011).
- 124 Ishibashi, K. *et al.* Cloning and functional expression of a new aquaporin (AQP9) abundantly expressed in the peripheral leukocytes permeable to water and urea, but not to glycerol. *Biochem. Biophys. Res. Commun.* 244, 268-274 (1998).
- 125 Tsukaguchi, H. *et al.* Molecular characterization of a broad selectivity neutral solute channel. *J. Biol. Chem.* 273, 24737-24743 (1998).
- 126 Elkjaer, M. *et al.* Immunolocalization of AQP9 in liver, epididymis, testis, spleen, and brain. *Biochem. Biophys. Res. Commun.* 276, 1118-1128 (2000).
- 127 Domeniconi, R. F. *et al.* Aquaporin 9 (AQP9) localization in the adult dog testis excurrent ducts by immunohistochemistry. *Anat Rec (Hoboken)* 290, 1519-1525 (2007).
- 128 Ohgusu, Y. *et al.* Functional characterization of human aquaporin 9 as a facilitative glycerol carrier. *Drug Metab. Pharmacokinet.* 23, 279-284 (2008).
- 129 Inoue, M. *et al.* Aquaporin 9 expression and its localization in normal skeletal myofiber. *Journal of molecular histology* 40, 165-170 (2009).
- 130 Karlsson, T. *et al.* Aquaporin 9 phosphorylation mediates membrane localization and neutrophil polarization. *J. Leukoc. Biol.* 90, 963-973 (2011).
- 131 Hatakeyama, S. *et al.* Cloning of a new aquaporin (AQP10) abundantly expressed in duodenum and jejunum. *Biochem. Biophys. Res. Commun.* 287, 814-819 (2001).
- 132 Morinaga, T. *et al.* Mouse aquaporin 10 gene (AQP10) is a pseudogene. *Biochem. Biophys. Res. Commun.* 294, 630-634 (2002).
- 133 Mobasher, A. *et al.* Immunohistochemical localization of aquaporin 10 in the apical membranes of the human ileum: a potential pathway for luminal water and small solute absorption. *Histochem. Cell Biol.* 121, 463-471 (2004).
- 134 Li, H. *et al.* Expression and localization of two isoforms of AQP10 in human small intestine. *Biol. Cell.* 97, 823-829 (2005).
- 135 Ishii, M. *et al.* Dual functional characteristic of human aquaporin 10 for solute transport. *Cell. Physiol. Biochem.* 27, 749-756 (2011).
- 136 Ishibashi, K. *et al.* in *Molecular Biology and Physiology of Water and Solute Transport* 123-126 (2000).
- 137 Morishita, Y. *et al.* Molecular mechanisms and drug development in aquaporin water channel diseases: aquaporin superfamily (superaquaporins): expansion of aquaporins restricted to multicellular organisms. *J. Pharmacol. Sci.* 96, 276-279 (2004).
- 138 Gorelick, D. A. *et al.* Aquaporin-11: a channel protein lacking apparent transport function expressed in brain. *BMC Biochem.* 7, 14 (2006).
- 139 Yakata, K. *et al.* Aquaporin-11 containing a divergent NPA motif has normal water channel activity. *Biochim. Biophys. Acta* 1768, 688-693 (2007).
- 140 Yeung, C. H. *et al.* Aquaporin AQP11 in the testis: molecular identity and association with the processing of residual cytoplasm of elongated spermatids. *Reproduction* 139, 209-216 (2010).
- 141 Larsen, H. S. *et al.* Aquaporin 11 in the developing mouse submandibular gland. *Eur. J. Oral Sci.* 118, 9-13 (2010).
- 142 Itoh, T. *et al.* Identification of a novel aquaporin, AQP12, expressed in pancreatic acinar cells. *Biochem. Biophys. Res. Commun.* 330, 832-838 (2005).
- 143 Ohta, E. *et al.* Pancreas-specific aquaporin 12 null mice showed increased susceptibility to caerulein-induced acute pancreatitis. *Am. J. Physiol. Cell Physiol.* 297, C1368-1378 (2009).
- 144 Nielsen, S. *et al.* Vasopressin increases water permeability of kidney collecting duct by inducing translocation of aquaporin-CD water channels to plasma membrane. *Proc. Natl. Acad. Sci. U. S. A.* 92, 1013-1017 (1995).
- 145 Yamamoto, T. *et al.* Vasopressin increases AQP-CD water channel in apical membrane of collecting duct cells in Brattleboro rats. *Am. J. Physiol. Renal Physiol.* 268, C1546-1551 (1995).
- 146 Hoffert, J. D. *et al.* Calmodulin is required for vasopressin-stimulated increase in cyclic AMP production in inner medullary collecting duct. *J. Biol. Chem.* 280, 13624-13630 (2005).
- 147 Strait, K. A. *et al.* Characterization of vasopressin-responsive collecting duct adenylyl cyclases in the mouse. *Am. J. Physiol. Renal Physiol.* 298, F859-867 (2010).
- 148 Rieg, T. *et al.* Adenylyl Cyclase 6 Determines cAMP Formation and Aquaporin-2 Phosphorylation and Trafficking in Inner Medulla. *J. Am. Soc. Nephrol.* 21, 2059-2068 (2010).
- 149 Roos, K. P. *et al.* Collecting duct-specific knockout of adenylyl cyclase type VI causes a urinary concentration defect in mice. *Am. J. Physiol. Renal Physiol.* 302, F78-84 (2012).
- 150 Klussmann, E. *et al.* Protein kinase A anchoring proteins are required for vasopressin-mediated translocation of aquaporin-2 into cell membranes of renal principal cells. *J. Biol. Chem.* 274, 4934-4938 (1999).
- 151 Henn, V. *et al.* Identification of a novel A-kinase anchoring protein 18 isoform and evidence for its role in the vasopressin-induced aquaporin-2 shuttle in renal principal cells. *J. Biol. Chem.* 279, 26654-26665 (2004).
- 152 Okutsu, R. *et al.* AKAP220 colocalizes with AQP2 in the inner medullary collecting ducts. *Kidney Int.* 74, 1429-1433 (2008).
- 153 Stefan, E. *et al.* Compartmentalization of cAMP-Dependent Signaling by Phosphodiesterase-4D Is Involved in the Regulation of Vasopressin-Mediated Water Reabsorption in Renal Principal Cells. *J. Am. Soc. Nephrol.* 18, 199-212 (2007).
- 154 Skroblin, P. *et al.* Mechanisms of protein kinase A anchoring. *Int. Rev. Cell Mol. Biol.* 283, 235-330 (2010).
- 155 Lande, M. B. *et al.* Phosphorylation of aquaporin-2 does not alter the membrane water permeability of rat papillary water channel-containing vesicles. *J. Biol. Chem.* 271, 5552-5557 (1996).
- 156 Nishimoto, G. *et al.* Arginine vasopressin stimulates phosphorylation of aquaporin-2 in rat renal tissue. *Am. J. Physiol. Renal Physiol.* 276, F254-259 (1999).
- 157 Kamsteeg, E. J. *et al.* The subcellular localization of an aquaporin-2 tetramer depends on the stoichiometry of phosphorylated and nonphosphorylated monomers. *J. Biol. Chem.* 275, 919-930 (2000).
- 158 Fenton, R. A. *et al.* Acute regulation of aquaporin-2 phosphorylation at Ser-264 by vasopressin. *Proc. Natl. Acad. Sci. U. S. A.* 105, 3134-3139 (2008).

- 159 Hoffert, J. D. *et al.* Vasopressin-stimulated Increase in Phosphorylation at Ser269 Potentiates Plasma Membrane Retention of Aquaporin-2. *J. Biol. Chem.* 283, 24617-24627 (2008).
- 160 Moeller, H. B. *et al.* Serine 269 phosphorylated aquaporin-2 is targeted to the apical membrane of collecting duct principal cells. *Kidney Int.* 75, 295-303 (2008).
- 161 Moeller, H. B. *et al.* Role of multiple phosphorylation sites in the COOH-terminal tail of aquaporin-2 for water transport: evidence against channel gating. *Am. J. Physiol. Renal Physiol.* 296, F649-657 (2009).
- 162 Bogum, J. *et al.* Small-Molecule Screening Identifies Modulators of Aquaporin-2 Trafficking. *J. Am. Soc. Nephrol.* (2013).
- 163 Hoffert, J. D. *et al.* Dynamics of aquaporin-2 serine-261 phosphorylation in response to short-term vasopressin treatment in collecting duct. *Am. J. Physiol. Renal Physiol.* 292, F691-700 (2007).
- 164 Tamma, G. *et al.* Regulation of AQP2 localization by Ser256 and S261 phosphorylation and ubiquitination. *AJP: Cell Physiology* (2010).
- 165 Noda, Y. *et al.* Reciprocal interaction with G-actin and tropomyosin is essential for aquaporin-2 trafficking. *J. Biol. Chem.* 182, 587-601 (2008).
- 166 Lang, P. *et al.* Protein kinase A phosphorylation of RhoA mediates the morphological and functional effects of cyclic AMP in cytotoxic lymphocytes. *EMBO J.* 15, 510-519 (1996).
- 167 Dong, J. M. *et al.* cAMP-induced morphological changes are counteracted by the activated RhoA small GTPase and the Rho kinase ROKalpha. *J. Biol. Chem.* 273, 22554-22562 (1998).
- 168 Klussmann, E. *et al.* An inhibitory role of Rho in the vasopressin-mediated translocation of aquaporin-2 into cell membranes of renal principal cells. *J. Biol. Chem.* 276, 20451-20457 (2001).
- 169 Tamma, G. *et al.* Rho inhibits cAMP-induced translocation of aquaporin-2 into the apical membrane of renal cells. *Am. J. Physiol. Renal Physiol.* 281, F1092-1101 (2001).
- 170 Tchernev, V. T. *et al.* The Chediak-Higashi protein interacts with SNARE complex and signal transduction proteins. *Mol. Med.* 8, 56-64 (2002).
- 171 Valenti, G. Minireview: Aquaporin 2 Trafficking. *Endocrinology* 146, 5063-5070 (2005).
- 172 Procino, G. *et al.* AQP2 exocytosis in the renal collecting duct - involvement of SNARE isoforms and the regulatory role of Munc18b. *J. Cell. Sci.* 121, 2097-2106 (2008).
- 173 Lehtonen, S. *et al.* Syntaxin 3 and Munc-18-2 in epithelial cells during kidney development. *Kidney Int.* 56, 815-826 (1999).
- 174 Frank, M. *et al.* rMAL is a glycosphingolipid-associated protein of myelin and apical membranes of epithelial cells in kidney and stomach. *J. Neurosci.* 18, 4901-4913 (1998).
- 175 Kamsteeg, E. J. *et al.* MAL decreases the internalization of the aquaporin-2 water channel. *Proc. Natl. Acad. Sci. U. S. A.* 104, 16696-16701 (2007).
- 176 van Balkom, B. W. *et al.* Hypertonicity is involved in redirecting the aquaporin-2 water channel into the basolateral, instead of the apical, plasma membrane of renal epithelial cells. *J. Biol. Chem.* 278, 1101-1107 (2003).
- 177 Yui, N. *et al.* Basolateral targeting and microtubule-dependent transcytosis of the aquaporin-2 water channel. *Am. J. Physiol. Cell Physiol.* 304, C38-48 (2013).
- 178 Sun, T. X. *et al.* Aquaporin-2 localization in clathrin-coated pits: inhibition of endocytosis by dominant-negative dynamin. *Am. J. Physiol. Renal Physiol.* 282, F998-1011 (2002).
- 179 Marples, D. *et al.* Dynein and dynactin colocalize with AQP2 water channels in intracellular vesicles from kidney collecting duct. *Am. J. Physiol. Renal Physiol.* 274, F384-394 (1998).
- 180 Lu, H. A. J. *et al.* Heat Shock Protein 70 Interacts with Aquaporin-2 and Regulates Its Trafficking. *J. Biol. Chem.* 282, 28721-28732 (2007).
- 181 Katzmann, D. J. *et al.* Receptor downregulation and multivesicular-body sorting. *Nat. Rev. Mol. Cell Biol.* 3, 893-905 (2002).
- 182 Piper, R. C. *et al.* Biogenesis and function of multivesicular bodies. *Annu. Rev. Cell Dev. Biol.* 23, 519-547 (2007).
- 183 Ward, D. M. *et al.* The role of LIP5 and CHMP5 in multivesicular body formation and HIV-1 budding in mammalian cells. *J. Biol. Chem.* 280, 10548-10555 (2005).
- 184 Azmi, I. *et al.* Recycling of ESCRTs by the AAA-ATPase Vps4 is regulated by a conserved VSL region in Vta1. *J. Cell Biol.* 172, 705-717 (2006).
- 185 Yu, Z. *et al.* Cryo-EM structure of dodecameric Vps4p and its 2:1 complex with Vta1p. *J. Mol. Biol.* 377, 364-377 (2008).
- 186 van Balkom, B. W. M. *et al.* LIP5 Interacts with Aquaporin 2 and Facilitates Its Lysosomal Degradation. *J. Am. Soc. Nephrol.* 20, 990-1001 (2009).
- 187 Pisitkun, T. *et al.* Identification and proteomic profiling of exosomes in human urine. *Proc. Natl. Acad. Sci. U. S. A.* 101, 13368-13373 (2004).
- 188 Gonzales, P. A. *et al.* Large-scale proteomics and phosphoproteomics of urinary exosomes. *J. Am. Soc. Nephrol.* 20, 363-379 (2009).
- 189 Hershko, A. *et al.* Components of ubiquitin-protein ligase system. Resolution, affinity purification, and role in protein breakdown. *J. Biol. Chem.* 258, 8206-8214 (1983).
- 190 Hershko, A. *et al.* Basic Medical Research Award. The ubiquitin system. *Nat. Med.* 6, 1073-1081 (2000).
- 191 Lee, Y. J. *et al.* E3 ubiquitin-protein ligases in rat kidney collecting duct: response to vasopressin stimulation and withdrawal. *Am. J. Physiol. Renal Physiol.* 301, F883-896 (2011).
- 192 Le, I. P. *et al.* Aquaporin-2 levels in vitro and in vivo are regulated by VACM-1, a cul 5 gene. *Cell. Physiol. Biochem.* 30, 1148-1158 (2012).
- 193 Schenk, L. K. *et al.* Quantitative proteomics identifies vasopressin-responsive nuclear proteins in collecting duct cells. *J. Am. Soc. Nephrol.* 23, 1008-1018 (2012).
- 194 Vossenkamper, A. *et al.* Microtubules are needed for the perinuclear positioning of aquaporin-2 after its endocytic retrieval in renal principal cells. *AJP: Cell Physiology* 293, C1129-C1138 (2007).
- 195 Nedvetsky, P. I. *et al.* A Role of Myosin Vb and Rab11-FIP2 in the Aquaporin-2 Shuttle. *Traffic* 8, 110-123 (2007).
- 196 Stenmark, H. Rab GTPases as coordinators of vesicle traffic. *Nat. Rev. Mol. Cell Biol.* 10, 513-525 (2009).
- 197 Hebert, R. L. *et al.* PGE2 inhibits AVP-induced water flow in cortical collecting ducts by protein kinase C activation. *Am. J. Physiol. Renal Physiol.* 259, F318-325 (1990).
- 198 van Balkom, B. W. *et al.* The role of putative phosphorylation sites in the targeting and shuttling of the aquaporin-2 water channel. *J. Biol. Chem.* 277, 41473-41479 (2002).
- 199 Brown, D. *et al.* Phosphorylation events and the modulation of aquaporin 2 cell surface expression. *Curr. Opin. Nephrol. Hypertens.* 17, 491-498 (2008).

- 200 Nunes, P. *et al.* A fluorimetry-based ssYFP secretion assay to monitor vasopressin-induced exocytosis in LLC-PK1 cells expressing aquaporin-2. *Am. J. Physiol. Cell Physiol.* 295, C1476-1487 (2008).
- 201 Bouley, R. *et al.* Aquaporin 2 (AQP2) and vasopressin type 2 receptor (V2R) endocytosis in kidney epithelial cells: AQP2 is located in 'endocytosis-resistant' membrane domains after vasopressin treatment. *Biol. Cell* 98, 215-232 (2006).
- 202 Moeller, H. B. *et al.* Phosphorylation of aquaporin-2 regulates its endocytosis and protein-protein interactions. *Proc. Natl. Acad. Sci. U. S. A.* 107, 424-429 (2010).
- 203 Nejsum, L. N. *et al.* Bidirectional regulation of AQP2 trafficking and recycling: involvement of AQP2-S256 phosphorylation. *Am. J. Physiol. Renal Physiol.* 288, F930-938 (2005).
- 204 Zelenina, M. *et al.* Prostaglandin E(2) interaction with AVP: effects on AQP2 phosphorylation and distribution. *Am. J. Physiol. Renal Physiol.* 278, F388-394 (2000).
- 205 Alexander, S. P. *et al.* Guide to Receptors and Channels (GRAC), 5th edition. *Br. J. Pharmacol.* 164 Suppl 1, S1-324 (2011).
- 206 Leeb-Lundberg, L. M. *et al.* International union of pharmacology. XLV. Classification of the kinin receptor family: from molecular mechanisms to pathophysiological consequences. *Pharmacol. Rev.* 57, 27-77 (2005).
- 207 Feinstein, T. N. *et al.* Retromer terminates the generation of cAMP by internalized PTH receptors. *Nat. Chem. Biol.* (2011).
- 208 Prie, D. *et al.* Principal cell-specific antigen and hormonal regulatory network in RC.SVtsA58 cell line. *Am. J. Physiol. Renal Physiol.* 266, C1628-1638 (1994).
- 209 Kamsteeg, E. J. *et al.* Missorting of the Aquaporin-2 mutant E258K to multivesicular bodies/lysosomes in dominant NDI is associated with its monoubiquitination and increased phosphorylation by PKC but is due to the loss of E258. *Pflugers Arch* 455, 1041-1054 (2008).
- 210 Pang, L. *et al.* PGE2 release by bradykinin in human airway smooth muscle cells: involvement of cyclooxygenase-2 induction. *Am. J. Physiol. Renal Physiol.* 273, L1132-1140 (1997).
- 211 Siragy, H. M. *et al.* Bradykinin B2 receptor modulates renal prostaglandin E2 and nitric oxide. *Hypertension* 29, 757-762 (1997).
- 212 Tamma, G. Bradykinin Signaling Counteracts cAMP-Elicited Aquaporin 2 Translocation in Renal Cells. *J. Am. Soc. Nephrol.* 16, 2881-2889 (2005).
- 213 Simon, H. *et al.* Vasopressin depolymerizes apical F-actin in rat inner medullary collecting duct. *Am. J. Physiol. Renal Physiol.* 265, C757-762 (1993).
- 214 Abramowitz, J. *et al.* Physiology and pathophysiology of canonical transient receptor potential channels. *FASEB J.* 23, 297-328 (2009).
- 215 Balasubramanian, L. *et al.* Calcium signaling in vasopressin-induced aquaporin-2 trafficking. *Pflugers Arch* 456, 747-754 (2008).
- 216 Sands, J. M. *et al.* Vasopressin-elicited water and urea permeabilities are altered in IMCD in hypercalcemic rats. *Am. J. Physiol. Renal Physiol.* 274, F978-985 (1998).
- 217 Earm, J. H. *et al.* Decreased aquaporin-2 expression and apical plasma membrane delivery in kidney collecting ducts of polyuric hypercalcemic rats. *J. Am. Soc. Nephrol.* 9, 2181-2193 (1998).
- 218 Bustamante, M. *et al.* Calcium-sensing receptor attenuates AVP-induced aquaporin-2 expression via a calmodulin-dependent mechanism. *J. Am. Soc. Nephrol.* 19, 109-116 (2008).
- 219 Procino, G. *et al.* Extracellular calcium antagonizes forskolin-induced aquaporin 2 trafficking in collecting duct cells. *Kidney Int.* 66, 2245-2255 (2004).
- 220 Procino, G. *et al.* Calcium-sensing receptor and aquaporin 2 interplay in hypercalciuria-associated renal concentrating defect in humans. An in vivo and in vitro study. *PLoS One* 7, e33145 (2012).
- 221 Brown, E. M. *et al.* The extracellular calcium-sensing receptor: its role in health and disease. *Annu. Rev. Med.* 49, 15-29 (1998).
- 222 Hasler, U. *et al.* Aquaporin-2 abundance in the renal collecting duct: new insights from cultured cell models. *Am. J. Physiol. Renal Physiol.* 297, F10-18 (2009).
- 223 Chou, C. L. *et al.* Non-muscle myosin II and myosin light chain kinase are downstream targets for vasopressin signaling in the renal collecting duct. *J. Biol. Chem.* 279, 49026-49035 (2004).
- 224 Soderling, T. R. *et al.* Structure and regulation of calcium/calmodulin-dependent protein kinases. *Chem. Rev.* 101, 2341-2352 (2001).
- 225 Li, S. Z. *et al.* Calcineurin-NFATc signaling pathway regulates AQP2 expression in response to calcium signals and osmotic stress. *Am. J. Physiol. Renal Physiol.* 292, C1606-1616 (2007).
- 226 Gooch, J. L. Loss of calcineurin A results in altered trafficking of AQP2 and in nephrogenic diabetes insipidus. *J. Cell. Sci.* 119, 2468-2476 (2006).
- 227 Defer, N. *et al.* Tissue specificity and physiological relevance of various isoforms of adenylyl cyclase. *Am. J. Physiol. Renal Physiol.* 279, F400-416 (2000).
- 228 Katsushika, S. *et al.* Cloning and characterization of a sixth adenylyl cyclase isoform: types V and VI constitute a subgroup within the mammalian adenylyl cyclase family. *Proc. Natl. Acad. Sci. U. S. A.* 89, 8774-8778 (1992).
- 229 Cooper, D. M. *et al.* Capacitative Ca²⁺ entry regulates Ca(2+)-sensitive adenylyl cyclases. *Biochem. J.* 297 (Pt 3), 437-440 (1994).
- 230 Wayman, G. A. *et al.* Ca²⁺ inhibition of type III adenylyl cyclase in vivo. *J. Biol. Chem.* 270, 21480-21486 (1995).
- 231 Wei, J. *et al.* Phosphorylation and inhibition of type III adenylyl cyclase by calmodulin-dependent protein kinase II in vivo. *J. Biol. Chem.* 271, 24231-24235 (1996).
- 232 Wei, J. *et al.* Phosphorylation and inhibition of olfactory adenylyl cyclase by CaM kinase II in Neurons: a mechanism for attenuation of olfactory signals. *Neuron* 21, 495-504 (1998).
- 233 Choi, E. J. *et al.* Stimulation of the type III olfactory adenylyl cyclase by calcium and calmodulin. *Biochemistry* 31, 6492-6498 (1992).
- 234 Mamluk, R. *et al.* Molecular identification of adenylyl cyclase 3 in bovine corpus luteum and its regulation by prostaglandin F2alpha-induced signaling pathways. *Endocrinology* 140, 4601-4608 (1999).
- 235 Ishikawa, S. *et al.* Arginine vasopressin increases cellular free calcium concentration and adenosine 3',5'-monophosphate production in rat renal papillary collecting tubule cells in culture. *Endocrinology* 123, 1376-1384 (1988).
- 236 Champigneulle, A. *et al.* V2-like vasopressin receptor mobilizes intracellular Ca²⁺ in rat medullary collecting tubules. *Am. J. Physiol. Renal Physiol.* 265, F35-45 (1993).

- 237 Maeda, Y. *et al.* Vasopressin and oxytocin receptors coupled to Ca²⁺ mobilization in rat inner medullary collecting duct. *Am. J. Physiol. Renal Physiol.* 265, F15-25 (1993).
- 238 Ecelbarger, C. A. *et al.* Evidence for dual signaling pathways for V2 vasopressin receptor in rat inner medullary collecting duct. *Am. J. Physiol. Renal Physiol.* 270, F623-633 (1996).
- 239 Yip, K. P. Coupling of vasopressin-induced intracellular Ca²⁺ mobilization and apical exocytosis in perfused rat kidney collecting duct. *J. Physiol.* 538, 891-899 (2002).
- 240 Christensen, A. E. *et al.* cAMP analog mapping of Epac1 and cAMP kinase. Discriminating analogs demonstrate that Epac and cAMP kinase act synergistically to promote PC-12 cell neurite extension. *J. Biol. Chem.* 278, 35394-35402 (2003).
- 241 Yip, K. P. Epac-mediated Ca(2+) mobilization and exocytosis in inner medullary collecting duct. *Am. J. Physiol. Renal Physiol.* 291, F882-890 (2006).
- 242 Cullere, X. *et al.* Regulation of vascular endothelial barrier function by Epac, a cAMP-activated exchange factor for Rap GTPase. *Blood* 105, 1950-1955 (2005).
- 243 Lorenz, D. *et al.* Cyclic AMP is sufficient for triggering the exocytic recruitment of aquaporin-2 in renal epithelial cells. *EMBO reports* 4, 88-93 (2003).
- 244 Siragy, H. M. *et al.* Evidence that intrarenal dopamine acts as a paracrine substance at the renal tubule. *Am. J. Physiol. Renal Physiol.* 257, F469-477 (1989).
- 245 Missale, C. *et al.* Dopamine receptors: from structure to function. *Physiol. Rev.* 78, 189-225 (1998).
- 246 Li, L. *et al.* Dopamine inhibits vasopressin-dependent cAMP production in the rat cortical collecting duct. *Am. J. Physiol. Renal Physiol.* 275, F62-67 (1998).
- 247 Boone, M. *et al.* Counteracting vasopressin-mediated water reabsorption by ATP, dopamine and phorbol esters: mechanisms of action. *AJP: Renal Physiology* (2011).
- 248 Bouley, R. *et al.* Nitric oxide and atrial natriuretic factor stimulate cGMP-dependent membrane insertion of aquaporin 2 in renal epithelial cells. *J. Clin. Invest.* 106, 1115-1126 (2000).
- 249 Garcia, N. H. *et al.* Nitric oxide inhibits ADH-stimulated osmotic water permeability in cortical collecting ducts. *Am. J. Physiol. Renal Physiol.* 270, F206-210 (1996).
- 250 Arreche, N. *et al.* Hypovolemic state: involvement of nitric oxide in the aged related alterations of aquaporins-2 abundance in rat kidney. *Vascul. Pharmacol.* 49, 19-25 (2008).
- 251 Klokke, J. *et al.* Atrial natriuretic peptide and nitric oxide signaling antagonizes vasopressin-mediated water permeability in inner medullary collecting duct cells. *Am. J. Physiol. Renal Physiol.* 297, F693-703 (2009).
- 252 Jun, D. W. *et al.* The role of nitric oxide in the expression of renal aquaporin 2 in a cirrhotic rat model: does an AVP-independent mechanism exist for the regulation of AQP2 expression? *Dig. Dis. Sci.* 55, 1296-1304 (2010).
- 253 Kortenoeven, M. L. *et al.* Hypotonicity-induced reduction of aquaporin-2 transcription in mpkCCD cells is independent of the tonicity responsive element, vasopressin, and cAMP. *J. Biol. Chem.* 286, 13002-13010 (2011).
- 254 Albertoni Borghese, M. F. *et al.* Aquaporin-2 promoter is synergistically regulated by nitric oxide and nuclear factor of activated T cells. *Nephron extra* 1, 124-138 (2011).
- 255 Hao, C. M. *et al.* Physiological regulation of prostaglandins in the kidney. *Annu. Rev. Physiol.* 70, 357-377 (2008).
- 256 Bachtseva, V. *et al.* Prostaglandin E2 inhibits vasotocin-induced osmotic water permeability in the frog urinary bladder by EP1-receptor-mediated activation of NO/cGMP pathway. *Am. J. Physiol. Regul. Integr. Comp. Physiol.* 293, R528-537 (2007).
- 257 Sugimoto, Y. *et al.* Cloning and expression of a cDNA for mouse prostaglandin E receptor EP3 subtype. *J. Biol. Chem.* 267, 6463-6466 (1992).
- 258 Tamma, G. *et al.* The prostaglandin E2 analogue sulprostone antagonizes vasopressin-induced antidiuresis through activation of Rho. *J. Cell. Sci.* 116, 3285-3294 (2003).
- 259 Yamaguchi, Y. *et al.* Galpha(12) and galpha(13) inhibit Ca(2+)-dependent exocytosis through Rho/Rho-associated kinase-dependent pathway. *J. Neurochem.* 75, 708-717 (2000).
- 260 Wells, C. D. *et al.* Mechanisms for reversible regulation between G13 and Rho exchange factors. *J. Biol. Chem.* 277, 1174-1181 (2002).
- 261 Namba, T. *et al.* Alternative splicing of C-terminal tail of prostaglandin E receptor subtype EP3 determines G-protein specificity. *Nature* 365, 166-170 (1993).
- 262 Hatae, N. *et al.* Prostaglandin receptors: advances in the study of EP3 receptor signaling. *J. Biochem.* 131, 781-784 (2002).
- 263 Olesen, E. T. *et al.* Is There a Role for PGE2 in Urinary Concentration? *J. Am. Soc. Nephrol.* 24, 169-178 (2013).
- 264 Olesen, E. T. *et al.* Vasopressin-independent targeting of aquaporin-2 by selective E-prostanoid receptor agonists alleviates nephrogenic diabetes insipidus. *Proc. Natl. Acad. Sci. U. S. A.* (2011).
- 265 Breyer, M. D. *et al.* G protein-coupled prostanoid receptors and the kidney. *Ann Rev Physiol* 63, 579-605 (2001).
- 266 Sugimoto, Y. *et al.* Distinct cellular localization of mRNAs for three subtypes of prostaglandin E receptor in kidney. *Am. J. Physiol. Renal Physiol.* 266, F823-828 (1994).
- 267 Breyer, M. D. *et al.* Differential localization of prostaglandin E receptor subtypes in human kidney. *Am. J. Physiol. Renal Physiol.* 270, F912-918 (1996).
- 268 Morath, R. *et al.* Immunolocalization of the four prostaglandin E2 receptor proteins EP1, EP2, EP3, and EP4 in human kidney. *J. Am. Soc. Nephrol.* 10, 1851-1860 (1999).
- 269 Jensen, B. L. *et al.* Localization of prostaglandin E(2) EP2 and EP4 receptors in the rat kidney. *Am. J. Physiol. Renal Physiol.* 280, F1001-1009 (2001).
- 270 Regan, J. W. EP2 and EP4 prostanoid receptor signaling. *Life Sci.* 74, 143-153 (2003).
- 271 Sugimoto, Y. *et al.* Prostaglandin E receptors. *J. Biol. Chem.* 282, 11613-11617 (2007).
- 272 Fujino, H. *et al.* EP(4) prostanoid receptor coupling to a pertussis toxin-sensitive inhibitory G protein. *Mol. Pharmacol.* 69, 5-10 (2006).
- 273 Fujino, H. *et al.* Prostaglandin E2 induced functional expression of early growth response factor-1 by EP4, but not EP2, prostanoid receptors via the phosphatidylinositol 3-kinase and extracellular signal-regulated kinases. *J. Biol. Chem.* 278, 12151-12156 (2003).
- 274 Tajika, Y. *et al.* Aquaporin-2 is retrieved to the apical storage compartment via early endosomes and phosphatidylinositol 3-kinase-dependent pathway. *Endocrinology* 145, 4375-4383 (2004).
- 275 Bustamante, M. *et al.* Insulin potentiates AVP-induced AQP2 expression in cultured renal collecting duct principal cells. *Am. J. Physiol. Renal Physiol.* 288, F334-344 (2005).
- 276 Kishore, B. K. *et al.* P2Y(2) receptors and water transport in the kidney. *Purinergic signalling* 5, 491-499 (2009).

- 277 Wildman, S. S. P. *et al.* Nucleotides Downregulate Aquaporin 2 via Activation of Apical P2 Receptors. *J. Am. Soc. Nephrol.* 20, 1480-1490 (2009).
- 278 Kishore, B. K. *et al.* Extracellular nucleotide receptor inhibits AVP-stimulated water permeability in inner medullary collecting duct. *Am. J. Physiol. Renal Physiol.* 269, F863-869 (1995).
- 279 Vallon, V. P2 receptors in the regulation of renal transport mechanisms. *Am. J. Physiol. Renal Physiol.* 294, F10-27 (2008).
- 280 Welch, B. D. *et al.* P2Y2 receptor-stimulated release of prostaglandin E2 by rat inner medullary collecting duct preparations. *Am. J. Physiol. Renal Physiol.* 285, F711-721 (2003).
- 281 Zhang, Y. *et al.* Genetic deletion of the P2Y2 receptor offers significant resistance to development of lithium-induced polyuria accompanied by alterations in PGE2 signaling. *Am. J. Physiol. Renal Physiol.* 302, F70-77 (2012).
- 282 Sauzeau, V. *et al.* P2Y(1), P2Y(2), P2Y(4), and P2Y(6) receptors are coupled to Rho and Rho kinase activation in vascular myocytes. *Am. J. Physiol. Heart Circ. Physiol.* 278, H1751-1761 (2000).
- 283 Umenishi, F. *et al.* cAMP regulated membrane diffusion of a green fluorescent protein-aquaporin 2 chimera. *Biophys. J.* 78, 1024-1035 (2000).
- 284 Noda, Y. *et al.* Water channel aquaporin-2 directly binds to actin. *Biochem. Biophys. Res. Commun.* 322, 740-745 (2004).
- 285 Noda, Y. *et al.* Identification of a multiprotein ?motor? complex binding to water channel aquaporin-2. *Biochem. Biophys. Res. Commun.* 330, 1041-1047 (2005).
- 286 Barile, M. *et al.* Large scale protein identification in intracellular aquaporin-2 vesicles from renal inner medullary collecting duct. *Mol. Cell. Proteomics* 4, 1095-1106 (2005).
- 287 Tamma, G. *et al.* Functional involvement of Annexin-2 in cAMP induced AQP2 trafficking. *Pflugers Arch* 456, 729-736 (2008).
- 288 Zwang, N. A. *et al.* Identification of Phosphorylation-Dependent Binding Partners of Aquaporin-2 Using Protein Mass Spectrometry. *J. Proteome Res.* 8, 1540-1554 (2009).
- 289 Yasui, M. *et al.* Adenylate cyclase-coupled vasopressin receptor activates AQP2 promoter via a dual effect on CRE and AP1 elements. *Am. J. Physiol. Renal Physiol.* 272, F443-450 (1997).
- 290 Irrarrazabal, C. E. *et al.* Activator protein-1 contributes to high NaCl-induced increase in tonicity-responsive enhancer/osmotic response element-binding protein transactivating activity. *J. Biol. Chem.* 283, 2554-2563 (2008).
- 291 Cai, Q. *et al.* Vasopressin increases expression of UT-A1, UT-A3, and ER chaperone GRP78 in the renal medulla of mice with a urinary concentrating defect. *Am. J. Physiol. Renal Physiol.* 299, F712-719 (2010).
- 292 Jo, I. *et al.* AQP2 is a substrate for endogenous PP2B activity within an inner medullary AKAP-signaling complex. *Am. J. Physiol. Renal Physiol.* 281, F958-965 (2001).
- 293 Valenti, G. *et al.* The phosphatase inhibitor okadaic acid induces AQP2 translocation independently from AQP2 phosphorylation in renal collecting duct cells. *J. Cell Sci.* 113 (Pt 11), 1985-1992 (2000).
- 294 Rinschen, M. M. *et al.* Different effects of CsA and FK506 on aquaporin-2 abundance in rat primary cultured collecting duct cells. *Pflugers Arch* 462, 611-622 (2011).
- 295 Bouley, R. *et al.* Calcitonin has a vasopressin-like effect on aquaporin-2 trafficking and urinary concentration. *J. Am. Soc. Nephrol.* 22, 59-72 (2011).
- 296 Aoki, T. *et al.* Close association of aquaporin-2 internalization with caveolin-1. *Acta Histochem. Cytochem.* 45, 139-146 (2012).
- 297 Rinschen, M. M. *et al.* Quantitative phosphoproteomic analysis reveals vasopressin V2-receptor-dependent signaling pathways in renal collecting duct cells. *Proc. Natl. Acad. Sci. U. S. A.* 107, 3882-3887 (2010).
- 298 Strange, K. *et al.* Apical membrane endocytosis via coated pits is stimulated by removal of antidiuretic hormone from isolated, perfused rabbit cortical collecting tubule. *J. Membrane Biol.* 103, 17-28 (1988).
- 299 Verkman, A. S. *et al.* Endosomes from kidney collecting tubule cells contain the vasopressin-sensitive water channel. *Nature* 333, 268-269 (1988).
- 300 Katsura, T. *et al.* Constitutive and regulated membrane expression of aquaporin 1 and aquaporin 2 water channels in stably transfected LLC-PK1 epithelial cells. *Proc. Natl. Acad. Sci. U. S. A.* 92, 7212-7216 (1995).
- 301 Norregaard, R. *et al.* COX-2 inhibition prevents downregulation of key renal water and sodium transport proteins in response to bilateral ureteral obstruction. *Am. J. Physiol. Renal Physiol.* 289, F322-333 (2005).
- 302 Norregaard, R. *et al.* Urinary tract obstruction induces transient accumulation of COX-2-derived prostanoids in kidney tissue. *Am. J. Physiol. Regul. Integr. Comp. Physiol.* 298, R1017-1025 (2010).
- 303 Norregaard, R. *et al.* COX-2 disruption leads to increased central vasopressin stores and impaired urine concentrating ability in mice. *Am. J. Physiol. Renal Physiol.* 301, F1303-1313 (2011).
- 304 Jensen, A. M. *et al.* Angiotensin II mediates downregulation of aquaporin water channels and key renal sodium transporters in response to urinary tract obstruction. *Am. J. Physiol. Renal Physiol.* 291, F1021-1032 (2006).
- 305 Jensen, A. M. *et al.* Cyclooxygenase 2 inhibition exacerbates AQP2 and pAQP2 downregulation independently of V2 receptor abundance in the postobstructed kidney. *Am. J. Physiol. Renal Physiol.* 298, F941-950 (2010).
- 306 Kim, G. H. *et al.* Treating lithium-induced nephrogenic diabetes insipidus with a COX-2 inhibitor improves polyuria via upregulation of AQP2 and NKCC2. *Am. J. Physiol. Renal Physiol.* 294, F702-709 (2008).
- 307 Kortenoeven, M. L. *et al.* Lithium reduces aquaporin-2 transcription independent of prostaglandins. *Am. J. Physiol. Renal Physiol.* (2011).
- 308 Matsumura, Y. *et al.* Transcriptional regulation of aquaporin-2 water channel gene by cAMP. *J. Am. Soc. Nephrol.* 8, 861-867 (1997).
- 309 Umenishi, F. *et al.* cAMP regulates vasopressin-induced AQP2 expression via protein kinase A-independent pathway. *Biochim. Biophys. Acta* 1758, 1100-1105 (2006).
- 310 Yu, M. J. *et al.* Systems-level analysis of cell-specific AQP2 gene expression in renal collecting duct. *Proc. Natl. Acad. Sci. U. S. A.* 106, 2441-2446 (2009).
- 311 Brunati, A. M. *et al.* Novel consensus sequence for the Golgi apparatus casein kinase, revealed using proline-rich protein-1 (PRP1)-derived peptide substrates. *Biochem. J.* 351 Pt 3, 765-768 (2000).
- 312 Procino, G. *et al.* Ser-256 phosphorylation dynamics of Aquaporin 2 during maturation from the ER to the vesicular compartment in renal cells. *FASEB J.* 17, 1886-1888 (2003).
- 313 Lu, H. *et al.* Inhibition of endocytosis causes phosphorylation (S256)-independent plasma membrane accumulation of AQP2. *Am. J. Physiol. Renal Physiol.* 286, F233-243 (2004).
- 314 Kortenoeven, M. L. *et al.* In mpkCCD cells, long-term regulation of aquaporin-2 by vasopressin occurs independent of protein kinase A and CREB, but may involve Epac. *Am. J. Physiol. Renal Physiol.* (2012).

- 315 Nielsen, J. *et al.* Proteomic analysis of lithium-induced nephrogenic diabetes insipidus: mechanisms for aquaporin 2 down-regulation and cellular proliferation. *Proc. Natl. Acad. Sci. U. S. A.* 105, 3634-3639 (2008).
- 316 Hasler, U. *et al.* Acute hypertonicity alters aquaporin-2 trafficking and induces a MAPK-dependent accumulation at the plasma membrane of renal epithelial cells. *J. Biol. Chem.* 283, 26643-26661 (2008).
- 317 Rao, R. *et al.* Lithium treatment inhibits renal GSK-3 activity and promotes cyclooxygenase 2-dependent polyuria. *Am. J. Physiol. Renal Physiol.* 288, F642-649 (2005).
- 318 Nielsen, J. *et al.* Dysregulation of renal aquaporins and epithelial sodium channel in lithium-induced nephrogenic diabetes insipidus. *Semin. Nephrol.* 28, 227-244 (2008).
- 319 Rao, R. *et al.* GSK3beta mediates renal response to vasopressin by modulating adenylate cyclase activity. *J. Am. Soc. Nephrol.* 21, 428-437 (2010).
- 320 Rice, W. L. *et al.* Differential, Phosphorylation Dependent Trafficking of AQP2 in LLC-PK1 Cells. *PLoS One* 7, e32843 (2012).
- 321 Park, E. J. *et al.* The role of 70-kDa heat shock protein in dDAVP-induced AQP2 trafficking in kidney collecting duct cells. *Am. J. Physiol. Renal Physiol.* 304, F958-971 (2013).
- 322 Wu, W. *et al.* Beta1-integrin is required for kidney collecting duct morphogenesis and maintenance of renal function. *Am. J. Physiol. Renal Physiol.* 297, F210-217 (2009).
- 323 Tamma, G. *et al.* Integrin Signaling Modulates AQP2 Trafficking via Arg-Gly-Asp (RGD) Motif. *Cell. Physiol. Biochem.* 27, 739-748 (2011).
- 324 Chen, Y. *et al.* Aquaporin 2 Promotes Cell Migration and Epithelial Morphogenesis. *J. Am. Soc. Nephrol.* (2012).
- 325 Boone, M. *et al.* The lysosomal trafficking regulator interacting protein-5 localizes mainly in epithelial cells. *J. Mol. Hist.* 41, 61-74 (2010).
- 326 Kang, D. Y. *et al.* Identification of vasopressin-induced genes in AQP2-transfected MDCK cells by suppression subtractive hybridization. *Biochem. Biophys. Res. Commun.* 324, 1234-1241 (2004).
- 327 Tamma, G. Actin remodeling requires ERM function to facilitate AQP2 apical targeting. *J. Cell. Sci.* 118, 3623-3630 (2005).
- 328 Hasler, U. *et al.* NF-kappaB modulates aquaporin-2 transcription in renal collecting duct principal cells. *J. Biol. Chem.* 283, 28095-28105 (2008).
- 329 Hocherl, K. *et al.* Inhibition of NF-kappaB ameliorates sepsis-induced downregulation of aquaporin-2/V2 receptor expression and acute renal failure in vivo. *Am. J. Physiol. Renal Physiol.* 298, F196-204 (2010).
- 330 Hasler, U. An example of functional interaction between NFAT5/TonEBP and nuclear factor-kappaB by hypertonic stress: aquaporin-2 transcription. *Cell cycle* 10, 364-365 (2011).
- 331 Pisitkun, T. *et al.* Akt and ERK1/2 pathways are components of the vasopressin signaling network in rat native IMCD. *Am. J. Physiol. Renal Physiol.* 295, F1030-1043 (2008).
- 332 Kuwahara, M. *et al.* cAMP-dependent phosphorylation stimulates water permeability of aquaporin-collecting duct water channel protein expressed in *Xenopus* oocytes. *J. Biol. Chem.* 270, 10384-10387 (1995).
- 333 Fushimi, K. *et al.* Phosphorylation of serine 256 is required for cAMP-dependent regulatory exocytosis of the aquaporin-2 water channel. *J. Biol. Chem.* 272, 14800-14804 (1997).
- 334 Katsura, T. *et al.* Protein kinase A phosphorylation is involved in regulated exocytosis of aquaporin-2 in transfected LLC-PK1 cells. *Am. J. Physiol. Renal Physiol.* 272, F817-822 (1997).
- 335 Jung, H. J. *et al.* Membrane Trafficking of Collecting Duct Water Channel Protein AQP2 Regulated by Akt/AS160. *Electrolyte Blood Press.* 8, 59-65 (2010).
- 336 Kim, H. Y. *et al.* Emerging role of Akt substrate protein AS160 in the regulation of AQP2 translocation. *Am. J. Physiol. Renal Physiol.* 301, F151-161 (2011).
- 337 Thai, T. L. *et al.* Lack of protein kinase C-alpha leads to impaired urine concentrating ability and decreased aquaporin-2 in angiotensin II-induced hypertension. *Am. J. Physiol. Renal Physiol.* 303, F37-44 (2012).
- 338 Bagnasco, S. M. Protein kinase C-alpha comes to the rescue of aquaporin-2. *Am. J. Physiol. Renal Physiol.* 303, F35-36 (2012).
- 339 Zhao, H. *et al.* PKCalpha regulates vasopressin-induced aquaporin-2 trafficking in mouse kidney collecting duct cells in vitro via altering microtubule assembly. *Acta Pharmacol. Sin.* (2012).
- 340 Douglass, J. *et al.* Identifying protein kinase target preferences using mass spectrometry. *Am. J. Physiol. Cell Physiol.* 303, C715-727 (2012).
- 341 Liebenhoff, U. *et al.* Identification of Rab3-, Rab5a- and synaptobrevin II-like proteins in a preparation of rat kidney vesicles containing the vasopressin-regulated water channel. *FEBS Lett.* 365, 209-213 (1995).
- 342 Tajika, Y. *et al.* Differential regulation of AQP2 trafficking in endosomes by microtubules and actin filaments. *Histochem. Cell Biol.* 124, 1-12 (2005).
- 343 Procino, G. *et al.* Fluvastatin modulates renal water reabsorption in vivo through increased AQP2 availability at the apical plasma membrane of collecting duct cells. *Pflugers Arch* (2011).
- 344 Tamma, G. cAMP-induced AQP2 translocation is associated with RhoA inhibition through RhoA phosphorylation and interaction with RhoGDI. *J. Cell. Sci.* 116, 1519-1525 (2003).
- 345 Inoue, T. *et al.* SNAP-23 in rat kidney: colocalization with aquaporin-2 in collecting duct vesicles. *Am. J. Physiol. Renal Physiol.* 275, F752-760 (1998).
- 346 Shukla, A. *et al.* SNAP-25-associated Hrs-2 protein colocalizes with AQP2 in rat kidney collecting duct principal cells. *Am. J. Physiol. Renal Physiol.* 281, F546-556 (2001).
- 347 Noda, Y. *et al.* Aquaporin-2 trafficking is regulated by PDZ-domain containing protein SPA-1. *FEBS Lett.* 568, 139-145 (2004).
- 348 Kishore, B. K. *et al.* Expression of synaptotagmin VIII in rat kidney. *Am. J. Physiol. Renal Physiol.* 275, F131-142 (1998).
- 349 Mandon, B. *et al.* Syntaxin-4 is localized to the apical plasma membrane of rat renal collecting duct cells: possible role in aquaporin-2 trafficking. *J. Clin. Invest.* 98, 906-913 (1996).
- 350 Mandon, B. *et al.* Expression of syntaxins in rat kidney. *Am. J. Physiol. Renal Physiol.* 273, F718-730 (1997).
- 351 Gouraud, S. *et al.* Functional involvement of VAMP/synaptobrevin-2 in cAMP-stimulated aquaporin 2 translocation in renal collecting duct cells. *J. Cell. Sci.* 115, 3667-3674 (2002).
- 352 Brooks, H. L. *et al.* cDNA array identification of genes regulated in rat renal medulla in response to vasopressin infusion. *Am. J. Physiol. Renal Physiol.* 284, F218-228 (2003).
- 353 Mistry, A. C. *et al.* Syntaxin specificity of aquaporins in the inner medullary collecting duct. *Am. J. Physiol. Renal Physiol.* 297, F292-300 (2009).

- 354 Li, Y. H. *et al.* Aquaporin-2 regulates cell volume recovery via tropomyosin. *Int. J. Biochem. Cell* 41, 2466-2476 (2009).
- 355 Storm, R. *et al.* Osmolality and solute composition are strong regulators of AQP2 expression in renal principal cells. *Am. J. Physiol. Renal Physiol.* 284, F189-198 (2003).
- 356 Lam, A. K. *et al.* Osmotic response element-binding protein (OREBP) is an essential regulator of the urine concentrating mechanism. *J. Biol. Chem.* 279, 48048-48054 (2004).
- 357 Lopez-Rodriguez, C. *et al.* Loss of NFAT5 results in renal atrophy and lack of tonicity-responsive gene expression. *Proc. Natl. Acad. Sci. U. S. A.* 101, 2392-2397 (2004).
- 358 Hasler, U. *et al.* Tonicity-responsive enhancer binding protein is an essential regulator of aquaporin-2 expression in renal collecting duct principal cells. *J. Am. Soc. Nephrol.* 17, 1521-1531 (2006).
- 359 Goel, M. *et al.* Vasopressin-induced membrane trafficking of TRPC3 and AQP2 channels in cells of the rat renal collecting duct. *Am. J. Physiol. Renal Physiol.* 293, F1476-1488 (2007).
- 360 Goel, M. *et al.* Role of cAMP/PKA signaling cascade in vasopressin-induced trafficking of TRPC3 channels in principal cells of the collecting duct. *AJP: Renal Physiology* 298, F988-F996 (2010).
- 361 Galizia, L. *et al.* Functional interaction between AQP2 and TRPV4 in renal cells. *J. Cell. Biochem.* 113, 580-589 (2012).
- 362 Sabolic, I. *et al.* The AQP2 water channel: effect of vasopressin treatment, microtubule disruption, and distribution in neonatal rats. *J. Membr. Biol.* 143, 165-175 (1995).
- 363 Breton, S. *et al.* Cold-induced microtubule disruption and relocalization of membrane proteins in kidney epithelial cells. *J. Am. Soc. Nephrol.* 9, 155-166 (1998).
- 364 Shaw, S. *et al.* A rat kidney tubule suspension for the study of vasopressin-induced shuttling of AQP2 water channels. *Am. J. Physiol. Renal Physiol.* 283, F1160-1166 (2002).
- 365 Lee, Y. J. *et al.* Ubiquitination of aquaporin-2 in the kidney. *Electrolyte Blood Press.* 7, 1-4 (2009).
- 366 Marples, D. *et al.* Redistribution of aquaporin-2 water channels induced by vasopressin in rat kidney inner medullary collecting duct. *Am. J. Physiol.* 269, C655-664 (1995).
- 367 Jo, I. *et al.* Rat kidney papilla contains abundant synaptobrevin protein that participates in the fusion of antidiuretic hormone-regulated water channel-containing endosomes in vitro. *Proc. Natl. Acad. Sci. U. S. A.* 92, 1876-1880 (1995).
- 368 Franki, N. *et al.* Water channel-carrying vesicles in the rat IMCD contain cellubrevin. *Am. J. Physiol. Renal Physiol.* 269, C797-801 (1995).
- 369 Nielsen, S. *et al.* Expression of VAMP-2-like protein in kidney collecting duct intracellular vesicles. Colocalization with Aquaporin-2 water channels. *J. Clin. Invest.* 96, 1834-1844 (1995).
- 370 Wang, C. C. *et al.* A role for VAMP8/endobrevin in surface deployment of the water channel aquaporin 2. *Mol. Cell. Biol.* 30, 333-343 (2010).
- 371 Fujiwara, T. M. *et al.* Molecular biology of hereditary diabetes insipidus. *J. Am. Soc. Nephrol.* 16, 2836-2846 (2005).
- 372 Stone, K. A. Lithium-induced nephrogenic diabetes insipidus. *J. Am. Board Fam. Pract.* 12, 43-47 (1999).
- 373 Cade, J. F. Lithium salts in the treatment of psychotic excitement. *Med. J. Aust.* 2, 349-352 (1949).
- 374 Kishore, B. K. *et al.* Lithium: a versatile tool for understanding renal physiology. *Am. J. Physiol. Renal Physiol.* 304, F1139-1149 (2013).
- 375 Kortenoeven, M. L. *et al.* Amiloride blocks lithium entry through the sodium channel thereby attenuating the resultant nephrogenic diabetes insipidus. *Kidney Int.* 76, 44-53 (2009).
- 376 Christensen, S. *et al.* Pathogenesis of nephrogenic diabetes insipidus due to chronic administration of lithium in rats. *J. Clin. Invest.* 75, 1869-1879 (1985).
- 377 Cogan, E. *et al.* Mechanisms of lithium-vasopressin interaction in rabbit cortical collecting tubule. *Am. J. Physiol.* 252, F1080-1087 (1987).
- 378 Li, Y. *et al.* Development of lithium-induced nephrogenic diabetes insipidus is dissociated from adenylyl cyclase activity. *J. Am. Soc. Nephrol.* 17, 1063-1072 (2006).
- 379 Wen, H. *et al.* Urinary excretion of aquaporin-2 in rat is mediated by a vasopressin-dependent apical pathway. *J. Am. Soc. Nephrol.* 10, 1416-1429 (1999).
- 380 Walker, R. J. *et al.* Lithium-induced reduction in urinary concentrating ability and urinary aquaporin 2 (AQP2) excretion in healthy volunteers. *Kidney Int.* 67, 291-294 (2005).
- 381 McIlraith, C. Notes on some cases of Diabetes Insipidus with marked family and hereditary tendencies. *The Lancet* 140, 767-768 (1892).
- 382 Bockenhauer, D. *et al.* Urinary concentration: different ways to open and close the tap. *Pediatr. Nephrol.* (2013).
- 383 Lolait, S. J. *et al.* Cloning and characterization of a vasopressin V2 receptor and possible link to nephrogenic diabetes insipidus. *Nature* 357, 336-339 (1992).
- 384 Rosenthal, W. *et al.* Molecular identification of the gene responsible for congenital nephrogenic diabetes insipidus. *Nature* 359, 233-235 (1992).
- 385 Birnbaumer, M. *et al.* Molecular cloning of the receptor for human antidiuretic hormone. *Nature* 357, 333-335 (1992).
- 386 van Lieburg, A. F. *et al.* Patients with autosomal nephrogenic diabetes insipidus homozygous for mutations in the aquaporin 2 water-channel gene. *Am. J. Hum. Genet.* 55, 648-652 (1994).
- 387 Robben, J. H. *et al.* Cell biological aspects of the vasopressin type-2 receptor and aquaporin 2 water channel in nephrogenic diabetes insipidus. *Am. J. Physiol. Renal Physiol.* 291, F257-270 (2006).
- 388 Moeller, H. B. *et al.* Nephrogenic diabetes insipidus: essential insights into the molecular background and potential therapies for treatment. *Endocr. Rev.* 34, 278-301 (2013).
- 389 Wesche, D. *et al.* Congenital nephrogenic diabetes insipidus: the current state of affairs. *Pediatr. Nephrol.* (2012).
- 390 Manning, M. *et al.* Solid phase synthesis of (1-deamino,4-valine)-8-D-arginine-vasopressin (DVEDAVP), a highly potent and specific antidiuretic agent possessing protracted effects. *J. Med. Chem.* 16, 975-978 (1973).
- 391 Schwartz, W. B. *et al.* A syndrome of renal sodium loss and hyponatremia probably resulting from inappropriate secretion of antidiuretic hormone. *Am. J. Med.* 23, 529-542 (1957).
- 392 Wilson, J. L. *et al.* Vasopressin and the regulation of aquaporin-2. *Clin. Exp. Nephrol.* (2013).
- 393 Fujita, N. *et al.* Role of water channel AQP-CD in water retention in SIADH and cirrhotic rats. *Am. J. Physiol.* 269, F926-931 (1995).
- 394 Saito, T. *et al.* Role of aquaporin-2 gene expression in hyponatremic rats with chronic vasopressin-induced antidiuresis. *Kidney Int.* 60, 1266-1276 (2001).
- 395 Feldman, B. J. *et al.* Nephrogenic syndrome of inappropriate antidiuresis. *N. Engl. J. Med.* 352, 1884-1890 (2005).

- 396 Ranchin, B. *et al.* Familial nephrogenic syndrome of inappropriate antidiuresis: dissociation between aquaporin-2 and vasopressin excretion. *J. Clin. Endocrinol. Metab.* 95, E37-43 (2010).
- 397 Bartter, F. C. *et al.* The syndrome of inappropriate secretion of antidiuretic hormone. *Am. J. Med.* 42, 790-806 (1967).
- 398 Xu, D. L. *et al.* Upregulation of aquaporin-2 water channel expression in chronic heart failure rat. *J. Clin. Invest.* 99, 1500-1505 (1997).
- 399 Weston, R. E. *et al.* The pathogenesis and treatment of hyponatremia in congestive heart failure. *Am. J. Med.* 25, 558-572 (1958).
- 400 Apostol, E. *et al.* Reduced renal medullary water channel expression in puromycin aminonucleoside-induced nephrotic syndrome. *J. Am. Soc. Nephrol.* 8, 15-24 (1997).
- 401 Ecelbarger, C. A. *et al.* Escape from vasopressin-induced antidiuresis: role of vasopressin resistance of the collecting duct. *Am. J. Physiol.* 274, F1161-1166 (1998).
- 402 Fernandez-Llama, P. *et al.* Concentrating defect in experimental nephrotic syndrome: altered expression of aquaporins and thick ascending limb Na⁺ transporters. *Kidney Int.* 54, 170-179 (1998).
- 403 Fernandez-Llama, P. *et al.* Impaired aquaporin and urea transporter expression in rats with adriamycin-induced nephrotic syndrome. *Kidney Int.* 53, 1244-1253 (1998).
- 404 Maric, K. *et al.* Aquaporin-2 expression in primary cultured rat inner medullary collecting duct cells. *Am. J. Physiol. Renal Physiol.* 275, F796-801 (1998).
- 405 Graham, F. L. *et al.* Characteristics of a human cell line transformed by DNA from human adenovirus type 5. *J. Gen. Virol.* 36, 59-74 (1977).
- 406 Stoos, B. A. *et al.* Characterization of a mouse cortical collecting duct cell line. *Kidney Int.* 39, 1168-1175 (1991).
- 407 Iolascon, A. *et al.* Characterization of Two Novel Missense Mutations in the *AQP2* Gene Causing Nephrogenic Diabetes Insipidus. *Nephron Physiol.* 105, p33-p41 (2007).
- 408 Steele, S. L. *et al.* Telomerase immortalization of principal cells from mouse collecting duct. *Am. J. Physiol. Renal Physiol.* 299, F1507-1514 (2010).
- 409 Faust, D. *et al.* Culturing primary rat inner medullary collecting duct cells. *J Vis Exp* (2013).
- 410 Bradford, M. M. A rapid and sensitive method for the quantitation of microgram quantities of protein utilizing the principle of protein-dye binding. *Anal. Biochem.* 72, 248-254 (1976).
- 411 Fire, A. *et al.* Potent and specific genetic interference by double-stranded RNA in *Caenorhabditis elegans*. *Nature* 391, 806-811 (1998).
- 412 Elbashir, S. M. *et al.* Duplexes of 21-nucleotide RNAs mediate RNA interference in cultured mammalian cells. *Nature* 411, 494-498 (2001).
- 413 Nykanen, A. *et al.* ATP requirements and small interfering RNA structure in the RNA interference pathway. *Cell* 107, 309-321 (2001).
- 414 Matranga, C. *et al.* Passenger-strand cleavage facilitates assembly of siRNA into Ago2-containing RNAi enzyme complexes. *Cell* 123, 607-620 (2005).
- 415 Martinez, J. *et al.* Single-stranded antisense siRNAs guide target RNA cleavage in RNAi. *Cell* 110, 563-574 (2002).
- 416 Hammond, S. M. *et al.* An RNA-directed nuclease mediates post-transcriptional gene silencing in *Drosophila* cells. *Nature* 404, 293-296 (2000).
- 417 Zhang, J. H. *et al.* A Simple Statistical Parameter for Use in Evaluation and Validation of High Throughput Screening Assays. *J. Biomol. Screen.* 4, 67-73 (1999).
- 418 Procino, G. *et al.* Adipocytes support cAMP-dependent translocation of aquaporin-2 from intracellular sites distinct from the insulin-responsive GLUT4 storage compartment. *Am. J. Physiol. Renal Physiol.* 290, F985-994 (2006).
- 419 Carpenter, A. E. *et al.* CellProfiler: image analysis software for identifying and quantifying cell phenotypes. *Genome Biol.* 7, R100 (2006).
- 420 Gustafson, C. E. *et al.* Vasopressin regulated trafficking of a green fluorescent protein-aquaporin 2 chimera in LLC-PK1 cells. *Histochem. Cell Biol.* 110, 377-386 (1998).
- 421 Atar, O. D. *et al.* Stability validation of paraformaldehyde-fixed samples for the assessment of the platelet PECAM-1, P-selectin, and PAR-1 thrombin receptor by flow cytometry. *J. Thromb. Thrombolysis* 30, 79-83 (2010).
- 422 Stoter, M. *et al.* CellProfiler and KNIME: Open Source Tools for High Content Screening. *Methods Mol. Biol.* 986, 105-122 (2013).
- 423 Lim, Y. S. *et al.* The Evi5 family in cellular physiology and pathology. *FEBS Lett.* 587, 1703-1710 (2013).
- 424 Bahassi el, M. Polo-like kinases and DNA damage checkpoint: beyond the traditional mitotic functions. *Exp. Biol. Med.* (Maywood) 236, 648-657 (2011).
- 425 Nikonova, A. S. *et al.* Aurora A kinase (AURKA) in normal and pathological cell division. *Cell. Mol. Life Sci.* 70, 661-687 (2013).
- 426 Cornils, H. *et al.* Downstream of human NDR kinases: impacting on c-myc and p21 protein stability to control cell cycle progression. *Cell cycle* 10, 1897-1904 (2011).
- 427 Bright, N. J. *et al.* The regulation and function of mammalian AMPK-related kinases. *Acta physiologica* 196, 15-26 (2009).
- 428 Bakke, O. *et al.* Emerging regulators of endosomal dynamics during mitosis. *Cell cycle* 13, 349-350 (2014).
- 429 van der Waal, M. S. *et al.* Cell division control by the Chromosomal Passenger Complex. *Exp. Cell Res.* 318, 1407-1420 (2012).
- 430 Rebocho, A. P. *et al.* ARAF acts as a scaffold to stabilize BRAF: CRAF heterodimers. *Oncogene* 32, 3207-3212 (2013).
- 431 Jaluria, P. *et al.* Enhancement of cell proliferation in various mammalian cell lines by gene insertion of a cyclin-dependent kinase homolog. *BMC Biotechnol.* 7, 71 (2007).
- 432 Horwood, N. J. *et al.* Tec family kinases in inflammation and disease. *Int. Rev. Immunol.* 31, 87-103 (2012).
- 433 Croucher, D. R. *et al.* Involvement of Lyn and the atypical kinase Sgk269/PEAK1 in a basal breast cancer signaling pathway. *Cancer Res.* 73, 1969-1980 (2013).
- 434 Lou, D. *et al.* Spatiotemporal expression of testicular protein kinase 1 after rat sciatic nerve injury. *J. Mol. Neurosci.* 47, 180-191 (2012).
- 435 Maloverjan, A. *et al.* Mammalian homologues of *Drosophila* fused kinase. *Vitam. Horm.* 88, 91-113 (2012).
- 436 Matitau, A. E. *et al.* MEKK2 kinase association with 14-3-3 protein regulates activation of c-Jun N-terminal kinase. *J. Biol. Chem.* 288, 28293-28302 (2013).
- 437 Stephenson, J. R. *et al.* Brain-specific angiogenesis inhibitor-1 signaling, regulation, and enrichment in the postsynaptic density. *J. Biol. Chem.* 288, 22248-22256 (2013).

- 438 Bettinger, B. T. *et al.* The MEK kinases MEKK4/Ssk2p facilitate complexity in the stress signaling responses of diverse systems. *J. Cell. Biochem.* 101, 34-43 (2007).
- 439 Diviani, D. *et al.* AKAP-Lbc: a molecular scaffold for the integration of cyclic AMP and Rho transduction pathways. *Eur. J. Cell Biol.* 85, 603-610 (2006).
- 440 Moelleken, J. *et al.* Differential localization of coatamer complex isoforms within the Golgi apparatus. *Proc. Natl. Acad. Sci. U. S. A.* 104, 4425-4430 (2007).
- 441 Ferre, S. *et al.* Insight into renal Mg²⁺ transporters. *Curr. Opin. Nephrol. Hypertens.* 20, 169-176 (2011).
- 442 Bunker, R. D. *et al.* Structure and function of human xylulokinase, an enzyme with important roles in carbohydrate metabolism. *J. Biol. Chem.* 288, 1643-1652 (2013).
- 443 Blonska, M. *et al.* NF-kappaB signaling pathways regulated by CARMA family of scaffold proteins. *Cell Res.* 21, 55-70 (2011).
- 444 Goyal, P. *et al.* Identifying and characterizing a novel protein kinase STK35L1 and deciphering its orthologs and close-homologs in vertebrates. *PLoS One* 4, e6981 (2009).
- 445 Manning, T. *et al.* Biologically inspired intelligent decision making: A commentary on the use of artificial neural networks in bioinformatics. *Bioengineered* 5 (2013).
- 446 Boland, M. V. *et al.* A neural network classifier capable of recognizing the patterns of all major subcellular structures in fluorescence microscope images of HeLa cells. *Bioinformatics* 17, 1213-1223 (2001).
- 447 Rosenblatt, F. The perceptron: a probabilistic model for information storage and organization in the brain. *Psychol. Rev.* 65, 386-408 (1958).
- 448 Simpson, K. J. *et al.* Comparative high-throughput RNAi screening methodologies in *C. elegans* and mammalian cells. *N. Biotechnol.* 29, 459-470 (2012).
- 449 Boutros, M. *et al.* The art and design of genetic screens: RNA interference. *Nat. Rev. Genet.* 9, 554-566 (2008).
- 450 Ashby, C. D. *et al.* Characterization of the interaction of a protein inhibitor with adenosine 3',5'-monophosphate-dependent protein kinases. I. Interaction with the catalytic subunit of the protein kinase. *J. Biol. Chem.* 247, 6637-6642 (1972).
- 451 Fantozzi, D. A. *et al.* Thermostable inhibitor of cAMP-dependent protein kinase enhances the rate of export of the kinase catalytic subunit from the nucleus. *J. Biol. Chem.* 269, 2676-2686 (1994).
- 452 Korsse, S. E. *et al.* Targeting LKB1 signaling in cancer. *Biochim. Biophys. Acta* 1835, 194-210 (2013).
- 453 Kelleher, F. C. *et al.* Fibroblast growth factor receptors, developmental corruption and malignant disease. *Carcinogenesis* 34, 2198-2205 (2013).
- 454 Cross, M. J. *et al.* The Shb adaptor protein binds to tyrosine 766 in the FGFR-1 and regulates the Ras/MEK/MAPK pathway via FRS2 phosphorylation in endothelial cells. *Mol. Biol. Cell* 13, 2881-2893 (2002).
- 455 Herath, N. I. *et al.* The role of Eph receptors and ephrin ligands in colorectal cancer. *Int. J. Cancer* 126, 2003-2011 (2010).
- 456 Orioli, D. *et al.* Sek4 and Nuk receptors cooperate in guidance of commissural axons and in palate formation. *EMBO J.* 15, 6035-6049 (1996).
- 457 Adams, R. H. *et al.* Roles of ephrinB ligands and EphB receptors in cardiovascular development: demarcation of arterial/venous domains, vascular morphogenesis, and sprouting angiogenesis. *Genes Dev.* 13, 295-306 (1999).
- 458 Batlle, E. *et al.* Beta-catenin and TCF mediate cell positioning in the intestinal epithelium by controlling the expression of EphB/ephrinB. *Cell* 111, 251-263 (2002).
- 459 Kotzsch, A. *et al.* Crystal structure analysis reveals a spring-loaded latch as molecular mechanism for GDF-5-type I receptor specificity. *EMBO J.* 28, 937-947 (2009).
- 460 Kang, T. H. *et al.* Negative regulation of ERK activity by VRK3-mediated activation of VHR phosphatase. *Nat. Cell Biol.* 8, 863-869 (2006).
- 461 Vega, F. M. *et al.* Expression of the VRK (vaccinia-related kinase) gene family of p53 regulators in murine hematopoietic development. *FEBS Lett.* 544, 176-180 (2003).
- 462 Napolitano, L. M. *et al.* TRIM family: Pleiotropy and diversification through homomultimer and heteromultimer formation. *IUBMB life* 64, 64-71 (2012).
- 463 Meroni, G. *et al.* TRIM/RBCC, a novel class of 'single protein RING finger' E3 ubiquitin ligases. *Bioessays* 27, 1147-1157 (2005).
- 464 Herskovits, A. Z. *et al.* The regulation of tau phosphorylation by PCTAIRE 3: implications for the pathogenesis of Alzheimer's disease. *Neurobiol. Dis.* 23, 398-408 (2006).
- 465 Noma, T. Dynamics of nucleotide metabolism as a supporter of life phenomena. *J. Med. Invest.* 52, 127-136 (2005).
- 466 Rickert, R. C. New insights into pre-BCR and BCR signalling with relevance to B cell malignancies. *Nat. Rev. Immunol.* 13, 578-591 (2013).
- 467 Abtahian, F. *et al.* Regulation of blood and lymphatic vascular separation by signaling proteins SLP-76 and Syk. *Science* 299, 247-251 (2003).
- 468 Luz, S. *et al.* Contribution of casein kinase 2 and spleen tyrosine kinase to CFTR trafficking and protein kinase A-induced activity. *Mol. Cell. Biol.* 31, 4392-4404 (2011).
- 469 Buitrago, L. *et al.* Tyrosine phosphorylation on spleen tyrosine kinase (Syk) is differentially regulated in human and murine platelets by protein kinase C isoforms. *J. Biol. Chem.* 288, 29160-29169 (2013).
- 470 Aufderklamm, S. *et al.* Thymidine kinase and cancer monitoring. *Cancer Lett.* 316, 6-10 (2012).
- 471 Priego, E. M. *et al.* Recent advances in thymidine kinase 2 (TK2) inhibitors and new perspectives for potential applications. *Curr. Pharm. Des.* 18, 2981-2994 (2012).
- 472 Bermudez, O. *et al.* The dual-specificity MAP kinase phosphatases: critical roles in development and cancer. *Am. J. Physiol. Cell Physiol.* 299, C189-202 (2010).
- 473 Schoneberg, T. *et al.* Structure and allosteric regulation of eukaryotic 6-phosphofructokinases. *Biol. Chem.* 394, 977-993 (2013).
- 474 Pisitkun, T. *et al.* High-throughput identification of IMCD proteins using LC-MS/MS. *Physiol. Genomics* 25, 263-276 (2006).
- 475 Yu, M. J. *et al.* LC-MS/MS analysis of apical and basolateral plasma membranes of rat renal collecting duct cells. *Mol. Cell. Proteomics* 5, 2131-2145 (2006).
- 476 Uawithya, P. *et al.* Transcriptional profiling of native inner medullary collecting duct cells from rat kidney. *Physiol. Genomics* 32, 229-253 (2008).
- 477 Mohr, S. *et al.* Genomic screening with RNAi: results and challenges. *Annu. Rev. Biochem.* 79, 37-64 (2010).
- 478 Elbashir, S. M. *et al.* Analysis of gene function in somatic mammalian cells using small interfering RNAs. *Methods* 26, 199-213 (2002).

- 479 Sharma, S. *et al.* RNAi screening: tips and techniques. *Nat. Immunol.* 10, 799-804 (2009).
- 480 Lambeth, L. S. *et al.* Short hairpin RNA-mediated gene silencing. *Methods Mol. Biol.* 942, 205-232 (2013).
- 481 Campeau, E. *et al.* RNA interference in mammals: behind the screen. *Briefings in functional genomics* 10, 215-226 (2011).
- 482 Birmingham, A. *et al.* 3' UTR seed matches, but not overall identity, are associated with RNAi off-targets. *Nat. Methods* 3, 199-204 (2006).
- 483 Jackson, A. L. *et al.* Widespread siRNA "off-target" transcript silencing mediated by seed region sequence complementarity. *RNA* 12, 1179-1187 (2006).
- 484 Rajewsky, N. microRNA target predictions in animals. *Nat. Genet.* 38 Suppl, S8-13 (2006).
- 485 Castanotto, D. *et al.* Combinatorial delivery of small interfering RNAs reduces RNAi efficacy by selective incorporation into RISC. *Nucleic Acids Res.* 35, 5154-5164 (2007).
- 486 Khan, A. A. *et al.* Transfection of small RNAs globally perturbs gene regulation by endogenous microRNAs. *Nat. Biotechnol.* 27, 549-555 (2009).
- 487 Brass, A. L. *et al.* Identification of host proteins required for HIV infection through a functional genomic screen. *Science* 319, 921-926 (2008).
- 488 Konig, R. *et al.* Global analysis of host-pathogen interactions that regulate early-stage HIV-1 replication. *Cell* 135, 49-60 (2008).
- 489 Zhou, H. *et al.* Genome-scale RNAi screen for host factors required for HIV replication. *Cell host & microbe* 4, 495-504 (2008).
- 490 Goff, S. P. Knockdown screens to knockout HIV-1. *Cell* 135, 417-420 (2008).
- 491 Haney, S. A. Increasing the robustness and validity of RNAi screens. *Pharmacogenomics* 8, 1037-1049 (2007).
- 492 Amarzguioui, M. *et al.* Tolerance for mutations and chemical modifications in a siRNA. *Nucleic Acids Res.* 31, 589-595 (2003).
- 493 Altschul, S. F. *et al.* Basic local alignment search tool. *J. Mol. Biol.* 215, 403-410 (1990).
- 494 Zhang, X. D. Novel Analytic Criteria and Effective Plate Designs for Quality Control in Genome-Scale RNAi Screens. *J. Biomol. Screen.* 13, 363-377 (2008).
- 495 Root, D. E. *et al.* Detecting spatial patterns in biological array experiments. *J. Biomol. Screen.* 8, 393-398 (2003).
- 496 Bushway, P. J. *et al.* Hybrid median filter background estimator for correcting distortions in microtiter plate data. *Assay Drug Dev. Technol.* 8, 238-250 (2010).
- 497 Levine, B. *et al.* Autophagy in cell death: an innocent convict? *J. Clin. Invest.* 115, 2679-2688 (2005).
- 498 Solaimani, P. *et al.* Genome-wide RNAi high-throughput screen identifies proteins necessary for the AHR-dependent induction of CYP1A1 by 2,3,7,8-tetrachlorodibenzo-p-dioxin. *Toxicol. Sci.* 136, 107-119 (2013).
- 499 Petrocca, F. *et al.* A genome-wide siRNA screen identifies proteasome addiction as a vulnerability of basal-like triple-negative breast cancer cells. *Cancer Cell* 24, 182-196 (2013).
- 500 Yang, S. H. *et al.* A genome-wide RNAi screen reveals MAP kinase phosphatases as key ERK pathway regulators during embryonic stem cell differentiation. *PLoS Genet.* 8, e1003112 (2012).
- 501 Groenendyk, J. *et al.* A genome-wide siRNA screen identifies novel phospho-enzymes affecting Wnt/beta-catenin signaling in mouse embryonic stem cells. *Stem cell reviews* 7, 910-926 (2011).
- 502 Farazi, T. A. *et al.* The growing catalog of small RNAs and their association with distinct Argonaute/Piwi family members. *Development* 135, 1201-1214 (2008).
- 503 Yin, Z. *et al.* Using iterative cluster merging with improved gap statistics to perform online phenotype discovery in the context of high-throughput RNAi screens. *BMC Bioinformatics* 9, 264 (2008).
- 504 Held, M. *et al.* CellCognition: time-resolved phenotype annotation in high-throughput live cell imaging. *Nat. Methods* 7, 747-754 (2010).
- 505 Conrad, C. *et al.* Micropilot: automation of fluorescence microscopy-based imaging for systems biology. *Nat. Methods* 8, 246-249 (2011).
- 506 de Chaumont, F. *et al.* Icy: an open bioimage informatics platform for extended reproducible research. *Nat. Methods* 9, 690-696 (2012).
- 507 Schindelin, J. *et al.* Fiji: an open-source platform for biological-image analysis. *Nat. Methods* 9, 676-682 (2012).
- 508 Rajaram, S. *et al.* PhenoRipper: software for rapidly profiling microscopy images. *Nat. Methods* 9, 635-637 (2012).
- 509 Li, F. *et al.* Chapter 17: bioimage informatics for systems pharmacology. *PLoS Computat. Biol.* 9, e1003043 (2013).
- 510 Jones, T. R. *et al.* Scoring diverse cellular morphologies in image-based screens with iterative feedback and machine learning. *Proc. Natl. Acad. Sci. U. S. A.* 106, 1826-1831 (2009).
- 511 Carpenter, A. E. Extracting rich information from images. *Methods Mol. Biol.* 486, 193-211 (2009).
- 512 Barrows, N. J. *et al.* Factors Affecting Reproducibility between Genome-Scale siRNA-Based Screens. *J. Biol. Chem.* 15, 735-747 (2010).
- 513 Horvath, P. *et al.* Machine Learning Improves the Precision and Robustness of High-Content Screens: Using Nonlinear Multiparametric Methods to Analyze Screening Results. *J. Biomol. Screen.* (2011).
- 514 Misselwitz, B. *et al.* Enhanced CellClassifier: a multi-class classification tool for microscopy images. *BMC Bioinformatics* 11, 30 (2010).
- 515 Zhang, X. D. *et al.* Integrating Experimental and Analytic Approaches to Improve Data Quality in Genome-wide RNAi Screens. *J. Biomol. Screen.* 13, 378-389 (2008).
- 516 Zhang, X. D. *et al.* Hit selection with false discovery rate control in genome-scale RNAi screens. *Nucleic Acids Res.* 36, 4667-4679 (2008).
- 517 Knepper, M. A. Systems biology in physiology: the vasopressin signaling network in kidney. *Am. J. Physiol. Cell Physiol.* 303, C1115-1124 (2012).
- 518 Griffiths-Jones, S. *et al.* miRBase: microRNA sequences, targets and gene nomenclature. *Nucleic Acids Res.* 34, D140-144 (2006).
- 519 Mikolcevic, P. *et al.* Orphan kinases turn eccentric: a new class of cyclin Y-activated, membrane-targeted CDKs. *Cell cycle* 11, 3758-3768 (2012).
- 520 Khawaja, X. *et al.* Proteomic analysis of protein changes developing in rat hippocampus after chronic antidepressant treatment: Implications for depressive disorders and future therapies. *J. Neurosci. Res.* 75, 451-460 (2004).
- 521 Daub, H. *et al.* Kinase-selective enrichment enables quantitative phosphoproteomics of the kinome across the cell cycle. *Mol. Cell* 31, 438-448 (2008).
- 522 Varjosalo, M. *et al.* The protein interaction landscape of the human CMGC kinase group. *Cell reports* 3, 1306-1320 (2013).

- 523 Rual, J. F. *et al.* Towards a proteome-scale map of the human protein-protein interaction network. *Nature* 437, 1173-1178 (2005).
- 524 Taipale, M. *et al.* Quantitative analysis of HSP90-client interactions reveals principles of substrate recognition. *Cell* 150, 987-1001 (2012).
- 525 Palmer, K. J. *et al.* PCTAIRE protein kinases interact directly with the COPII complex and modulate secretory cargo transport. *J. Cell Sci.* 118, 3839-3847 (2005).
- 526 Gloeckner, C. J. *et al.* A novel tandem affinity purification strategy for the efficient isolation and characterisation of native protein complexes. *Proteomics* 7, 4228-4234 (2007).
- 527 Walsh, D. A. *et al.* Krebs EG: Purification and characterization of a protein inhibitor of adenosine 3',5'-monophosphate-dependent protein kinases. *J. Biol. Chem.* 246, 1977-1985 (1971).
- 528 Snel, B. *et al.* STRING: a web-server to retrieve and display the repeatedly occurring neighbourhood of a gene. *Nucleic Acids Res.* 28, 3442-3444 (2000).
- 529 Pilo-Boyl, P. *et al.* Profilin2 contributes to synaptic vesicle exocytosis, neuronal excitability, and novelty-seeking behavior. *EMBO J.* 26, 2991-3002 (2007).
- 530 Huang da, W. *et al.* Bioinformatics enrichment tools: paths toward the comprehensive functional analysis of large gene lists. *Nucleic Acids Res.* 37, 1-13 (2009).

9 PUBLICATIONS

ARTICLES

Faust D, Geelhaar A, Eisermann B, Eichhorst J, Wiesner B, Rosenthal W and Enno Klussman. Culturing primary rat inner medullary collecting duct cells. *J Vis Exp*. 2013 Jun 21; (76):e5115

Bogum J, Faust D, Zühlke K, Eichhorst J, Moutty MC, Furkert J, Eldahshan A, Neuenschwander M, von Kries JP, Wiesner B, Trimpert C, Deen PM, Valenti G, Rosenthal W and Enno Klussmann. Small-Molecule Screening Identifies Modulators of Aquaporin-2 Trafficking. *J Am Soc of Nephrol*. 2013 Apr; 24(5):744-58

ORAL PRESENTATIONS

Faust D, Wippich M, Lazarow K, Neuenschwander M, Graeber S, Fontaine JF, Andrade M, Kries JP, Rosenthal W and Enno Klussmann. Silencing of mouse kinome reveals novel players controlling the localisation of the water channel aquaporin-2. 9th Transport Colloquium, Rauischholzhausen, Germany, May 8-9, 2014

Faust D, Neuenschwander M, Lazarow K, Graeber S, Kries JP, Rosenthal W and Enno Klussmann. Identification of proteins involved in the trafficking of aquaporin-2 (AQP2) *via* genome-wide siRNA screening. American Society of Nephrology, Kidney Week, San Diego, United States of America, October 30-November 4, 2012

Faust D, Neuenschwander M, Lazarow K, Graeber S, Kries JP, Rosenthal W and Enno Klussmann. Genome-wide siRNA screening for the identification of novel players controlling AQP2. Pre-American Society of Nephrology Kidney Week Young Investigators Forum in Epithelial Biology 2012, San Diego, United States of America, October 31, 2012

Faust D, da Costa-Goncalves AC, Tabor V, Kirschner A, Eisermann B, Geelhaar A, Rosenthal W and Enno Klussmann. Increased AQP2 protein stability by SPN-PP1-mediated dephosphorylation-new insights into AVP-induced renal water reabsorption. 13th MDC/ FMP PhD Retreat, Liebenwalde, Germany, September 1-3, 2011.

POSTER PRESENTATIONS

Faust D, Neuenschwander M, Lazarow K, Graeber S, Kries JP, Rosenthal W and Enno Klussmann. A genome-wide siRNA screening to identify proteins involved in the trafficking of aquaporin-2. 14th MDC/ FMP PhD Retreat, Liebenwalde, Germany, August 30-September 1, 2012.

Faust D, Tabor V, Eisermann B, Milic J, Hill K, Kirschner A, Neumann A, Geelhaar A, Schaefer M, Rosenthal W and Enno Klussmann. A novel class of small molecules for the treatment of hyponatremia in chronic heart failure. 12th MDC/ FMP PhD Retreat, Reinsberg, Germany, September 9-11, 2010.

Faust D, Tabor V, Eisermann B, Milic J, Hill K, Kirschner A, Neumann A, Geelhaar A, Schaefer M, Rosenthal W and Enno Klussmann. Regulation of AQP2 trafficking *via* a TRPC6-dependent mechanism. MDC/ FMP Symposium, Berlin, Germany, May 27, 2010

1	Set Variable	volume "enter the volume in ul to transfer" "enter the volume in ul to transfer"
2	Aspirate	 volume µl Water wet contact MCA 384 DITI 125 slow for Optimem "AB0781" (Col. 1, Rows 1-16)
3	Dispense	 volume µl Water wet contact MCA 384 DITI 125 slow for Optimem "Greiner µClear" (Col. 1, Rows 1-16)
4	Move	 Positioning with global Z-Travel "Adapter384ComboDiti" (Col. 1, Rows 1-16)
5	Set Variable	answer "shall the tips be washed now?" "shall the tips be washed now?"
6	If - Then	answer = yes
7	Group	wash tips and dry them with ethanol
8	Comment	wash tips and dry them with ethanol
9	Mix	 100.0 µl Water wet contact MCA384 DITI 125 "water tip wash" (Col. 1, Rows 1-16)
10	Aspirate	 100.0 µl Ethanol Wash MCA Diti "ethanol" (Col. 1, Rows 1-16)
11	Dispense	 100.0 µl Ethanol Wash MCA Diti "ethanol" (Col. 1, Rows 1-16)
12	Mix	 80.0 µl Air Dry MCA Diti "ethanol" (Col. 1, Rows 1-16)
13	Start Timer	1
14	Wait for Timer	Timer 1 : 15 sec
15	Mix	 80.0 µl Air Dry MCA Diti "ethanol" (Col. 1, Rows 1-16)
16	Start Timer	2
17	Wait for Timer	Timer 1 : 120 sec
18	Move	 Positioning with global Z-Travel "Adapter384ComboDiti" (Col. 1, Rows 1-16)
19	Group End	wash tips and dry them with ethanol
20	Else	
21	End If	

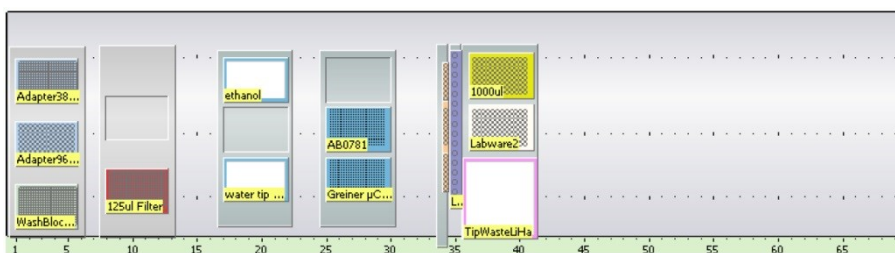


Fig. S 2. Protocol for automated siRNA transfer using TECAN Freedom EVO. Volume (step 1) was set to 4.3 µl, resulting in 4 µl transferred volume per well of a 384 well plate.

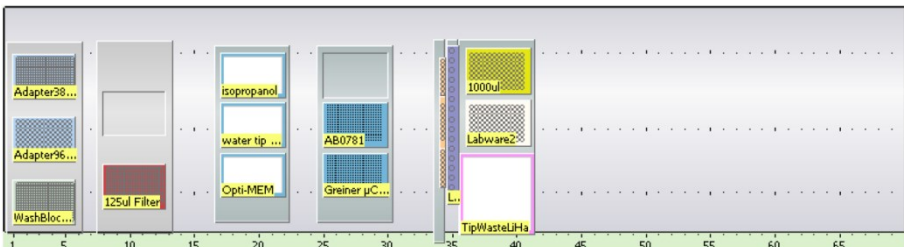
Set Variable	volume "enter the volume in ul to transfer" "enter the volume in ul to transfer"
Aspirate	 volume µl Water wet contact MCA 384 DITI 125 slow for Optimem "AB0781" (Col. 1, Rows 1-16)
Dispense	 volume µl Water wet contact MCA 384 DITI 125 slow for Optimem "Greiner µClear" (Col. 1, Rows 1-16)
Mix	 8.0 µl Water wet contact MCA 384 DITI 125 slow for Optimem "Greiner µClear" (Col. 1, Rows 1-16)
Mix	 50.0 µl Water wet contact MCA384 DITI 125 "Opti-MEM" (Col. 1, Rows 1-16)
Move	 Positioning with global Z-Travel "Adapter384ComboDiti" (Col. 1, Rows 1-16)
Set Variable	answer "shall the tips be washed now?" "shall the tips be washed now?"
If - Then	answer = yes
Group	wash tips and dry them with isopropanol
Comment	wash tips and dry them with isopropanol
Get Head Adapter	Grid 1; Site: 1 (Adapter DITI Combo MCA384)
Mix	 100.0 µl Water wet contact MCA384 DITI 125 "water tip wash" (Col. 1, Rows 1-16)
Aspirate	 100.0 µl Ethanol Wash MCA Diti "isopropanol" (Col. 1, Rows 1-16)
Dispense	 100.0 µl Ethanol Wash MCA Diti "isopropanol" (Col. 1, Rows 1-16)
Mix	 80.0 µl Air Dry MCA Diti "isopropanol" (Col. 1, Rows 1-16)
Start Timer	1
Wait for Timer	Timer 1 : 15 sec
Mix	 80.0 µl Air Dry MCA Diti "isopropanol" (Col. 1, Rows 1-16)
Drop Head Adapter	Grid 1; Site: 1 (Adapter DITI Combo MCA384)
Start Timer	2
Wait for Timer	Timer 1 : 120 sec
Move	 Positioning with global Z-Travel "Adapter384ComboDiti" (Col. 1, Rows 1-16)
Group End	wash tips and dry them with isopropanol
	

Fig. S 3. Protocol for automated transfer of Lipofectamine® 2000 using TECAN Freedom EVO. Volume (step 1) was set to 6.3 µl, resulting in 6 µl transferred volume per well of a 384 well plate.

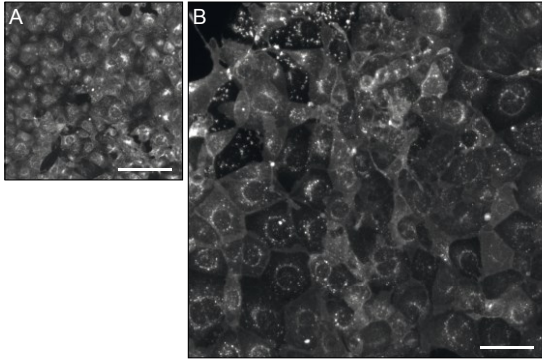


Fig. S 4. High quality imaging of MCD4 cells in microtiter plates. **A)** Standard acquisition camera mode includes 2 x 2 binning and resulted in 512 x 512 images. Cells were seeded on Corning “Optical Imaging” microtiter plates (#3985) having a polystyrene bottom of 900 μm thickness. **B)** High resolution acquisition camera mode generated 1024 x 1024 images without binning (1 x 1). Cells were seeded on cell culture microtiter plates “ μ clear” from Greiner (#781091) that have 190 μm thick polystyrene bottoms. Images were acquired *via* automated immunofluorescence microscopy using an ArrayScan V^{TI} HCS Reader (40x magnification). Scale bars indicate 50 μm .

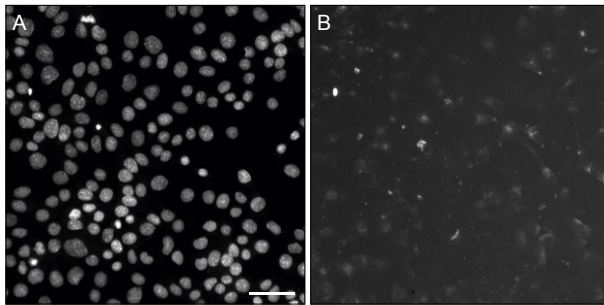


Fig. S 5. Mouse-derived α -rabbit Cy3-conjugated secondary antibody showed weak background staining on MCD4 cells. **A)** Nuclei were visualised with DAPI. **B)** Secondary antibody #211-165-109 without primary antibody. Images were acquired *via* automated immunofluorescence microscopy using an ArrayScan V^{TI} HCS Reader (40x magnification). The scale bar indicates 50 μm . Representative images are shown.

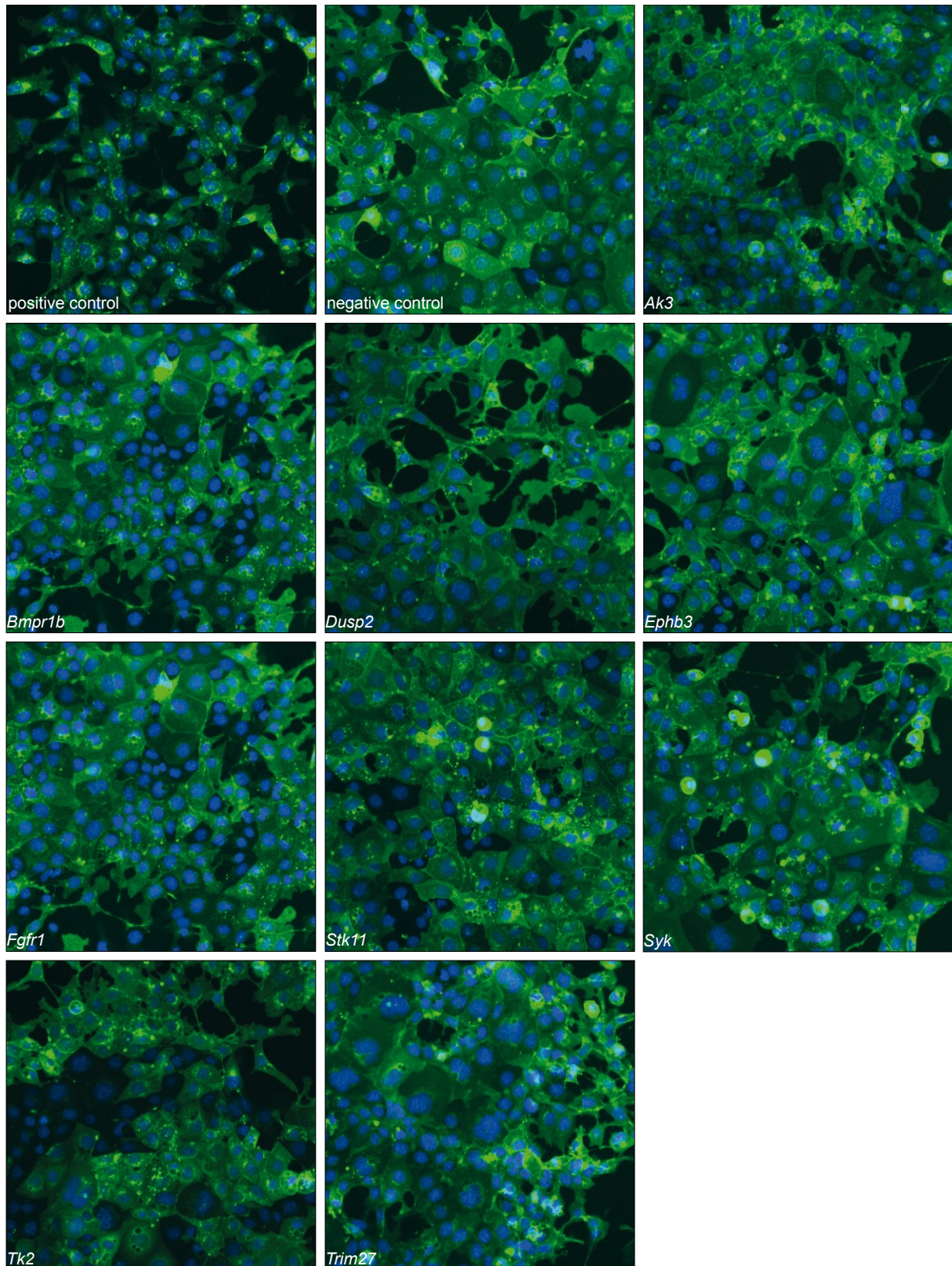


Fig. S 6. Down regulation of indicated genes impaired the AQP2 translocation to the plasma membrane in MCD4 cells. Control images show NT#2-transfected cells. Except for the positive control, all cells were stimulated with 30 μ M FSK for 60 min. For images of four additional hits refer to Fig. 26. Images were acquired via automated immunofluorescence microscopy using an ArrayScan V^{TI} HCS Reader (40x magnification). AQP2 depicted in green, nuclei shown in blue. *Ak3*, Adenylate kinase 3; *Bmpr1b*, Bone morphogenic protein receptor type 1B; *Dusp2*, dual specificity phosphatase 2; *Ephb3*, Ephrin receptor B3; *Fgfr1*, Fibroblast growth factor receptor 1; *Stk11*, Serine/threonine kinase 11; *Syk*, Spleen tyrosine kinase; *Tk2*, Thymidine kinase 2; *Trim27*, Tripartite motif-containing 27. Representative images are shown.

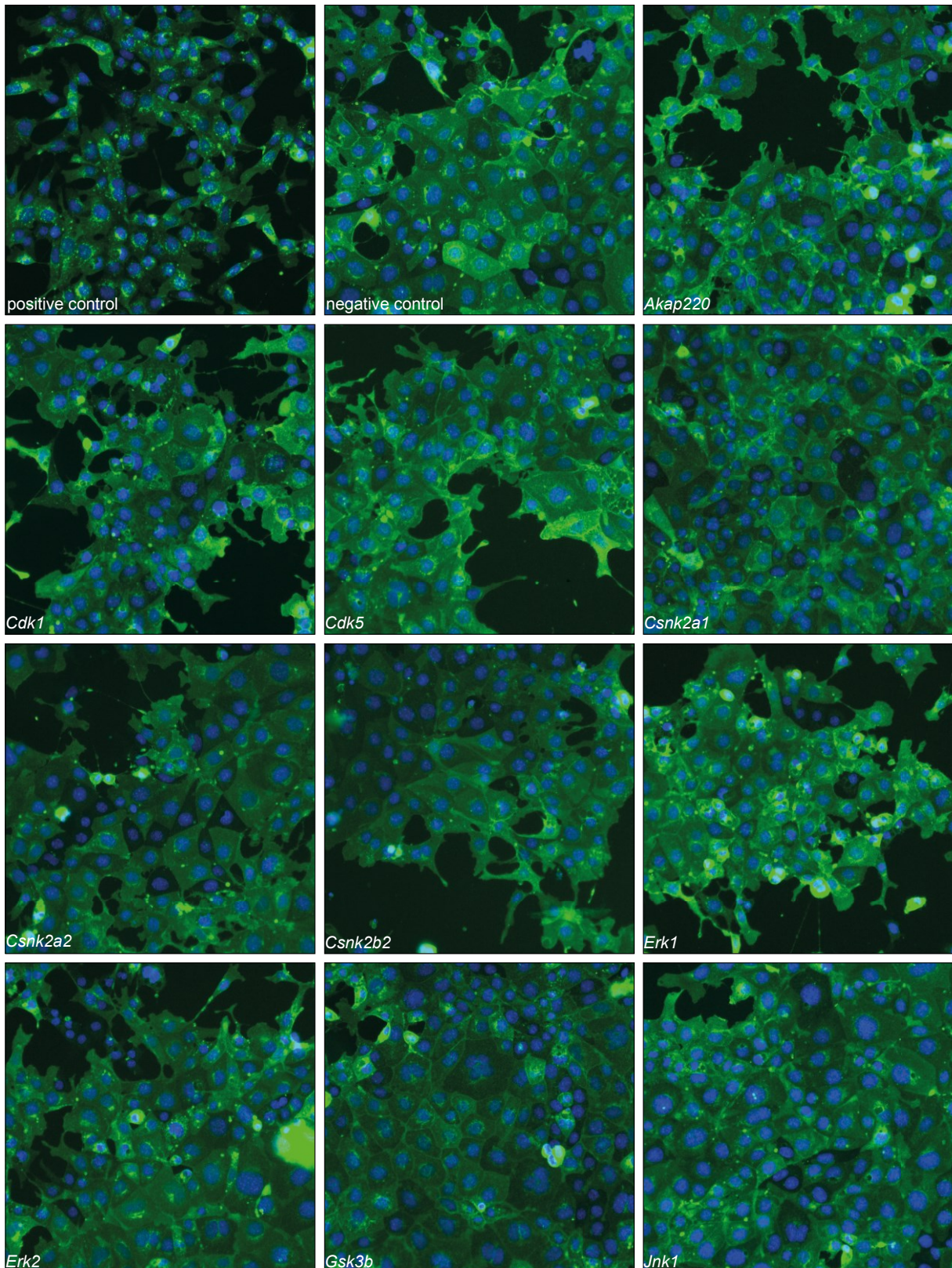


Fig. S 7. Down regulation of proteins or protein subunits that are involved in AQP2 control did not impair the AQP2 translocation to the plasma membrane. Proteins involved in AQP2 translocation are listed in Tab. 2. Control images show NT#2-transfected cells. Except for the positive control, all cells were stimulated with 30 μ M FSK for 60 min. Images were acquired via automated immunofluorescence microscopy using an ArrayScan V^{TI} HCS Reader (40x magnification). AQP2 depicted in green, nuclei shown in blue. AKAP220, A kinase (PKA) anchor protein 220; Cdk1/5, Cyclin-dependent kinase 1/5; Csnk2a1/2, Casein kinase 2 alpha 1 polypeptide/alpha prime polypeptide; Csnk2b2, Casein kinase 2 beta polypeptide; Erk1/2, extracellular signal-related kinase 1/2, MAPK3/1; Gsk3b, Glycogen synthase kinase 3 beta; Jnk1, c-Jun N-terminal kinase 1, MAPK8. Representative images are shown.

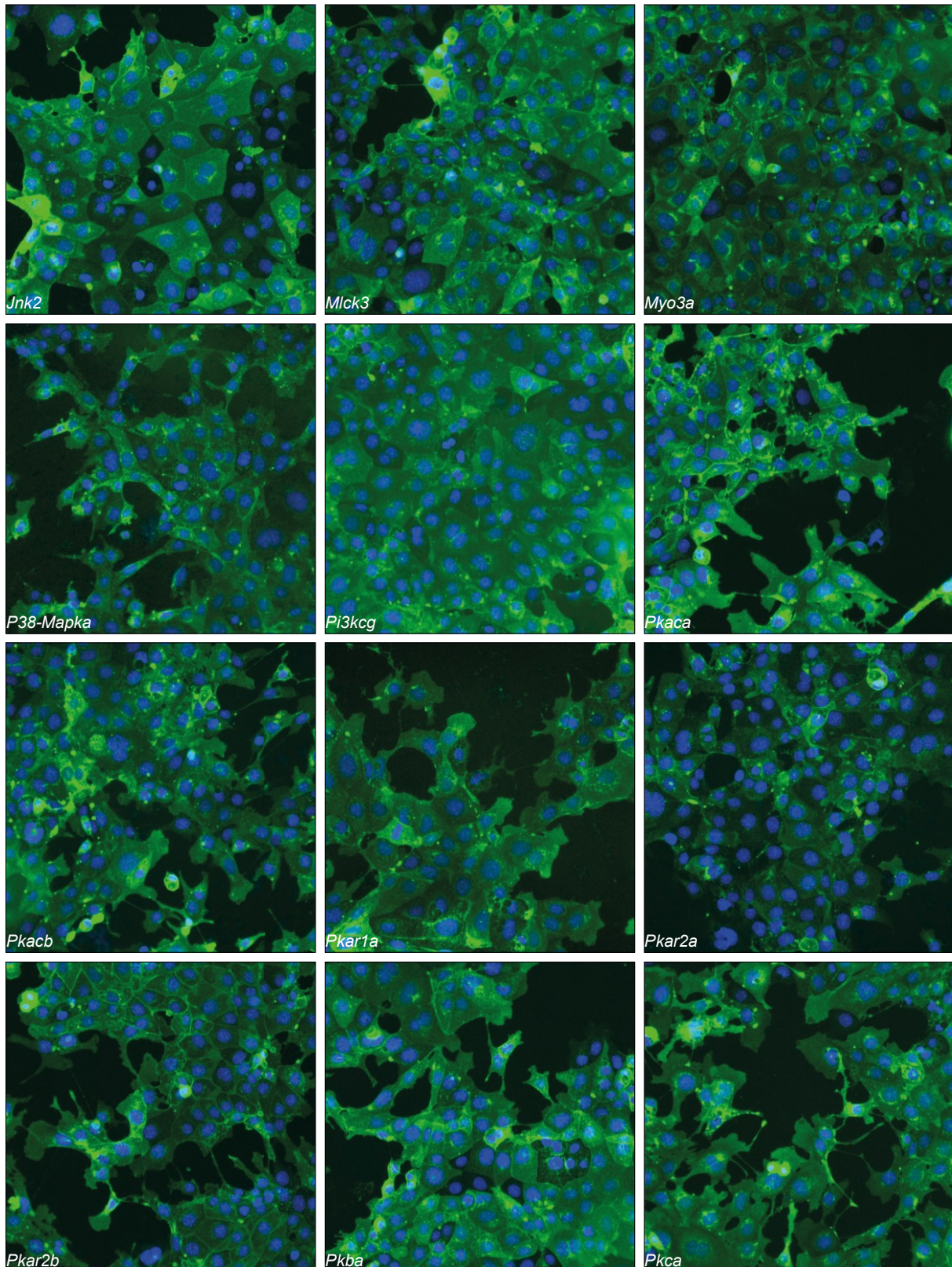


Fig. S7 continued. Jnk2, c-Jun N-terminal kinase 2, MAPK9; Mlck3, myosin light chain kinase 3; Myo3a, Myosin IIIA; P38-MAKPA, Mitogen-activated protein kinase p38 alpha; Pi3kcg, Phosphoinositide 3-kinase catalytic gamma polypeptide; Pkaca/b, Protein kinase cAMP dependent catalytic alpha/beta; Pkar1a, Protein kinase cAMP dependent regulatory type I alpha; Pkar2a/b, Protein kinase cAMP dependent regulatory type II alpha/beta; Pkba, Protein kinase B alpha, Akt1; Pkca, Protein kinase C alpha. Representative images are shown.

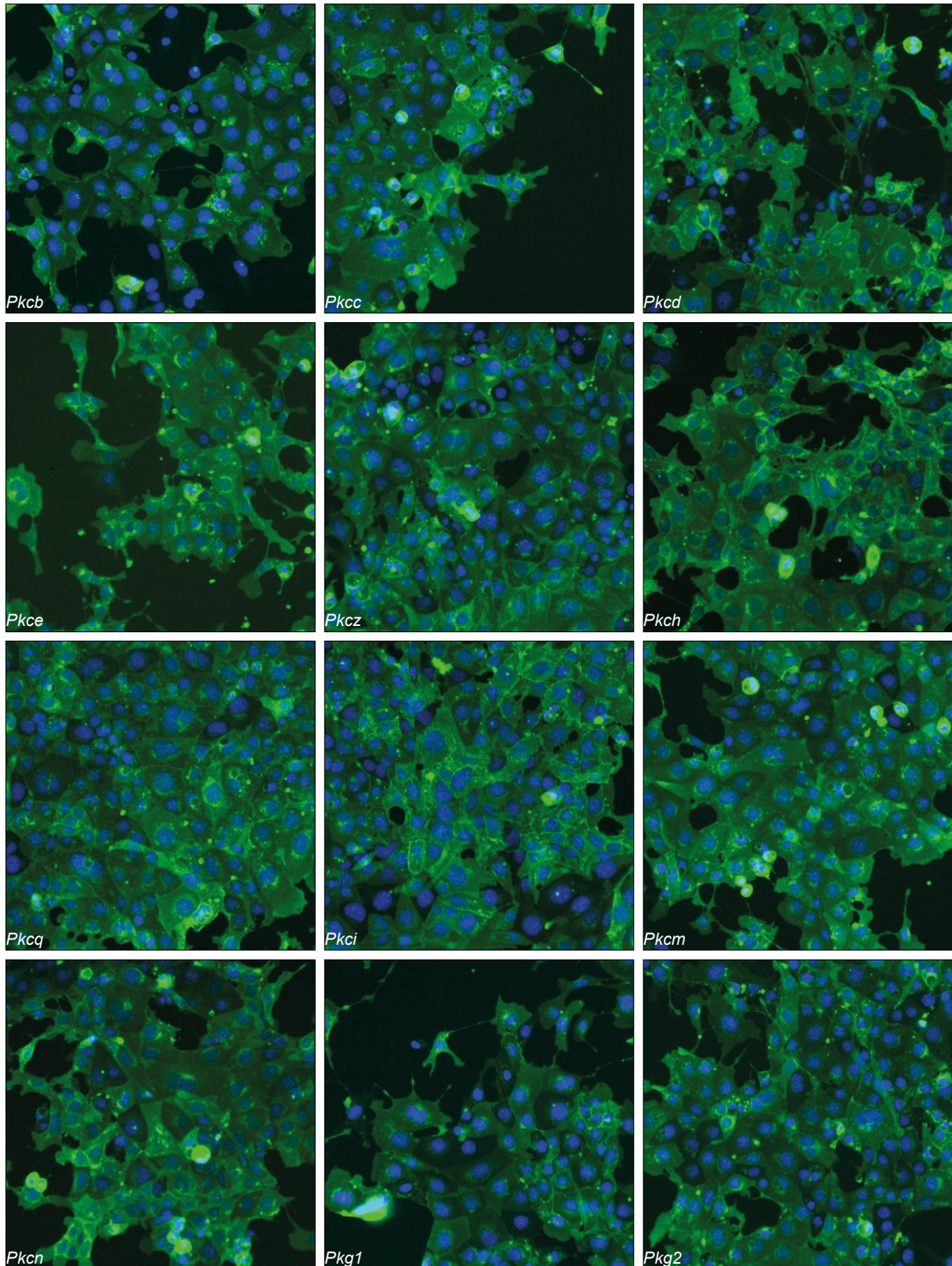


Fig. S7 continued. Pkcb/c/d/e/z/h/q/i/m/n/, Protein kinase C beta/gamma/delta/epsilon/zeta/eta/theta/ iota/mu/nu. Pkg1/2, Protein kinase cGMP-dependent type 1/2. Representative images are shown.

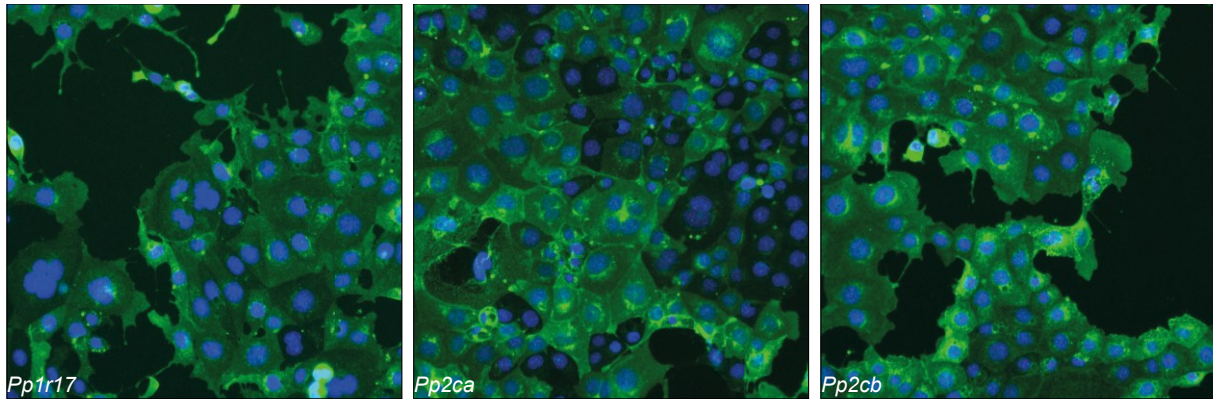


Fig. S7 continued. Pp1r17, Protein phosphatase 1 regulatory subunit 17; Pp2ca/b, Protein phosphatase 2 (formerly 2A) catalytic subunit alpha isoform/beta isoform. Representative images are shown.

MNKMKNFKRR	L SLSVPRPET	IEESLAEFTE	QFNQLHTQTN	EDGTDEPEQL	SPGMQYQQRQ	60
-----	-S-----	-----	-----	-----	-----	PKA
-----	-S-----	-----	-----	-----	-----	PKG
-----	-S-----	-----	-----	-----	-----	ATM
NQRRFSMEDL	NKRLSLPMDI	RLPQEFLOKL	QLENPGLPKP	LTRMSRRASL	SDIGFGKLET	120
-----	-S-----	-----	-----	-----S-----	-----	PKA
-----	-----	-----	-----	-----S-----	-----	PKC
-----	-----	-----	-----	-----S-----	-----	PKA
-----	-----	-----	-----	-----S-----	-----	PKC
-----	-----	-----	-----	-----S-----	-----	CaM-II
-----	-----	-----	-----	-----S-----	-----	PKG
-----	-----	-----	-----	-----S-----	-----	PKB
-----	-----	-----	-----	-----S-----	-----T-----	PKC
Y VKLDKLGEG	T YATVFKGRS	KLTENLVALK	EIRLEHEEGA	PCTAIREV S L	LKDCLKHANIV	180
Y-----	-Y-----	-----	-----	-----S-----	-----	INSR
-----	-Y-----	-----	-----	-----S-----	-----	EGFR
-----	-Y-----	-----	-----	-----S-----	-----	PKG
TLHDLIHTDR	S TLVFEYLD	SDLKQYLDHC	GNLMMHNHVK	IFMFQLLRGL	AYCHHRKILH	240
-----	--T-----	-----	-----	-----	-----	PKC
RDLKPQNLLI	NERGELKLAD	FGLARAK S VP	TKTYSNEVVT	LWYRPPDVLL	GSTE Y STPID	300
-----	-----	-----S-----	-----	-----	-----Y-----	PKG
-----	-----	-----S-----	-----	-----	-----Y-----	INSR
-----	-----	-----S-----	-----	-----	-----Y-----	Abl
MWGVGCILYE	MATGKPLFPG	S TVKEELHLI	FRLLG T PTEE	SWPGVTSISE	FRAYNFPRYL	360
-----	-----	-T-----	-----	-----	-----	PKC
-----	-----	-----	-----T-----	-----	-----	MAPK
-----	-----	-----	-----T-----	-----	-----	MAPK
PQPLLSHAPR	LDTEGINLLS	SLL L YESKSR	M SAAEALNHP	YFQSLGDRVH	QLHDTASIF S	420
-----	-----	-----Y-----	-----	-----	-----	INSR
-----	-----	-----Y-----	-----S-----	-----	-----	PKG
-----	-----	-----Y-----	-----S-----	-----	-----S-----	CKI
LKEIQLQKDP	G YRGLAFQHP	GRGKSRRQSI	F 451	-----	-----	
-----	-Y-----	-----	- INSR	-----	-----	

Fig. S 8. The predicted phosphorylation sites of mouse CDK18. Phosphosites were predicted using KinasePhos database (kinasephos.mbc.nctu.edu.tw/). ABL, Tyrosine-protein kinase ABL1/Abelson tyrosine-protein kinase 1; ATM, Serine-protein kinase ATM/Ataxia telangiectasia mutated homolog; CaM-II, Calmodulin-dependent protein kinase II; CKI, Casein kinase I isoform delta; EGFR, Epidermal growth factor receptor; INSR, Insulin receptor; MAPK, Mitogen-activated protein kinase; PKA, Protein kinase A; PKB, Protein kinase B/Akt1 kinase; PKC, Protein kinase C; PKG, Protein kinase G.

10.2 Supplementary tables

Tab. S 1. MCD4 cell viability upon the down regulation of listed genes.

Plate	Well	Viability (%)	Gene name	Accession	Cat number	Pool number
1	A03	85	<i>Cytidine monophosphate (UMP-CMP) kinase 1</i>	NM_025647	D-063389-01	M-063389-00
1	A04	60	<i>Integrin-linked kinase-associated serine/threonine phosphatase 2C</i>	NM_023343	D-048470-01	M-048470-00
1	A05	78	<i>PDZ and LIM domain 5</i>	NM_019808	D-047511-01	M-047511-00
1	A06	71	<i>Adenylate kinase 8</i>	XM_130050	D-045649-01	M-045649-00
1	A07	82	<i>NUAK family SNF1-like kinase 2</i>	NM_028778	D-051199-01	M-051199-00
1	A08	86	<i>SCY1-like 3 (S. Cerevisiae)</i>	NM_028776	D-058290-01	M-058290-00
1	A09	87	<i>Phosphoribosyl pyrophosphate synthetase 1-like 1</i>	NM_029294	D-056856-01	M-056856-00
1	A10	103	<i>Serine/threonine kinase 35</i>	NM_183262	D-042007-01	M-042007-00
1	A11	43	<i>Serine/threonine kinase 36 (fused homolog Drosophila)</i>	NM_175031	D-056017-01	M-056017-00
1	A12	68	<i>Phosphoenolpyruvate carboxykinase 2 (mitochondrial)</i>	NM_028994	D-062380-01	M-062380-00
1	A13	69	<i>Cyclin-dependent kinase 5 regulatory subunit 2 (p39)</i>	NM_009872	D-049225-01	M-049225-00
1	A14	80	<i>CDK5 regulatory subunit associated protein 1</i>	NM_025876	D-056922-01	M-056922-00
1	A15	99	<i>CDK5 regulatory subunit associated protein 3</i>	NM_030248	D-046463-01	M-046463-00
1	A16	88	<i>Cyclin-dependent kinase 6</i>	NM_009873	D-043101-01	M-043101-00
1	A17	93	<i>Cyclin-dependent kinase 7</i>	NM_009874	D-040601-01	M-040601-00
1	A18	90	<i>Cyclin-dependent kinase 8</i>	NM_153599	D-053848-01	M-053848-00
1	A19	86	<i>Cyclin-dependent kinase 9 (CDC2-related kinase)</i>	NM_130860	D-040602-01	M-040602-00
1	A20	95	<i>Cyclin-dependent kinase-like 1 (CDC2-related kinase)</i>	NM_183294	D-042035-01	M-042035-00
1	A21	82	<i>Cyclin-dependent kinase-like 2 (CDC2-related kinase)</i>	NM_016912	D-040603-01	M-040603-00
1	A22	55	<i>Cyclin-dependent kinase-like 3</i>	NM_153785	D-054266-01	M-054266-00
1	B03	80	<i>Dual-specificity tyrosine-(Y)-phosphorylation regulated kinase 2</i>	NM_001014390	D-065611-01	M-065611-00
1	B04	90	<i>Inositol 13456-pentakisphosphate 2-kinase</i>	NM_199056	D-050560-01	M-050560-00
1	B05	88	<i>WNK lysine deficient protein kinase 2</i>	XM_127323	D-045498-01	M-045498-00
1	B06	91	<i>Serine/threonine kinase 40</i>	NM_028800	D-060998-01	M-060998-00
1	B07	87	<i>Acyl-Coenzyme A dehydrogenase family member 10</i>	NM_028037	D-047158-01	M-047158-00
1	B08	78	<i>RIKEN cdna 2610018G03 gene</i>	NM_133729	D-051436-01	M-051436-00
1	B09	91	<i>STE20-related kinase adaptor alpha</i>	NM_028126	D-044725-01	M-044725-00
1	B10	102	<i>Acylglycerol kinase</i>	NM_023538	D-046451-01	M-046451-00
1	B11	89	<i>Cyclin-dependent kinase 19</i>	NM_198164	D-059630-01	M-059630-00
1	B12	90	<i>CDC42 small effector 2</i>	NM_178626	D-057779-01	M-057779-00
1	B13	92	<i>Cyclin-dependent kinase inhibitor 1A (P21)</i>	NM_007669	D-058636-01	M-058636-00
1	B14	83	<i>Cyclin-dependent kinase inhibitor 1B</i>	NM_009875	D-040178-01	M-040178-00
1	B15	99	<i>Cyclin-dependent kinase inhibitor 1C (P57)</i>	NM_009876	D-062494-01	M-062494-00
1	B16	89	<i>Cyclin-dependent kinase inhibitor 2B (p15 inhibits CDK4)</i>	NM_007670	D-060290-01	M-060290-00
1	B17	95	<i>Cyclin-dependent kinase inhibitor 2C (p18 inhibits CDK4)</i>	NM_007671	D-061423-01	M-061423-00
1	B18	71	<i>Cyclin-dependent kinase inhibitor 2D (p19 inhibits CDK4)</i>	NM_009878	D-062496-01	M-062496-00
1	B19	93	<i>Cyclin-dependent kinase inhibitor 3</i>	XM_354809	D-047568-01	M-047568-00
1	B20	84	<i>Ceramide kinase</i>	NM_145475	D-040107-01	M-040107-00
1	B21	85	<i>Checkpoint kinase 1</i>	NM_007691	D-058640-05	M-058640-01
1	B22	83	<i>Checkpoint kinase 2</i>	NM_016681	D-040604-01	M-040604-00
1	C03	70	<i>Cyclin-dependent kinase 2 interacting protein</i>	NM_026048	D-045958-01	M-045958-00
1	C04	67	<i>Adaptor protein phosphotyrosine interaction PH domain and leucine zipper containing 1</i>	NM_145221	D-053641-01	M-053641-00
1	C05	58	<i>Membrane associated guanylate kinase WW and PDZ domain containing 3</i>	NM_133853	D-051390-01	M-051390-00
1	C06	70	<i>IQ motif containing H</i>	XM_134960	D-061985-01	M-061985-00
1	C07	89	<i>RIKEN cdna 4930444A02 gene</i>	NM_029037	D-059713-01	M-059713-00

Plate	Well	Viability (%)	Gene name	Accession	Cat number	Pool number
1	C08	74	<i>Tumor protein D52-like 3</i>	NM_025741	D-049852-01	M-049852-00
1	C09	91	<i>Testis-specific serine kinase 4</i>	NM_027673	D-057012-01	M-057012-00
1	C10	90	<i>Phosphoribosyl pyrophosphate synthetase-associated protein 1</i>	XM_181343	D-064396-01	M-064396-00
1	C11	73	<i>Doublecortin-like kinase 2</i>	NM_027539	D-041657-01	M-041657-00
1	C12	68	<i>Mixed lineage kinase domain-like</i>	XM_356104	D-061420-01	M-061420-00
1	C13	64	<i>Choline kinase alpha</i>	NM_013490	D-065301-01	M-065301-00
1	C14	81	<i>Choline kinase beta</i>	NM_007692	D-065344-01	M-065344-00
1	C15	71	<i>Cholinergic receptor muscarinic 1 CNS</i>	NM_007698	D-058643-01	M-058643-00
1	C16	103	<i>Conserved helix-loop-helix ubiquitous kinase</i>	NM_007700	D-041014-01	M-041014-00
1	C17	92	<i>Citron</i>	NM_007708	D-044420-01	M-044420-00
1	C18	85	<i>Creatine kinase brain</i>	NM_021273	D-062038-01	M-062038-00
1	C19	82	<i>Creatine kinase muscle</i>	NM_007710	D-044437-01	M-044437-00
1	C20	84	<i>Creatine kinase mitochondrial 1 ubiquitous</i>	NM_009897	D-049314-01	M-049314-00
1	C21	84	<i>Creatine kinase mitochondrial 2</i>	NM_198415	D-042830-01	M-042830-00
1	C22	83	<i>CDC28 protein kinase 1b</i>	NM_016904	D-043790-01	M-043790-00
1	D03	77	<i>Ankyrin repeat and kinase domain containing 1</i>	NM_172922	D-052432-01	M-052432-00
1	D04	76	<i>PITPNM family member 3</i>	XM_354620	D-063825-01	M-063825-00
1	D05	75	<i>Eph receptor A10</i>	NM_177671	D-053504-01	M-053504-00
1	D06	85	<i>Lemur tyrosine kinase 2</i>	XM_132499	D-053835-01	M-053835-00
1	D07	82	<i>TBC1 domain containing kinase</i>	NM_173032	D-055508-01	M-055508-00
1	D08	90	<i>Uridine-cytidine kinase 2</i>	NM_030724	D-047637-01	M-047637-00
1	D09	70	<i>DBF4 homolog (S. Cerevisiae)</i>	NM_013726	D-046785-01	M-046785-00
1	D10	96	<i>Abl-interactor 1</i>	NM_007380	D-056816-01	M-056816-00
1	D11	70	<i>C-abl oncogene 1 non-receptor tyrosine kinase</i>	NM_009594	D-040285-01	M-040285-00
1	D12	75	<i>V-abl Abelson murine leukemia viral oncogene homolog 2 (arg Abelson-related gene)</i>	XM_136360	D-044204-01	M-044204-00
1	D13	76	<i>CDC28 protein kinase regulatory subunit 2</i>	NM_025415	D-045245-01	M-045245-00
1	D14	75	<i>CDC-like kinase 2</i>	NM_007712	D-040830-01	M-040830-00
1	D15	79	<i>CDC-like kinase 3</i>	NM_007713	D-040838-01	M-040838-00
1	D16	91	<i>CDC like kinase 4</i>	NM_007714	D-040839-01	M-040839-00
1	D17	77	<i>Connector enhancer of kinase suppressor of Ras 1</i>	XM_110525	D-050791-01	M-050791-00
1	D18	80	<i>Coenzyme A synthase</i>	NM_027896	D-062384-01	M-062384-00
1	D19	67	<i>Collagen type IV alpha 3 (Goodpasture antigen) binding protein</i>	NM_023420	D-054738-01	M-054738-00
1	D20	25	<i>Coatomer protein complex subunit beta 2 (beta prime)</i>	NM_015827	D-045228-01	M-045228-00
1	D21	84	<i>Cyclin-dependent kinase 12</i>	NM_026952	D-064510-01	M-064510-00
1	D22	80	<i>V-crk sarcoma virus CT10 oncogene homolog (avian)-like</i>	NM_007764	D-058646-01	M-058646-00
1	E03	80	<i>Activin A receptor type 1</i>	NM_007394	D-042047-01	M-042047-00
1	E04	83	<i>Activin A receptor type 1B</i>	NM_007395	D-043507-01	M-043507-00
1	E05	69	<i>Activin receptor IIA</i>	NM_007396	D-040676-01	M-040676-00
1	E06	64	<i>Activin receptor IIB</i>	NM_007397	D-040629-01	M-040629-00
1	E07	72	<i>Activin A receptor type II-like 1</i>	NM_009612	D-043004-01	M-043004-00
1	E08	81	<i>A disintegrin and metallopeptidase domain 9 (meltrin gamma)</i>	NM_007404	D-041144-01	M-041144-00
1	E09	78	<i>Aarf domain containing kinase 2</i>	NM_178873	D-057241-01	M-057241-00
1	E10	79	<i>Aarf domain containing kinase 4</i>	NM_133770	D-057610-01	M-057610-00
1	E11	84	<i>Aarf domain containing kinase 5</i>	NM_172960	D-055456-01	M-055456-00
1	E12	82	<i>Adenosine kinase</i>	NM_134079	D-062728-01	M-062728-00
1	E13	74	<i>Colony stimulating factor 1 receptor</i>	NM_007779	D-044650-01	M-044650-00
1	E14	80	<i>C-src tyrosine kinase</i>	NM_007783	D-060300-01	M-060300-00
1	E15	60	<i>Casein kinase 1 alpha 1</i>	NM_146087	D-062865-01	M-062865-00
1	E16	69	<i>Casein kinase 1 delta</i>	NM_027874	D-044377-01	M-044377-00
1	E17	83	<i>Casein kinase 1 epsilon</i>	NM_013767	D-040108-01	M-040108-00
1	E18	72	<i>Casein kinase 1 gamma 1</i>	NM_173185	D-055555-01	M-055555-00
1	E19	77	<i>Casein kinase 1 gamma 2</i>	NM_134002	D-040465-01	M-040465-00
1	E20	108	<i>Casein kinase 1 gamma 3</i>	NM_152809	D-064761-01	M-064761-00
1	E21	88	<i>Casein kinase 2 alpha 1 polypeptide</i>	NM_007788	D-058653-01	M-058653-00
1	E22	69	<i>Casein kinase 2 alpha prime polypeptide</i>	NM_009974	D-051582-01	M-051582-00

Plate	Well	Viability (%)	Gene name	Accession	Cat number	Pool number
1	F03	78	<i>Adrenergic receptor alpha 1a</i>	NM_013461	D-059194-01	M-059194-00
1	F04	98	<i>Adrenergic receptor alpha 1b</i>	NM_007416	D-043437-01	M-043437-00
1	F05	87	<i>Adrenergic receptor beta 2</i>	NM_007420	D-042042-01	M-042042-00
1	F06	75	<i>Adrenergic receptor kinase beta 1</i>	NM_130863	D-040967-01	M-040967-00
1	F07	81	<i>Adrenergic receptor kinase beta 2</i>	NM_177078	D-051179-01	M-051179-00
1	F08	73	<i>Angiotensin 4</i>	NM_009641	D-043390-01	M-043390-00
1	F09	85	<i>Angiotensin II receptor type 2</i>	NM_007429	D-061951-01	M-061951-00
1	F10	57	<i>Xylulokinase homolog (H. Influenzae)</i>	NM_001033209	D-062361-01	M-062361-00
1	F11	75	<i>Protein kinase D2</i>	NM_178900	D-040693-01	M-040693-00
1	F12	75	<i>Serine/threonine/tyrosine kinase 1</i>	NM_172891	D-055398-01	M-055398-00
1	F13	60	<i>Casein kinase 2 beta polypeptide</i>	NM_009975	D-049417-01	M-049417-00
1	F14	83	<i>Chemokine (C-X-C motif) ligand 10</i>	NM_021274	D-042605-01	M-042605-00
1	F15	78	<i>SCY1-like 2 (S. Cerevisiae)</i>	NM_198021	D-063381-01	M-063381-00
1	F16	67	<i>Pyruvate dehydrogenase kinase isoenzyme 1</i>	NM_172665	D-054066-01	M-054066-00
1	F17	67	<i>Inositol hexaphosphate kinase 3</i>	NM_173027	D-052483-01	M-052483-00
1	F18	65	<i>Myosin light chain kinase 3</i>	NM_175441	D-052765-01	M-052765-00
1	F19	66	<i>DNA segment Chr 8 ERATO Doi 82 expressed</i>	NM_172911	D-055423-01	M-055423-00
1	F20	81	<i>Death associated protein kinase 1</i>	NM_029653	D-040260-01	M-040260-00
1	F21	81	<i>Death-associated protein kinase 2</i>	NM_010019	D-042162-01	M-042162-00
1	F22	82	<i>Death-associated protein kinase 3</i>	NM_007828	D-044800-01	M-044800-00
1	G03	90	<i>Mitogen-activated protein kinase-activated protein kinase 3</i>	NM_178907	D-058176-01	M-058176-00
1	G04	90	<i>Adenylate kinase 1</i>	NM_021515	D-040896-01	M-040896-00
1	G05	84	<i>Adenylate kinase 2</i>	NM_016895	D-040897-01	M-040897-00
1	G06	69	<i>Adenylate kinase 3</i>	NM_021299	D-040898-01	M-040898-00
1	G07	80	<i>Adenylate kinase 4</i>	NM_009647	D-065422-01	M-065422-00
1	G08	83	<i>A kinase (PRKA) anchor protein 1</i>	NM_009648	D-042815-01	M-042815-00
1	G09	102	<i>A kinase (PRKA) anchor protein 11</i>	XM_127854	D-048015-01	M-048015-00
1	G10	58	<i>A kinase (PRKA) anchor protein 13</i>	XM_133543	D-059232-01	M-059232-00
1	G11	76	<i>A kinase (PRKA) anchor protein 3</i>	NM_009650	D-043482-01	M-043482-00
1	G12	86	<i>A kinase (PRKA) anchor protein 4</i>	NM_009651	D-043498-01	M-043498-00
1	G13	72	<i>Doublecortin-like kinase 1</i>	NM_019978	D-062033-01	M-062033-00
1	G14	81	<i>Deoxycytidine kinase</i>	NM_007832	D-055649-01	M-055649-00
1	G15	78	<i>Discoidin domain receptor family member 1</i>	NM_007584	D-040109-01	M-040109-00
1	G16	63	<i>Discoidin domain receptor family member 2</i>	NM_022563	D-047913-01	M-047913-00
1	G17	102	<i>Diacylglycerol kinase alpha</i>	NM_016811	D-041106-01	M-041106-00
1	G18	106	<i>Diacylglycerol kinase beta</i>	NM_178681	D-059281-01	M-059281-00
1	G19	77	<i>Diacylglycerol kinase epsilon</i>	NM_019505	D-049658-01	M-049658-00
1	G20	93	<i>Diacylglycerol kinase gamma</i>	NM_138650	D-042616-01	M-042616-00
1	G21	76	<i>Diacylglycerol kinase theta</i>	NM_199011	D-042776-01	M-042776-00
1	G22	86	<i>Diacylglycerol kinase zeta</i>	NM_138306	D-040327-01	M-040327-00
1	H03	97	<i>A kinase (PRKA) anchor protein 8</i>	NM_019774	D-060714-01	M-060714-00
1	H04	76	<i>Thymoma viral proto-oncogene 1</i>	NM_009652	D-040709-01	M-040709-00
1	H05	72	<i>Thymoma viral proto-oncogene 2</i>	NM_007434	D-040782-01	M-040782-00
1	H06	85	<i>Thymoma viral proto-oncogene 3</i>	NM_011785	D-040891-01	M-040891-00
1	H07	88	<i>Anaplastic lymphoma kinase</i>	NM_007439	D-040104-01	M-040104-00
1	H08	93	<i>STE20-related kinase adaptor beta</i>	NM_172656	D-042808-01	M-042808-00
1	H09	88	<i>Anti-Mullerian hormone type 2 receptor</i>	NM_144547	D-053605-01	M-053605-00
1	H10	74	<i>Receptor-interacting serine-threonine kinase 4</i>	NM_023663	D-048568-01	M-048568-00
1	H11	59	<i>V-raf murine sarcoma 3611 viral oncogene homolog</i>	NM_009703	D-042948-01	M-042948-00
1	H12	86	<i>ADP-ribosylation factor-like 6 interacting protein 1</i>	XM_133792	D-063637-01	M-063637-00
1	H13	86	<i>Deoxyguanosine kinase</i>	NM_013764	D-042284-01	M-042284-00
1	H14	91	<i>Discs large homolog 1 (Drosophila)</i>	NM_007862	D-042037-01	M-042037-00
1	H15	96	<i>Discs large homolog 2 (Drosophila)</i>	NM_011807	D-043520-01	M-043520-00
1	H16	90	<i>Discs large homolog 3 (Drosophila)</i>	NM_016747	D-062296-01	M-062296-00
1	H17	97	<i>Discs large homolog 4 (Drosophila)</i>	NM_007864	D-040099-01	M-040099-00
1	H18	81	<i>Dystrophia myotonica-protein kinase</i>	NM_032418	D-050244-01	M-050244-00
1	H19	98	<i>Dnaj (Hsp40) homolog subfamily C member 3</i>	NM_008929	D-058434-01	M-058434-00

Plate	Well	Viability (%)	Gene name	Accession	Cat number	Pool number
1	H20	67	<i>Docking protein 1</i>	NM_010070	D-062538-01	M-062538-00
1	H21	70	<i>Deoxythymidylate kinase</i>	NM_023136	D-045682-01	M-045682-00
1	H22	67	<i>Dual specificity phosphatase 1</i>	NM_013642	D-040753-01	M-040753-00
1	I03	63	<i>Ataxia telangiectasia mutated homolog (human)</i>	NM_007499	D-042892-01	M-042892-00
1	I04	33	<i>Aurora kinase B</i>	NM_011496	D-063793-01	M-063793-00
1	I05	65	<i>Aurora kinase C</i>	NM_020572	D-050161-01	M-050161-00
1	I06	66	<i>RIKEN cDNA B230120H23 gene</i>	NM_023057	D-045169-01	M-045169-00
1	I07	65	<i>Ropporin 1-like</i>	NM_145852	D-052427-01	M-052427-00
1	I08	94	<i>Arginine vasopressin receptor 1A</i>	NM_016847	D-044411-01	M-044411-00
1	I09	61	<i>Arginine vasopressin receptor 1B</i>	NM_011924	D-043452-01	M-043452-00
1	I10	71	<i>Protein kinase membrane associated tyrosine/threonine 1</i>	NM_023058	D-045252-01	M-045252-00
1	I11	77	<i>Alpha-kinase 3</i>	NM_054085	D-047437-01	M-047437-00
1	I12	57	<i>Threonine synthase-like 1 (bacterial)</i>	NM_001001297	D-057298-01	M-057298-00
1	I13	74	<i>Dual specificity phosphatase 10</i>	NM_022019	D-060807-01	M-060807-00
1	I14	65	<i>Dual specificity phosphatase 2</i>	NM_010090	D-040331-01	M-040331-00
1	I15	77	<i>Dual specificity phosphatase 4</i>	NM_176933	D-061306-01	M-061306-00
1	I16	66	<i>Dual specificity phosphatase 6</i>	NM_026268	D-040050-01	M-040050-00
1	I17	64	<i>Dual specificity phosphatase 7</i>	NM_153459	D-040051-01	M-040051-00
1	I18	74	<i>Dual specificity phosphatase 8</i>	NM_008748	D-048028-01	M-048028-00
1	I19	95	<i>Dual-specificity tyrosine-(Y)-phosphorylation regulated kinase 1a</i>	NM_007890	D-040110-01	M-040110-00
1	I20	74	<i>Dual-specificity tyrosine-(Y)-phosphorylation regulated kinase 1b</i>	NM_010092	D-041083-01	M-041083-00
1	I21	81	<i>Dual-specificity tyrosine-(Y)-phosphorylation regulated kinase 3</i>	NM_145508	D-053268-01	M-053268-00
1	I22	91	<i>Dual-specificity tyrosine-(Y)-phosphorylation regulated kinase 4</i>	NM_207210	D-057308-01	M-057308-00
1	J03	72	<i>Protein serine kinase H1</i>	NM_173432	D-058302-01	M-058302-00
1	J04	77	<i>Protein kinase domain containing cytoplasmic</i>	NM_134117	D-055034-01	M-055034-00
1	J05	99	<i>AXL receptor tyrosine kinase</i>	NM_009465	D-040941-01	M-040941-00
1	J06	50	<i>Ecotropic viral integration site 5 like</i>	NM_153536	D-054740-01	M-054740-00
1	J07	80	<i>NUAK family SNF1-like kinase 1</i>	XM_196007	D-063024-01	M-063024-00
1	J08	80	<i>TAF1 RNA polymerase II TATA box binding protein (TBP)-associated factor</i>	XM_194622	D-058598-01	M-058598-00
1	J09	74	<i>NIMA (never in mitosis gene a)-related expressed kinase 5</i>	NM_177898	D-061319-01	M-061319-00
1	J10	71	<i>NAD kinase</i>	NM_138671	D-053672-01	M-053672-00
1	J11	65	<i>Nuclear receptor binding protein 2</i>	NM_144847	D-051705-01	M-051705-00
1	J12	64	<i>Cam kinase-like vesicle-associated</i>	NM_145621	D-052770-01	M-052770-00
1	J13	85	<i>RIKEN cDNA E130304F04 gene</i>	NM_175538	D-056574-01	M-056574-00
1	J14	63	<i>Endothelin 2</i>	NM_007902	D-056620-01	M-056620-00
1	J15	73	<i>Eukaryotic elongation factor-2 kinase</i>	NM_007908	D-060315-01	M-060315-00
1	J16	71	<i>Epidermal growth factor receptor</i>	NM_007912	D-040411-01	M-040411-00
1	J17	79	<i>Eukaryotic translation initiation factor 2 alpha kinase 1</i>	NM_013557	D-045523-01	M-045523-00
1	J18	64	<i>Eukaryotic translation initiation factor 2 alpha kinase 3</i>	NM_010121	D-044901-01	M-044901-00
1	J19	79	<i>Eph receptor A1</i>	NM_023580	D-063644-01	M-063644-00
1	J20	83	<i>Eph receptor A2</i>	NM_010139	D-040412-01	M-040412-00
1	J21	98	<i>Eph receptor A3</i>	NM_010140	D-043335-01	M-043335-00
1	J22	78	<i>Eph receptor A4</i>	NM_007936	D-055030-01	M-055030-00
1	K03	66	<i>Regulation of nuclear pre-mRNA domain containing 1A</i>	NM_144861	D-051920-01	M-051920-00
1	K04	69	<i>Cdna sequence BC021891</i>	NM_145608	D-052680-01	M-052680-00
1	K05	63	<i>Dihydroxyacetone kinase 2 homolog (yeast)</i>	NM_145496	D-051984-01	M-051984-00
1	K06	56	<i>PDLIM1 interacting kinase 1 like</i>	NM_146156	D-054631-01	M-054631-00
1	K07	73	<i>Fructosamine 3 kinase related protein</i>	NM_181420	D-053981-01	M-053981-00
1	K08	76	<i>CDC42 binding protein kinase gamma (DMPK-like)</i>	XM_140553	D-056686-01	M-056686-00
1	K09	70	<i>Obscurin cytoskeletal calmodulin and titin-interacting rhogef</i>	NM_001003914	D-063726-01	M-063726-00
1	K10	63	<i>Doublecortin-like kinase 3</i>	NM_172928	D-052448-01	M-052448-00

Plate	Well	Viability (%)	Gene name	Accession	Cat number	Pool number
1	K11	76	<i>Branched chain ketoacid dehydrogenase kinase</i>	NM_009739	D-061516-01	M-061516-00
1	K12	71	<i>Breakpoint cluster region</i>	XM_125706	D-040584-01	M-040584-00
1	K13	93	<i>Eph receptor A7</i>	NM_010141	D-040413-01	M-040413-00
1	K14	68	<i>Eph receptor A8</i>	NM_007939	D-045134-01	M-045134-00
1	K15	79	<i>Eph receptor B1</i>	NM_173447	D-057003-01	M-057003-00
1	K16	77	<i>Eph receptor B2</i>	NM_010142	D-050820-01	M-050820-00
1	K17	78	<i>Eph receptor B3</i>	NM_010143	D-043340-01	M-043340-00
1	K18	81	<i>Eph receptor B4</i>	NM_010144	D-060469-01	M-060469-00
1	K19	108	<i>Eph receptor B6</i>	NM_007680	D-040414-01	M-040414-00
1	K20	75	<i>V-erb-b2 erythroblastic leukemia viral oncogene homolog 2 neuro/glioblastoma derived oncogene homolog (avian)</i>	XM_109715	D-064147-01	M-064147-00
1	K21	71	<i>V-erb-b2 erythroblastic leukemia viral oncogene homolog 3 (avian)</i>	XM_125954	D-040415-01	M-040415-00
1	K22	87	<i>V-erb-a erythroblastic leukemia viral oncogene homolog 4 (avian)</i>	XM_136682	D-043436-01	M-043436-00
1	L03	84	<i>Bradykinin receptor beta 2</i>	NM_009747	D-060441-01	M-060441-00
1	L04	83	<i>B lymphoid kinase</i>	NM_007549	D-061983-01	M-061983-00
1	L05	61	<i>B cell linker</i>	NM_008528	D-040345-01	M-040345-00
1	L06	73	<i>BMP2 inducible kinase</i>	NM_080708	D-040720-01	M-040720-00
1	L07	86	<i>Bone morphogenetic protein receptor type 1A</i>	NM_009758	D-040598-01	M-040598-00
1	L08	75	<i>Bone morphogenetic protein receptor type 1B</i>	NM_007560	D-051071-01	M-051071-00
1	L09	68	<i>Bone morphogenetic protein receptor type II (serine/threonine kinase)</i>	NM_007561	D-040599-01	M-040599-00
1	L10	90	<i>BMX non-receptor tyrosine kinase</i>	NM_009759	D-062471-01	M-062471-00
1	L11	94	<i>Braf transforming gene</i>	XM_355754	D-040325-01	M-040325-00
1	L12	87	<i>Bromodomain containing 2</i>	NM_010238	D-043404-01	M-043404-00
1	L13	81	<i>Endoplasmic reticulum (ER) to nucleus signalling 1</i>	NM_023913	D-041030-01	M-041030-00
1	L14	78	<i>Ethanolamine kinase 1</i>	XM_284250	D-057481-01	M-057481-00
1	L15	84	<i>Ethanolamine kinase 2</i>	NM_175443	D-063930-01	M-063930-00
1	L16	83	<i>MDS1 and EVI1 complex locus</i>	NM_007963	D-045212-01	M-045212-00
1	L17	74	<i>Exosome component 10</i>	NM_016699	D-049286-01	M-049286-00
1	L18	62	<i>Fas-activated serine/threonine kinase</i>	NM_023229	D-048817-01	M-048817-00
1	L19	81	<i>Feline sarcoma oncogene</i>	NM_010194	D-043381-01	M-043381-00
1	L20	79	<i>Fibroblast growth factor receptor 1</i>	NM_010206	D-040832-01	M-040832-00
1	L21	78	<i>Fibroblast growth factor receptor 2</i>	NM_201601	D-040288-01	M-040288-00
1	L22	76	<i>Fibroblast growth factor receptor 3</i>	NM_008010	D-065558-01	M-065558-00
1	M03	76	<i>Bromodomain testis-specific</i>	NM_054054	D-045525-01	M-045525-00
1	M04	80	<i>Bruton agammaglobulinemia tyrosine kinase</i>	NM_013482	D-040985-01	M-040985-00
1	M05	66	<i>Budding uninhibited by benzimidazoles 1 homolog (S. Cerevisiae)</i>	NM_009772	D-042998-01	M-042998-00
1	M06	84	<i>Budding uninhibited by benzimidazoles 1 homolog beta (S. Cerevisiae)</i>	NM_009773	D-044095-01	M-044095-00
1	M07	63	<i>T cell receptor associated transmembrane adaptor 1</i>	NM_198297	D-041911-01	M-041911-00
1	M08	76	<i>Diacylglycerol kinase iota</i>	XM_284192	D-055942-01	M-055942-00
1	M09	88	<i>Protein kinase AMP-activated alpha 1 catalytic subunit</i>	XM_139298	D-041035-01	M-041035-00
1	M10	59	<i>RIKEN cDNA C230081A13 gene</i>	NM_172924	D-055433-01	M-055433-00
1	M11	68	<i>6-phosphofructo-2-kinase/fructose-26-biphosphatase 4</i>	NM_173019	D-054640-01	M-054640-00
1	M12	59	<i>Phosphoinositide-3-kinase class 2 beta polypeptide</i>	XM_136225	D-044033-01	M-044033-00
1	M13	85	<i>Fibroblast growth factor receptor 4</i>	NM_008011	D-045345-01	M-045345-00
1	M14	82	<i>Gardner-Rasheed feline sarcoma viral (Fgr) oncogene homolog</i>	NM_010208	D-041086-01	M-041086-00
1	M15	72	<i>FMS-like tyrosine kinase 1</i>	NM_010228	D-040636-01	M-040636-00
1	M16	84	<i>FMS-like tyrosine kinase 3</i>	NM_010229	D-040111-01	M-040111-00
1	M17	70	<i>FMS-like tyrosine kinase 4</i>	NM_008029	D-045433-01	M-045433-00
1	M18	79	<i>Fructosamine 3 kinase</i>	NM_022014	D-050096-01	M-050096-00
1	M19	77	<i>Mechanistic target of rapamycin (serine/threonine kinase)</i>	NM_020009	D-065427-01	M-065427-00
1	M20	92	<i>Fyn-related kinase</i>	NM_010237	D-059001-01	M-059001-00

Plate	Well	Viability (%)	Gene name	Accession	Cat number	Pool number
1	M21	87	<i>Fucokinase</i>	NM_172283	D-064057-01	M-064057-00
1	M22	87	<i>FYN binding protein</i>	NM_011815	D-043701-01	M-043701-00
1	N03	69	<i>Calmodulin 3</i>	NM_007590	D-065395-01	M-065395-00
1	N04	87	<i>Calcium/calmodulin-dependent protein kinase I</i>	NM_133926	D-040624-01	M-040624-00
1	N05	79	<i>Calcium/calmodulin-dependent protein kinase ID</i>	NM_177343	D-063690-01	M-063690-00
1	N06	77	<i>Calcium/calmodulin-dependent protein kinase I gamma</i>	NM_144817	D-053402-01	M-053402-00
1	N07	82	<i>Calcium/calmodulin-dependent protein kinase II alpha</i>	NM_009792	D-059173-01	M-059173-00
1	N08	87	<i>Calcium/calmodulin-dependent protein kinase II beta</i>	NM_007595	D-062002-01	M-062002-00
1	N09	83	<i>Calcium/calmodulin-dependent protein kinase II delta</i>	NM_023813	D-040821-01	M-040821-00
1	N10	75	<i>Calcium/calmodulin-dependent protein kinase IV</i>	NM_009793	D-043023-01	M-043023-00
1	N11	83	<i>Calcium/calmodulin-dependent protein kinase kinase 1 alpha</i>	NM_018883	D-049735-01	M-049735-00
1	N12	65	<i>Calcium/calmodulin-dependent protein kinase kinase 2 beta</i>	NM_145358	D-040625-01	M-040625-00
1	N13	91	<i>Fyn proto-oncogene</i>	NM_008054	D-040112-01	M-040112-00
1	N14	71	<i>Cyclin G associated kinase</i>	NM_153569	D-052494-01	M-052494-00
1	N15	92	<i>Galactokinase 1</i>	NM_016905	D-044069-01	M-044069-00
1	N16	81	<i>Galactokinase 2</i>	NM_175154	D-056130-01	M-056130-00
1	N17	85	<i>Growth associated protein 43</i>	NM_008083	D-042499-01	M-042499-00
1	N18	66	<i>Glucokinase</i>	NM_010292	D-040844-01	M-040844-00
1	N19	75	<i>Glial cell line derived neurotrophic factor family receptor alpha 2</i>	NM_008115	D-045746-01	M-045746-00
1	N20	87	<i>Glycerol kinase 2</i>	NM_010294	D-065424-01	M-065424-00
1	N21	75	<i>Predicted gene 711</i>	XM_205054	D-058364-01	M-058364-00
1	N22	91	<i>Glia maturation factor beta</i>	NM_022023	D-050170-01	M-050170-00
1	O03	60	<i>Caspase recruitment domain family member 10</i>	NM_130859	D-050635-01	M-050635-00
1	O04	58	<i>Caspase recruitment domain family member 14</i>	NM_130886	D-063872-01	M-063872-00
1	O05	65	<i>Sedoheptulokinase</i>	NM_029031	D-042391-01	M-042391-00
1	O06	84	<i>Calcium/calmodulin-dependent serine protein kinase (MAGUK family)</i>	NM_009806	D-048887-01	M-048887-00
1	O07	63	<i>Chemokine (C-C motif) ligand 12</i>	NM_011331	D-043193-01	M-043193-00
1	O08	89	<i>Chemokine (C-C motif) ligand 4</i>	NM_013652	D-047365-01	M-047365-00
1	O09	83	<i>Cyclin-dependent kinase 20</i>	NM_053180	D-053874-01	M-053874-00
1	O10	67	<i>CD3 antigen epsilon polypeptide</i>	NM_007648	D-056107-01	M-056107-00
1	O11	77	<i>CD4 antigen</i>	NM_013488	D-049309-01	M-049309-00
1	O12	77	<i>CD7 antigen</i>	NM_009854	D-043076-01	M-043076-00
1	O13	71	<i>Glia maturation factor gamma</i>	NM_022024	D-050175-01	M-050175-00
1	O14	73	<i>Glucosamine (UDP-N-acetyl)-2-epimerase/N-acetylmannosamine kinase</i>	NM_015828	D-062937-01	M-062937-00
1	O15	89	<i>G protein-coupled receptor kinase 4</i>	NM_019497	D-040342-01	M-040342-00
1	O16	69	<i>G protein-coupled receptor kinase 5</i>	NM_018869	D-040343-01	M-040343-00
1	O17	95	<i>G protein-coupled receptor kinase 1</i>	NM_011881	D-040341-01	M-040341-00
1	O18	79	<i>Protein phosphatase 1 regulatory subunit 17</i>	NM_011153	D-061575-01	M-061575-00
1	O19	97	<i>Germ cell-specific gene 2</i>	NM_010353	D-048815-01	M-048815-00
1	O20	90	<i>Glycogen synthase kinase 3 beta</i>	NM_019827	D-041080-01	M-041080-00
1	O21	89	<i>General transcription factor II H polypeptide 1</i>	NM_008186	D-062142-01	M-062142-00
1	O22	98	<i>Guanylate cyclase 2c</i>	XM_132928	D-057453-01	M-057453-00
1	P03	62	<i>Cytidine and dcmp deaminase domain containing 1</i>	XM_127813	D-047908-01	M-047908-00
1	P04	75	<i>Cyclin-dependent kinase 1</i>	NM_007659	D-058633-01	M-058633-00
1	P05	92	<i>Cyclin-dependent kinase 11B</i>	NM_007661	D-040105-01	M-040105-00
1	P06	86	<i>Cyclin-dependent kinase 13</i>	XM_127221	D-045210-01	M-045210-00
1	P07	77	<i>CDC42 binding protein kinase beta</i>	NM_183016	D-041756-01	M-041756-00
1	P08	83	<i>Cell division cycle 7 (S. Cerevisiae)</i>	NM_009863	D-043093-01	M-043093-00
1	P09	81	<i>Cyclin-dependent kinase 10</i>	NM_194444	D-064531-01	M-064531-00
1	P10	90	<i>Cyclin-dependent kinase 4</i>	NM_009870	D-040106-01	M-040106-00

Plate	Well	Viability (%)	Gene name	Accession	Cat number	Pool number
1	P11	89	<i>Cyclin-dependent kinase 5</i>	NM_007668	D-040544-01	M-040544-00
1	P12	95	<i>Cyclin-dependent kinase 5 regulatory subunit 1 (p35)</i>	NM_009871	D-041971-01	M-041971-00
1	P13	77	<i>Guanylate cyclase 2e</i>	NM_008192	D-046044-01	M-046044-00
1	P14	71	<i>Guanylate cyclase 2f</i>	XM_142224	D-059040-01	M-059040-00
1	P15	79	<i>Glycerol kinase</i>	NM_008194	D-065587-01	M-065587-00
1	P16	76	<i>Alpha-kinase 2</i>	XM_128981	D-056166-01	M-056166-00
1	P17	72	<i>Hemopoietic cell kinase</i>	NM_010407	D-040986-01	M-040986-00
1	P18	78	<i>Homeodomain interacting protein kinase 1</i>	NM_010432	D-040113-01	M-040113-00
1	P19	83	<i>Homeodomain interacting protein kinase 2</i>	NM_010433	D-040114-01	M-040114-00
1	P20	76	<i>Homeodomain interacting protein kinase 3</i>	NM_010434	D-041001-01	M-041001-00
1	P21	84	<i>Hexokinase 1</i>	NM_010438	D-043574-01	M-043574-00
1	P22	76	<i>Leucine-rich repeat kinase 2</i>	NM_025730	D-049666-01	M-049666-00
2	A03	74	<i>Hexokinase 2</i>	NM_013820	D-051128-01	M-051128-00
2	A04	82	<i>Hexokinase 3</i>	NM_001033245	D-045823-01	M-045823-00
2	A05	66	<i>Heat shock protein 8</i>	NM_030704	D-055174-01	M-055174-00
2	A06	77	<i>Hormonally upregulated Neu-associated kinase</i>	NM_015755	D-046705-01	M-046705-00
2	A07	114	<i>Intestinal cell kinase</i>	NM_019987	D-049932-01	M-049932-00
2	A08	97	<i>Insulin-like growth factor I receptor</i>	NM_010513	D-056843-01	M-056843-00
2	A09	101	<i>Inositol hexaphosphate kinase 1</i>	NM_013785	D-041917-01	M-041917-00
2	A10	89	<i>Inhibitor of kappa light polypeptide enhancer in B cells kinase complex-associated protein</i>	NM_026079	D-050005-01	M-050005-00
2	A11	98	<i>Inhibitor of kappab kinase beta</i>	NM_010546	D-040630-01	M-040630-00
2	A12	80	<i>Inhibitor of kappab kinase epsilon</i>	NM_019777	D-040798-01	M-040798-00
2	A13	80	<i>Pantothenate kinase 4</i>	NM_172990	D-055475-01	M-055475-00
2	A14	84	<i>3'-phosphoadenosine 5'-phosphosulfate synthase 1</i>	NM_011863	D-045089-01	M-045089-00
2	A15	101	<i>3'-phosphoadenosine 5'-phosphosulfate synthase 2</i>	NM_011864	D-044941-01	M-044941-00
2	A16	84	<i>PAS domain containing serine/threonine kinase</i>	NM_080850	D-065533-01	M-065533-00
2	A17	102	<i>PDZ binding kinase</i>	NM_023209	D-055354-01	M-055354-00
2	A18	107	<i>Phosphoenolpyruvate carboxykinase 1 cytosolic</i>	NM_011044	D-048453-01	M-048453-00
2	A19	83	<i>Cyclin-dependent kinase 16</i>	NM_011049	D-040144-01	M-040144-00
2	A20	83	<i>Cyclin-dependent kinase 17</i>	NM_146239	D-051660-01	M-051660-00
2	A21	70	<i>Cyclin-dependent kinase 18</i>	NM_008795	D-040145-01	M-040145-00
2	A22	73	<i>Platelet derived growth factor receptor alpha polypeptide</i>	NM_011058	D-048730-01	M-048730-00
2	B03	75	<i>Interleukin 2</i>	NM_008366	D-061458-01	M-061458-00
2	B04	83	<i>Integrin linked kinase</i>	NM_010562	D-040115-01	M-040115-00
2	B05	90	<i>Inositol polyphosphate multikinase</i>	XM_125641	D-062885-01	M-062885-00
2	B06	91	<i>Insulin receptor</i>	NM_010568	D-043748-01	M-043748-00
2	B07	87	<i>Insulin receptor-related receptor</i>	NM_011832	D-047791-01	M-047791-00
2	B08	98	<i>Interleukin-1 receptor-associated kinase 1</i>	NM_008363	D-040116-01	M-040116-00
2	B09	75	<i>Interleukin-1 receptor-associated kinase 2</i>	NM_172161	D-060091-01	M-060091-00
2	B10	88	<i>Interleukin-1 receptor-associated kinase 3</i>	NM_028679	D-059683-01	M-059683-00
2	B11	85	<i>Insulin receptor substrate 1</i>	NM_010570	D-040503-01	M-040503-00
2	B12	86	<i>Integrin beta 1 binding protein 1</i>	NM_008403	D-060350-01	M-060350-00
2	B13	79	<i>Platelet derived growth factor receptor beta polypeptide</i>	NM_008809	D-048218-01	M-048218-00
2	B14	101	<i>Pyruvate dehydrogenase kinase isoenzyme 2</i>	NM_133667	D-051566-01	M-051566-00
2	B15	86	<i>Pyruvate dehydrogenase kinase isoenzyme 3</i>	NM_145630	D-052920-01	M-052920-00
2	B16	106	<i>Pyruvate dehydrogenase kinase isoenzyme 4</i>	NM_013743	D-043425-01	M-043425-00
2	B17	78	<i>3-phosphoinositide dependent protein kinase 1</i>	NM_011062	D-040658-01	M-040658-00
2	B18	75	<i>Pyridoxal (pyridoxine vitamin B6) kinase</i>	NM_172134	D-054035-01	M-054035-00
2	B19	97	<i>6-phosphofructo-2-kinase/fructose-26-biphosphatase 2</i>	NM_008825	D-041829-01	M-041829-00
2	B20	92	<i>6-phosphofructo-2-kinase/fructose-26-biphosphatase 3</i>	NM_133232	D-050027-01	M-050027-00
2	B21	82	<i>Phosphofructokinase liver B-type</i>	NM_008826	D-060388-01	M-060388-00
2	B22	81	<i>Phosphofructokinase muscle</i>	NM_021514	D-065512-01	M-065512-00

Plate	Well	Viability (%)	Gene name	Accession	Cat number	Pool number
2	C03	97	<i>IL2 inducible T cell kinase</i>	NM_010583	D-040679-01	M-040679-00
2	C04	76	<i>Inositol 134-triphosphate 5/6 kinase</i>	NM_172584	D-055096-01	M-055096-00
2	C05	84	<i>Inositol 145-triphosphate 3-kinase A</i>	NM_146125	D-062876-01	M-062876-00
2	C06	77	<i>Inositol 145-triphosphate 3-kinase B</i>	XM_205854	D-041024-01	M-041024-00
2	C07	68	<i>Inositol 145-triphosphate 3-kinase C</i>	NM_181593	D-041107-01	M-041107-00
2	C08	87	<i>Janus kinase 1</i>	NM_146145	D-040117-01	M-040117-00
2	C09	93	<i>Janus kinase 2</i>	NM_008413	D-040118-01	M-040118-00
2	C10	88	<i>Janus kinase 3</i>	NM_010589	D-040119-01	M-040119-00
2	C11	95	<i>Kinase insert domain protein receptor</i>	NM_010612	D-040634-01	M-040634-00
2	C12	80	<i>Ketohexokinase</i>	NM_008439	D-062217-01	M-062217-00
2	C13	64	<i>Phosphofructokinase platelet</i>	NM_019703	D-059341-01	M-059341-00
2	C14	77	<i>Cyclin-dependent kinase 14</i>	NM_011074	D-040146-01	M-040146-00
2	C15	81	<i>Phosphoglycerate kinase 1</i>	NM_008828	D-040302-01	M-040302-00
2	C16	91	<i>Phosphoglycerate kinase 2</i>	NM_031190	D-043374-01	M-043374-00
2	C17	79	<i>Phosphorylase kinase alpha 1</i>	NM_008832	D-048299-01	M-048299-00
2	C18	97	<i>Phosphorylase kinase alpha 2</i>	NM_172783	D-055256-01	M-055256-00
2	C19	96	<i>Phosphorylase kinase gamma 1</i>	NM_011079	D-043266-01	M-043266-00
2	C20	88	<i>Phosphorylase kinase gamma 2 (testis)</i>	NM_026888	D-059847-01	M-059847-00
2	C21	75	<i>Phosphatidylinositol 4-kinase type 2 alpha</i>	NM_145501	D-065311-01	M-065311-00
2	C22	74	<i>Phosphatidylinositol 4-kinase type 2 beta</i>	NM_025951	D-065308-01	M-065308-00
2	D03	84	<i>Kinesin family member 13B</i>	XM_283218	D-047951-01	M-047951-00
2	D04	64	<i>U2AF homology motif (UHM) kinase 1</i>	NM_010633	D-041701-01	M-041701-00
2	D05	86	<i>Kit oncogene</i>	NM_021099	D-042174-01	M-042174-00
2	D06	79	<i>Large tumor suppressor 2</i>	NM_015771	D-044602-01	M-044602-00
2	D07	62	<i>Lymphocyte protein tyrosine kinase</i>	NM_010693	D-043878-01	M-043878-00
2	D08	87	<i>Lymphocyte cytosolic protein 2</i>	NM_010696	D-059042-01	M-059042-00
2	D09	85	<i>LIM-domain containing protein kinase</i>	NM_010717	D-043923-01	M-043923-00
2	D10	62	<i>LIM motif-containing protein kinase 2</i>	NM_010718	D-043932-01	M-043932-00
2	D11	79	<i>Myosin light polypeptide kinase 2 skeletal muscle</i>	XM_130630	D-046735-01	M-046735-00
2	D12	83	<i>Leukocyte tyrosine kinase</i>	NM_008523	D-063855-01	M-063855-00
2	D13	70	<i>Phosphatidylinositol 3-kinase C2 domain containing alpha polypeptide</i>	NM_011083	D-049318-01	M-049318-00
2	D14	68	<i>Phosphatidylinositol 3-kinase C2 domain containing gamma polypeptide</i>	NM_011084	D-065486-01	M-065486-00
2	D15	91	<i>Phosphatidylinositol 3-kinase catalytic alpha polypeptide</i>	NM_008839	D-040730-01	M-040730-00
2	D16	88	<i>Phosphatidylinositol 3-kinase catalytic beta polypeptide</i>	NM_029094	D-040088-01	M-040088-00
2	D17	89	<i>Phosphoinositide-3-kinase catalytic gamma polypeptide</i>	NM_020272	D-040929-01	M-040929-00
2	D18	86	<i>Phosphatidylinositol 3-kinase regulatory subunit polypeptide 1 (p85 alpha)</i>	NM_011085	D-041079-01	M-041079-00
2	D19	78	<i>Phosphatidylinositol 3-kinase regulatory subunit polypeptide 2 (p85 beta)</i>	NM_008841	D-041085-01	M-041085-00
2	D20	85	<i>Phosphatidylinositol 3 kinase regulatory subunit polypeptide 3 (p55)</i>	NM_181585	D-041300-01	M-041300-00
2	D21	85	<i>Phosphatidylinositol 3 kinase regulatory subunit polypeptide 4 p150</i>	XM_135116	D-062225-01	M-062225-00
2	D22	60	<i>Phosphatidylinositol 4-kinase catalytic beta polypeptide</i>	NM_175356	D-056390-01	M-056390-00
2	E03	70	<i>Yamaguchi sarcoma viral (v-yes-1) oncogene homolog</i>	NM_010747	D-040987-01	M-040987-00
2	E04	82	<i>Male germ cell-associated kinase</i>	NM_008547	D-047244-01	M-047244-00
2	E05	73	<i>Mucosa associated lymphoid tissue lymphoma translocation gene 1</i>	NM_172833	D-051221-01	M-051221-00
2	E06	79	<i>Mitogen-activated protein kinase kinase 1</i>	NM_008927	D-040605-01	M-040605-00
2	E07	85	<i>Late endosomal/lysosomal adaptor MAPK and MTOR activator 3</i>	NM_019920	D-049984-01	M-049984-00
2	E08	71	<i>Mitogen-activated protein kinase kinase 2</i>	NM_023138	D-040606-01	M-040606-00
2	E09	74	<i>Mitogen-activated protein kinase kinase 3</i>	NM_008928	D-040121-01	M-040121-00
2	E10	58	<i>Mitogen-activated protein kinase kinase 4</i>	NM_009157	D-040122-01	M-040122-00
2	E11	73	<i>Mitogen-activated protein kinase kinase 5</i>	NM_011840	D-040607-01	M-040607-00
2	E12	82	<i>Mitogen-activated protein kinase kinase 6</i>	NM_011943	D-043421-01	M-043421-00

Plate	Well	Viability (%)	Gene name	Accession	Cat number	Pool number
2	E13	82	<i>Proviral integration site 1</i>	NM_008842	D-040685-01	M-040685-00
2	E14	81	<i>Proviral integration site 2</i>	NM_138606	D-052724-01	M-052724-00
2	E15	75	<i>Proviral integration site 3</i>	NM_145478	D-052883-01	M-052883-00
2	E16	80	<i>PTEN induced putative kinase 1</i>	NM_026880	D-044666-01	M-044666-00
2	E17	69	<i>Phosphatidylinositol-4-phosphate 5-kinase type 1 alpha</i>	NM_008847	D-041183-01	M-041183-00
2	E18	87	<i>Phosphatidylinositol-5-phosphate 4-kinase type II alpha</i>	NM_008845	D-040163-01	M-040163-00
2	E19	77	<i>Phosphatidylinositol-5-phosphate 4-kinase type II beta</i>	NM_054051	D-054851-01	M-054851-00
2	E20	93	<i>Phosphatidylinositol-5-phosphate 4-kinase type II gamma</i>	NM_054097	D-040164-01	M-040164-00
2	E21	78	<i>Phosphatidylinositol-4-phosphate 5-kinase-like 1</i>	NM_198191	D-057347-01	M-057347-00
2	E22	97	<i>Protein kinase inhibitor alpha</i>	NM_008862	D-058432-01	M-058432-00
2	F03	83	<i>Mitogen-activated protein kinase kinase 7</i>	NM_011944	D-040610-01	M-040610-00
2	F04	85	<i>Mitogen-activated protein kinase kinase kinase 1</i>	NM_011945	D-041090-01	M-041090-00
2	F05	80	<i>Mitogen-activated protein kinase kinase kinase 10</i>	XM_194344	D-058190-01	M-058190-00
2	F06	82	<i>Mitogen-activated protein kinase kinase kinase 11</i>	NM_022012	D-040101-01	M-040101-00
2	F07	94	<i>Mitogen-activated protein kinase kinase kinase 12</i>	NM_009582	D-040608-01	M-040608-00
2	F08	72	<i>Mitogen-activated protein kinase kinase kinase 14</i>	NM_016896	D-040771-01	M-040771-00
2	F09	55	<i>Mitogen-activated protein kinase kinase kinase 2</i>	NM_011946	D-040920-01	M-040920-00
2	F10	81	<i>Mitogen-activated protein kinase kinase kinase 3</i>	NM_011947	D-040123-01	M-040123-00
2	F11	79	<i>Mitogen-activated protein kinase kinase kinase 4</i>	NM_011948	D-040609-01	M-040609-00
2	F12	106	<i>Mitogen-activated protein kinase kinase kinase 5</i>	NM_008580	D-041179-01	M-041179-00
2	F13	81	<i>Protein kinase inhibitor beta camp dependent testis specific</i>	NM_008863	D-058816-01	M-058816-00
2	F14	68	<i>Pyruvate kinase liver and red blood cell</i>	NM_013631	D-057382-01	M-057382-00
2	F15	64	<i>Pyruvate kinase muscle</i>	NM_011099	D-062711-01	M-062711-00
2	F16	78	<i>Protein kinase N1</i>	NM_177262	D-065212-01	M-065212-00
2	F17	82	<i>Protein kinase N2</i>	NM_178654	D-065210-01	M-065210-00
2	F18	69	<i>Protein kinase N3</i>	NM_153805	D-065208-01	M-065208-00
2	F19	25	<i>Polo-like kinase 1 (Drosophila)</i>	NM_011121	D-040566-01	M-040566-00
2	F20	50	<i>Polo-like kinase 2 (Drosophila)</i>	NM_152804	D-040151-01	M-040151-00
2	F21	79	<i>Polo-like kinase 3 (Drosophila)</i>	NM_013807	D-051404-01	M-051404-00
2	F22	85	<i>Polo-like kinase 4 (Drosophila)</i>	NM_011495	D-051400-01	M-051400-00
2	G03	94	<i>Mitogen-activated protein kinase kinase kinase 6</i>	NM_016693	D-043402-01	M-043402-00
2	G04	87	<i>Mitogen-activated protein kinase kinase kinase 7</i>	NM_172688	D-040718-01	M-040718-00
2	G05	88	<i>Mitogen-activated protein kinase kinase kinase 8</i>	NM_007746	D-040683-01	M-040683-00
2	G06	81	<i>Mitogen-activated protein kinase kinase kinase 9</i>	NM_177395	D-057199-01	M-057199-00
2	G07	85	<i>Mitogen-activated protein kinase kinase kinase kinase 1</i>	NM_008279	D-042597-01	M-042597-00
2	G08	62	<i>Mitogen-activated protein kinase kinase kinase kinase 2</i>	NM_009006	D-047980-01	M-047980-00
2	G09	105	<i>Mitogen-activated protein kinase kinase kinase kinase 3</i>	XM_128800	D-040611-01	M-040611-00
2	G10	78	<i>Mitogen-activated protein kinase kinase kinase kinase 4</i>	NM_008696	D-040100-01	M-040100-00
2	G11	83	<i>Mitogen-activated protein kinase kinase kinase kinase 5</i>	NM_024275	D-040124-01	M-040124-00
2	G12	90	<i>Misshapen-like kinase 1 (zebrafish)</i>	NM_016713	D-040612-01	M-040612-00
2	G13	66	<i>Phosphomevalonate kinase</i>	NM_026784	D-041051-01	M-041051-00
2	G14	83	<i>Polynucleotide kinase 3'-phosphatase</i>	NM_021549	D-048839-01	M-048839-00
2	G15	79	<i>Protein phosphatase 1 regulatory (inhibitor) subunit 1B</i>	NM_144828	D-040427-01	M-040427-00

Plate	Well	Viability (%)	Gene name	Accession	Cat number	Pool number
2	G16	111	<i>Protein phosphatase 2 (formerly 2A) catalytic subunit alpha isoform</i>	NM_019411	D-040657-01	M-040657-00
2	G17	95	<i>Protein phosphatase 2 (formerly 2A) catalytic subunit beta isoform</i>	NM_017374	D-041905-01	M-041905-00
2	G18	82	<i>Protein phosphatase 4 catalytic subunit</i>	NM_019674	D-040058-01	M-040058-00
2	G19	87	<i>Protein kinase AMP-activated alpha 2 catalytic subunit</i>	XM_131633	D-040809-01	M-040809-00
2	G20	69	<i>Protein kinase camp dependent catalytic alpha</i>	NM_008854	D-047080-01	M-047080-00
2	G21	85	<i>Protein kinase camp dependent catalytic beta</i>	NM_011100	D-042579-01	M-042579-00
2	G22	91	<i>Protein kinase AMP-activated gamma 1 non-catalytic subunit</i>	NM_016781	D-048876-01	M-048876-00
2	H03	95	<i>Mitogen-activated protein kinase 1</i>	NM_011949	D-040613-01	M-040613-00
2	H04	96	<i>Mitogen-activated protein kinase 10</i>	NM_009158	D-045023-01	M-045023-00
2	H05	88	<i>Mitogen-activated protein kinase 11</i>	NM_011161	D-050928-01	M-050928-00
2	H06	77	<i>Mitogen-activated protein kinase 12</i>	NM_013871	D-062913-01	M-062913-00
2	H07	73	<i>Mitogen-activated protein kinase 13</i>	NM_011950	D-043774-01	M-043774-00
2	H08	71	<i>Mitogen-activated protein kinase 14</i>	NM_011951	D-040125-01	M-040125-00
2	H09	83	<i>Mitogen-activated protein kinase 3</i>	NM_011952	D-040126-01	M-040126-00
2	H10	83	<i>Mitogen-activated protein kinase 4</i>	NM_172632	D-055010-01	M-055010-00
2	H11	87	<i>Mitogen-activated protein kinase 6</i>	NM_015806	D-040133-01	M-040133-00
2	H12	92	<i>Mitogen-activated protein kinase 7</i>	NM_011841	D-040333-01	M-040333-00
2	H13	78	<i>Protein kinase AMP-activated gamma 3 non-catalytic subunit</i>	NM_153744	D-057924-01	M-057924-00
2	H14	71	<i>Protein kinase camp dependent regulatory type I alpha</i>	NM_021880	D-040846-01	M-040846-00
2	H15	99	<i>Protein kinase camp dependent regulatory type II alpha</i>	NM_008924	D-042734-01	M-042734-00
2	H16	82	<i>Protein kinase camp dependent regulatory type II beta</i>	NM_011158	D-063792-01	M-063792-00
2	H17	87	<i>Protein kinase C alpha</i>	NM_011101	D-040348-01	M-040348-00
2	H18	105	<i>Protein interacting with C kinase 1</i>	NM_008837	D-048339-01	M-048339-00
2	H19	80	<i>Protein kinase C beta</i>	NM_008855	D-048412-01	M-048412-00
2	H20	88	<i>Protein kinase C gamma</i>	NM_011102	D-050293-01	M-050293-00
2	H21	86	<i>Protein kinase C delta</i>	NM_011103	D-040147-01	M-040147-00
2	H22	80	<i>Protein kinase C epsilon</i>	NM_011104	D-040148-01	M-040148-00
2	I03	95	<i>Mitogen-activated protein kinase 8</i>	NM_016700	D-040128-01	M-040128-00
2	I04	73	<i>Mitogen-activated protein kinase 8 interacting protein 1</i>	NM_011162	D-042191-01	M-042191-00
2	I05	84	<i>Mitogen-activated protein kinase 8 interacting protein 2</i>	NM_021921	D-061724-01	M-061724-00
2	I06	83	<i>Mitogen-activated protein kinase 8 interacting protein 3</i>	NM_013931	D-043334-01	M-043334-00
2	I07	79	<i>Mitogen-activated protein kinase 9</i>	NM_016961	D-040134-01	M-040134-00
2	I08	93	<i>MAP kinase-activated protein kinase 2</i>	NM_008551	D-040135-01	M-040135-00
2	I09	79	<i>MAP kinase-activated protein kinase 5</i>	NM_010765	D-040095-01	M-040095-00
2	I10	77	<i>MAP/microtubule affinity-regulating kinase 1</i>	NM_145515	D-053815-01	M-053815-00
2	I11	73	<i>MAP/microtubule affinity-regulating kinase 2</i>	NM_007928	D-040137-01	M-040137-00
2	I12	59	<i>MAP/microtubule affinity-regulating kinase 3</i>	NM_021516	D-040138-01	M-040138-00
2	I13	75	<i>Protein kinase C eta</i>	NM_008856	D-040158-01	M-040158-00
2	I14	71	<i>Protein kinase C iota</i>	NM_008857	D-040822-01	M-040822-00
2	I15	71	<i>Protein kinase D1</i>	NM_008858	D-048415-01	M-048415-00
2	I16	70	<i>Protein kinase D3</i>	NM_029239	D-040692-01	M-040692-00
2	I17	100	<i>Protein kinase C theta</i>	NM_008859	D-048426-01	M-048426-00
2	I18	68	<i>Protein kinase C substrate 80K-H</i>	NM_008925	D-048665-01	M-048665-00
2	I19	74	<i>Protein kinase C zeta</i>	NM_008860	D-040823-01	M-040823-00
2	I20	75	<i>Protein kinase DNA activated catalytic polypeptide</i>	NM_011159	D-040958-01	M-040958-00
2	I21	89	<i>Protein kinase cgmp-dependent type I</i>	NM_011160	D-048829-01	M-048829-00
2	I22	76	<i>Protein kinase cgmp-dependent type II</i>	NM_008926	D-062310-01	M-062310-00
2	J03	76	<i>MAP/microtubule affinity-regulating kinase 4</i>	NM_172279	D-054377-01	M-054377-00
2	J04	97	<i>Microtubule associated serine/threonine kinase 2</i>	NM_008641	D-040614-01	M-040614-00
2	J05	89	<i>Microtubule associated serine/threonine kinase-like</i>	NM_025979	D-063943-01	M-063943-00

Plate	Well	Viability (%)	Gene name	Accession	Cat number	Pool number
2	J06	104	<i>Megakaryocyte-associated tyrosine kinase</i>	NM_010768	D-044002-01	M-044002-00
2	J07	89	<i>MAP3K12 binding inhibitory protein 1</i>	NM_145442	D-062812-01	M-062812-00
2	J08	69	<i>Maternal embryonic leucine zipper kinase</i>	NM_010790	D-059459-01	M-059459-00
2	J09	87	<i>C-mer proto-oncogene tyrosine kinase</i>	NM_008587	D-040357-01	M-040357-00
2	J10	71	<i>Met proto-oncogene</i>	NM_008591	D-040878-01	M-040878-00
2	J11	78	<i>MAP kinase-interacting serine/threonine kinase 1</i>	NM_021461	D-040139-01	M-040139-00
2	J12	86	<i>MAP kinase-interacting serine/threonine kinase 2</i>	NM_021462	D-041005-01	M-041005-00
2	J13	78	<i>Eukaryotic translation initiation factor 2-alpha kinase 2</i>	NM_011163	D-040807-01	M-040807-00
2	J14	81	<i>Protein kinase interferon inducible double stranded RNA dependent activator</i>	NM_011871	D-040713-01	M-040713-00
2	J15	89	<i>WNK lysine deficient protein kinase 1</i>	NM_198703	D-041543-01	M-041543-00
2	J16	80	<i>WNK lysine deficient protein kinase 3 pseudogene</i>	XM_205148	D-059069-01	M-059069-00
2	J17	76	<i>WNK lysine deficient protein kinase 4</i>	NM_175638	D-040229-01	M-040229-00
2	J18	88	<i>Protein kinase X-linked</i>	NM_016979	D-056757-01	M-056757-00
2	J19	68	<i>PRP4 pre-mrna processing factor 4 homolog B (yeast)</i>	NM_013830	D-051113-01	M-051113-00
2	J20	83	<i>Phosphoribosyl pyrophosphate synthetase 1</i>	NM_021463	D-063233-01	M-063233-00
2	J21	91	<i>Phosphoribosyl pyrophosphate synthetase 2</i>	NM_026662	D-057480-01	M-057480-00
2	J22	80	<i>Phosphoribosyl pyrophosphate synthetase-associated protein 2</i>	NM_144806	D-053452-01	M-053452-00
2	K03	64	<i>Moloney sarcoma oncogene</i>	NM_020021	D-049882-01	M-049882-00
2	K04	78	<i>Membrane protein palmitoylated</i>	NM_008621	D-062246-01	M-062246-00
2	K05	72	<i>Membrane protein palmitoylated 2 (MAGUK p55 subfamily member 2)</i>	NM_016695	D-040140-01	M-040140-00
2	K06	75	<i>Membrane protein palmitoylated 3 (MAGUK p55 subfamily member 3)</i>	NM_007863	D-044887-01	M-044887-00
2	K07	88	<i>Myelin protein zero-like 1</i>	XM_129565	D-044264-01	M-044264-00
2	K08	73	<i>Mannose receptor C type 2</i>	NM_008626	D-040940-01	M-040940-00
2	K09	92	<i>Macrophage stimulating 1 receptor (c-met-related tyrosine kinase)</i>	NM_009074	D-046427-01	M-046427-00
2	K10	75	<i>Muscle skeletal receptor tyrosine kinase</i>	NM_010944	D-046617-01	M-046617-00
2	K11	80	<i>Mevalonate (diphospho) decarboxylase</i>	NM_138656	D-053575-01	M-053575-00
2	K12	74	<i>Mevalonate kinase</i>	NM_023556	D-063629-01	M-063629-00
2	K13	73	<i>PTK2 protein tyrosine kinase 2</i>	NM_007982	D-041099-01	M-041099-00
2	K14	68	<i>PTK2 protein tyrosine kinase 2 beta</i>	NM_172498	D-040719-01	M-040719-00
2	K15	73	<i>PTK6 protein tyrosine kinase 6</i>	NM_009184	D-044700-01	M-044700-00
2	K16	80	<i>PTK7 protein tyrosine kinase 7</i>	NM_175168	D-040788-01	M-040788-00
2	K17	76	<i>Twinfilin actin-binding protein homolog 1 (Drosophila)</i>	NM_008971	D-060402-01	M-060402-00
2	K18	74	<i>Twinfilin actin-binding protein homolog 2 (Drosophila)</i>	NM_011876	D-062823-01	M-062823-00
2	K19	74	<i>Protein tyrosine phosphatase non-receptor type 5</i>	NM_013643	D-046680-01	M-046680-00
2	K20	82	<i>Protein tyrosine phosphatase receptor type G</i>	NM_008981	D-048271-01	M-048271-00
2	K21	82	<i>Protein tyrosine phosphatase receptor type J</i>	NM_008982	D-050291-01	M-050291-00
2	K22	92	<i>Protein tyrosine phosphatase receptor type R</i>	NM_011217	D-040062-01	M-040062-00
2	L03	85	<i>Myosin light polypeptide kinase</i>	NM_139300	D-041418-01	M-041418-00
2	L04	84	<i>Myosin IIIA</i>	NM_148413	D-054332-01	M-054332-00
2	L05	81	<i>N-acetylglucosamine kinase</i>	NM_019542	D-049645-01	M-049645-00
2	L06	85	<i>NIMA (never in mitosis gene a)-related expressed kinase 11</i>	NM_172461	D-056397-01	M-056397-00
2	L07	91	<i>NIMA (never in mitosis gene a)-related expressed kinase 2</i>	NM_010892	D-045662-01	M-045662-00
2	L08	89	<i>NIMA (never in mitosis gene a)-related expressed kinase 3</i>	NM_011848	D-045726-01	M-045726-00
2	L09	64	<i>NIMA (never in mitosis gene a)-related expressed kinase 4</i>	NM_011849	D-045512-01	M-045512-00
2	L10	86	<i>NIMA (never in mitosis gene a)-related expressed kinase 6</i>	NM_021606	D-059408-01	M-059408-00
2	L11	89	<i>NIMA (never in mitosis gene a)-related expressed kinase 7</i>	NM_021605	D-063266-01	M-063266-00
2	L12	82	<i>NIMA (never in mitosis gene a)-related expressed kinase 8</i>	NM_080849	D-044403-01	M-044403-00

Plate	Well	Viability (%)	Gene name	Accession	Cat number	Pool number
2	L13	92	<i>Protein tyrosine phosphatase receptor type T</i>	NM_021464	D-048432-01	M-048432-00
2	L14	70	<i>PX domain containing serine/threonine kinase</i>	NM_145458	D-055422-01	M-055422-00
2	L15	77	<i>Aldehyde dehydrogenase 18 family member A1</i>	NM_019698	D-049794-01	M-049794-00
2	L16	81	<i>RAS-related C3 botulinum substrate 1</i>	NM_009007	D-041170-01	M-041170-00
2	L17	77	<i>V-raf-leukemia viral oncogene 1</i>	NM_029780	D-040149-01	M-040149-00
2	L18	95	<i>Serine/threonine kinase 30</i>	NM_011973	D-048657-01	M-048657-00
2	L19	81	<i>Rap guanine nucleotide exchange factor (GEF) 3</i>	NM_144850	D-057800-01	M-057800-00
2	L20	82	<i>Rap guanine nucleotide exchange factor (GEF) 4</i>	NM_019688	D-057784-01	M-057784-00
2	L21	91	<i>RAS protein-specific guanine nucleotide-releasing factor 2</i>	NM_009027	D-047527-01	M-047527-00
2	L22	62	<i>Ribokinase</i>	NM_153196	D-062934-01	M-062934-00
2	M03	77	<i>NIMA (never in mitosis gene a)-related expressed kinase 9</i>	NM_145138	D-040141-01	M-040141-00
2	M04	75	<i>Nemo like kinase</i>	NM_008702	D-042021-01	M-042021-00
2	M05	76	<i>Non-metastatic cells 1 protein (NM23A) expressed in</i>	NM_008704	D-040142-01	M-040142-00
2	M06	82	<i>Non-metastatic cells 2 protein (NM23B) expressed in</i>	NM_008705	D-040143-01	M-040143-00
2	M07	77	<i>Non-metastatic cells 3 protein expressed in</i>	NM_019730	D-049492-01	M-049492-00
2	M08	101	<i>Non-metastatic cells 4 protein expressed in</i>	NM_019731	D-049846-01	M-049846-00
2	M09	78	<i>Non-metastatic cells 5 protein expressed in (nucleoside-diphosphate kinase)</i>	NM_080637	D-049199-01	M-049199-00
2	M10	95	<i>Non-metastatic cells 6 protein expressed in (nucleoside-diphosphate kinase)</i>	NM_018757	D-045821-01	M-045821-00
2	M11	90	<i>Non-metastatic cells 7 protein expressed in (nucleoside-diphosphate kinase)</i>	NM_138314	D-053365-01	M-053365-00
2	M12	76	<i>Natriuretic peptide receptor 1</i>	NM_008727	D-042648-01	M-042648-00
2	M13	63	<i>Ret proto-oncogene</i>	NM_009050	D-047013-01	M-047013-00
2	M14	74	<i>Riboflavin kinase</i>	NM_019437	D-046077-01	M-046077-00
2	M15	82	<i>RIO kinase 1 (yeast)</i>	NM_024242	D-056893-01	M-056893-00
2	M16	88	<i>RIO kinase 3 (yeast)</i>	NM_024182	D-050639-01	M-050639-00
2	M17	79	<i>Receptor (TNFRSF)-interacting serine-threonine kinase 1</i>	NM_009068	D-040150-01	M-040150-00
2	M18	74	<i>Receptor (TNFRSF)-interacting serine-threonine kinase 2</i>	NM_138952	D-052248-01	M-052248-00
2	M19	100	<i>Receptor-interacting serine-threonine kinase 3</i>	NM_019955	D-049919-01	M-049919-00
2	M20	84	<i>Ribonuclease L (2' 5'-oligoadenylate synthetase-dependent)</i>	NM_011882	D-043480-01	M-043480-00
2	M21	96	<i>Rho-associated coiled-coil containing protein kinase 1</i>	NM_009071	D-046504-01	M-046504-00
2	M22	94	<i>Rho-associated coiled-coil containing protein kinase 2</i>	NM_009072	D-040429-01	M-040429-00
2	N03	80	<i>Natriuretic peptide receptor 2</i>	NM_173788	D-050423-01	M-050423-00
2	N04	76	<i>Nuclear receptor binding protein 1</i>	NM_147201	D-054243-01	M-054243-00
2	N05	75	<i>Neuregulin 3</i>	NM_008734	D-047955-01	M-047955-00
2	N06	83	<i>Nik related kinase</i>	NM_013724	D-046446-01	M-046446-00
2	N07	71	<i>Neurotrophic tyrosine kinase receptor type 1</i>	XM_283871	D-049564-01	M-049564-00
2	N08	77	<i>Neurotrophic tyrosine kinase receptor type 2</i>	NM_008745	D-048017-01	M-048017-00
2	N09	84	<i>Neurotrophic tyrosine kinase receptor type 3</i>	NM_008746	D-041561-01	M-041561-00
2	N10	88	<i>Oxidative-stress responsive 1</i>	XM_135264	D-062357-01	M-062357-00
2	N11	79	<i>Protein kinase C and casein kinase substrate in neurons 1</i>	NM_011861	D-062209-01	M-062209-00
2	N12	80	<i>Phosphoprotein associated with glycosphingolipid microdomains 1</i>	NM_053182	D-055487-01	M-055487-00
2	N13	85	<i>Receptor tyrosine kinase-like orphan receptor 1</i>	NM_013845	D-053825-01	M-053825-00
2	N14	81	<i>Receptor tyrosine kinase-like orphan receptor 2</i>	NM_013846	D-041074-01	M-041074-00
2	N15	72	<i>Ros1 proto-oncogene</i>	NM_011282	D-042212-01	M-042212-00
2	N16	89	<i>Retinitis pigmentosa 2 homolog (human)</i>	NM_133669	D-042964-01	M-042964-00
2	N17	79	<i>Ribosomal protein S6 kinase polypeptide 1</i>	NM_009097	D-045777-01	M-045777-00
2	N18	67	<i>Ribosomal protein S6 kinase polypeptide 2</i>	NM_011299	D-042672-01	M-042672-00
2	N19	85	<i>Ribosomal protein S6 kinase polypeptide 3</i>	NM_148945	D-054432-01	M-054432-00

Plate	Well	Viability (%)	Gene name	Accession	Cat number	Pool number
2	N20	87	<i>Ribosomal protein S6 kinase polypeptide 5</i>	NM_153587	D-040751-01	M-040751-00
2	N21	85	<i>Ribosomal protein S6 kinase polypeptide 6</i>	NM_025949	D-046138-01	M-046138-00
2	N22	77	<i>Ribosomal protein S6 kinase polypeptide 2</i>	NM_021485	D-040894-01	M-040894-00
2	O03	81	<i>P21 protein (Cdc42/Rac)-activated kinase 1</i>	NM_011035	D-048101-01	M-048101-00
2	O04	83	<i>P21 protein (Cdc42/Rac)-activated kinase 2</i>	NM_177326	D-040615-01	M-040615-00
2	O05	79	<i>P21 protein (Cdc42/Rac)-activated kinase 3</i>	NM_008778	D-040616-01	M-040616-00
2	O06	60	<i>P21 protein (Cdc42/Rac)-activated kinase 4</i>	NM_027470	D-059484-01	M-059484-00
2	O07	69	<i>P21 protein (Cdc42/Rac)-activated kinase 6</i>	XM_111790	D-047118-01	M-047118-00
2	O08	86	<i>P21 protein (Cdc42/Rac)-activated kinase 7</i>	NM_172858	D-055362-01	M-055362-00
2	O09	99	<i>Pantothenate kinase 1</i>	NM_023792	D-042165-01	M-042165-00
2	O10	88	<i>Pantothenate kinase 3</i>	NM_145962	D-051419-01	M-051419-00
2	O11	94	<i>Yeast Sps1/Ste20-related kinase 4 (S. Cerevisiae)</i>	XM_136210	D-044094-01	M-044094-00
2	O12	90	<i>Adenylate kinase domain containing 1</i>	XM_137065	D-063402-01	M-063402-00
2	O13	68	<i>Ribosomal protein S6 kinase-like 1</i>	NM_146244	D-057689-01	M-057689-00
2	O14	73	<i>Receptor-like tyrosine kinase</i>	XM_135104	D-064592-01	M-064592-00
2	O15	84	<i>Microtubule associated serine/threonine kinase 1</i>	NM_019945	D-055903-01	M-055903-00
2	O16	77	<i>SCY1-like 1 (S. Cerevisiae)</i>	NM_023912	D-047892-01	M-047892-00
2	O17	83	<i>Selenophosphate synthetase 1</i>	NM_175400	D-057100-01	M-057100-00
2	O18	85	<i>Selenophosphate synthetase 2</i>	NM_009266	D-050751-01	M-050751-00
2	O19	85	<i>Serum/glucocorticoid regulated kinase 1</i>	NM_011361	D-040774-01	M-040774-00
2	O20	92	<i>Serum/glucocorticoid regulated kinase 2</i>	NM_013731	D-047584-01	M-047584-00
2	O21	105	<i>Serum/glucocorticoid regulated kinase 3</i>	NM_133220	D-050771-01	M-050771-00
2	O22	68	<i>Src homology 2 domain-containing transforming protein C1</i>	NM_011368	D-040793-01	M-040793-00
2	P03	80	<i>Homeodomain interacting protein kinase 4</i>	XM_133316	D-058179-01	M-058179-00
2	P04	91	<i>A kinase (PRKA) anchor protein 5</i>	XM_138063	D-043936-01	M-043936-00
2	P05	81	<i>Dual specificity phosphatase 5</i>	XM_140740	D-057231-01	M-057231-00
2	P06	97	<i>Ataxia telangiectasia and Rad3 related</i>	XM_147046	D-062167-01	M-062167-00
2	P07	68	<i>Cyclin-dependent kinase 15</i>	XM_194683	D-043393-01	M-043393-00
2	P08	90	<i>Src family associated phosphoprotein 1</i>	XM_203404	D-064190-01	M-064190-00
2	P09	94	<i>Kinase suppressor of ras 2</i>	XM_285897	D-054277-01	M-054277-00
2	P10	88	<i>Cyclin-dependent kinase-like 4</i>	XM_355031	D-055022-01	M-055022-00
2	P11	83	<i>RIKEN cDNA 2810408M09 gene</i>	XM_355368	D-046643-01	M-046643-00
2	P12	94	<i>NIMA (never in mitosis gene a)-related expressed kinase 1</i>	XM_356077	D-061162-01	M-061162-00
2	P13	90	<i>Salt inducible kinase 2</i>	NM_178710	D-041008-01	M-041008-00
2	P14	76	<i>MAD homolog 7 (Drosophila)</i>	NM_008543	D-047242-01	M-047242-00
2	P15	88	<i>Salt inducible kinase 1</i>	NM_010831	D-044399-01	M-044399-00
2	P16	90	<i>SNF related kinase</i>	NM_133741	D-051065-01	M-051065-00
2	P17	86	<i>Suppressor of cytokine signalling 1</i>	NM_009896	D-043120-01	M-043120-00
2	P18	87	<i>Suppressor of cytokine signalling 5</i>	NM_019654	D-042294-01	M-042294-00
2	P19	87	<i>Sperm autoantigenic protein 17</i>	NM_011449	D-045569-01	M-045569-00
2	P20	87	<i>Sphingosine kinase 1</i>	NM_025367	D-040671-01	M-040671-00
2	P21	82	<i>Sphingosine kinase 2</i>	NM_020011	D-041258-01	M-041258-00
2	P22	85	<i>Sequestosome 1</i>	NM_011018	D-047628-01	M-047628-00
3	A03	83	<i>Rous sarcoma oncogene</i>	NM_009271	D-040877-01	M-040877-00
3	A04	86	<i>Src-related kinase lacking C-terminal regulatory tyrosine and N-terminal myristylation sites</i>	NM_011481	D-062777-01	M-062777-00
3	A05	78	<i>Serine/arginine-rich protein specific kinase 1</i>	NM_016795	D-061647-01	M-061647-00
3	A06	89	<i>Serine/arginine-rich protein specific kinase 2</i>	NM_009274	D-055142-01	M-055142-00
3	A07	79	<i>Testis-specific serine kinase 6</i>	NM_032004	D-046069-01	M-046069-00
3	A08	74	<i>Serine/threonine kinase 10</i>	NM_009288	D-044001-01	M-044001-00
3	A09	87	<i>Serine/threonine kinase 11</i>	NM_011492	D-044342-01	M-044342-00
3	A10	89	<i>Serine/threonine kinase 16</i>	NM_011494	D-040152-01	M-040152-00
3	A11	87	<i>Serine/threonine kinase 17b (apoptosis-inducing)</i>	NM_133810	D-040944-01	M-040944-00
3	A12	81	<i>Serine/threonine kinase 19</i>	NM_019442	D-063053-01	M-063053-00
3	B03	87	<i>STE20-like kinase (yeast)</i>	NM_009289	D-040579-01	M-040579-00

Plate	Well	Viability (%)	Gene name	Accession	Cat number	Pool number
3	B04	86	<i>Testis-specific serine kinase 1</i>	NM_009435	D-042335-01	M-042335-00
3	B05	78	<i>Testis-specific serine kinase 2</i>	NM_009436	D-051637-01	M-051637-00
3	B06	90	<i>Testis-specific serine kinase 3</i>	NM_080442	D-049881-01	M-049881-00
3	B07	87	<i>Testis-specific serine kinase substrate</i>	NM_011651	D-043849-01	M-043849-00
3	B08	85	<i>Serine/arginine-rich protein specific kinase 3</i>	NM_019684	D-049832-01	M-049832-00
3	B09	73	<i>Serine/threonine kinase 24 (STE20 homolog yeast)</i>	NM_145465	D-062796-01	M-062796-00
3	B10	72	<i>Serine/threonine kinase 25 (yeast)</i>	NM_021537	D-065319-01	M-065319-00
3	B11	85	<i>Serine/threonine kinase 3 (Ste20 yeast homolog)</i>	NM_019635	D-040440-01	M-040440-00
3	B12	84	<i>Serine threonine kinase 31</i>	NM_029916	D-046426-01	M-046426-00
3	C03	67	<i>Serine/threonine kinase 32B</i>	NM_022416	D-049086-01	M-049086-00
3	C04	78	<i>Serine/threonine kinase 32C</i>	NM_021302	D-047534-01	M-047534-00
3	C05	77	<i>Serine/threonine kinase 33</i>	XM_358897	D-060060-01	M-060060-00
3	C06	66	<i>Serine/threonine kinase 38</i>	NM_134115	D-062731-01	M-062731-00
3	C07	59	<i>Serine/threonine kinase 38 like</i>	NM_172734	D-040297-01	M-040297-00
3	C08	85	<i>Serine/threonine kinase 39 STE20/SPS1 homolog (yeast)</i>	NM_016866	D-050614-01	M-050614-00
3	C09	66	<i>Serine/threonine kinase 4</i>	NM_021420	D-059385-01	M-059385-00
3	C10	52	<i>Aurora kinase A</i>	NM_011497	D-065109-01	M-065109-00
3	C11	69	<i>Spleen tyrosine kinase</i>	NM_011518	D-041084-01	M-041084-00
3	C12	80	<i>TANK-binding kinase 1</i>	NM_019786	D-063162-01	M-063162-00
3	D03	58	<i>Tec protein tyrosine kinase</i>	NM_013689	D-040988-01	M-040988-00
3	D04	70	<i>Endothelial-specific receptor tyrosine kinase</i>	NM_013690	D-045325-01	M-045325-00
3	D05	59	<i>Testis specific protein kinase 1</i>	NM_011571	D-059125-01	M-059125-00
3	D06	75	<i>Testis-specific kinase 2</i>	NM_146151	D-064149-01	M-064149-00
3	D07	66	<i>Testis expressed gene 14</i>	NM_031386	D-045638-01	M-045638-00
3	D08	86	<i>Transforming growth factor beta receptor I</i>	NM_009370	D-040617-01	M-040617-00
3	D09	71	<i>Transforming growth factor beta receptor II</i>	NM_009371	D-040618-01	M-040618-00
3	D10	69	<i>Tyrosine kinase with immunoglobulin-like and EGF-like domains 1</i>	NM_011587	D-046547-01	M-046547-00
3	D11	73	<i>Tight junction protein 2</i>	NM_011597	D-046662-01	M-046662-00
3	D12	72	<i>Thymidine kinase 1</i>	NM_009387	D-042809-01	M-042809-00
3	E03	66	<i>Thymidine kinase 2 mitochondrial</i>	NM_021028	D-047803-01	M-047803-00
3	E04	79	<i>Tousled-like kinase 1</i>	NM_172664	D-040153-01	M-040153-00
3	E05	88	<i>Tousled-like kinase 2 (Arabidopsis)</i>	NM_011903	D-040154-01	M-040154-00
3	E06	70	<i>Toll-like receptor 1</i>	NM_030682	D-050626-01	M-050626-00
3	E07	74	<i>Toll-like receptor 3</i>	NM_126166	D-059850-01	M-059850-00
3	E08	73	<i>Toll-like receptor 4</i>	NM_021297	D-047487-01	M-047487-00
3	E09	85	<i>Toll-like receptor 6</i>	NM_011604	D-046763-01	M-046763-00
3	E10	76	<i>Tumor necrosis factor receptor superfamily member 10b</i>	NM_020275	D-050949-01	M-050949-00
3	E11	78	<i>TRAF2 and NCK interacting kinase</i>	XM_130797	D-049830-01	M-049830-00
3	E12	85	<i>Tyrosine kinase non-receptor 1</i>	NM_031880	D-063130-01	M-063130-00
3	F03	74	<i>Tyrosine kinase non-receptor 2</i>	NM_016788	D-040775-01	M-040775-00
3	F04	83	<i>Thiamine pyrophosphokinase</i>	NM_013861	D-044055-01	M-044055-00
3	F05	64	<i>Tribbles homolog 1 (Drosophila)</i>	NM_144549	D-057134-01	M-057134-00
3	F06	83	<i>Tribbles homolog 2 (Drosophila)</i>	NM_144551	D-040469-01	M-040469-00
3	F07	62	<i>Tribbles homolog 3 (Drosophila)</i>	NM_144554	D-040943-01	M-040943-00
3	F08	70	<i>Tripartite motif-containing 27</i>	NM_009054	D-046932-01	M-046932-00
3	F09	66	<i>Transformation related protein 53 regulating kinase</i>	NM_023815	D-061023-01	M-061023-00
3	F10	52	<i>Transient receptor potential cation channel subfamily M member 6</i>	NM_153417	D-053986-01	M-053986-00
3	F11	73	<i>Transient receptor potential cation channel subfamily M member 7</i>	NM_021450	D-040716-01	M-040716-00
3	F12	66	<i>Tau tubulin kinase 2</i>	NM_080788	D-047640-01	M-047640-00
3	G03	88	<i>Ttk protein kinase</i>	NM_009445	D-047162-01	M-047162-00
3	G04	81	<i>Titin</i>	NM_011652	D-045920-01	M-045920-00
3	G05	75	<i>TXK tyrosine kinase</i>	NM_013698	D-045811-01	M-045811-00
3	G06	64	<i>Thioredoxin domain containing 3 (spermatozoa)</i>	NM_181591	D-061399-01	M-061399-00

Plate	Well	Viability (%)	Gene name	Accession	Cat number	Pool number
3	G07	61	<i>Tyrosine kinase 2</i>	NM_018793	D-050349-01	M-050349-00
3	G08	89	<i>TYRO3 protein tyrosine kinase 3</i>	NM_019392	D-043798-01	M-043798-00
3	G09	89	<i>UDP-glucose pyrophosphorylase 2</i>	NM_139297	D-061150-01	M-061150-00
3	G10	96	<i>Unc-51 like kinase 1 (C. Elegans)</i>	NM_009469	D-040155-01	M-040155-00
3	G11	77	<i>Unc-51 like kinase 2 (C. Elegans)</i>	NM_013881	D-040619-01	M-040619-00
3	G12	79	<i>Uridine-cytidine kinase 1</i>	NM_011675	D-043765-01	M-043765-00
3	H03	85	<i>Uridine-cytidine kinase 1-like 1</i>	NM_026765	D-056528-01	M-056528-00
3	H04	96	<i>Vaccinia related kinase 1</i>	NM_011705	D-040620-01	M-040620-00
3	H05	79	<i>Vaccinia related kinase 2</i>	NM_027260	D-040621-01	M-040621-00
3	H06	70	<i>Vaccinia related kinase 3</i>	NM_133945	D-040622-01	M-040622-00
3	H07	18	<i>WEE 1 homolog 1 (S. Pombe)</i>	NM_009516	D-040623-01	M-040623-00
3	H08	82	<i>Wnt inhibitory factor 1</i>	NM_011915	D-046832-01	M-046832-00
3	H09	88	<i>Yamaguchi sarcoma viral (v-yes) oncogene homolog 1</i>	NM_009535	D-040156-01	M-040156-00
3	H10	81	<i>Tyrosine 3-monooxygenase/tryptophan 5-monooxygenase activation protein eta polypeptide</i>	NM_011738	D-043652-01	M-043652-00
3	H11	85	<i>Zeta-chain (TCR) associated protein kinase</i>	NM_009539	D-062434-01	M-062434-00

Mean viability of three independent experiments (repetitions 1.1-1.3 are averaged to 1, 2.1-2.3 to 2, 3.1-3.3 to 3) is shown. NT#2-transfected cells were considered as 100 % viable. MCD4 cell viability of less than 60 % and more than 100 % is highlighted. All genes that are targeted within the Mouse Protein Kinases siRNA sublibrary are listed and are sorted by plate and well. Accessions refer to National Center for Biotechnology Information (NCBI, www.ncbi.nlm.nih.gov/) entries. Genes indicated in italics were removed from NCBI due to standard genome processing. Catalogue (Cat) and pool number refer to Dharmacon catalogue.

Tab. S 2. Different mRNA regions are targeted by pooled and single siRNAs.

Pk α siRNA	Start at bp	Sequence 5'-3'
pool 1	232	GAAGAAATGCAATACATGA
pool 2	347	GAGAAGCTCCACCGAACAA
pool 3	278	CAGCAATGAATTAGCCTTA
pool 4	296	AAACTAGCAGGCCTTGATA
single	2778	CCAAATGTACCATTAGTT

mRNA binding regions and sequences of four pooled and one single siRNA (located on Mouse Protein Kinase plate 2, well E22) targeting mouse *Pkia* transcript (NM_008862.3) are indicated. siRNAs comprise 19 nucleotides. Pk α pooled siRNAs, M-058432-01-0005/18767, Thermo Fisher Scientific (Bonn, DE); Pk α single siRNA, AM16708A; ID, 150159, Life Technologies GmbH (Darmstadt, DE).

Tab. S 3. Settings of prime program PRIME_200 of BioTek ELx405 Select CW Microtiter plate Washer.

	Range	Selected
Prime volume	1-999	200 ml
Low flow prime vol	1-999	000 ml
Prime flow rate	1-9	07
Soak after prime	Yes/no	No

Tab. S 4. Settings of aspiration program GREINER 10 of BioTek ELx405 Select CW Microtiter plate Washer.

	Range	Selected
Plate type	96/384	384
Aspirate height	12-180	034 (4,318 mm)
Horizontal aspr pos	-25-25	-07 (-0,320 mm)
Horiz y aspr pos	-10-20	-07 (-0,320 mm)
Aspiration rate	1-10	07 (3,0 mm/sec)
Aspirate delay	0-5000	000 msec
Crosswise aspir	Yes/no	No

Tab. S 5. Settings of washing program GREINER of BioTek ELx405 Select CW Microtiter plate Washer.

		Range	Selected
	Plate type	96/384	384
Method	Nuber of cycles	1-10	03
	Wash formatt	Plate/sector	Plate
	Soak/shake	Yes/no	No
Disp	Dispense volume	50-30000	0100 µl/well
	Dispense flow rate	1-11	01
	Dispense height	12-180	115 (14,605mm)
	Horizontal disp pos	-25-25	-25 (-1,143m)
	Horiz y dsip pos	-10-20	-08 (-0,366mm)
	Bottom wash first	Yes/no	No
	Prime before start	Yes/no	No
Aspir	Aspirate height	12-180	078 (9,906 mm)
	Horizontal aspr pos	-25-25	-07 (-0,320mm)
	Horiz y aspr pos	-10-20	-07 (-0,320mm)
	Aspiration rate	1-10	07 (3,0 mm/sec)
	Aspirate delay	0-5000	000 msec
	Crosswise aspir	Yes/no	No
	Final aspiration	Yes/no	Yes
	Final aspir delay	0-5000	0000 msec

Tab. S 6. MCD4 cell viability upon the siRNA-mediated down regulation of proteins that are involved in the AQP2 control.

	Viability (%)	Protein symbol	Gene name	Accession
1	59	PI3KC2B	<i>Phosphoinositide-3-kinase class 2 beta polypeptide</i>	NM_001099276.2
2	60	CSNK2B	<i>Casein kinase 2 beta polypeptide</i>	NM_009975.2
3	65	MLCK3	<i>Myosin light chain kinase 3</i>	NM_175441.5
4	69	PRKACA	<i>Protein kinase cAMP dependent catalytic alpha</i>	NM_008854.4
5	69	CSNK2A2	<i>Casein kinase 2 alpha prime polypeptide</i>	NM_009974.3
6	70	PKCN	<i>Protein kinase C nu</i>	NM_029239.3
7	71	PKCI	<i>Protein kinase C iota</i>	NM_008857.3
8	71	PKCM	<i>Protein kinase C mu</i>	NM_008858.3
9	71	PKAR1A	<i>Protein kinase cAMP dependent regulatory type I alpha</i>	NM_021880.2
10	71	P38-MAPK	<i>Mitogen-activated protein kinase p38 alpha</i>	NM_001146200.1
11	74	PKCZ	<i>Protein kinase C zeta</i>	NM_008860.2
12	75	CDK1	<i>Cyclin-dependent kinase 1</i>	NM_007659.3
13	75	PKCH	<i>Protein kinase C eta</i>	NM_008856.3
14	76	PKBA	<i>Protein kinase B alpha</i>	NM_009652.3
15	76	PKG2	<i>Protein kinase cGMP-dependent type II</i>	NM_008926.4
16	79	JNK2	<i>c-Jun N-terminal kinase 2</i>	NM_207692.2
17	79	PP1R17	<i>Protein phosphatase 1 regulatory subunit 17</i>	NM_011153.3
18	80	PKCE	<i>Protein kinase C epsilon</i>	NM_011104.3
19	80	PKCB	<i>Protein kinase C beta</i>	NM_008855.2
20	82	PKAR2B	<i>Protein kinase cAMP dependent regulatory type II beta</i>	NM_011158.3
21	83	ERK1	<i>Extracellular signal-related kinase 1</i>	NM_011952.2
22	84	MYO3A	<i>Myosin IIIA</i>	NM_148413.3
23	85	PKACB	<i>Protein kinase cAMP dependent catalytic beta</i>	NM_001164199.1
24	86	PKCD	<i>Protein kinase C delta</i>	NM_011103.3
25	87	PKCA	<i>Protein kinase C alpha</i>	NM_011101.3
26	88	PKCC	<i>Protein kinase C gamma</i>	NM_011102.3
27	88	CSNK2A1	<i>Casein kinase 2 alpha 1 polypeptide</i>	NM_007788.3
28	89	CDK5	<i>Cyclin-dependent kinase 5</i>	NM_007668.3
29	89	PKG1	<i>Protein kinase cGMP-dependent type I</i>	NM_011160.3
30	89	PI3KCG	<i>Phosphoinositide-3-kinase catalytic gamma polypeptide</i>	NM_001146200.1
31	90	GSK3B	<i>Glycogen synthase kinase 3 beta</i>	NM_019827.6
32	95	ERK2	<i>Extracellular signal-related kinase 2</i>	NM_011949.3
33	95	PP2CB	<i>Protein phosphatase 2 (formerly 2A) catalytic subunit beta isoform</i>	NM_017374.3
34	95	JNK1	<i>c-Jun N-terminal kinase 1</i>	NM_016700.4
35	99	PKAR2A	<i>Protein kinase cAMP dependent regulatory type II alpha</i>	NM_008924.2
36	100	PKCQ	<i>Protein kinase C theta</i>	NM_008859.2
37	102	AKAP220	<i>A kinase (PRKA) anchor protein 220</i>	NM_001164503.1
38	111	PP2CA	<i>Protein phosphatase 2 (formerly 2A) catalytic subunit alpha isoform</i>	NM_019411.4

Accessions refer to National Center for Biotechnology Information (NCBI, www.ncbi.nlm.nih.gov/) entries.

Tab. S 7. siRNA molecules that are not complementary to target mRNA.

	Protein symbol	Gene name	Original targeted accession	Current untargeted accession	siRNA sequence 5'-3'
1	ADK	Adenosine Kinase	NM_134079.1	NM_001243041.1 NM_134079.4	GAACUUGUCUGCGUGCAU
2	AKAP1	A kinase (PKA) anchor protein 1	NM_009648.1	NM_009648.2 NM_001042541.1	GAUAUAAGAGGGUGAAAGU
3	AKAP13	A kinase (PKA) anchor protein 13	XM_133543.3	NM_029332.1	UAGCGAACAUUGUCAGUUU
4	ALDH18A1	Aldehyde Dehydrogenase 18 Family Member A1	NM_153554.1 NM_019698.1	NM_019698.2 NM_153554.2	GCACGGAAGCCUCAAGUAU
5	APPL1	Adaptor Protein Phosphotyrosine Interaction PH Domain And Leucine Zipper Containing 1	NM_145221.1	NM_145221.2	GACGGAAUCACAUUUUAUA
6	AURKC	Aurora Kinase C	NM_020572.1	NM_001080965.1 NM_001080966.1 NM_020572.2	GGAACACUCUCGACGGGUG
7	AVPR1B	Arginine Vasopressin Receptor 1B	NM_011924.1	NM_011924.2	GAGAUUGGUAUCCUAGCUA
8	BUB1	Budding Uninhibited By Benzimidazoles 1 Homolog	NM_009772.1	NM_001113179.1 NM_009772.2	GAACGGCAGCAUUAUAGUA
9	BUB1	Budding Uninhibited By Benzimidazoles 1 Homolog	NM_009772.1	NM_001113179.1 NM_009772.2	CCCAUGGGAUGAUGAAUUG
10	CDC7	Cell Division Cycle 7	NM_009863.1	NM_009863.3 NM_001271567.1 NM_001271568.1 NM_001271566.1	AAUAGAGUCUCGACGCUUU
11	CDK15	Cyclin-Dependent Kinase 15	XM_194683.2	NM_001033373.2	GCGAAUACCAUCAUUGAGU
12	CDK5R2	Cyclin-Dependent Kinase 5 Regulatory Subunit 2 (P39)	NM_009872.1	NM_009872.3	GCAAGCGUCUACCGGCGAA
13	CDKN2B	Cyclin-Dependent Kinase Inhibitor 2B	NM_007670.2	NM_007670.4	CCGCCUGCCGGUAGACUUA
14	CLK2	CDC-like kinase 2	NM_007712.1	NM_001163432.1 NM_007712.3	GAACACGAGUUGCCUGAA
15	CMPK1	Cytidine Monophosphate (UMP-CMP) Kinase 1	NM_025647.2	NM_025647.3	CUAAUGCUCAGAAGAAUAA
16	COL4A3BP	Collagen Type IV Alpha 3 (Goodpasture Antigen) Binding Protein	NM_023420.1	NM_023420.2 NM_001164222.1	GGCGCCAGCUUCGGUCUUA
17	CSF1R	Colony Stimulating Factor 1 Receptor	NM_007779.1	NM_001037859.2	CCAUGGCGAGGUUCGAUUA
18	DOK1	Docking Protein 1	NM_010070.3	NM_010070.4	CAAGAAACCUCUCUACUGG
19	DUSP5	Dual Specificity Phosphatase 5	XM_140740.3	NM_001085390.1	CAUCUCGGCUCUACUCAGA
20	DUSP5	Dual Specificity Phosphatase 5	XM_140740.3	NM_001085390.1	CCAAGCGUCUACACAAGA
21	EVI5L	Ecotropic Viral Integration Site 5 Like	NM_153536.2	NM_001039578.3	GGAUUGAGACCCUAGAGAA
22	FN3KRP	Fructosamine 3 Kinase Related Protein	NM_181420.2	NM_181420.3	GUAGUGACAUUCUGCGGAU
23	GUCY2F	Guanylate Cyclase 2f	XM_142224.3	NM_001007576.2	GAACAGAGCUCAAGGCAAG
24	IKBKAP	Inhibitor Of Kappa Light Polypeptide Enhancer In B Cells Kinase Complex-Associated Protein	NM_026079.1	NM_026079.3	CGAAAGUUCUGCCUGUCA
25	IPMK	Inositol Polyphosphate Multikinase	XM_125641.3	NM_027184.1	GCACUCACCAGAUUUAGUU
26	IRS1	Insulin Receptor Substrate 1	NM_010570.2	NM_010570.4	AGGAGGAGCUGAGUAAUUA
27	KIF13B	Kinesin Family Member 13B	XM_283218.2	NM_001081177.1	GUACUUAGAUGCUGCCUUA
28	MAP3K6	Mitogen-Activated Protein Kinase Kinase 6	NM_016693.2	NM_016693.5	GACAAUGAGAGCACUAUUA
29	MAP3K6	Mitogen-Activated Protein Kinase Kinase 6	NM_016693.2	NM_016693.5	GAUCUAGUCUACACCAGAA
30	MAP3K9	Mitogen-Activated Protein Kinase Kinase 9	NM_177395.2	NM_177395.5 NM_001174107.1	GCAAGACCAUAGAGAACGU
31	MAP4K1	Mitogen-Activated Protein Kinase Kinase Kinase 1	NM_008279.1	NM_008279.2	GCCAGUGUCUACUCAUUA
32	MAP4K1	Mitogen-Activated Protein Kinase Kinase Kinase 1	NM_008279.1	NM_008279.2	GGAAUUCUGUGGAGCCGGU
33	MAPK10	Mitogen-Activated Protein Kinase 10	NM_009158.1	NM_001081567.1 NM_009158.2	GGAAGGAGCUAUUUGACC
34	MARK1	MAP/microtubule affinity-regulating kinase 1	NM_145515.1	NM_145515.2	GACGUC AACUGGGAUAAUC
35	MARK1	MAP/microtubule affinity-regulating kinase 1	NM_145515.1	NM_145515.2	CCACGAAACGGGUGCACUU
36	MARK3	MAP/microtubule affinity-regulating kinase 3	NM_021516.1 NM_022801.1	NM_021516.4 NM_022801.4	GAAGCAAGAGCUAAGUUUA
37	MECOM	MDS1 and EVI1 complex locus	NM_007963.1	NM_021442.2 NM_007963.2	GAACCCAAAUCAAGUGCAA
38	MECOM	MDS1 and EVI1 complex locus	NM_007963.1	NM_021442.2 NM_007963.2	UAAAGGCUAUUGCGUCUAU
49	MECOM	MDS1 and EVI1 complex locus	NM_007963.1	NM_021442.2 NM_007963.2	UGGCUUCGAUAACUAAUUA
40	MYLK2	Myosin Light Polypeptide Kinase 2 Skeletal Muscle	XM_130630.4	NM_001081044.2	GAGUGGAGCUUGUAUCUAA

	Protein symbol	Gene name	Original targeted accession	Current untargeted accession	siRNA sequence 5'-3'
41	MYLK2	<i>Myosin Light Polypeptide Kinase 2 Skeletal Muscle</i>	XM_130630.4	NM_001081044.2	GGUGUCAGCUAGAAAGACU
42	MYO3A	<i>Myosin IIIA</i>	NM_148413.1	NM_148413.3	GCAAGUGUAUUAUGUGUAC
43	NADK	<i>NAD kinase</i>	NM_138671.1	NM_001159637.1 NM_138671.2	GCAGUGUGCCUCCUGUUUAU
44	PAK1	<i>p21 protein (Cdc42/Rac)-activated kinase 1</i>	NM_011035.1	NM_011035.2	GUACACACCGUUCGAGAAG
45	PINK1	<i>PTEN induced putative kinase 1</i>	NM_026880.1	NM_026880.2	GUACACUGUCCUCGUUUAU
46	PKBA	<i>Protein kinase B alpha</i>	NM_009652.1	NM_009652.3 JNM_001165894.1	GGAAAGUGAUUCUGGUGAA
47	PKCD	<i>Protein Kinase C Delta</i>	NM_011103.1	NM_011103.3	GAUAAGUACUUUGCAAUCA
48	PKDC	<i>Protein Kinase DNA Activated Catalytic Polypeptide</i>	NM_011159.1	NM_011159.2	GGACCUAUGUGAUGUAUAC
49	PKN2	<i>Protein Kinase N2</i>	NM_178654.2	NM_178654.4	UAGACAGCCUGAUGUGUAA
50	PPP2CB	<i>Protein Phosphatase 2 (Formerly 2A) Catalytic Subunit Beta Isoform</i>	NM_017374.2	NM_017374.3	GACUCUUCUUGUAGCGUUA
51	PTK2B	<i>PTK2 protein tyrosine kinase 2 beta</i>	NM_172498.1	NM_172498.3 NM_001162365.1 NM_001162366.1	GAACAUGGCUGAUCUCAUA
52	RIPK3	<i>Receptor-Interacting Serine-Threonine Kinase 3</i>	NM_019955.1	NM_019955.2 NM_001164108.1 NM_001164107.1	ACCCAGAGCUGUUUUUAA
53	ROS1	<i>Ros1 proto-oncogene</i>	NM_011282.1	NM_011282.2	GGUACCAGCUACUGAAUUA
54	RPRD1A	<i>Regulation Of Nuclear Pre-Mrna Domain Containing 1A</i>	NM_144861.1	NM_144861.2	GCAACUCACUCGAAUGUUA
55	RPS6KA1	<i>Ribosomal Protein S6 Kinase Polypeptide 1</i>	NM_009097.1	NM_009097.4	UGAAAGAUGUGUACGACGA
56	RPS6KA1	<i>Ribosomal Protein S6 Kinase Polypeptide 1</i>	NM_009097.1	NM_009097.4	GUAAUAUCCUCUAUGUGGA
57	SPHK1	<i>Sphingosine Kinase 1</i>	NM_011451.1 NM_025367.3	NM_025367.6 NM_001172475.1 NM_011451.3 NM_001172473.1 NM_001172472.1	GGAGGUAGCUGAACUGAAU
58	SPHK1	<i>Sphingosine Kinase 1</i>	NM_011451.1 NM_025367.3	NM_025367.6 NM_001172475.1 NM_011451.3 NM_001172473.1 NM_001172472.1	GGAGAGAGCUGUGAAUUG
59	SPHK1	<i>Sphingosine Kinase 1</i>	NM_011451.1 NM_025367.3	NM_025367.6 NM_001172475.1 NM_011451.3 NM_001172473.1 NM_001172472.1	GCUAUACGUUGAACAAUUU
60	SPHK1	<i>Sphingosine Kinase 1</i>	NM_011451.1 NM_025367.3	NM_025367.6 NM_001172475.1 NM_011451.3 NM_001172473.1 NM_001172472.1	UAAAGAAACUCUACCAGAU
61	TK2	<i>Thymidine Kinase 2 Mitochondrial</i>	NM_021028.2	NM_021028.3 NR_045642.1	GUUAGAGGUGGGAAGAUG
62	TLR6	<i>Toll-Like Receptor 6</i>	NM_011604.1	NM_011604.3	GAUUUAGUGCUGCCAAGUU
63	TRIM27	<i>Tripartite Motif-Containing 27</i>	NM_009054.1	NM_009054.3	GAGCGCAGUCCUUUGAUC
64	TXK	<i>TXK tyrosine kinase</i>	NM_013698.1	NM_013698.2 NM_001122754.1	GAUAGAUCGUCAGAGUUG
65	YSK4	<i>Yeast Sps1/Ste20-related kinase 4</i>	XM_136210.4	NM_011737.1	GAUCCUAAGCUUUGUGAUU

siRNAs were generated based on accessions of RefSeq release 32 (Reference Sequence Database, Original targeted accession). Listed oligonucleotides do not match current target accessions based on RefSeq release 58 (Current untargeted accession). Accession numbers refer to National Center for Biotechnology Information (NCBI, www.ncbi.nlm.nih.gov/) entries. Several transcript variants per gene are considered.

Tab. S 8. Sequences of siRNAs directed against 13 hits.

	Protein symbol	Gene Name	Duplex number	siRNA sequence 5'-3'
1	AK3	<i>Adenylate kinase 3</i>	D-040898-01	GAACAGAAACCAACAAGAU
2	AK3	<i>Adenylate kinase 3</i>	D-040898-02	GAAAGCUGAUCCAGAUAGA
3	AK3	<i>Adenylate kinase 3</i>	D-040898-03	GUAUACUCCUCCUACAGA
4	AK3	<i>Adenylate kinase 3</i>	D-040898-04	GAUAGACACAGUAAUAAU
5	BMPR1B	<i>Bone morphogenetic protein receptor type 1B</i>	D-051071-01	GACGAGAGCUUGAAUAGAA
6	BMPR1B	<i>Bone morphogenetic protein receptor type 1B</i>	D-051071-02	GAGGUUAUGUGGAAGAAUA
7	BMPR1B	<i>Bone morphogenetic protein receptor type 1B</i>	D-051071-03	GCACAGAUGGGUACUGCUU
8	BMPR1B	<i>Bone morphogenetic protein receptor type 1B</i>	D-051071-04	ACGAAGCUCUGGAAAAUUA
9	CDK18	<i>Cyclin-dependent kinase 18</i>	D-040145-01	CCAAUUCAGUGCCUACAAA
10	CDK18	<i>Cyclin-dependent kinase 18</i>	D-040145-02	ACAGUGACCUGAAACAGUA
11	CDK18	<i>Cyclin-dependent kinase 18</i>	D-040145-03	GGAAACAUAUGUGAAACUG
12	CDK18	<i>Cyclin-dependent kinase 18</i>	D-040145-04	GAAACACGCCAAUUAUGUG
13	DUSP2	<i>Dual specificity phosphatase 2</i>	D-040331-01	GGACGAGCCUUGACUUU
14	DUSP2	<i>Dual specificity phosphatase 2</i>	D-040331-02	UCACAGCAGUUCUCAUUGU
15	DUSP2	<i>Dual specificity phosphatase 2</i>	D-040331-03	GCAUUCAGUAGAAGAUAA
16	DUSP2	<i>Dual specificity phosphatase 2</i>	D-040331-04	UAGACUCGGUGAAGAAUAG
17	EPHB3	<i>Eph receptor B3</i>	D-043340-01	GAGAUGACCUCUUUUAUAA
18	EPHB3	<i>Eph receptor B3</i>	D-043340-02	GCACGUUACAGGUGUGUAA
19	EPHB3	<i>Eph receptor B3</i>	D-043340-03	GCACCUGCCAUAUUAACUU
20	EPHB3	<i>Eph receptor B3</i>	D-043340-04	AGAGCAAGACUAUCGGUUA
21	FGFR1	<i>Fibroblast growth factor receptor 1</i>	D-040832-01	GAAGACUCUGGAGUUAAU
22	FGFR1	<i>Fibroblast growth factor receptor 1</i>	D-040832-02	GAAGAGAGACCAGCUGUGA
23	FGFR1	<i>Fibroblast growth factor receptor 1</i>	D-040832-03	GAUCGCAGACUUUGCCUUA
24	FGFR1	<i>Fibroblast growth factor receptor 1</i>	D-040832-04	UGGAGUAUCUUGCCUCUAA
25	PFKP	<i>Phosphofructokinase 1</i>	D-059341-01	GGAAUGGUGAUUCGAUAA
26	PFKP	<i>Phosphofructokinase 1</i>	D-059341-02	UAUAAGCGUCUUGCCAUAU
27	PFKP	<i>Phosphofructokinase 1</i>	D-059341-03	GAGGCGACUAUGACAUGU
28	PFKP	<i>Phosphofructokinase 1</i>	D-059341-01	GGAGCAAUCGACAUCAAAA
29	PKIA	<i>Protein kinase inhibitor alpha</i>	D-058432-01	GAAGAAAUGCAAUACAUGA
30	PKIA	<i>Protein kinase inhibitor alpha</i>	D-058432-02	GAGAAGCUCCACCGAACAA
31	PKIA	<i>Protein kinase inhibitor alpha</i>	D-058432-03	CAGCAAUGAAUUAAGCCUUA
32	PKIA	<i>Protein kinase inhibitor alpha</i>	D-058432-04	AAACUAGCAGGCCUUGAUUA
33	STK11	<i>Serine/threonine kinase 11</i>	D-044342-01	CCAAUGGACUGGACACCUU
34	STK11	<i>Serine/threonine kinase 11</i>	D-044342-02	GCGCCAAUCUACUGGCAA
35	STK11	<i>Serine/threonine kinase 11</i>	D-044342-03	GGUCACACUUUACAACAUC
36	STK11	<i>Serine/threonine kinase 11</i>	D-044342-04	GUGAUGGAGUACUGCGUAU
37	SYK	<i>Spleen tyrosine kinase</i>	D-041084-01	GGAAUAAUCUCAAGGAUCA
38	SYK	<i>Spleen tyrosine kinase</i>	D-041084-02	GCAAUUAACUGGGUGGUUU
39	SYK	<i>Spleen tyrosine kinase</i>	D-041084-03	GAACUGAGGCUUCGCAAUU
40	SYK	<i>Spleen tyrosine kinase</i>	D-041084-04	GGCCUUAUCUGCCUCCUUA
41	TK2	<i>Thymidine kinase 2 mitochondrial</i>	D-047803-02	GGAGAAAUGUCCAUUGGCCA
42	TK2	<i>Thymidine kinase 2 mitochondrial</i>	D-047803-03	CCUGUACGGUUGAUGGAAA
43	TK2	<i>Thymidine kinase 2 mitochondrial</i>	D-047803-04	GCAAGUGGGAAGACGACAU
44	TK2	<i>Thymidine kinase 2 mitochondrial</i>	D-047803-01	GUUAGAGGUGGGAAGAUG
45	TRIM27	<i>Tripartite motif-containing 27</i>	D-046932-01	GCAGCUCUAUCACUGUUG
46	TRIM27	<i>Tripartite motif-containing 27</i>	D-046932-03	UGAGUGGGAUUGAUGGDUU
47	TRIM27	<i>Tripartite motif-containing 27</i>	D-046932-04	GAGAUGGGCUGUGCGAGA
48	TRIM27	<i>Tripartite motif-containing 27</i>	D-046932-02	GAGCGCACGUCCUUGAUC
49	VRK3	<i>Vaccinia related kinase 3</i>	D-040622-01	GCAGCGAUCUCCAGACCUU
50	VRK3	<i>Vaccinia related kinase 3</i>	D-040622-02	GGUGAUGGCCUCAAUUAU
51	VRK3	<i>Vaccinia related kinase 3</i>	D-040622-03	CAAAGCAUGUGUAUCAGA
52	VRK3	<i>Vaccinia related kinase 3</i>	D-040622-04	GUACAGGUCCUAGUAUUC

Duplex number refers to Dharmacon catalogue. The down regulation of the listed genes did not decrease MCD4 cell viability to less than 60 %.